Development of a Design-Phase Assessment Tool for Double Façades in Retrofit Applications

by

Emily Vance

A thesis

presented to the University of Waterloo

in fulfillment of the

thesis requirement for the degree of

Master of Applied Science

in

Civil Engineering

Waterloo, Ontario, Canada, 2013

AUTHOR'S DECLARATION

I hereby declare that I am the sole author of this thesis. This is a true copy of the thesis, including any required final revisions, as accepted by my examiners.

I understand that my thesis may be made electronically available to the public.

Abstract

Much of the existing commercial building stock is aging and will be in need of upgrades now or within the next twenty years. Typically, enclosure retrofits consist of adding insulation to the exterior or interior of the existing façade. In this thesis, an alternative solution is examined, whereby a glass façade is added to the exterior of the existing building, forming a double façade. For historic buildings, this could preserve and protect the existing façade without completely covering it up. For outdated buildings, this could modernize the existing façade, giving it the all-glazed appearance that is currently so popular among architects.

Regardless of the retrofit motive, it is important to be able to quantitatively compare retrofit solutions to make informed design decisions. As such, building simulation can be an important design tool. At present, there is no available simulation tool that can easily and accurately model a double façade; therefore, a double façade (DoFa) model was developed to fill this gap.

A spreadsheet-based, lumped model was created and validated using current complex fenestration models and limited experimental data. Further experimental data is required to validate all aspects of the model. Results showed that the DoFa model can achieve accurate results; however, further development is needed to predict optical properties of venetian blinds and convective coefficients for natural airflow in double façade cavities.

The model was used to compare double façades to traditional glazing systems. Results indicated that double façades can perform comparably to double glazing with outdoor shading in summer, and triple glazing in winter. However, the results are only valid for the tested glazing systems. In a second application, the DoFa model was modified to simulate an entire enclosure to compare a double façade retrofit to more traditional retrofit strategies. Results suggested that a double façade provides a good improvement in winter performance, though summer overheating is a concern. For the case study examined, a double façade would have performed better than the chosen retrofit of replacing the windows with double glazing and indoor shading, without insulating the opaque components.

The DoFa model can be very useful in creating double façade preliminary design and operation strategies. At present, the DoFa model is an instantaneous, stand-alone tool. Further development is needed to pair the DoFa model with whole building energy simulations.

Acknowledgements

First and foremost, I would like to thank my supervisor, Dr. John Straube, for his help and guidance throughout this project. His incredible wealth of knowledge and enthusiasm towards building science provide a true inspiration for me.

I would also like to thank my friends and colleagues in the BEG office: Rob LePage, Lorne Ricketts and Trevor Trainor. Their shared knowledge and experiences from various building science backgrounds were much appreciated. Thanks also to the staff at BSC, who allowed me to work on interesting projects beyond the scope of my thesis.

Thank you to my family, whose love and support were invaluable throughout my graduate studies, not to mention my entire life. Finally, a big thanks to my friends and fellow graduate students, who made these past two (and a half) years so much fun.

Financial support from the Natural Sciences and Engineering Research Council of Canada (NSERC) and University of Waterloo Presidents Scholarship are also gratefully acknowledged.

Table of Contents

List of Figures

List of Tables

Nomenclature

Greek Symbols

θ	Incidence angle [°]
β	Surface tilt angle [°]
γ	Surface solar azimuth angle [°]
φ	Venetian blind slat angle [°]
α	Absorptivity
ρ	Reflectivity
τ	Transmissivity
ε	Emissivity
σ	Stefan-Boltzmann constant [5.67 W/m^2K^4]
β	Coefficient of volumetric thermal expansion [1/K]
v	Kinematic viscosity [m^2/s]
Δ	Change

Symbols

q	heat flux [W/m^2]
Q	heat flow [W]
A	Area [m^2]
G	Incident solar radiation [W/m^2]
C	Ratio of diffuse irradiation on a horizontal surface to direct normal irradiation
F	Angle factor
A	Apparent solar irradiation at air mass equal to zero [W/m^2]
B	Atmospheric extinction coefficient
C_N	Clearness number
t	Top-of-stack transmittance
a	Top-of-stack absorptance
T	Temperature [K unless otherwise specified]
h_r	Radiative heat transfer coefficient [W/m^2K]
h_c	Convective heat transfer coefficient [W/m^2K]
I_{lw}	Longwave radiation exchange [W/m^2]
C	Thermal conductance [W/m^2K]
k	Thermal conductivity [W/m·K]
l	length/material thickness [m]
U	Overall thermal conductance excluding surface films [W/m^2K]
R	Thermal resistance [m^2K/W]
V	Air velocity [m/s]
L	Characteristic length [m]
Nu	Nusselt number
Ra	Rayleigh number
Pr	Prandtl number
c_p	Specific heat of cavity air [approx. 1005 J/kg·K]
g	Acceleration of gravity [m/s^2]
A_r	Aspect ratio
H	Height [m]
s	Cavity depth [m]
Re	Reynolds number
y	Entrance length [m]
D_h	Hydraulic diameter [m]
m_a	Mass flow rate of air [kg/s]

I_{lwc}	Longwave radiation exchange to a clear sky [W/m^2]
k	Function of the type of cloud [0.26]
c	Fractional cloud cover
O_p	Openness [%]
Fe	Exterior Flowing Fraction
$\dot{Q}$	Volumetric flow rate of air [m^3/s]
h	height to neutral pressure plane [m]
C_d	Discharge coefficient of opening
z	Elevation [m]
P	Pressure [Pa]
y	Height above inlet [m]

Subscripts

SWR	Solar (Shortwave) radiation
LWR	Longwave radiation
Cond	Conduction
Conv	Convection
e	Effective
t	Total
D	Direct
d	Diffuse
g	Ground
sky	Sky
S	Solid layer
F	Fluid layer
n	Solid layer number increasing from the inside
j	Fluid layer number increasing from the inside
MRT	Mean radiant temperature
a	Air
ext	Exterior (Outdoors)
int	Interior (Indoors)
i	inner
o	outer
m	Mean
eq	Equivalent
for	Forced
nat	Natural
f	Flow
th	Thermal
D	Diameter
dir	Direct
ind	Indirect
cav	Cavity
dp	Dew point
w	Vapour
ws	Saturation vapour

Chapter 1
Introduction

1.1 Background

Approximately one third of Canada's secondary energy consumption and greenhouse gas emissions are due to the operation of buildings (NRCan, 2010). Similar statistics are true in Europe and the United States. As such, there is much opportunity within the building industry for energy savings. This is especially important now, when rising energy costs, energy security and the environmental impacts of energy production are becoming significant concerns.

1.1.1 Existing Buildings

Although energy efficiency in new construction is important and significant reductions can be achieved, upgrading the existing building stock is where the largest total energy savings potential lies. The North American commercial and institutional building stock is aging (Figure 1.1) and is in need of upgrades and retrofits in the near future.

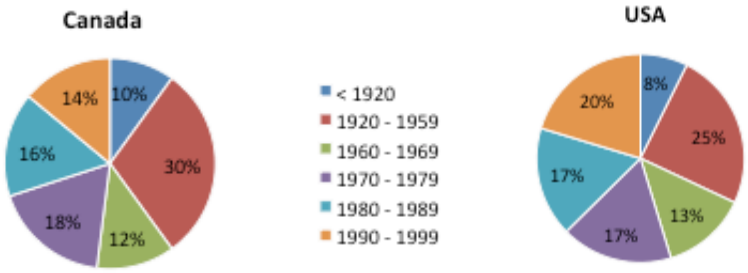

(NRCan, 2003) (U.S. DOE, 2006)

Figure 1.1 Age of Commercial and Institutional Building Stock

In the year 2000, approximately half of the buildings in North America were built before 1970 and two thirds were built before 1980. Similar statistics are true in Europe, where two thirds of the office-stock is also older than 30 years (Hoffmann, 2006). According to Ebbert (2011), most modern façades and mechanical systems reach the end of their technical life-span at 30 years and these buildings show poor performance in terms of user comfort and energy consumption. Based on the literature review and discussion with an expert in the industry, Table 1.1 lists very rough estimates of the expected lifetimes of various enclosure types before a retrofit is required.

Table 1.1 Expected Façade Lifetime for Typical Commercial/Institutional Buildings

Year Built	Enclosure Type	**Expected Service Life** [years]
< 1920	Load-bearing masonry	60 - 200
	Metal frame masonry infill	50 - 120
1920 - 1959	Load-bearing masonry	60 - 200
	Hybrid block/veneer	50 - 100
1960 - 1980	Brick veneer/CMU	60 - 100
	Steel stud brick veneer	50 - 100
	Metal curtain wall	40 - 60
1980 - present	Curtain wall	35 - 50
	Steel stud EIFS	30 - 40

The ages in Table 1.1 vary depending on the specific construction and exposure of each building. However, older buildings are generally constructed with more massive and durable enclosures (e.g., stone or masonry) while newer façades are constructed with lightweight and less durable enclosures (e.g., curtain wall or EIFS). Consequently, many of the enclosure types by age group can be expected to require retrofits at the same time (i.e., currently or within the next 20 years). Accordingly, there will soon be an explosion in the number of retrofit projects, which presents a great opportunity to include energy efficiency upgrades.

1.1.2 Drivers for Retrofit

Currently, countries around the world are setting targets to improve energy efficiency and reduce greenhouse gas emissions. Conservation is generally seen as the cheapest way to accomplish these goals; therefore, government incentives may create a driving force for retrofitting inefficient buildings. For the owner, rising energy costs and the desire to “go green” can also be factors.

For comparison, Figure 1.2 shows the site energy consumption intensity (i.e., the site energy use per unit floor area) of North American commercial and institutional buildings by the year built.

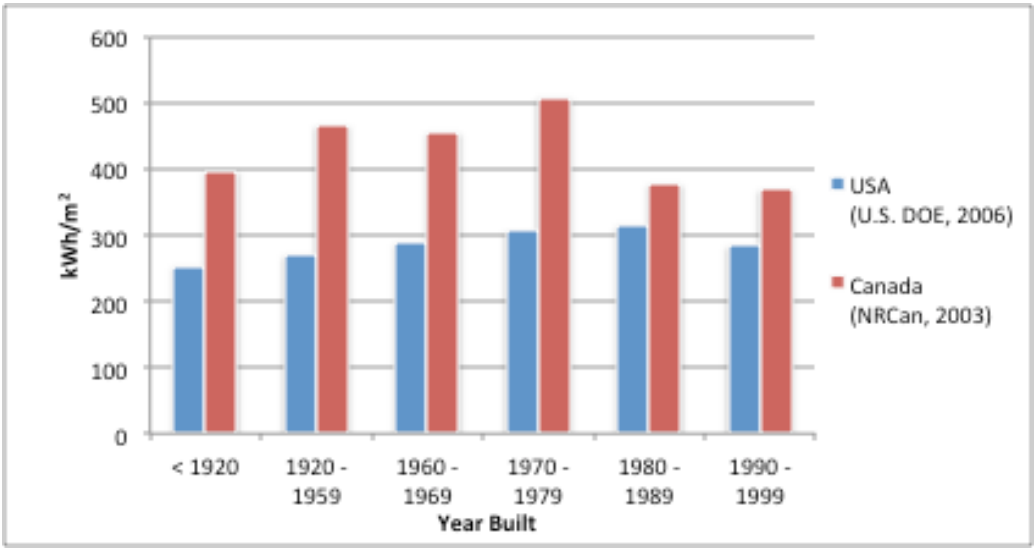

Figure 1.2 Energy Consumption per Unit Floor Area of North American Commercial and Institutional Buildings

Different energy consumption between the two countries is expected due to major climatic differences as well as other factors such as occupancy type, energy source, construction type, etc. Nevertheless, overall trends show that highest energy consumption in Canada is for buildings built between 1970 and 1980, while highest consumption in the United States is for buildings built between 1980 and 1990. Upgrading these energy inefficient buildings should become an important priority if conservation is the goal.

Although improving energy efficiency is an important concern, it often comes as a side benefit to retrofits initiated for more urgent or compelling reasons. Much of the aging building stock must be retrofitted simply because the building enclosure is failing, in need of major repair and/or users are uncomfortable. Common problems that could drive a building-enclosure retrofit are described in Table 1.2.

Table 1.2 Potential Causes for Retrofit

Problem	Associated Concerns
Water leakage	Structural damage, rot, mold and staining
Air leakage	Draughts, interstitial condensation and air quality complaints
Poor thermal insulation	Cold surfaces causing surface condensation, water damage and comfort complaints
Appearance	Efflorescence, spalling, rusting, cracking, deterioration and staining
Safety	Façade components falling off

In addition to the above listed drivers for retrofit, many existing buildings are simply aesthetically out of date, or look "tired". Companies often wish to portray a modern appearance or create a bold statement with a beautiful building, hence driving the desire for retrofit. Additional perceived benefits of improved aesthetics are increased company image, property value, worker pride and productivity, etc.

1.1.3 Retrofit Options

Retrofitting an older building, as opposed to demolishing and rebuilding, has many advantages, including:

- Significant components of the existing building (e.g., structure, service, etc.) may be reused, saving on materials, time and money;
- large amounts of demolition waste are prevented from ending up in a landfill;
- buildings can be updated where new zoning ordinances (e.g., height/area restrictions) would not allow a new building of the same size to replace the old.

Traditionally, energy efficiency retrofits for commercial buildings (excluding equipment and appliances) have included four aspects: 1) building enclosure; 2) heating, ventilation and air conditioning (HVAC) systems; 3) artificial lighting; and 4) renewable technologies. Retrofit strategies discussed in this thesis focus primarily on the building enclosure.

The two basic options for enclosure retrofits are to either insulate on the interior or insulate on the exterior of the existing structure. The two strategies are illustrated in Figure 1.3 and Figure 1.4 respectively.

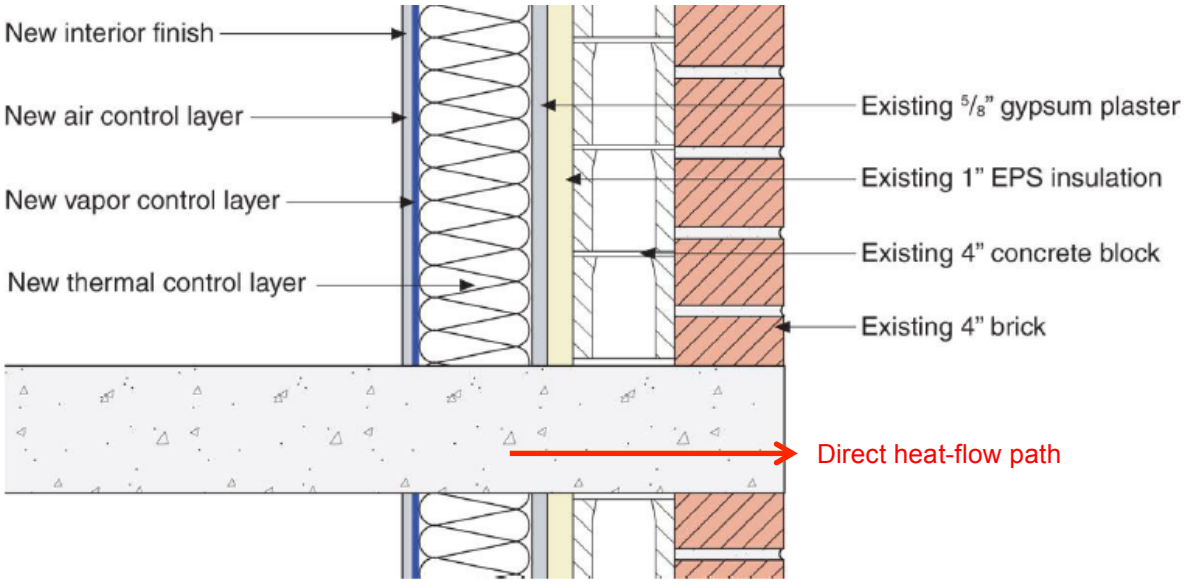

Figure 1.3 Interior Insulation Retrofit (Charbonneau, 2011)

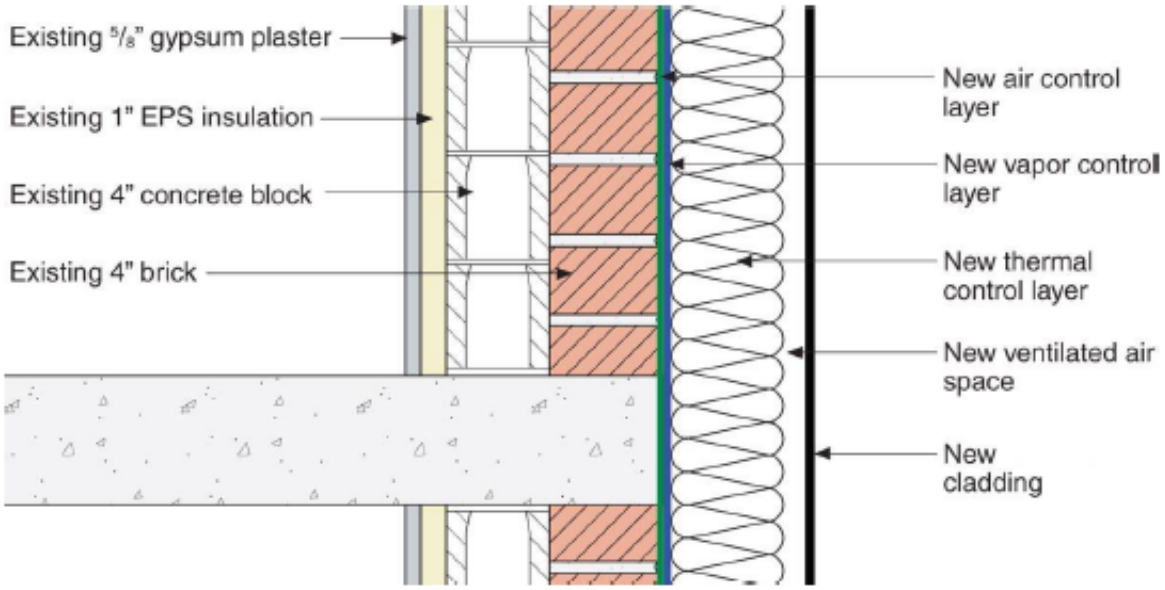

Figure 1.4 Exterior Insulation Retrofit (Charbonneau, 2011)

Insulating on the exterior, or overcladding, is the preferred option from a performance perspective because it is easier to make the control layers continuous (i.e., air, water, vapour and thermal control layers). Applying control layers on the interior necessitates connections at the floor, ceiling and penetrations, which creates more opportunity for discontinuities.

Furthermore, continuity of the thermal layer is impossible where structural elements penetrate to the outside (Figure 1.3). This creates a direct heat-flow path out of the building (i.e., thermal bridge), reducing the overall R-value of the wall and creating a cold surface at the floor slab where condensation may occur. Interior retrofits also leave the existing system exposed to weather, which could cause further deterioration. In his thesis, Charbonneau (2011) compared exterior and interior insulation retrofits for high-rise apartment buildings. A summary of his findings is presented in Table 1.3.

Table 1.3 Comparison Between Interior and Exterior Retrofits

Criteria	Interior Retrofit	Exterior Retrofit
Control Layers	Discontinuous	Continuous
Rainscreen Opportunity	No	Yes
Moisture Tolerant Materials	Not required	**Required**
Effective Thermal Resistance	Less effective	2 to 4 times more effective
Annual Energy Consumption	Less efficient	Saves 3% more than interior
Brick Durability	Less durable	Significantly more durable
Condensation Potential	Potential improvement	Significantly Improved
Aesthetics (Curb Appeal)	No opportunity for improvement	Opportunity for improvement
Economies of scale	Good	Better
Construction interference to occupants	Significant	Minimal
Construction displacement of tenants	Yes	No
Construction scaffolding required	No	**Yes**
Construction weather sensitive	No	**Yes**
Finished Floor Area	Reduced	Unaffected or increased

The exterior retrofit proved better in every category except those shown in bold in Table 1.3. Essentially, the only disadvantages of an exterior retrofit are that it requires moisture tolerant insulation, scaffolding and good weather for construction. However, regardless of the advantages, an exterior retrofit is not possible if the owner wants to maintain the existing building appearance, as is true for many older buildings with historic or sentimental value. In these cases, an interior retrofit is necessary, which causes several problems and creates some performance risk.

1.1.4 Interior Retrofit Difficulties for Load-Bearing Masonry

Retrofitting beautiful older buildings can be a challenge. In North America, many older buildings have load-bearing brick masonry or hybrid block/veneer enclosures. While these are very

durable constructions, they are also air leaky and often have little to no insulation (total approximate R-value of 4). Consequently, retrofits are required to provide thermal comfort. Some building examples are shown in Figure 1.5.

Figure 1.5 Examples of Solid Load-bearing Masonry Buildings in North America

In order to maintain the appearance and character of these buildings, an interior retrofit would be necessary. However, moisture-related performance and durability problems can result, counteracting the very preservation goals of the retrofit.

Load-bearing masonry walls use the mass approach to control rain water penetration. Essentially, the enclosure materials are allowed to get wet, though the high moisture storage capacity of the masonry prevents water from wicking or penetrating to the inside. The materials then dry to both the exterior and the interior, and no damage occurs. However, adding insulation to the interior effectively decreases the temperature of the masonry and reduces the drying potential (Figure 1.6).

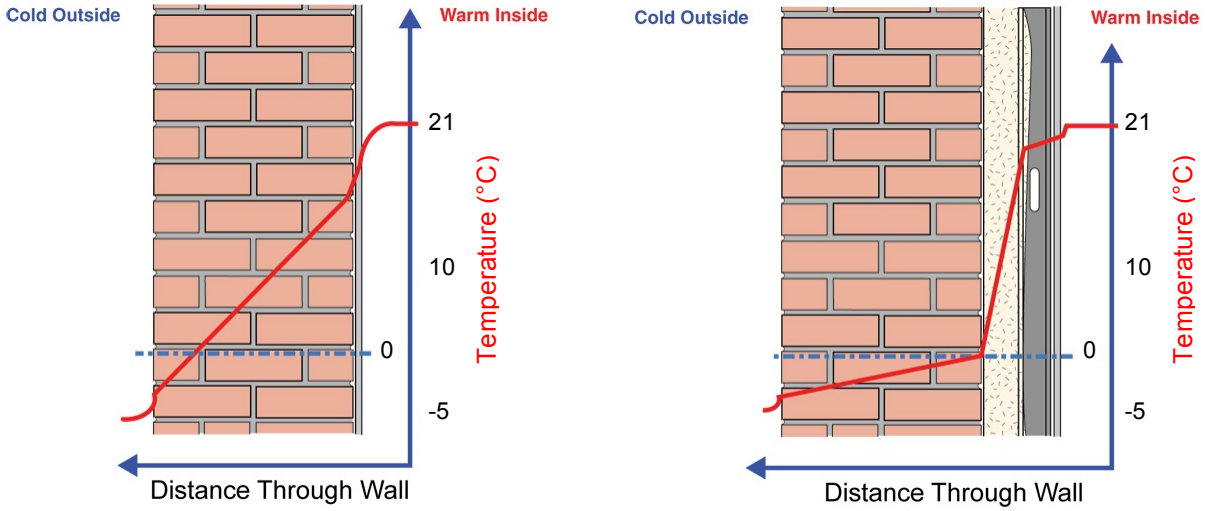

Figure 1.6 Temperature Profile for Uninsulated and Insulated Masonry Walls (Straube & Schumacher, 2007)

Adding insulation causes the entire masonry wall to become colder in winter conditions, thereby reducing drying by diffusion and surface evaporation. Consequently, the brick is wetter and the risk of freeze-thaw damage increases. Schumacher (2011) has found, through extensive brick testing, that there is a critical degree of saturation for each type of brick. If that brick experiences freezing temperatures even once while its moisture content is above this critical degree of saturation, damage will occur. Therefore, causing the bricks to be colder and wetter will subject them to more freeze-thaw conditions that could cause damage and spalling. Although the critical degree of saturation varies between bricks, it tends to be lower for older bricks and especially for older bricks forming the interior wythes of multi-wythe assemblies. In the past, lesser-quality bricks were often used for the inner wythes because they were not expected to experience extreme conditions. However, adding insulation to the interior essentially exposes the inner-wythe bricks to conditions similar to outside conditions. Consequently, freeze-thaw becomes a higher risk for bricks throughout the entire assembly.

Another moisture concern is surface condensation due to air leakage and diffusion, especially in buildings where the relative humidity is kept high during cold weather (e.g., museums). Because the interior face of the masonry is now colder in winter, it has a higher potential to be below the dew point temperature of the interior air. Consequently, any air leakage contacting this surface could result in condensation and cause damage and mold (Figure 1.7).

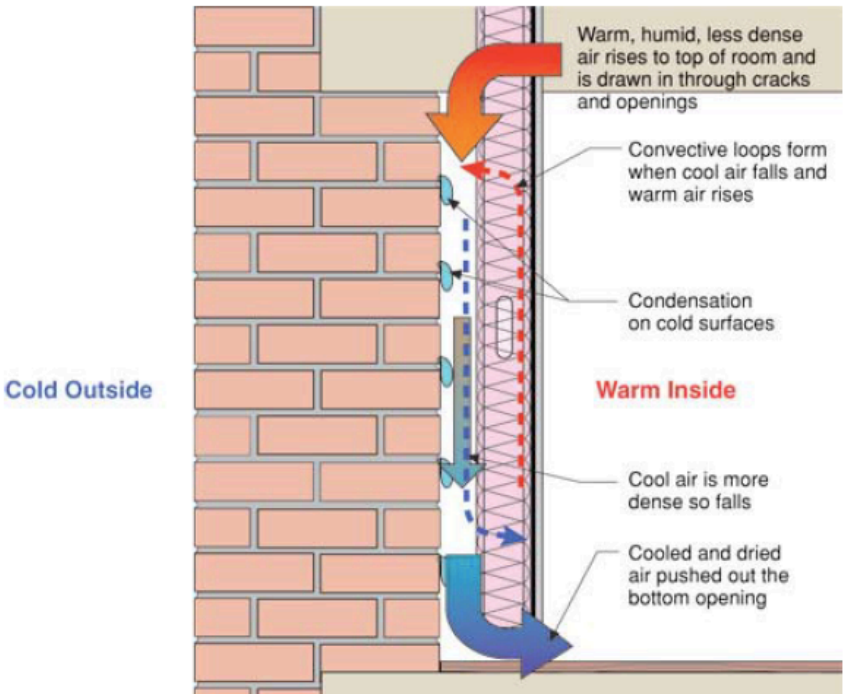

Figure 1.7 Air Leakage Condensation in an Interior Retrofit with Stud Wall and Batt Insulation (Straube & Schumacher, 2007)

To control air leakage, it is important to have a continuous air barrier on the interior of the insulation. However, continuity can be difficult to achieve at connections and penetrations. Straube and Schumacher (2007) state that spraying airtight insulating foam directly to the back of the existing masonry is the best method to achieve maximum airtightness and eliminate air movement behind the insulation.

Similarly, outward flowing vapour diffusion can cause condensation at the cold interior masonry surface. Therefore, the vapour permeability of interior finishes is important. Some vapour control is needed to stop cold-weather diffusion condensation, though low permeance interior finishes and barriers can be detrimental because they resist or eliminate the potential for inward

drying after rain events (Straube & Schumacher, 2007). Hence, it is important to choose appropriate materials to control vapour diffusion wetting while allowing inward drying for building-specific indoor and outdoor conditions.

Another concern is the floor structure, which is often imbedded in the masonry to transfer loads to the wall. This cannot be insulated from the inside and creates a thermal bridge. If the floor structure is concrete, it will be colder at the wall connection and could experience surface condensation. If the floor structure is comprised of wood beams, more serious problems may occur. With the decreased temperature of the masonry, the embedded wood beam temperature is also decreased and its drying potential is reduced. Furthermore, any air leakage into the beam pocket could cause condensation. This increases the risk of rot, which could be dangerous to the structural integrity of the building (Figure 1.8).

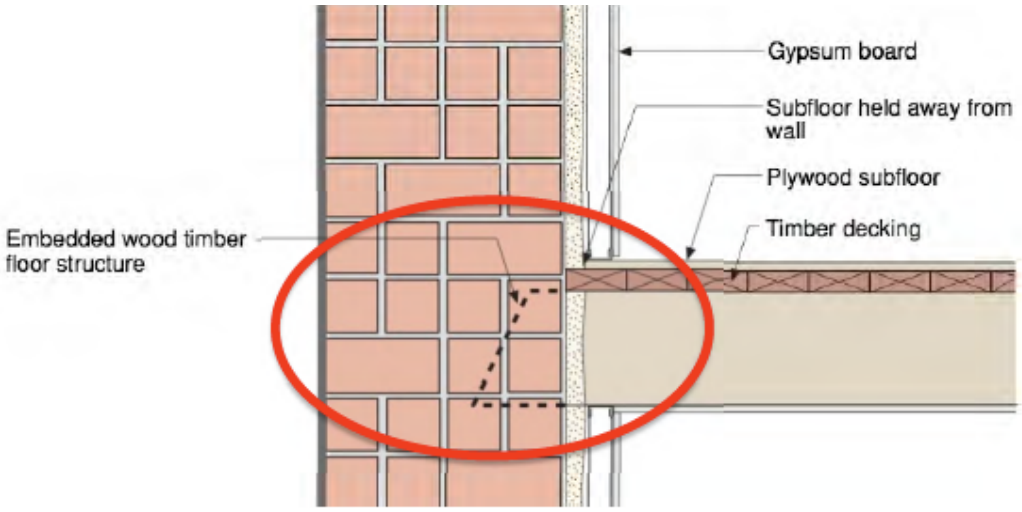

Figure 1.8 Embedded Wood Timber Floor Structure (Ueno, 2011)

Possible solutions include installing metal “heat spreader” plates at the sides of the member (bypassing the insulation) or omitting/reducing the insulation surrounding the embedded wood to effectively raise the temperature; however, an energy penalty is incurred (Ueno, 2011).

1.1.5 Alternative Solution

An alternate retrofit strategy, as an intermediate approach between exterior and interior insulation retrofits, could be to apply a glass façade to the exterior of the existing structure, thereby creating a double façade (DF). This would provide continuous exterior control layers to

preserve and protect the existing building without completely covering it up. For a historical retrofit, a very clear glazing might be chosen to display the building behind. Conversely, for a retrofit where a modern and sleek look is desired, a colored or reflective glazing might be chosen to hide the building behind.

Regardless of the retrofit objectives, it is important to be able to quantitatively compare retrofit strategies to make informed design decisions. As such, building simulation can be an important design tool. At present, there is no available simulation tool that can easily and accurately model a double façade. Therefore, the main focus of this thesis is to create a tool to facilitate quick comparisons between double façades and more traditional retrofit strategies.

1.2 Project Objective

The objective of the research reported in this thesis is to develop a simple computer program or tool to model the behaviour of double façades in retrofit applications. It is meant to facilitate early design-phase decision making. As such, it should be easy to use and computationally light while still providing important design information. The main uses of such a tool would be to 1) provide quantitative performance data (e.g., energy loads and interior surface temperatures) to allow comparisons between DF options and more traditional retrofit strategies, 2) determine design loads and expected performance under specific outdoor conditions and 3) allow designers to quickly assess the impact of design choices to optimize their design.

1.3 Scope

The scope of this thesis is to create a model to accept basic user inputs and quickly provide outputs useful for preliminary design. These include heat flux, Solar Heat Gain Coefficient (SHGC), U-value, average layer temperatures, bulk airflow rates, etc. However, the tool is intended to provide general performance results and not detailed design information such as local surface temperatures or airflow distribution. If detailed design information is required, more complex modeling tools are necessary.

The model approach and calculations are documented and validated for natural airflow. Note that mechanical convection is included as an option but is not validated in the present work. Furthermore, natural airflow calculations include buoyancy only, excluding wind effects. Finally, the model is developed for assembly sections of uniform composition. At present, the model is

a stand-alone model to predict instantaneous performance. Future development is needed to couple the model developed here with whole building energy models to determine annual energy performance at early stages of design.

1.4 Approach

The research presented in this thesis begins by investigating the DF concept to determine the advantages, disadvantages and possible configurations. Selected DF retrofits are examined as case studies to determine the motives, design strategies and concerns of each project.

Next, the literature is reviewed to establish the main approaches to modeling DFs. Whole building energy models, complex fenestration models and purpose-built DF models are investigated.

The chosen modeling approach is then presented and the calculations are documented. Calculations may be separated into the optical element (incident and absorbed solar radiation), thermal element (conductive, radiative and convective heat flux) and the airflow element (convective heat flow and air velocity). Energy balances for each type of component (i.e., single glazing, shading, multi-glazing, opaque wall) are presented as well as overall performance indices calculations.

The developed model was validated, first against existing complex fenestration models and second against published experimental data. A parametric study was also conducted to determine the importance of various inputs.

Finally, the model was used in two example applications. First, DF options were compared to more traditional glazing options of double and triple glazing with indoor, outdoor and intermediate shading. Second, whole building retrofit options were compared for an existing building.

Chapter 2
Double Façades

2.1 History & Definition

In modern architecture, there is a large fascination with all-glazed façades. From the exterior they are seen as modern and sleek, creating a uniform and transparent appearance. From the interior they are seen as occupant friendly, providing daylight and a visual connection to the outdoors. However, an all-glazed façade is not energy efficient. While a typical Canadian opaque wall might have an R-value of 15-20, Straube (2008) warns that most so-called "high-performance" curtain walls with a mix of vision glass and spandrel panels have overall R-values of less than 4. The low thermal resistance and high transparency cause excessive heat loss when it is cold, excessive heat gain when the sun shines and even excessive daylighting (Braham, 2005). Consequently, the double façade (DF) was introduced as a more energy efficient version of the traditional curtain wall system. Originally implemented in Northern Europe, there now exist several examples in North America, including the Manitoba Hydro Building, which was labeled a "green" building achieving LEED (Leadership in Energy and Environmental Design) Platinum certification.

The DF has been referred to by many titles in different works, namely multiple skin façade, double glass façade, ventilated façade, air supply/extract window, active glass envelope, intelligent façade, etc. Regardless of the title, it can generally be defined as:

> *An envelope construction consisting of a ventilated cavity bounded by semi-transparent or fully transparent surfaces.*

Saelens (2002) suggests that there are three important elements to a DF: 1) the envelope construction, 2) the cavity airflow and 3) the transparency of the bounding surfaces. The first element suggests that the DF must be part of the building enclosure and not an occupied zone requiring a certain comfort level. This excludes atria, ventilated greenhouses and glazed corridors, unless large temperature swings are allowable in these areas. The second element suggests that there must be airflow within the cavity, which excludes sealed windows and airtight constructions. However, a DF may be closed in certain operation modes to avoid ventilation. The third element suggests that the bounding surfaces must be at least partially

glazed, which excludes ventilated cavities and Trombe walls. A general schematic of a DF is shown in Figure 2.1.

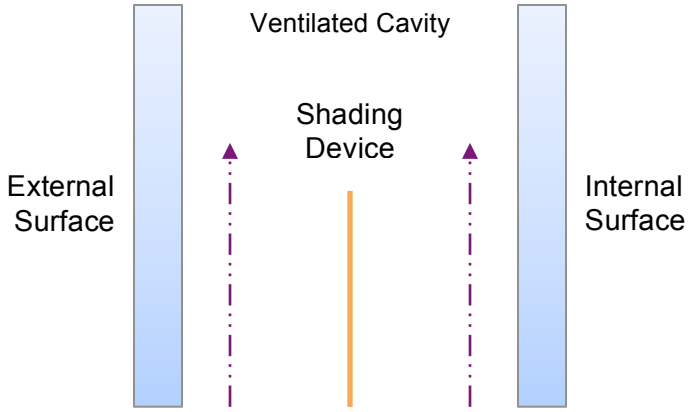

Figure 2.1 Double Façade Concept

The external surface is generally all glazed and can extend over the entire building or only a portion of it. The internal surface can be a mix of opaque and glazed elements. The ventilated cavity can range from about 20 cm to 200 cm, and some sort of operable shading device is usually installed within this space, either a roller blind or louver-type blind. The direction and pathway of airflow within the cavity is dependent on the design intentions of the façade.

The main concept behind the DF is that it may gather or exclude solar heat to save energy in both winter and summer. In winter, the façade cavity is closed to trap solar heated air between the inner and outer façades, hence creating a buffer zone between the inner façade and the outdoor environment. In the summer, the façade cavity is opened so that natural airflow induced by buoyancy and wind pressures may flush out the solar heated cavity air and prevent overheating. Furthermore, shading devices installed in the cavity space reduce solar heat gain to the office space behind, thereby reducing cooling loads. However, the operation strategy is very dependent on the façade configuration, of which there are many options.

2.2 Configurations

It is difficult to give a general definition of the DF, since there exist so many possible designs and configurations. However, numerous researchers have categorized DFs in a similar manner (Saelens, 2002; Lancour et al., 2004; Braham, 2005; Haase et al., 2007; Intelligent Energy Europe, 2008). The main categories may be defined by three parameters: 1) the driving force of

the cavity airflow, 2) the façade compartmentalization and 3) the airflow path. While definitions and vocabulary vary within the literature, a common DF classification is shown in Figure 2.2.

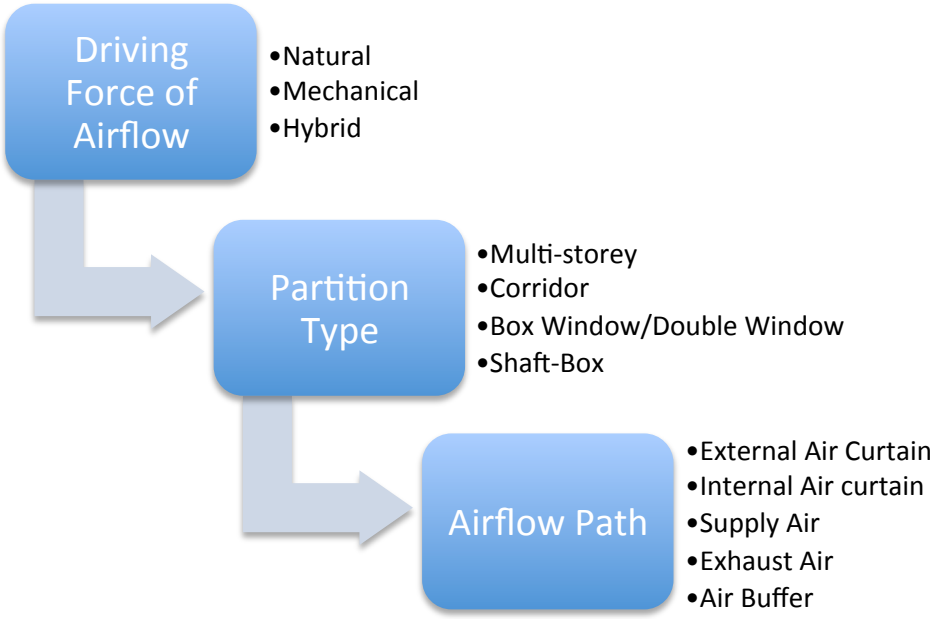

Figure 2.2 Classification of Double Façades

2.2.1 Driving Force of Airflow

The airflow within a double façade cavity may be driven either naturally, mechanically or by a mixture of both. Naturally driven airflow relies on natural buoyancy and wind-induced pressures and is therefore dependent on external climatic conditions. Mechanically driven airflow is much more predictable, though requires energy to run fans constantly. A hybrid system allows the use of both naturally and mechanically driven airflow when necessary. This requires a complex, centralized control system to switch modes depending on climate and user need.

2.2.2 Façade Compartmentalization

The façade can be compartmentalized in a variety of ways, though Oesterle et al. (2001) define the four main types listed in Figure 2.2. Much of the literature agrees with this classification.

Firstly, the multi-storey DF has no compartmentalization at all (Figure 2.3). The outer façade extends over the entire height and length of the building without intermediate divisions. In general, metallic grids are installed at each level to allow access for cleaning and maintenance.

Large openings at the bottom and top of the façade allow air intake and exhaust, though intermediate openings may also be distributed over the building height. The driving force of airflow is generally natural, as there will be large stack pressures (Oesterle et al., 2001). The problems with this type of façade are that fire and smoke may spread freely through the cavity space, which may not comply with local fire regulations. Also, high temperatures will be experienced in the top of the façade cavity, making natural ventilation undesirable during most seasons. Furthermore, high airflow rates and sound transmission in the cavity space make operable windows in the inner façade undesirable. However, warmed air from the façade may be used as preheated supply air to the HVAC system in winter. Additionally, the outer façade provides good separation with outdoor noise, so this façade is especially suitable where external noise levels are high (Oesterle et al., 2001).

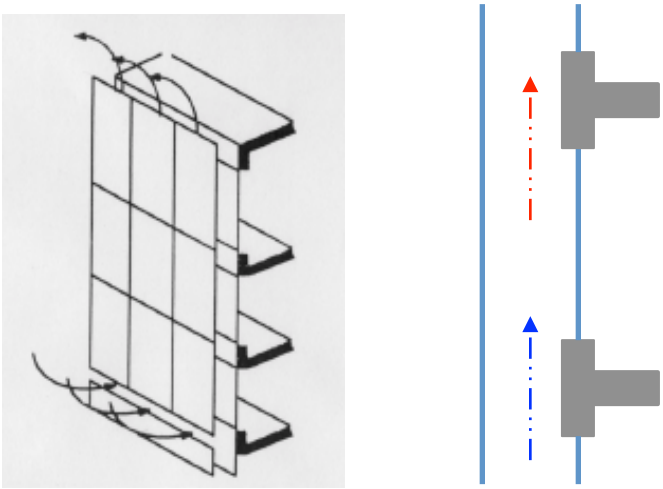

Profile (Uuttu, 2001) Section

Figure 2.3 Multi-Storey Double Façade

The corridor DF has vertical compartmentalization, where the façade cavity is separated by storey (Figure 2.4). The corridor may extend for a number of rooms or for an entire floor, depending on acoustic, fire-protection or ventilation objectives. Air intake and exhaust openings are situated at the floor and ceiling level of each corridor, and should be staggered from floor to floor to avoid exhaust air from one floor being supplied to the next floor. In this configuration, natural ventilation via windows or openings in the inner façade is possible and the risk of overheating is less. Also, separating the cavity space provides fire protection and reduces sound transmission, though sound transmission between rooms on the same level is still a

concern. This type of façade can have naturally or mechanically driven airflow within the cavity, depending on the airflow and ventilation strategy. However, naturally driven airflow will be limited due to the small height available for stack effect.

The box window DF incorporates horizontal separations so that the cavity is separated vertically at every storey and horizontally at every room (Figure 2.4). The same principles apply here as with the corridor façade, though the horizontal separations provide more sound insulation between rooms. This type of façade is suited for solid interior façades with punched openings and where greater importance is attached to privacy between rooms (Oesterle et al., 2001). Another similar form of DF is the ventilated double window or airflow window, which functions in the same way as a box window but is only at the window portion of the façade.

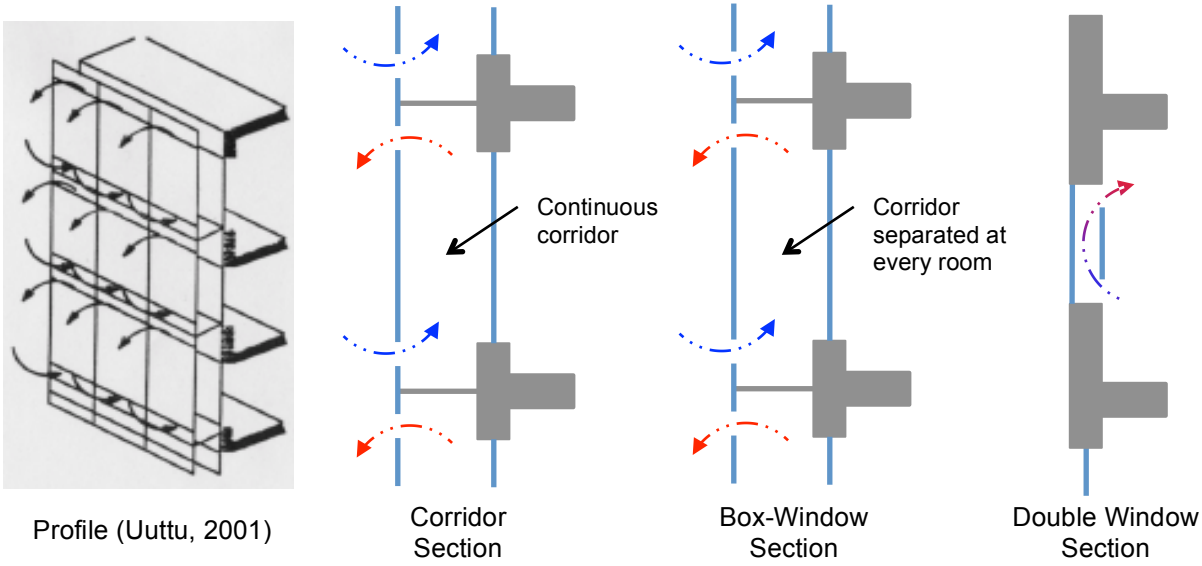

Figure 2.4 Corridor, Box Window and Double Window Double Façades

The shaft-box DF is a hybrid façade incorporating alternating box windows and multi-storey shafts (Figure 2.5). Air intake is at the bottom of each box window, while exhaust is through a ceiling-level bypass opening into the multi-storey shaft, where natural buoyancy draws the air up to a top outlet. In this way, naturally-driven airflow is possible while preventing overheating in the box windows and allowing natural ventilation to the office space behind. Also, openings in the outer façade can be smaller, which provides improved acoustic separation with the outdoors. The shaft height must be limited to provide correct exhaust rates from the box windows; therefore, this solution is suitable for lower-rise buildings, though high-rise buildings

may be divided into several tiers (Oesterle et al., 2001). As with multi-storey façades, fire protection may be a concern as smoke can enter the vertical shafts through several floors.

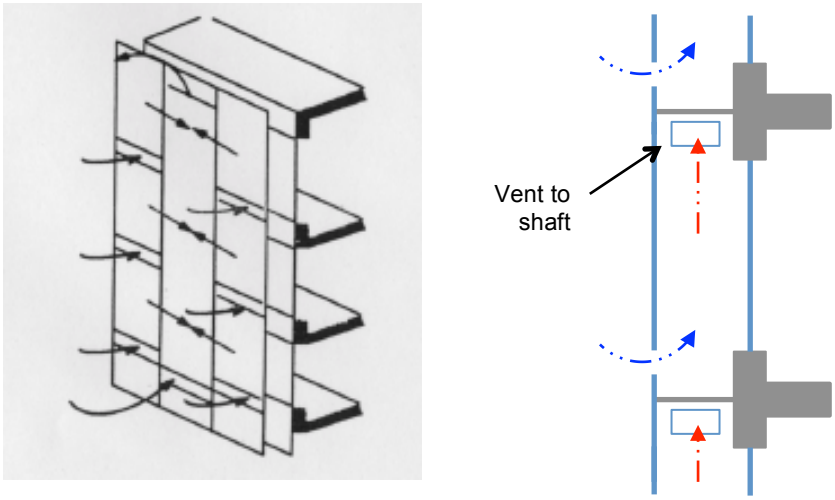

Figure 2.5 Box-Shaft Double Façade

A summary of the various types and their properties is provided in Table 2.1.

Table 2.1 Summary of Double Façade Compartmentalization

Façade Type	Separa-tions	Airflow Force	Natural Ventilation	Acoustic Insulation	Fire Protection
Multi-Storey	None	• Natural/ Hybrid	• Not recommended	• Good separation with outdoors • Sound transmission b/w rooms and storeys	High risk (all rooms are linked)
Corridor	Vertical	• Natural/ Hybrid/ Mechanical	• Stagger intake/extract openings to avoid exhaust entering the next storey as supply	• Poor separation with outdoors if open • Sound transmission b/w rooms	Medium risk (rooms of the same storey are linked)
Box Window	Vertical and Horizon tal	• Natural/ Hybrid/ Mechanical	• Same as corridor	• Poor separation with outdoors if open • No sound transmission b/w rooms	Low risk (rooms are separated)
Shaft-Box	Vertical and Horizon tal	• Natural/ Hybrid	• Size outlets carefully to provide correct exhaust rates from multiple stories to a shingle shaft	• Separation with outdoors (more openings than multi-storey but fewer than corridor or box window) • Little sound transmission between rooms	Low risk (rooms are separated)

2.2.3 Airflow Path

The airflow path depends on the origin and destination of the air moving within the cavity space. In general, there are five different paths as shown in Figure 2.6.

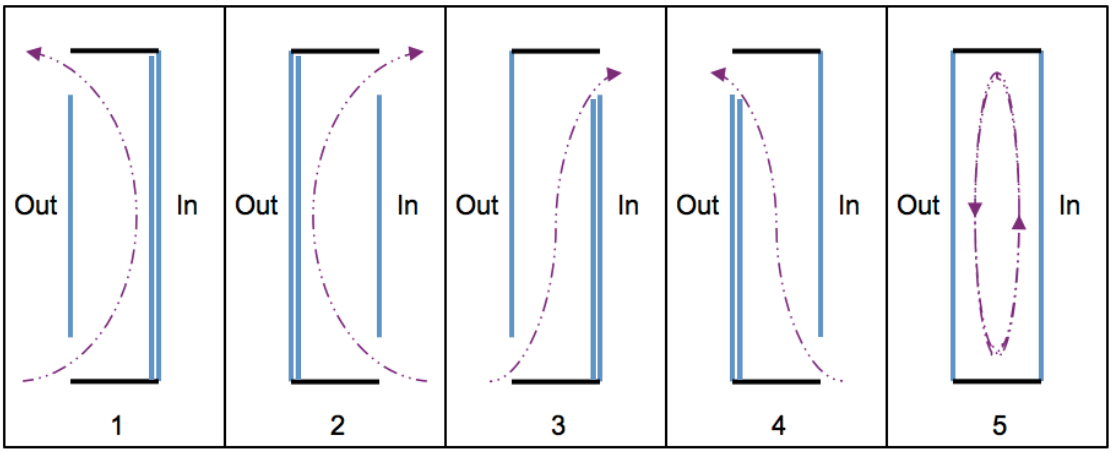

Figure 2.6 Airflow Paths in Double Façades

In general, the literature agrees on the following naming convention:

1) External air curtain - air is supplied from and returned to the outside. This is typically done with naturally-driven airflow, with the main insulating layer at the inner façade.

2) Internal air curtain – air is supplied from and returned to the inside (room or ventilation system). This is typically done with mechanically-driven airflow, with the main insulating layer at the outer façade.

3) Supply air – outdoor air is supplied to the building (room or ventilation system) via the cavity. This can be done through naturally or mechanically-driven airflow, with the main insulating layer at the inner façade.

4) Exhaust air – indoor air is exhausted from the building (room or ventilation system) via the cavity. This can be done through naturally or mechanically-driven airflow, with the main insulating layer at the outer façade.

5) Air buffer – the cavity is closed to trap solar-heated air.

When indoor air is flowing through the cavity space, the insulating layer is usually on the exterior to avoid condensation on the outer façade. When outdoor air is flowing through the cavity

space, the opposite is true. This is reflected in Figure 2.6. However, any given DF can have multiple operation modes, controllable by openings in the inner and outer façades. Therefore, there is no standard set of rules for DF design.

Note that the airflow direction may be the opposite of that shown in Figure 2.6, though the nomenclature remains the same (Figure 2.7)

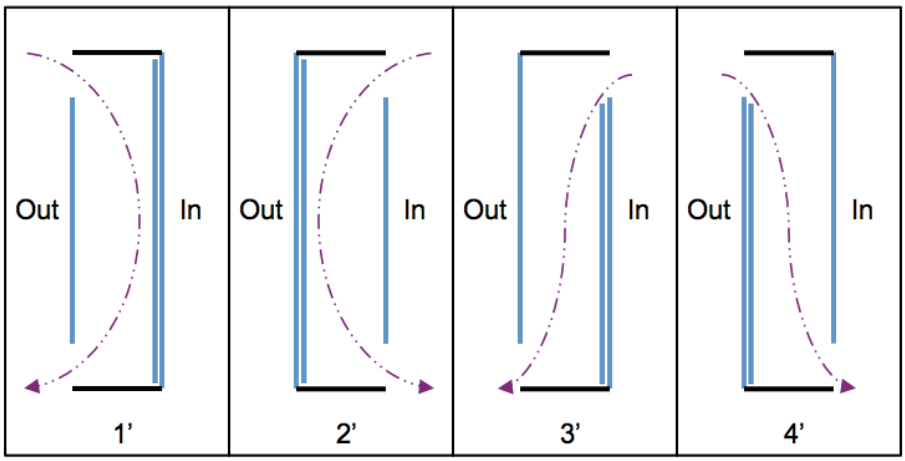

Figure 2.7 Reversed Airflow Paths in Double Façades

While the airflow path can oppose natural buoyancy, mechanical ventilation would be necessary if this were the design intention. Note that Case 1' may occur naturally if wind forces causing downward flow overpowered natural buoyancy forces.

The various airflow paths are appropriate for different configurations, climates and design intentions. Naturally ventilated façades are usually applied for Case 1 in fully conditioned offices or Case 3 for naturally conditioned offices. Mechanically ventilated façades are usually applied for Case 2, where solar heating is intended to reduce the heating load, or Case 4, where natural buoyancy is intended to aid in air extraction. Case 5 is usually employed in the heating season and can be used by any type of DF. In general, mode switching is necessary between summer and winter operation, either automatically by the HVAC system or manually by occupants or maintenance personnel. There is an important link between proper operation and good performance.

2.3 Perceived Benefits

In the literature, the stated benefits of a DF over a traditional curtain wall system are that it:

- allows natural ventilation;
- reduces solar heat gain, thereby reducing summer cooling loads;
- provides protection for shading devices;
- increases acoustic insulation; and
- reduces heating loads (i.e., increases thermal insulation and can provide preheated ventilation air).

However, researchers often report DF benefits compared to poor-performing single façades (e.g., double-glazed curtain wall with interior shading). Therefore, the perceived benefits are not necessarily true when compared to higher performance systems. Each perceived benefit is conditional based on the specific building, location and design.

The argument for natural ventilation is one of the main arguments in Europe. Natural ventilation is often thought impossible for high-rise buildings in urban centers due to high wind pressures and high outdoor noise levels. However, the outer façade of the DF provides protection for operable windows or openings in the inner façade. Also, natural buoyancy creates airflow in the cavity that helps deliver natural ventilation. Nighttime cooling is also possible with a DF because the second skin supplies security and wind/rain protection for interior openings when the building is unoccupied. Consequently, DFs have been popular in European countries with mild climates, where natural ventilation is possible for large portions of the year. Unfortunately, natural ventilation would provide limited benefits in countries with more extreme climates. Furthermore, Straube and van Straaten (2001) argue that protected, operable, screened and sound baffled openings are preferable to operable windows and can be used in high-rise buildings.

The benefit of providing acoustic insulation depends on the DF configuration. For buildings with high outside noise levels, such as those in urban centers, the second skin provides an extra sound barrier. However, when openings exist in the outer façade, as would be necessary for natural ventilation, the acoustic benefits are somewhat compromised. Also, sound disruption may be increased when the cavity space extends over multiple openings in the inner façade, thereby creating an acoustic connection between neighbouring zones. Furthermore, in certain cases sound disruption due to air leakage and high airflow rates in the cavity space has been a problem (Solaripedia, 2008). Again, if natural ventilation is desired, dedicated ventilation

openings and fixed triple-glazed windows would provide better sound insulation than a DF (Straube & van Straaten, 2001).

Another main argument for the DF is that it reduces solar heat gain by providing a protected space to mount shading devices. External shading is highly effective at blocking solar heat gain because much of the solar radiation never enters the interior space. When compared to indoor shading, the same shading device installed on the outside can be 9.5 times more effective at blocking solar heat gain (CS™, 2012). However, outdoor shading is generally not installed on high-rise buildings in North America because of high wind pressures that could damage or dislodge the shading device. Therefore, a double façade is attractive because shading devices installed in the cavity are protected from wind and weather, eliminating safety concerns and saving on maintenance and cleaning costs. Although shading within a cavity will absorb solar radiation and heat the cavity, the idea is that the cavity airflow will carry this heat away. Nevertheless, intermediate shading is not as effective as outdoor shading and should not be the main reason for choosing a DF. Outdoor shading can, in fact, be used on commercial buildings and is a more cost effective option. Although it is uncommon in North America, outdoor shading is common practice in Europe and suitable products are emerging in the North American market (e.g., Solarmotion®, as shown in Figure 2.8).

Figure 2.8 Commercial Building Outdoor Shading Examples (CS™, 2012)

Finally, the benefit of reducing heating loads is generally true when comparing to a poorly insulated single façade. In winter, the cavity air temperature is higher and the airflow rate is lower than at the outdoor surface, which lowers the heat transfer rate at the interior façade

(Poirazis, 2006). Consequently, heat loss through the enclosure is reduced and the indoor surface temperature is increased, providing better thermal comfort. However, a DF is rarely compared to high performing options such as triple/quadruple glazing or an insulated opaque wall. In these cases, a DF may perform worse. The other stated benefit in heating conditions is that solar-heated air from the cavity may be used as preheated air to the ventilation system. However, it is important to realize that allowing ventilation through the cavity would decrease the thermal insulation of the façade. Furthermore, no one has compared the energy savings of preheated ventilation air over that provided by a standard energy recovery ventilator (ERV). This should be investigated for each individual building and climate before choosing a DF. Combining preheated ventilation air with an ERV is also an option.

2.4 Drawbacks

Despite the many optimistic viewpoints regarding DFs, there are various associated problems and obstacles, some of which were discussed in the previous section. Hens et al. (2008) suggest that DFs "are not the high-tech blessing expected by many, but may act as expensive troublemakers". Some acknowledged disadvantages for DFs in new construction are:

- risk of overheating in summer;
- fire-protection difficulties;
- condensation within the cavity space;
- additional cost for construction;
- cost of operation and maintenance;
- reduced daylighting and visual contact with the outdoor environment;
- decreased rentable floor space; and
- Noise in the cavity from airflow, air leakage or a connection with neighbouring zones

On sunny days, surfaces within the cavity absorb solar radiation and heat the cavity space above the outdoor temperature. Natural airflow in the cavity evacuates some of this heat, though not all of it. Consequently, heat gain and cooling loads are increased in summer when compared to a single façade. Furthermore, the indoor surface temperature is increased, leading

to occupant discomfort. Excessively high temperatures in the cavity could also cause material deformation. Supplying adequate airflow through the cavity (either naturally or mechanically) and/or limiting the cavity height can reduce cavity temperatures.

In cases where a DF extends over multiple rooms, it is possible for smoke and fire to spread between rooms via the cavity space. This is a safety concern and may not meet local fire safety regulations. In some cases, a design must be altered to incorporate more separations. Otherwise, specialized sprinkler systems, fire extinguishing gasses, operable fire separations, etc. may be necessary.

Condensation in the cavity space could be a risk depending on the cavity design and airflow path. Where indoor air flows through the cavity, condensation may form on the exterior façade if its temperature is below the indoor air dew-point temperature. However, this is also a risk for traditional glazing units in a single façade. Controlling the indoor relative humidity and ensuring adequate thermal insulation of the exterior façade may avoid this.

Increased capital cost is a large drawback of DFs. There are many different design possibilities and configurations (Section 2.2); therefore, significant engineering expertise is required to create a good design. Furthermore, if the system is intended to be adaptable to outdoor conditions, an advanced building automation system (BAS) is required along with indoor/outdoor sensors and adjustable devices for shading, vent openings, etc. These features accommodate strategies for shading, ventilation, fire emergencies, closure against heavy rains, etc. Lee et al. (2002) suggest that commissioning and tuning are essential to the proper operation of such a complex system. Each of these elements presents an initial cost. Moreover, a DF incorporates an additional skin, which is obviously more costly than a single skin façade. Oesterle et al. (2001) estimate a capital cost increase of 25% over traditional curtain wall construction. Others put the estimate at up to 80% higher (Intelligent Energy Europe, 2008), though this is compared to a low-cost curtain wall without outdoor shading. Although cladding manufacturers now offer prefabricated solutions to reduce production and development costs (e.g., Gartner, Permasteelisa Group, etc.), the initial cost remains higher than the cost of single skin façades.

Maintenance and operation costs must also be considered. Complex systems require qualified personnel for upkeep and sophisticated devices must be monitored and calibrated regularly

(Saelens, 2002). While cleaning costs of a DF are higher, as there are four surfaces instead of two, the frequency of cleaning depends on the source of airflow. More cleaning is necessary if the airflow is from the outdoors, depending on the outdoor pollution level. Also, any material durability problems caused by high cavity temperatures must be addressed (e.g. sealants). However, cleaning and maintenance costs of the shading device are reduced compared to outdoor shading. Furthermore, Oesterle et al. (2001) suggest that increased energy efficiency and the use of natural ventilation decrease necessary HVAC-plant capacity and ventilation fans, reducing the cost of inspection, servicing and maintenance. Consequently, they state that maintenance costs between a DF and single skin façade level out. However, this claim depends on the proper design and operation of the DF. In some existing cases, constructed DFs have proven to be less energy efficient than conventional curtain wall buildings due to improper design and operation (Rowe et al., 2010).

The final drawbacks not yet discussed are decreased daylighting and rentable floor space. Adding an additional glazing layer reduces the transmittance of a DF compared to a single façade with the same glazing area. This is typically compensated for by increasing the window-to-wall ratio, thereby increasing solar heat gains and potentially causing excessive daylighting and glare close to the façade. Another option is to incorporate daylighting systems in the cavity space (e.g., incorporated in the shading device), to reduce daylighting near the façade while increasing penetration depth. Finally, the depth required for a DF decreases the rentable floor space compared to the same sized building with a single façade. This is only a problem for new construction and will not be discussed in detail here.

There are differing opinions regarding the DF for new construction, though many of the optimistic viewpoints either are not founded on quantitative results or compare DFs to poor-performing alternatives. Braham (2005) argues that DFs are employed because they are interesting and exciting, though high-performance glass assemblies can deliver similar performance at lower cost. Hens et al. (2008) state that except for acoustic insulation, none of the perceived benefits stand up when compared to a high-performance single façade with outdoor shading. Straube and van Straaten (2006) share this opinion, giving alternative design options that provide superior performance to a DF. They suggest that the best option (from a cost and energy perspective) would be to reduce the glazing area and increase the quality of

the glazing product, thereby eliminating the energy and comfort problems created by using excessive areas of poor-performance glazing.

Although reducing window-to-wall ratios can, and should, be used for new construction, it is generally not possible in retrofit projects. Furthermore, for a building with a reasonable window-to-wall ratio and poorly insulated walls, applying a second glazed façade over the entire building may prove to be more beneficial than simply replacing the windows with better glazing. This has not been studied in detail and could prove to be a better application for DFs. Moreover, the DF provides a retrofit solution where other options are not possible (Section 1.1.4).

2.5 Double Façades for Retrofit Applications

To date, the DF has been implemented mostly in new construction projects; however, it may provide a more competitive solution for retrofit applications. While a DF for retrofit is not a wide-spread solution, design teams are starting to find this option attractive for various reasons. The energy benefits listed in Section 2.3 hold true when the base building is an uninsulated or poorly-insulated older façade with indoor shading. In addition to these and the other benefits listed in Section 2.3, DFs provide specific benefits relevant for retrofits. Recurring benefits in the literature and case studies are that a DF:

- protects the existing structure from weather and further degradation (i.e., it provides water and airtightness);
- does not completely cover up any historic or sentimental value of the existing building, since the existing structure is still visible behind the façade;
- presents little interference with the indoor space, so the building may stay occupied throughout construction;
- does not decrease useable floor space as would occur if interior insulation were added;
- presents a modern look for older buildings, which is often very important to the owner.

Although there are many perceived benefits of a double façade retrofit, it has not always been as successful as planned. Except for the drawback of decreased rentable floor space, all drawbacks listed in Section 2.4 also apply to retrofit projects. Also, there is the possibility that a

DF would provide poor energy performance compared to other retrofit strategies. This will be investigated in the following chapters.

Table 2.2 Design-Phase Criteria Checklist (Lancour et al., 2004)

	Criteria	High priority	Medium priority	Low priority	Not relevant
Architecture	Highly glazed façade	☐	☐	☐	☐
	High-tech image	☐	☐	☐	☐
	Increase of the space use	☐	☐	☐	☐
Thermal Comfort	During heating season	☐	☐	☐	☐
	During cooling season	☐	☐	☐	☐
Acoustics	High acoustic performance relatively to the outdoor noise	☐	☐	☐	☐
	Attention paid to the potential flanking problems	☐	☐	☐	☐
Visual comfort	Glare control	☐	☐	☐	☐
	Privacy reasons	☐	☐	☐	☐
Energy consumption	Limiting heating consumption	☐	☐	☐	☐
	Limiting cooling consumption	☐	☐	☐	☐
Ventilation	Realizing natural ventilation of the offices	☐	☐	☐	☐
	Realizing night cooling of the offices	☐	☐	☐	☐
Systems	Avoiding a full air-conditioning system	☐	☐	☐	☐
	Avoiding heating element in offices	☐	☐	☐	☐
	Possibility to use the solar shading in nearly all meteorological conditions	☐	☐	☐	☐
Maintenance	Limiting maintenance of the solar shading	☐	☐	☐	☐
	Limiting maintenance of the cooling system	☐	☐	☐	☐
Users	Need to give the user control on the system (solar shading, etc…)	☐	☐	☐	☐
	Possibility to open the windows – contact with the exterior	☐	☐	☐	☐
Other	Green image – low consumption building	☐	☐	☐	☐

The next question is, “Which configuration is best for a retrofit project?” Hilmarsson (2008) suggests that the box window double façade is a relatively easy type to apply to older buildings to improve their performance. Conversely, Brunoro (2008) suggests that the multi-storey DF is best for retrofits because it facilitates natural airflow and presents the least interference with the

existing façade. The compartmentalization and airflow strategies depend on the design intentions and the outdoor climate. The Belgian Building Research Institute (BBRI) suggests a qualitative criteria checklist (Table 2.2) when deciding if a DF is an appropriate solution and which type would be most appropriate.

2.6 Case Studies

While DF retrofits are far from common, a few projects have chosen this option for various reasons. Four selected case studies are discussed in detail, as well as a variety of projects that chose alternate retrofit strategies similar to a DF. The motives, design strategies and concerns of each project are examined.

2.6.1 Telus William Farrell Building - Vancouver, Canada

Built in 1947, the Telus Building is an 8-storey, 11,800-m^2 office building located in downtown Vancouver (CRGBC, 2001). When built, it consisted of a concrete structure with brick veneer and punched, double-hung, wood-frame windows. In 1998, the building had to be upgraded to meet seismic requirements. Instead of demolition, Telus required that the existing building be recycled and re-used, and that green strategies be incorporated (oikos, 2001).

The design solution was to overclad the street-facing façades (south and west) with a fully glazed exterior skin to create a sleek, modern image for the company. The original brick veneer was removed and a low-E, double-glazed curtain wall was hung 900 mm from the exposed concrete structure (Boake, 2006). For the exterior skin, clear vision glass was used in a band aligning with the interior windows while fritted glass was used in the intermediate sections to block high angle summer sun. This differentiated glazing was intended to promote daylighting while reducing unnecessary heat transfer and glare. The existing single-glazed windows were restored to operating condition so that natural ventilation could be used in shoulder seasons.

The new curtain wall extends from the second level to the full height of the building, without compartmentalization. The first level was left unglazed to avoid encroaching on sidewalk space, since the existing building already extended to the property line. Motorized dampers at the top and bottom allow the cavity to be opened or closed according to weather conditions. Additional openings throughout the height of the exterior façade may also be opened to encourage ventilation. Figure 2.9 illustrates the different operation modes of the façade.

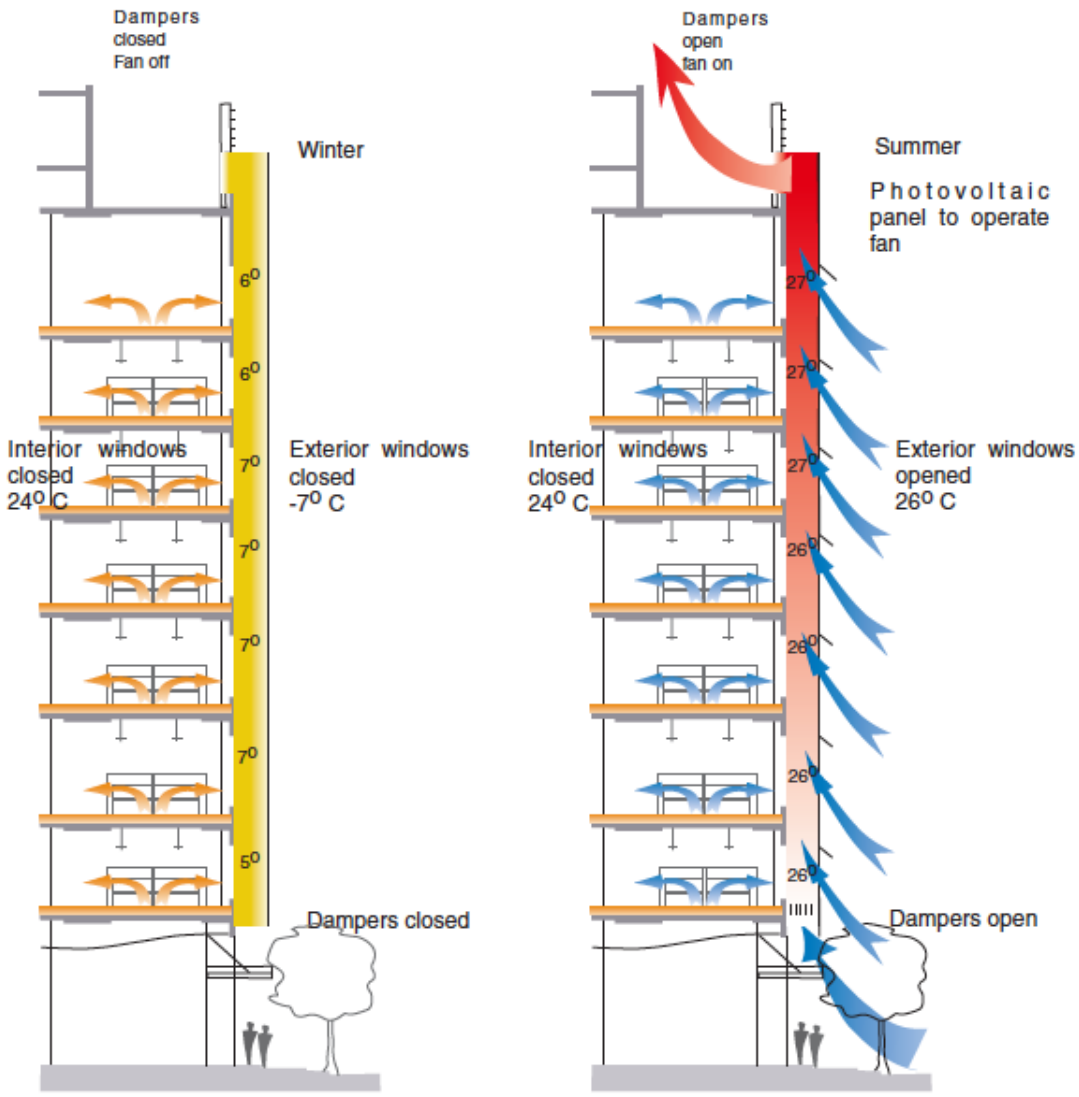

Figure 2.9 Winter/Summer Operation of the Telus Building DF (Boake, 2006)

In winter, the cavity is closed and the air space acts as an insulation layer, trapping incident solar radiation that warms the concrete mass of the building. The cavity is also closed during peak traffic hours to avoid noise and air pollution. During the summer, the cavity is fully opened so that ventilation may flush out excess heat. Photovoltaic-powered ventilation fans were provided at the roof level to aid in summertime ventilation and avoid overheating. A PV array was an attractive source of energy for the fans because power is generated during sunny periods when ventilation is required. The solar modules are incorporated directly into the glazed façade and provide 2.2 kilowatts to 12 high-efficiency DC exhaust fans, each rated for an air

volume of 2,800 cfm (1.32 m^3/s) (Prasad & Snow, 2005). Electronic temperature sensors within the cavity control the fans, windows and dampers to provide optimal conditions within the cavity and ensure that the temperature does not exceed 27°C at the top.

Additional features of the retrofit include an underfloor air distribution system with individual user-controlled diffusers at each station. Also, 85% of the building's heating load is sourced from excess heat generated by a chiller unit in an ancillary part of the building complex (Taylor, 2010). Light-shelves coupled with whitewashed concrete ceilings increase daylight penetration into the building core and much of the interior materials and fittings were re-used or recycled during construction. Also, by performing the retrofit on a floor-by-floor basis, the Telus building was able to remain occupied and operational throughout construction.

Figure 2.10 William Farrell Telus Building Before and After Retrofit (oikos, 2001)

The addition of the second skin effectively gave the vintage façade a contemporary facelift. Completed in 2001, the refurbishment cost $13 million and the retrofitted building attained energy performance 39% better than ASHRAE standards at the time, receiving various awards for excellence in design and energy efficiency (CRGBC, 2001). However, exact energy numbers were not published. The end energy use breakdown is not known; however, with 85% of heating needs supplied by waste heat, cooling is likely the primary energy user. In this

situation, a DF retrofit (with a main risk of overheating) seems like a peculiar choice, though for a moderate climate such as Vancouver, overheating is not a large concern. In 2007, the building went through further retrofits whereby the atrium was replaced to meet seismic requirements and high performance lighting was installed. In 2008, the direct digital control system was optimized in a recommissioning project to further improve energy performance. The recommissioning report revealed that the building had an annual energy consumption of 644 kWh/m^2 prior to recommissioning (NRCan, 2008).

For comparison, the average Canadian annual energy consumption of commercial and institutional buildings in year 2000 was 439 kWh/m^2 (NRCan, 2003), while the most energy efficient office building in Canada uses only 69 kWh/m^2 (NRCan, 2012). Consequently, the retrofitted Telus building cannot be considered energy efficient by modern standards. However, energy-intensive telecommunications equipment could be contributing to the high overall energy use. Regardless, the Telus building stands as an example of a DF retrofit from which lessons can be learned. In this case, a preliminary design-phase modeling tool could have aided in decision making and perhaps found that a DF was not the best option.

2.6.2 The Albatros – Den Helder, Netherlands

Built in 1972, the Albatros building is an 8-storey, 6,200-m^2 concrete structure in northern Holland (Solaripedia, 2008). Owned by the Royal Dutch Navy, the building was used as housing for navy officers until 2004, when the navy decided to convert the building into office space. A life cycle analysis showed that the most cost-effective way of gaining the required office space was to strip and refurbish the existing building instead of demolishing it and re-building (Kurstjens et al., 2004).

The existing building was built with single glazing, no insulation and artificial lighting. The building was heated using radiators (gas boiler) and ventilation was supplied and exhausted through a mechanical system. The ambition in this project (part of the European REVIVAL consortium) was to develop a high performance, sustainably renovated and healthy building in an uncomplicated and low-tech way (Kurstjens et al., 2004). The chosen solution was to maintain the existing façade and add a single-glazed second skin, which provided rain and wind protection, an exhaust/supply path for natural ventilation and a protected area to mount shading-devices.

Figure 2.11 Albatros Before and After Retrofit (Solaripedia, 2008)

The old façade was made airtight and windows were replaced with operable, low-E double-glazing (U-value = 1.8 W/m^{2}K). Opaque elements were insulated (U-value = 0.3 W/m^{2}K) and upgraded using exterior foam insulation and new tile cladding. Louvered blinds were mounted in the DF cavity on the inside of the outer glazing. The building energy management system (BEMS) automatically deploys the blinds when incoming solar radiation is higher than 200 W/m^2, though the BEMS may be manually overridden (Baker, 2009). The second skin was compartmentalized at each floor to avoid summer overheating. Also, thermal mass provided by the uncovered, concrete ceilings helps to level off peak loads. Unwanted sound transmission was minimized by noise absorbing material at the cavity ceiling at each level.

Ventilation air is supplied passively via the space between the two skins, allowing for preheating in winter and nighttime cooling in summer. Adjustable grilles/windows in both skins are controlled by the BEMS to allow adequate winter or summer ventilation. In winter, all vents are closed at nighttime to provide additional insulation. During the daytime however, vents in both skins are opened slightly to provide preheated natural ventilation. Air is mechanically extracted from the offices via grills in the ceiling to a heat recovery ventilator (HRV) and heat pump at the rooftop level. In summer, the exterior skin vents are opened to allow natural airflow through the cavity. At nighttime, vents in the inner skin are also opened to allow night ventilation to the offices. Air is extracted by fans located in the corridor outside the offices (Baker, 2009).

Other improvements to the building include high efficiency lighting, with daylight sensors and occupancy detectors. For efficient heating, the building was connected to an existing CHP plant on the Navy site, with a low temperature delivery system.

The retrofit was completed in 2006; however, Solaripedia (2008) described several operational problems that became apparent in the commissioning period. The BEMS was set up incorrectly and the ventilation grills in the exterior skin as well as the new operable windows in the interior skin were not airtight. This caused occupants to complain of uncomfortably low temperatures in winter and excessive noise in windy conditions. Also, small holes in metal components within the cavity acted like organ pipes, amplifying the noise problem. However, after resolving the initial problems, the general experience of the users was good and the Navy was very proud of the building. Initial energy aims were to achieve a 50% reduction in overall energy use (Kurstjens et al., 2004). It is unknown whether this aim was met, though the mild Dutch climate presents favourable conditions for a DF retrofit.

2.6.3 Sparkasse Vorderpfalz - Ludwigshafen, Germany

Ebbert (2011) describes the retrofit of the headquarters of Sparkasse Vorderpfalz, a German regional bank. Built in 1972, the building is 12 stories and totals 8000 m^2. The structure was built of concrete slabs supported by steel columns and beams, clad with a mix of curtain wall and aluminum panels. In 2006, retrofit plans were implemented because the building was outdated and performing poorly. Located on the most prominent square in the city centre of Ludwigshafen, the bank desired a more modern building to represent their corporate image. Furthermore, rainwater was entering the façade and users were uncomfortable due to poor thermal insulation and airtightness. According to Ebbert (2011), the client stated the following goals for the retrofit:

- Updated HVAC system meeting the German Energy Saving Directive for new construction;
- more user control over indoor climate and improved daylight quality;
- modernized exterior appearance with a more open and communicative design; and
- minimized disruption to building interior to allow ongoing operation during construction.

The original façade of the building had three different constructions: 1) the office façade, 2) the wings and 3) the base. The office façade was primarily a stick-system curtain wall comprised of IGUs and steel frames. The concrete parapets and spandrel areas were clad with un-insulated, ventilated aluminum panels. All air intake and exhaust occurred directly through vents in these panels to decentralized HVAC units located in the cavity behind. The HVAC system was controlled centrally and was not adjustable by the user. The wings were similarly clad, with un-insulated, ventilated aluminum panels fixed to a steel framework attached to concrete block. The base comprised of a conference area clad in floor-to-ceiling IGUs with thermally unbroken aluminum frames. Exterior concrete louvers in front of the base served for solar protection and decoration. Figure 2.12 illustrates the original building.

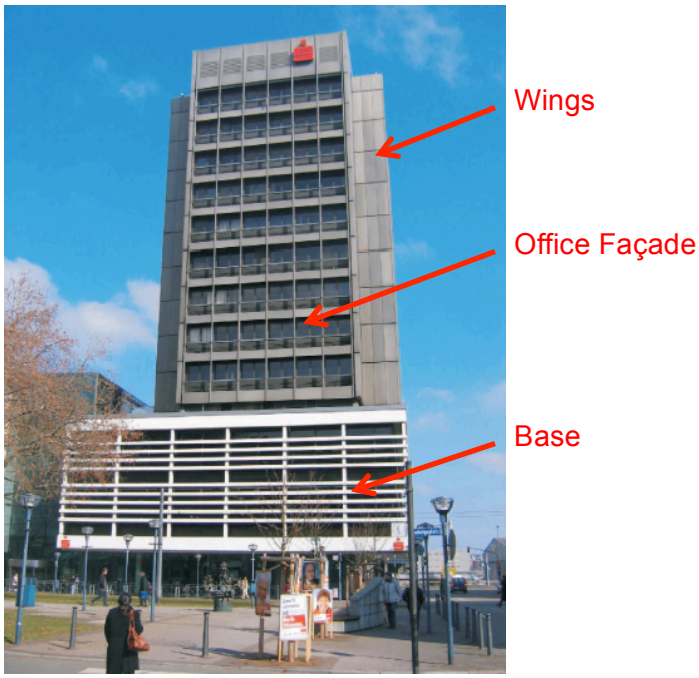

Figure 2.12 Sparkasse Vorderpfalz Pre-Retrofit (Ebbert, 2011)

The chosen retrofit strategy for the office façade was to hang a single glazed curtain wall 75 cm from the original building. The façade cavity was not compartmentalized, though a service platform was provided at each level. Fire protection was provided by installing sprinklers on either side of the interior façade (i.e., cavity side and office side). A cleaning platform was added at the roof level, which was used to mount the outer glass panes during construction.

The interior façade was then retrofitted with new windows and insulated panels. By completing the exterior façade first, the interior façade could be renovated independently of the weather.

The decentralized HVAC units behind the original aluminum cladding were replaced with newer units that incorporated heat recovery. In winter, fresh air is let in at the bottom of the façade cavity and preconditioned by solar irradiation before entering the HVAC units. Exhaust air is let out through a duct directly connected to the outside. Also, air within the DF cavity can be transported from the east to the west cavity in the morning and vice versa in the afternoon to optimize the air temperatures in both cavities. In summer the system is reversed; the cavity is opened on the top and closed on the bottom. Supply air is provided via the duct directly connected to the outside, while exhaust air is let out through the DF cavity. The stack effect created in the DF cavity helps extract the air from the rooms; thus, less electric energy is needed to run the mechanical fans in the HVAC units. Figure 2.13 shows the operation modes.

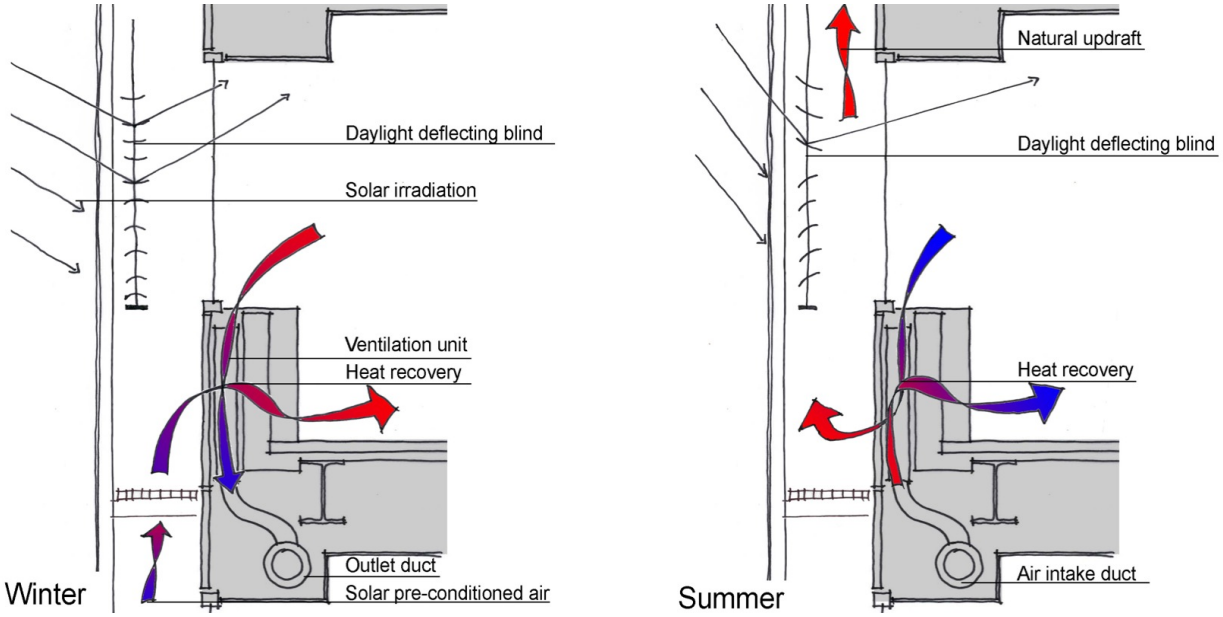

Figure 2.13 Winter/Summer Operation of the Sparkasse Vorderpfalz DF (Ebbert, 2011)

Shading devices in the cavity reduce solar heat gain while deflecting light into the offices. White ceilings facilitate further reflections to provide day lighting deep into the building.

For the base section, a second single-glazed façade was also installed. The glazing in the original façade was replaced and insulated frames were mounted on top of the existing frames. The second skin provided a water and airtight cover while the increased thermal insulation

effectively prevented condensation. For the wings, 100 mm of mineral wool was added and the original aluminum panels were cleaned, recoated and remounted onto the existing structure. The completed retrofit is shown in Figure 2.14.

Figure 2.14 Sparkasse Vorderpfalz Post-Retrofit (Ebbert, 2011)

Each office room was equipped with a user interface to control the desired temperature and light level. The decentralized HVAC system is intended to react rapidly to settings. Motion and CO_2 sensors control lighting and ventilation respectively so that both are turned off when a room is unoccupied. Also, the building's heat is supplied by district heating generated in a waste incineration plant in close proximity.

The retrofit was completed in 2009 for a cost of €7.2 million, which was considered an economical retrofit. Based on cost savings from energy use and HVAC maintenance, a payback period of 13 years was expected. Further cost savings such as higher rental rates were not included. Also, the retrofit avoided any costs associated with relocation, since the building was occupied during the entire retrofit. Computer simulation results estimated that primary energy use was reduced by 64%. The final energy demand was 289 kWh/m^2 annually, while the primary energy demand was lower due to the district heating. While this is not exceptionally efficient, it is better than the Canadian average.

2.6.4 ERGO Tower – Milan, Italy

The ERGO tower, located in Milan, was built in the 1990s. Complete details regarding the retrofit are unknown because many of the applicable articles are written in Italian; however, it provides an interesting case study. As a finalist of the 2011 Re-skinning awards, Zerofootprint (2011) describes some of the strategies and achievements of the retrofit.

The building is comprised of a 5-storey square block to the north, attached to a 3-storey rectangular block to the south Figure 2.16. The exact area of the building is unknown, though approximate dimensions taken from Google maps give 8250 m^2. According to Zerofootprint (2011), the original building was poorly designed; it was heavily air conditioned, poorly insulated, and overly reliant on artificial lighting. Furthermore, the exterior tiles were already deteriorating by 2007, less than 20 years after construction. Therefore, ERGO, a major Italian insurance company, set out to transform the building from a mediocre, outdated structure, to a highly energy-efficient and modern head office.

Based on energy performance, comfort and economic goals, the design team chose to overclad the building. The walls were overclad with mineral fiber insulation and new cladding to appear more modern (U-value = 0.25 to 0.3 W/m^2K). Rigid foam insulation was added to the roof (U-value = 0.28 W/m^2K), while existing, tinted windows were replaced (U-value = 1.8 W/m^2K). Based on the reported U-value, it is assumed that low-E, double-pane IGUs were used. Windows were covered with outdoor shading devices that are controlled according to the angle of the sun. Figure 2.15 shows the façade before and after the retrofit while Figure 2.16 shows the building layout.

Figure 2.15 ERGO Building Before and After Retrofit (Zerofootprint, 2011)

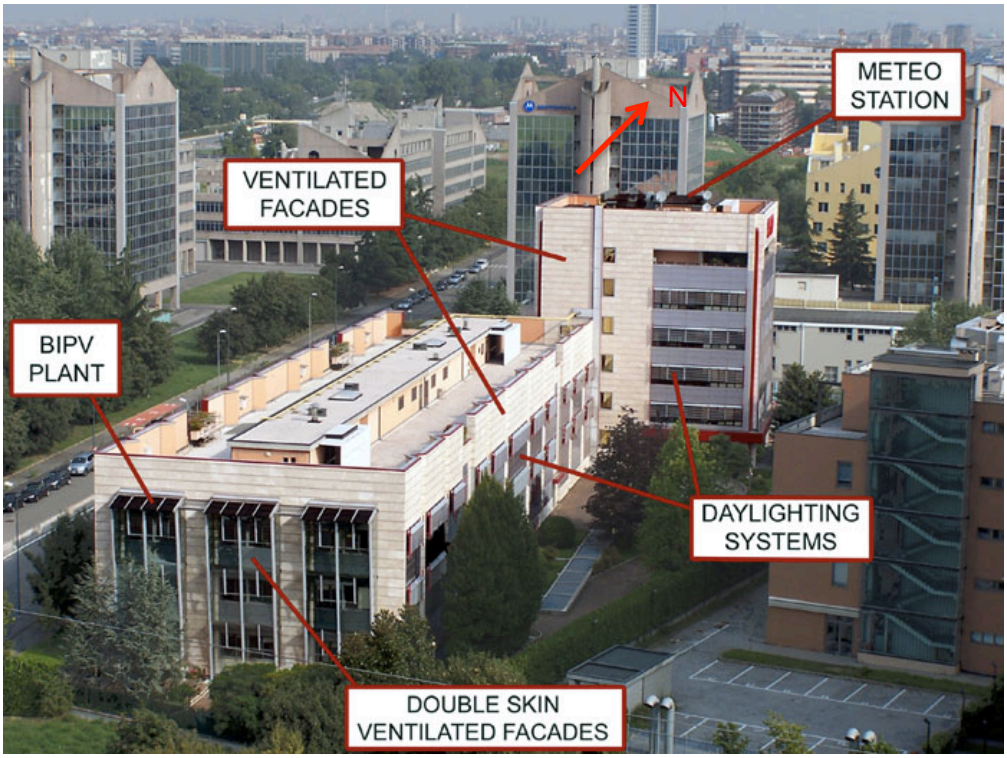

Figure 2.16 ERGO Building Layout (Zerofootprint, 2011)

On the south face of the 3-storey block, three separate DFs were added, topped with solar panels that provide approximately 3 KWp (ERGO Italia, 2009) (Figure 2.17).

Figure 2.17 South-Facing Double Façades (Zerofootprint, 2011)

The façades appear to be compartmentalized at each floor, though the separations do not appear to be airtight. Due to their size, the DFs appear to be either for demonstration or for testing. Unfortunately, the design intentions are unknown. From the architect's rendering and photos, it appears that the north face of the 5-storey block has a second glazed façade as well (Figure 2.18). However, it is unclear whether or not this façade is ventilated.

Figure 2.18 5-Storey Block (Zerofootprint, 2011)

The west face of the 5-storey block seems to be an opaque ventilated façade, with louvered shading at window locations acting as ventilation grills. Figure 2.16 confirms that at least two of the opaque façades are ventilated. It is possible that all façades of this construction are ventilated, though it is difficult to tell. Regardless, it is apparent that ventilated façades with both glazed and opaque exterior skins were employed in the ERGO tower retrofit.

The ERGO tower retrofit, costing €2.38 million, was completed in 2010. After the retrofit, annual primary energy consumption was reduced by 40% (1,871,000 KWh to 1,134,000 KWh) saving approximately €65,000 per year. Using the estimated floor area of the building, the annual primary energy consumption is approximately 140 kWh/m^2. Although the climate in Milan differs from the Canadian climate, this would be considered an energy efficient building by Canadian standards. In Italy, the retrofit was hailed as a reproducible strategy serving as a model in an urban renewal project for an industrial area of Milan.

2.6.5 Other Retrofit Examples

Retrofit strategies other than DFs have also been used to either preserve or completely modernize an existing building. Some examples are examined here.

To preserve historic buildings, a concept similar to the DF has been used in multiple cases: encasing the existing building completely or partially with a new glass enclosure. For example, the Hespeler Library in Cambridge, Ontario was encased in a larger glass structure to provide additional space while preserving the original building. In this case, the new glass façade formed an entirely new enclosure, creating useable space around the existing building.

Figure 2.19 Hespeler Library in Cambridge, Ontario

The Bank of Canada building in Ottawa, Ontario was renovated in a similar manner, though only half of the building was encased in the new glass structure. The new structure spans between the glazed office buildings located on either side of the historic building, creating a large atrium space around it.

Figure 2.20 Bank of Canada, Ottawa

Another example is the Library of Parliament located at 125 Sparks Street in Ottawa, Ontario (Figure 2.21). In this case, only the back face of the building was encased in a new glass enclosure. The motive for the retrofit is unknown, though potential causes could be to improve energy performance or air and water tightness. From the appearance and location of the glass enclosure (back face), it is unlikely the retrofit was completed for aesthetic reasons.

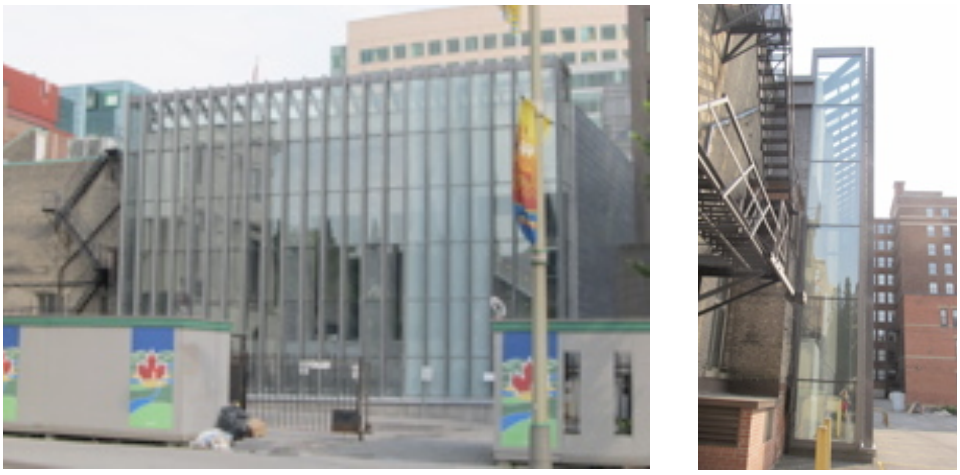

Figure 2.21 Ottawa Library of Parliament Glass Façade

In other examples, such as a building located in Prague, Czech Republic, the completely opposite approach was taken. Instead of encasing the building in a new glass enclosure, a glass façade was added completely outboard of the main enclosure. In this example, a single-glazed façade was used, which appears to be completely open to the atmosphere. The

purpose of the additional façade could be to protect the main enclosure from rain and wind, though it would do little else to improve the building performance.

Figure 2.22 Glazed-Façade Retrofit in Prague, Czech Republic

Other retrofits have been implemented to completely transform and modernize an outdated building, such as the skyscraper located at 100 Park Avenue, New York City. Instead of a DF, the designers chose to overclad the existing 36-storey building with a flush, unitized curtain wall. It appears that the existing windows were removed in the retrofit.

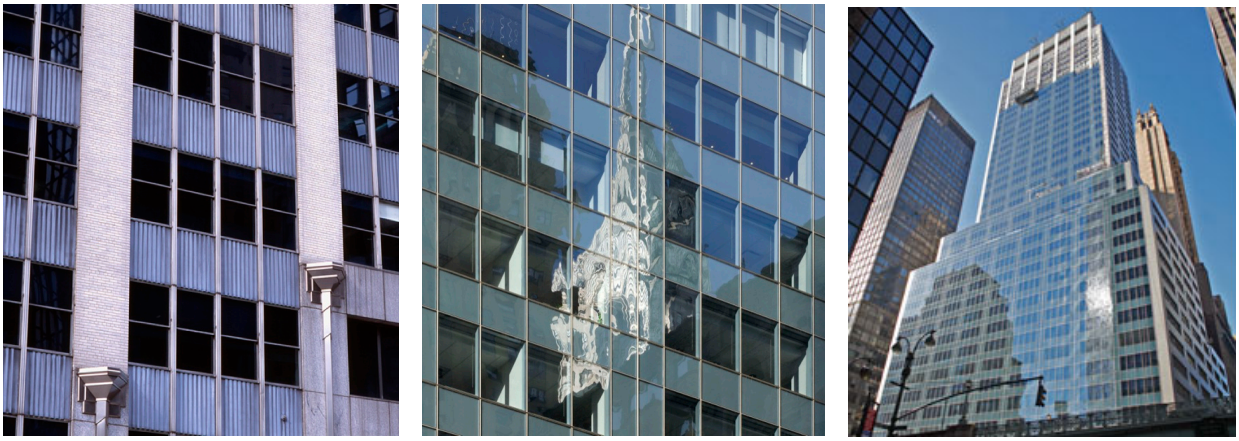

Figure 2.23 100 Park Avenue Façade Retrofit (Zerofootprint, 2010)
Left: Pre-retrofit, Middle: Post-retrofit, Right: Mid-retrofit

Discussions with a consulting firm in Toronto, Ontario revealed that clients were interested in similar retrofits because an all-glazed appearance was desired. In multiple cases, both a DF and flush curtain wall retrofit were being considered. In the flush curtain wall option, a curtain wall would be installed over the existing façade, with vision glass at existing windows and

insulated spandrel panels at opaque components. The existing windows would be removed and the new curtain wall would be connected to the existing window openings. This is likely the approach used at 100 Park Ave.

In one example, designers chose to completely remove the existing brick façade and replace it with an entirely glazed DF. The Industriens Hus, located in the main square of Copenhagen, Denmark, was built in 1979 and displayed a dark, brick façade covered in large, neon signs. Accused of being outdated and forbidding, the original façade was stripped and completely replaced. The retrofit was undertaken to provide a more modern and impressive presence in the city centre, one of the first places seen by tourists and visitors to the city (Danish Architecture Centre, 2012).

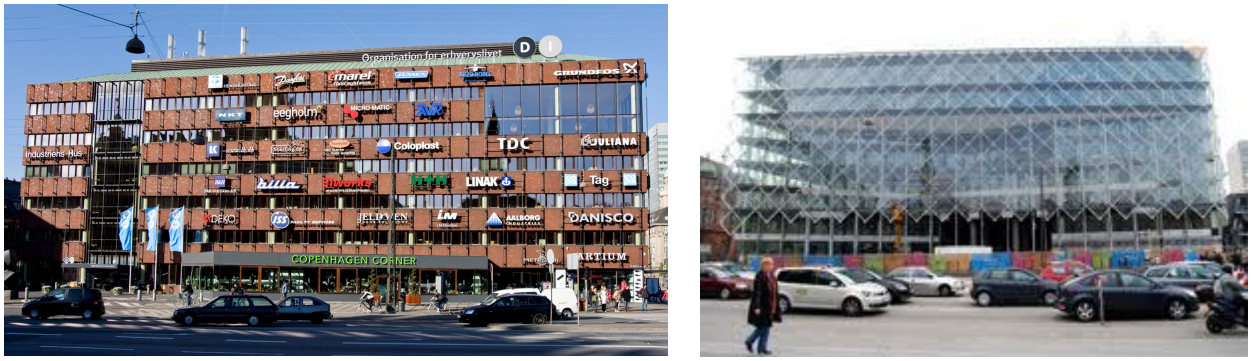

Figure 2.24 Industriens Hus, Copenhagen, Denmark (Danish Architecture Centre, 2012)

The retrofits described in this section present a small selection of the potential examples. There are many similar retrofit projects, showing that all-glazed retrofits, whether DFs or otherwise, are being considered and employed worldwide.

2.6.6 Conclusions

Double façade retrofits have been used in the past and are gaining interest for the future. The case studies examined show that DF retrofits can provide energy savings, though proper design and operation are important. In some situations, a DF may not be the best retrofit solution. A summary of the DF case studies is presented in Table 2.3. The ERGO tower was excluded due to lack of information.

Table 2.3 Case Study Summary

	Telus	Albatros	Sparkasse Vorderpfalz
Location	Vancouver, Canada	Den Helder, Netherlands	Ludwigshafen, Germany
Year Built	1947	1972	1972
Storeys	8	8	12
Cavity Depth	900	Unknown	750
Shading	Fritted glass	Louvered blinds	Venetian blinds
Exterior Skin	Low-e, double glazing	Single glazing	Single glazing
Interior Skin	Original: exposed concrete and existing, single-glazed windows (operable)	Refurbished: insulated opaque envelope and new low-E, double-glazed windows (operable)	Refurbished: insulated panels and new, fixed windows (assumed low-E, double-glazed)
Partitioning	Multi-storey	Corridor	Multi-storey
Summer Operation	Exterior air curtain	Day: exterior air curtain Night: supply	Exhaust
Winter Operation	Buffer zone	Day: supply Night: buffer zone	Supply
Airflow Force	Hybrid (PV powered fans ensure that temperature does not exceed 27°C)	Natural	Mechanical (decentralized HVAC units with heat recovery)
Control	Electronic temperature sensors control fans and dampers so cavity temperature < 27°C.	BEMS controls vents in inner and outer skin. Operation mode dependent on outdoor conditions.	BEMS controls vents in inner and outer skin. Set to prevent excessive heat gains centrally and also value user wishes.
Acoustic Precautions	None	Noise absorbing material installed at the ceiling of each cavity	Dedicated openings to HVAC units
Goals	• Meet seismic requirements; • Recycle and re-use existing building; • Incorporate green retrofit strategies • Minimize disruption to inside (i.e., keep in operation during construction); and • Update and modernize façade to reflect the corporate image.	• Provide sustainable, uncomplicated and low-tech retrofit; • Increase energy performance (50% reduction in overall energy use); • Provide healthy Indoor environment satisfying all new-build criteria; • Minimize over-cost of eco-refurbishment; and • Create an architectural highlight.	• Update HVAC system to meet the German Energy Saving Directive for new construction; • Increase user control over indoor climate and improve daylight quality; • Minimize disruption to inside (i.e., keep in operation during construction); and • Modernize appearance and provide a more open and communicative design.

Different approaches were used in each example. According to Ebbert and Knaack (2007), a multi-storey façade is a relatively cheap solution providing good extra insulation; though, corridor façades and box-type façades provide different levels of horizontal and vertical

separation, which keeps the façade controllable. Summer overheating, fire protection and sound transfer must always be considered. Also, any connections to or penetrations of the existing structure must be detailed correctly to minimize air leakage and heat transfer. However, the cases examined showed that interference with the interior façade can be minimal. Both the Telus and Sparkasse Vorderpfalz buildings remained occupied during construction, reducing costs of relocation and work interruption.

Operation modes and ventilation strategies differed between buildings. In the Sparkasse Vorderpfalz building, the building services were integrated into the façade in the form of decentralized units. This solution provided good flexibility and user control. In both the Sparkasse Vorderpfalz and Albatros buildings, preheating ventilation air through the DF was used in conjunction with HRVs, thereby maximizing efficiency.

In all DF cases, the retrofits were conducted to improve energy performance and provide an updated appearance. Other retrofit examples using all-glazed façades were completed for similar reasons. Alternate solutions were to encase the existing building in a glazed enclosure, add a glazed façade flush to the existing façade or completely replace the existing façade with a glazed façade. These examples show that there is an interest in retrofits giving a modern, all-glazed appearance. However, energy performance is also very important. Therefore, a tool is needed to predict energy performance of DF retrofits at the preliminary design stage. Such a tool would allow comparisons between DFs and alternate retrofit solutions based on quantitative results, allowing design teams to make informed decisions.

Chapter 3
Modeling Double Façades

3.1 Overview

In recent years, double façades have garnered much attention in the academic world and many papers have dealt with various aspects of their design and operation. Entire publications have been devoted to literature reviews on the subject (e.g., Poirazis, 2006; Zhou & Chen, 2010; Shameri et al., 2011). This section will attempt to cover the main approaches to modeling DFs developed to date. Regardless of the model type, the governing heat and mass transfer phenomena can be grouped into three elements (Poirazis, 2006):

1) Optical element - incident solar radiation (direct, diffuse and reflected) and layer optical properties (transmission, reflectance and absorptance);
2) Thermal element - radiative, convective and conductive heat transfer; and
3) Airflow element - air movement through the DF cavity.

In the following sections, the calculations employed for each element are discussed in detail; therefore, background knowledge may be required for full comprehension. For reference, Chapter 4 discusses the physics of heat and mass transfer in more detail.

Both commercially available software and models developed by researchers are examined. Commercially available software can be divided into two categories: 1) whole building energy models and 2) complex fenestration models. These models were not developed specifically for DFs, but are discussed here to establish what is currently available. Various researchers have developed models specific to DFs, which can be divided into four main types: 1) lumped, 2) control volume, 3) zonal and 4) computational fluid dynamics (CFD). Selected studies using each model type are discussed in detail and a summary is provided in Appendix B.

3.2 Whole Building Energy Models

Whole building energy models present an economical method to assess the energy impact of design choices, making them important design tools. However, the majority of current energy modeling is not conducted for design purposes. Presently, the vast majority of energy modeling

is done to demonstrate compliance with building codes or green building certification programs, such as LEED or BOMA. Consequently, while a large variety of building energy models exist, there are various challenges in using them for preliminary design and especially, for preliminary design of complex façades.

In a review of existing energy models, Hanam (2010) found that easy-to-use programs lack accuracy and the ability to model new, innovative systems, while programs that allow the simulation of new systems are very complex and have a steep learning curve. Consequently, the programs necessary to model DFs would be too technical for most architects. Furthermore, such programs require detailed knowledge of the building design and system parameters, which are often unknown at the design stage. Finally, it is not straightforward to model a DF using whole building energy models, even if detailed design information is available.

The BBRI (2004) identified three whole building modeling programs capable of modeling a DF: 1) TRNSYS, 2) ESP-r and 3) TAS. These are all transient energy simulation programs that allow the coupling between thermal and airflow models. Various authors have linked TRNSYS with commercially available airflow models such as LOOPDA (Ballestini et al., 2005) and COMIS (Haase et al., 2009). Authors including Hensen et al. (2002) and Høseggen et al. (2008) used ESP-r for their simulations; however, Dickson (2004) found that results are dependent on proper treatment of solar irradiation, cavity convection regimes, surface view-factors, airflow resistances and fictitious cavity divisions. Finally, Gratia and DeHerde have published multiple studies using the TAS software, which employs a 2D CFD package. The BBRI (2004) warns that the above programs are complex, requiring time and experience to use them properly. Furthermore, detailed knowledge of DF physics and behaviour is required, which is expected for DF researchers but unlikely for most consultants.

Various authors have chosen to create their own models specifically meant for DFs. These have been developed as stand-alone models or coupled with whole building energy models such as TRNSYS (Saelens, 2002; Eicker et al., 2008) and EnergyPlus (Griffith, 2006; Pappas & Shai, 2008). While EnergyPlus was not listed as capable of modeling a DF on its own, it allows a relatively easy coupling with external, user defined routines (Zanghirella et al., 2010). An alternative model that could easily be coupled with an external DF model might be the BELA program (Building Energy and Loads Analysis). This program, developed by Hanam (2010),

has a “transparent, open architecture to allow additions and changes, and it facilitates the simulation of simple early design”.

3.3 Complex Fenestration Models

Complex fenestration models are used to assess the performance of glazing units. Available programs do not incorporate an airflow element; however, optical and thermal calculations are transferable to DFs. The two most widely used programs in North America are VISION and WINDOW. Both programs include a one-dimensional model for center-of-glass heat transfer and are capable of modeling a wide variety of glazings, fill-gases, pane spacings and environmental conditions (Wright, 1996).

3.3.1 VISION

VISION, created at the University of Waterloo, is now in its 5th version. In her Master’s Thesis, Rogalsky (2011) builds upon various works from Wright, Kotey and Collins (e.g., Barnaby et al., 2009; Wright et al., 2009) to update the calculations used in the previous version and to develop a user interface. The model may be used as a stand-alone tool for education and research purposes, or it may be integrated into building simulation programs.

In the optical element, the incoming solar radiation, diffuse fraction and incidence angle are user inputs. The overall transmittance of the system and the absorbed solar radiation in each layer are calculated based on Edwards’ (1977) embedding method, which accounts for multiple reflections within the system. The method has been extended to account for diffuse radiation and beam-to-diffuse conversion in reflection and transmission (Wright & Kotey, 2006). Various shading layers can be incorporated, including venetian blinds, roller blinds, insect screens and pleated drapes. The shading layer models were developed by Kotey (2009) and are based on a combination of theory and empirical results. All shading layer models determine angle dependent reflectance and transmittance properties for beam and diffuse radiation based on the angle of incidence and the material normal incidence properties.

In the thermal element, a resistor network is used for both radiative and convective heat transfer. This network allows heat transfer between any two layers via jump resistors.

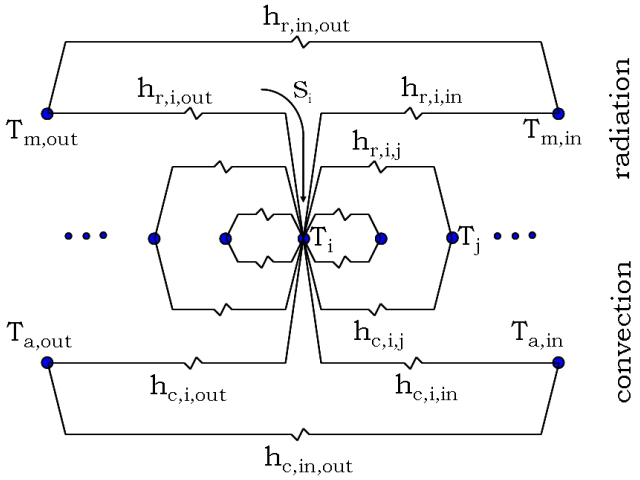

Figure 3.1 VISION Resistor Network (Rogalsky, 2011)

At outdoor and indoor surfaces, convective heat transfer coefficients are user input while the radiative heat transfer coefficients are connected to the outdoor/indoor mean radiant temperatures (MRT), which are also user input. Cavity radiative coefficients are calculated from the radiosity of each surface as per (Wright, 2008). In the method, the network energy balance is solved through matrix inversion. Cavity convective coefficients are calculated from the Nusselt number, which is determined using empirical correlations developed by Wright (1996) and Wright et al. (2009). The correlations are based on experiments of ElSherbiny et al. (1982) and Shewen (1986) for sealed cavities with aspect ratios over 40. Conductive resistance of the layer materials is neglected. Energy balances performed at each layer are solved for layer temperatures. Because layer temperatures and convective/radiative heat transfer coefficients are interdependent, a short iterative process is used to reach convergence.

The model does allow airflow in the outermost and innermost cavities to represent outdoor or indoor unsealed shading cavities. In these cases, the convective coefficients are determined as per Appendix C of ASHRAE RP-1311 (Barnaby et al., 2009; Wright et al., 2009). For indoor shading, the glass layer convects to both the shading layer and the ambient air. Convective coefficients of the glass and shading layer are dependent on the defined indoor convective coefficient and the gap width. Where a venetian blind is used, the convective coefficient is augmented by as much as 20% to account for airflow through the slats. For outdoor shading, the glass convective coefficient equals the defined outdoor convective coefficient while the

shading convective coefficient is twice the defined outdoor convective coefficient to account for exposure of both sides to the ambient.

Along with the temperature profile, the model outputs four indices of merit for the environmental conditions specified: U-value, solar heat gain coefficient (SHGC), $f_{r,in}$ and $f_{r,out}$. $f_{r,in}$ and $f_{r,out}$ are weighting factors used to determine the effective ambient temperatures. These indices of merit may be used in whole building simulations (e.g., Wright et al., 2011). Although VISION is a useful and powerful tool, problems with applying it to DF systems are:

- maximum cavity depth is 100 mm;
- there is no airflow element (airflow is only simulated in shading cavities via convection coefficients); and
- opaque/mixed façades cannot be modeled.

3.3.2 WINDOW

The complex-fenestration modeling program WINDOW, which is currently at version 6.3, is distributed by the Lawrence Berkley National Laboratory (LBNL, 2011). The program conforms to NFRC procedures and calculates specular optical properties in accordance with ISO 15099. For NFRC certification, fixed environmental conditions are used. In general, the calculations are very similar to those used in earlier versions of VISION.

In the optical element, NFRC conditions use 783 W/m^2 of direct solar radiation at normal incidence. To correctly model layers with spectrally selective coatings (e.g., low-e), WINDOW uses a multi-band model requiring a spectral data file updated and maintained by LBNL. The multi-band model calculates the layer properties for each wavelength and weights the properties by weighting functions to obtain total solar, visible and infrared properties. If spectral data is not available, WINDOW assumes a flat spectral behavior based on the stated visible and solar properties. The absorptance of each layer is determined using recursive, spectrally-dependent equations that account for multiple internal reflections within the glazing system. Various shading layers can be incorporated, including venetian blinds, roller blinds, laminates and frits. Shading-layer calculations account for direct and diffuse reflection and transmission.

In the thermal element, a one-dimensional, steady-state resistance network is used (Figure 3.2). The concept is similar to that used in VISION, though “jump resistors” are not included so heat flux is only permitted between adjacent layers.

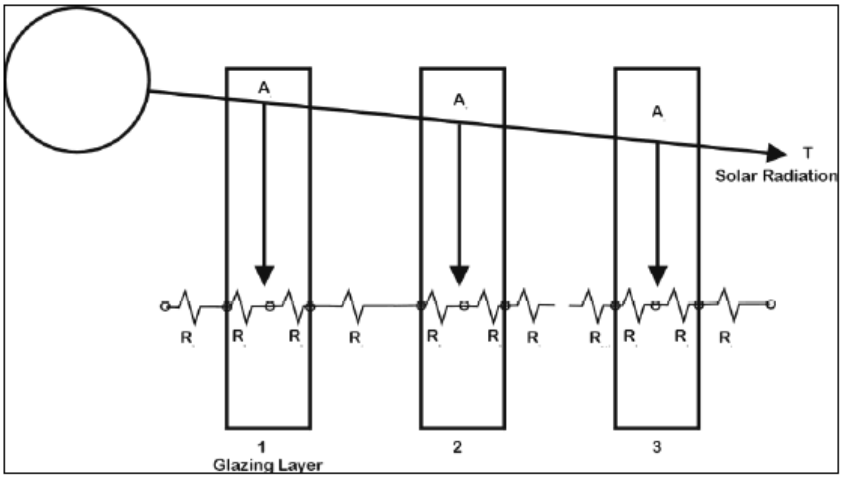

Figure 3.2 WINDOW Resistance Network (LBNL, 2011)

The outdoor surface convection heat transfer coefficient is calculated from the set NFRC wind speed. The indoor surface convective coefficient is calculated from the Nusselt number, which is determined from empirical correlations based on window height and tilt. The outdoor and indoor surface radiative heat transfer coefficients are calculated from the MRT, which is assumed equal to the ambient temperature for NFRC conditions. Within the cavity, convective coefficients are calculated from the empirical Nusselt number based on window tilt. Wright’s (1996) correlations are used for tilt angles of 90°, while correlations by Hollands et al. (1976) and ElSherbiny et al. (1982) are used for other tilt angles. Radiative heat transfer within the cavity is calculated using surface radiosity, which is the net radiation leaving a surface including emitted, reflected and transmitted portions. Conductive heat transfer coefficients through solid layers are calculated from the thickness and conductivity of the material. To solve the surface temperatures, a set of non-linear equations derived from the layer energy balances are solved in a matrix solution. Once again, because layer temperatures and convective heat transfer coefficients/radiosities are interdependent, an iterative solution method is used to converge upon the correct temperature distribution.

Along with the temperature distribution, model outputs include center-of-glazing U-value, SHGC and visual transmittance (VT). A companion program, THERM, can then be used to calculate

frame and edge-of-glazing properties, which are imported into WINDOW to calculate total product properties. Note that the U-value and SHGC calculations are not for specific conditions as they are in VISION. In WINDOW, U-value calculations assume nighttime conditions ($G_{t\theta}$=0) and SHGC calculations assume no indoor/outdoor temperature difference ($T_{a,int}$=$T_{a,ext}$). Again, although WINDOW is a useful and powerful tool, it cannot model airflow and is therefore not capable of modeling DFs.

3.4 Double Façade Models

The existing DF models treat each element (i.e., optical, thermal and airflow) with varying degrees of complexity. However, Poirazis (2006) warns that the structure of the model becomes unbalanced and weak if one element is neglected or "guestimated" while other elements are more thoroughly investigated. The current models can be divided into four categories: 1) lumped, 2) control volume, 3) zonal and 4) CFD. The distinction between models is primarily based on how the façade is divided. At one extreme, the lumped model only considers horizontal divisions created by the façade layers (e.g., glass, air cavity, shading device). At the other extreme, the CFD model uses multiple horizontal and vertical divisions to create a grid of small cells. Both forced (mechanical) and natural (buoyancy and wind) airflows are modeled. For forced airflow, the velocity is a known input while for natural airflow, velocity is calculated based on the pressure difference between the cavity air and the inlet air. Distinction is made between the airflow network approach and the CFD approach.

Each model has benefits and drawbacks. The simpler models are quicker and easier to use; however, they only provide average temperature estimates and bulk airflow rates. More complicated models provide detailed knowledge of the temperature and airflow distributions; however, they require substantial computation time and user knowledge. Zanghirella et al. (2010) suggest that simpler models may be more appropriate to develop sensitivity analyses or for use as preliminary decision/design tools, whereas more complicated models (CFD) are more suitable for final, detailed design and optimization.

3.4.1 Lumped model

The lumped model is a simple, one-dimensional model constructed from first principles conservation laws, similar to the complex fenestration models. The temperature of each surface

and cavity in the DF system is lumped in the vertical direction and treated as a single node. In this way, vertical temperature stratification and complicated airflow paths are neglected. Also, heat transfer coefficients are assumed uniform for the entire height. Energy balances are performed on each surface and cavity. The layer temperatures and heat transfer coefficients are interdependent and therefore, must be solved in an iterative process. Note that airflow due to buoyancy is dependent on the thermal system and must be solved in the iterative process. In the airflow network, only two nodes exist: 1) inlet and 2) cavity (average). Figure 3.3 shows the lumped model concept.

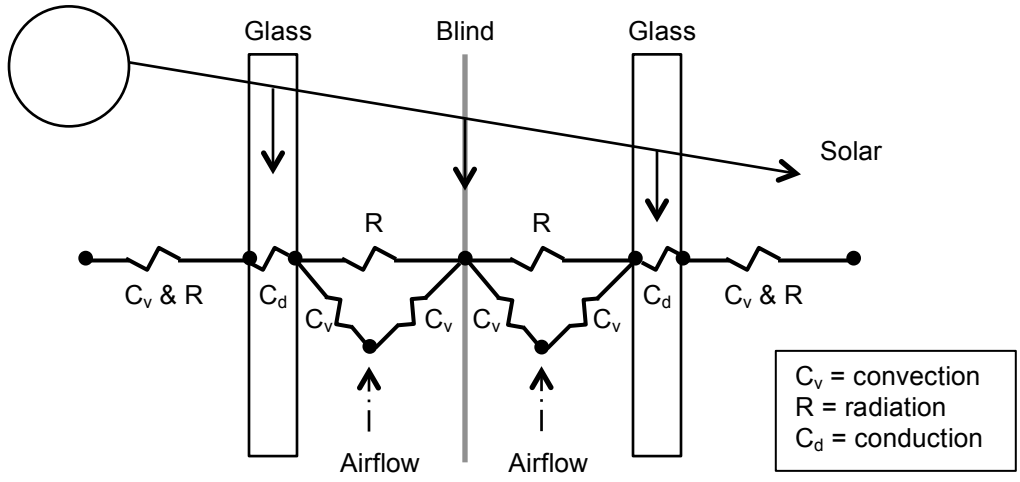

Figure 3.3 Lumped Model

The calculation setup is essentially the same as WINDOW, though cavity nodes are included to account for airflow. Therefore, convection is calculated to the cavity air instead of between the solid surfaces. Note that the lumped models are not listed in chronological order, but in order of complexity.

3.4.1.1 Todorovic and Maric (1998)

Todovoric and Maric (1998) produced one of the earlier models focused on predicting DF performance. In their study, a lumped model is proposed to estimate the cavity air temperature in a DF in Belgrade. They address a single-storey façade with an exterior layer of single glazing and an interior layer of mixed single glazing and opaque wall. Different cavity depths are modeled with no shading device. Associated heating/cooling loads are calculated for one-hour time steps.

In the optical element, solar radiation is defined simply as the "intensity of solar radiation through standard glass", without separating into direct and diffuse components. The absorbed portion in each layer is calculated from the absorption of the layer and the transmittance of the previous layer. There is no treatment of multiple reflections.

In the thermal element, energy balances are set up for each layer, including the air cavity. Convection coefficients are used at each surface, though calculations are not discussed. Instead of radiative coefficients, an undefined "temperature coefficient" is used to linearize radiation equations that calculate heat transfer from each surface to the adjacent air. Note that it is more realistic to calculate radiation between solid surfaces only. Radiant heat transfer to and from the opaque wall is neglected as the authors consider it "negligible for the required accuracy". Similarly, it appears that convective heat transfer from the opaque wall to the indoor environment is also neglected. The conductive heat transfer coefficient through the opaque wall is calculated from the thickness and conductivity of the material. Conduction resistance through the glazed elements is neglected. For the cavity space energy balance, nomenclature and discussion is vague, making the exact calculations difficult to comprehend. However, it appears that airflow, convection and heat transmission through each solid component is included. It is unclear what "heat transmission" represents, since it is not simply conduction, though convection is accounted for separately.

For the airflow element, both closed and open cavities are considered. For the closed cavity, the air volume is heated from its temperature in the previous hour. For the open cavity, the heat exchange depends on the airflow velocity, which must be known, imposed or assumed. The developed model was used to compare the thermal performance of DFs to a conventional single façade. It was found that with proper operation, a DF could reduce cooling and heating loads when compared to an uninsulated single façade.

3.4.1.2 Yilmaz and Çetintas (2005)

Yilmaz and Çetintas (2005) build upon Todorovic's model, using the same DF setup. Calculations are conducted for winter conditions, when vent openings to the cavity space are closed. The method consists of two steps: 1) calculating the cavity temperature under steady-state conditions using the method developed by Todorovic and 2) calculating unsteady-state

heat transfer from opaque components of the inner façade to account for heat storage capacity. Noted differences in Step 1 to Todorovic's method are:

- solar radiation is separated into direct and diffuse components;
- convective heat transfer coefficients within the cavity are calculated based on air velocity (McAdams, 1954);
- longwave radiation from the opaque wall is included in the cavity energy balance; otherwise, longwave radiation is neglected completely; and
- a term accounting for the previous hour's glass temperature is included in the glazed surface energy balances. The term is intended to represent the heat in the glass mass.

For Step 2, cavity temperatures calculated in Step 1 are accepted as outdoor air temperatures (i.e., boundary conditions) to calculate heat flux through the components of the inner skin. A differential equation calculating unsteady-state heat transfer through the opaque component is solved by the finite difference method. The indoor surface temperatures of the opaque and glazed components are then used to determine the room temperature, assuming there is no mechanical heat source. This is very similar to coupling the DF model to a whole building energy model. Note that thermal mass was not considered in step one, although it would affect the cavity temperature. The developed calculations were used to model a building in Turkey, finding that a south-facing DF could reduce heat loss up to 40%. However, the façade used for comparison was uninsulated (wall U-value= 2 W/m^2K, window U-value= 2.1 W/m^2K).

3.4.1.3 Griffith (2006)

Griffith's (2006) model was developed for naturally ventilated cavities that are formed by lightweight baffles on the exterior of opaque building thermal envelopes. Griffith found that existing building simulation programs did not provide explicit models for vented exterior cavities; therefore, he created a model to provide outdoor boundary conditions for convection and radiation heat transfer as inputs into EnergyPlus. Although this model is not intended for glazed exterior surfaces, similar principles are used.

In the optical element, direct and diffuse incident solar radiation are calculated as per EnergyPlus, including models for sky conditions, solar radiation, shading and ground reflection. Absorbed solar radiation is only applicable to the outdoor surface because it is opaque.

In the thermal element, energy balances are formulated for the opaque baffle surface and the air cavity. The outdoor surface convective coefficient is treated in the "usual" way for surfaces that are exposed to outdoor weather conditions. It is assumed that the "usual" way means that it is calculated from the wind speed. Linearized, outdoor-surface radiative coefficients are calculated to the sky, air and ground using the Stefan-Boltzmann law and view factors. The same method of calculating linearized radiative coefficients is used within the cavity. Convection coefficients within the cavity are calculated using empirical correlations for window gaps, as documented in ISO 15099. However, Griffith advises that the convection coefficients should be revisited. The energy balance on the cavity air includes convection from the bounding surfaces and natural ventilation.

In the airflow element, simplistic correlations are used for single-side natural ventilation based on user-provided discharge coefficients, as presented by ASHRAE (2001). Velocities calculated from natural buoyancy and wind forces are combined by addition. The natural buoyancy calculation is for turbulent flow through a sharp-edged orifice, derived from Bernoulli's basic flow equation. It is based on the area of the openings, a discharge coefficient, the height to the neutral pressure plane and the difference between the average cavity temperature and the inlet temperature. For these calculations, the area of the vent openings is modeled as the average area of the upper and lower openings. When implemented in EnergyPlus, the Heat Balance Model with conduction transfer functions was used to model the underlying heat transfer surface. The cavity model provided a method of updating the outdoor boundary conditions, using sequential substitution to handle the interdependence of the two energy balances within the model. Griffith expressed the need for experimental data to calibrate input values for the ventilation opening areas and discharge coefficients.

3.4.1.4 Park et al. (2004)

In this study, Park et al. (2004) use a lumped model calibrated with in-situ measurements to model a DF with operable shading (i.e., venetian blinds) and natural ventilation. The goal was to determine optimal settings in real time for various components (louver slat angles and ventilation openings) to respond to changing weather and desired internal conditions. As such, a quick and simple method was desired over intensive numerical computation. Furthermore,

the authors expressed concerns that even the most accurate flow simulations cannot model cavity airflow and convective heat exchange correctly if the input parameters are unknown.

In the optical element, solar radiation is separated into direct and diffuse components. To determine overall system transmittance and the absorptance of each layer, the net radiation model suggested by Rheault and Bilgen (1989) was used. This model uses a fictitious cavity to simplify the solution of multiple reflections between the two glass panes and the venetian blind slats (Figure 3.4). Beam-diffuse reflection and transmission is incorporated.

In the thermal element, convection is the focus of the study. Radiation calculations are not described, though the method by Rheault and Bilgen (1989) is referenced for radiation exchange within the cavity. The method calculates radiosities, i.e., the net radiation leaving each surface including emitted, reflected and transmitted portions. Convection coefficients for each surface are considered unknowns and are determined using a parameter estimation technique based on extensive data points obtained from experiments. In addition to the six convection coefficients displayed in Figure 3.4, parameter estimation technique is used to find the form loss factor (f), the flow coefficient (c) and the flow exponent (n) used in natural ventilation calculations.

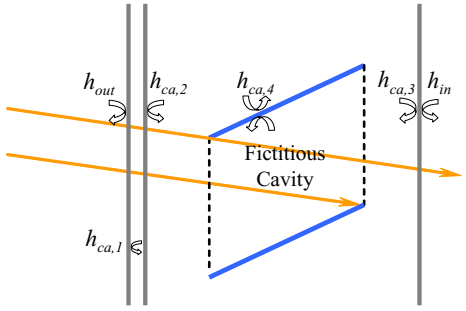

Figure 3.4 Fictitious Cavity and Convective Coefficients (Park et al., 2004)

In the airflow element, air velocity is calculated from buoyancy, wind and mechanical pressure differences for eight different flow regimes. Buoyancy flow is based on a conventional one-dimensional formulation similar to Griffith (2006). However, it includes the calibrated parameter *f* instead of a discharge coefficient. Also, instead of using an effective vent area, the open height of the ventilation inlet/outlet dampers is divided by the cavity depth. Also, the entire height of the façade is used instead of the height to the neutral pressure plane. In operation

modes where only buoyancy and wind are factors, air velocities from each factor are calculated and combined by taking the square root of the sum/difference of squares. In modes where mechanical pressure is also a factor, each factor is expressed as a pressure difference and combined using the power law equation to determine overall airflow. Calibrated parameters c and n are used in the equation. Only bulk flows are calculated with no consideration of the distribution on either side of the shading device.

When compared to measured results from the experimental test facility, the model proved accurate. However, the authors infer that an un-calibrated model would not predict the system's behavior accurately because "the literature values of convective coefficients are empirically driven for general cases and thus, can significantly vary according to the system configuration, location, surroundings, the nature of the surface, micro-climatic environment, etc.". For this same reason, the results presented by the authors are also limited to the test facility for which they were calibrated. However, the findings show that published empirical Nusselt number correlations underestimate convective coefficients within a DF cavity.

3.4.1.5 von Grabe (2002)

In this paper, a modeling tool is developed for energy consultants to make quick design decisions without using fairly complicated CFD tools. It is essentially a lumped model with shading devices; however, it differs from previously described models in that the cavity temperature is height dependent. This makes it a compromise between a one-dimensional and two-dimensional model.

In the optical element, the solar calculations and optical model are not described. While the material absorption coefficients are used to determine absorbed solar energy in each layer, it is unknown whether multiple reflections are taken into account.

In the thermal element, all heat transfer coefficients are averaged over the height of the system. Outdoor and indoor surface heat exchange is calculated using combined radiative and convective heat transfer coefficients as per CIBSE Guide A3 (1999). Within the cavity, linearized radiative heat transfer coefficients are used for infinite parallel plates. Convective heat transfer coefficients within the cavity are calculated using the approach of Michejew for free convection at vertical planes. The approach is not described; however, a reference for the calculation is given. The cavity is divided into two separate shafts on either side of the shading

device and convective heat transfer coefficients are calculated separately for each shaft. Equations for the two shaft air temperatures are based on convection and mass flow over the height of the system. This gives a two-dimensional system of first-order, linear differential equations that is solved in two steps: 1) the homogeneous solution is found by calculating the eigenvalues and eigenvectors and 2) the non-homogeneous solution is determined using the method of undetermined coefficients. The two shaft temperatures are found by integrating over the height of the system.

In the airflow element, only buoyancy forces are taken into account. The calculation is similar to Park et al. (2002), though densities are used instead of temperatures. The loss factor is determined in a similar way to the turbulence losses of pipes and incorporates local area reductions (e.g., inlet and outlet). Consequently, the opening areas do not appear in the velocity equation. The height used is the full cavity height and the velocity in each shaft is calculated separately. All flow is assumed to be in the y-direction, with no consideration of diagonal flow. Therefore, the model is mostly applicable to roller blinds.

A purpose-built DF was monitored to test the algorithm. Depending on the location of the shading device, the flow resistance was predicted best by different types of turbulence losses (e.g., flange, diffuser, abrupt enlargement/contraction, etc.). This is because natural ventilation velocity profiles are not symmetric like mechanical ventilation velocity profiles in ducts and pipes. The authors warn that using turbulence losses from mechanical engineering tables does not always model natural airflow resistance accurately.

3.4.2 Control Volume Approach

Control volume models provide a two-dimensional analysis, allowing for vertical temperature stratification. In this approach, the façade is divided into a number of control volumes in the vertical direction. For each volume, the heat balance for each surface is written similarly to the lumped method. The mass flow rate for each control-volume is set equal to the inlet mass flow rate, and the set of equations is solved using a finite volume method. When the airflow rate is not known (i.e., natural ventilation), the thermal system and airflow rate must be solved iteratively. With the presence of a shading device, the pressure distribution in the cavity must be known. Furthermore, airflow calculations are generally one dimensional in the y-axis. Therefore, this method has mostly been applied for cavities with roller blinds, since the

extension to other shading devices such as venetian blinds is not straightforward (Jiru & Haghighat, 2008).

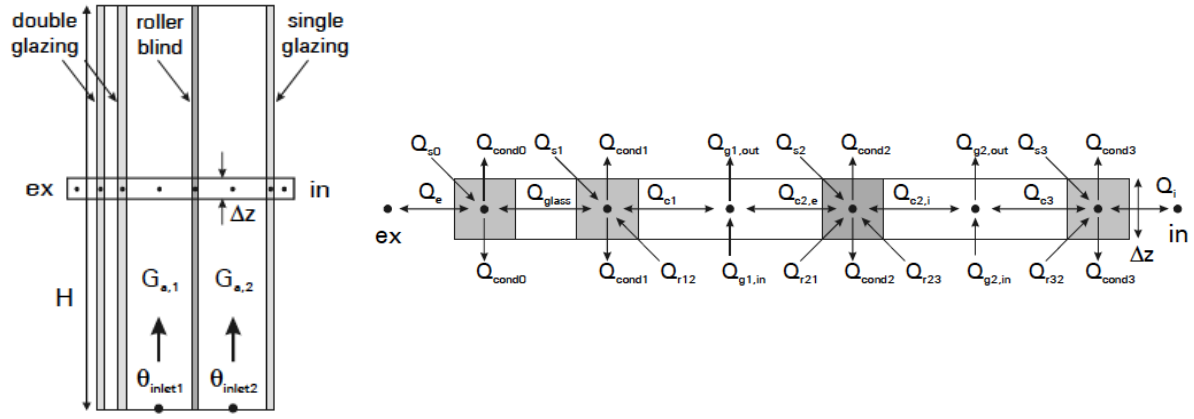

Figure 3.5 Control Volume Model (Saelens, 2002)

3.4.2.1 Balocco, 2001

Balocco (2001) uses the control volume method to simulate a ventilated cavity with an opaque exterior. Cavity widths between 7 and 35 cm are investigated, with a cavity height of 6 and 14 m. Buoyancy-induced, natural airflow is modeled for an exterior air curtain flow path. It is proposed that the model is also adaptable to a mechanically-ventilated, interior air curtain.

In the optical element, solar irradiation is a set value and is not divided into direct and diffuse components. Absorbed solar radiation is only applicable to the outdoor surface as it is opaque.

In the thermal element, the system is solved using four steady-state energy balances representing each surface and the air in the cavity. For the opaque wall, heat transfer to the indoor environment is calculated via conduction using an overall U-value. While not explicitly stated, it is likely that radiation and convection were included in the U-value using equivalent conductances. For the outdoor surface, conduction, radiation and convection are separated. Radiative heat transfer is calculated to the sky and ambient using linearized radiative heat transfer coefficients, though they are not defined or discussed. Convective heat transfer coefficients are calculated differently depending on wind speed. For wind speeds above 4 m/s, the convective coefficient is calculated from the wind speed using the McAdams (1954) formula. Note that this formula is generally used for wind velocities between 1 and 5 m/s (Straube &

Burnett, 2005). For wind speeds under 4 m/s, a Nusselt number correlation for vertical walls is used. Within the cavity, a Nusselt number correlation for turbulent flow is used. References for the correlations are given. Note that for all surfaces, convective heat exchange is calculated using difference in specific enthalpy rather than temperature. Radiative heat exchange within the cavity is calculated using linearized radiative coefficients. The overall energy balances are solved through an iterative procedure using a finite element code Ventilcam.

In the airflow element, only buoyancy forces are considered. The calculation is a one-dimensional formulation based on mass and energy conservation, similar to the calculations employed in the lumped models. Pressure losses are evaluated by a friction factor, which is "calculated with the Moody formula as a function of the Reynolds number".

The model is validated using experimental data from Moshfegh and Sandberg (1996), who investigated fluid flow and heat transfer in a vertical channel heated from one side by PV elements. The mean error between experimental and calculated airflow was 21%. Findings showed that increasing width and airflow rate reduced frictional resistance of the cavity.

3.4.2.2 Saelens (2002)

In his PhD thesis, Saelens (2002) created a numerical model for single-storey, all-glazed DFs with roller blinds. He presents an in-depth discussion of all thermal processes and input parameters. The model was validated using a test facility in Belgium.

In the optical element, incident solar radiation is calculated. Direct, sky diffuse and ground reflected components are determined using a clearness index and ground reflectance. For diffuse radiation on a tilted surface, the Reindl model (1990) is used, which takes into account circumsolar radiation and horizon brightening. Edwards' (1977) embedded method is used to determine overall system transmittance and individual layer absorptances accounting for multiple reflections. Spectrally averaged values are used and polarization is not considered. However, angle dependent optical properties are used. Diffuse radiation is estimated using optical properties for an incidence angle of 60°, as per (Brandemuehl & Beckman, 1980).

In the thermal element, convective and radiative heat exchanges with the outdoor/indoor environments are considered separately unless required information is not available (e.g., air velocity or MRT). In these cases, standardized combined surface film coefficients of 23 and 8

W/m²K are used for the outdoor and indoor surfaces respectively. Note that an equivalent outdoor or "sol-air" temperature is used instead of the air temperature. When all information is known, the outdoor convective coefficient is calculated based on the wind speed and direction using empirical correlations by Loveday and Taki (1996). Radiative heat exchange is calculated using a typical Stefan-Boltzmann fourth-order radiation equation assuming equal view factors with the sky and surroundings (Appendix B). At the indoor surface, the radiation calculations are not presented. The convective coefficient at the indoor surface is calculated using empirical correlations with distinction between no heating device and a radiator or fan. Within the cavity, radiative heat exchange is calculated using the net-radiation method initially developed by Hottel (1954) for non-isothermal walls. This method accounts for incoming flux from all other surfaces (including those from other control volumes) using view factors.

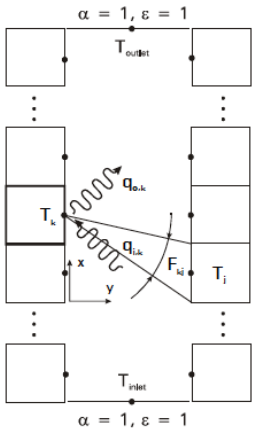

Figure 3.6 Radiation Heat Exchange Model for Non-Isothermal Walls (Saelens, 2002)

The convective heat transfer coefficients used within the cavity are discussed thoroughly. Distinction is made between natural, forced and mixed convection for both wide and narrow channels. Different equations are used for each regime, based on existing relations obtained from experimental research and numerical simulations. A limited experimental evaluation of the correlations is presented, though the spread of the results "shows that obtaining a reliable expression for the heat transfer coefficient is difficult". However, results indicated that natural convection was generally predicted better by Nusselt number relationships for laminar flow.

In the airflow model, both naturally ventilated and mechanically ventilated façades are considered. The airflow rate in the mechanical flow variant is a known variable, while the airflow

rate in the natural flow variant is calculated based on buoyancy and wind-induced pressure differences. The pressure difference due to buoyancy is determined using a calculation very similar to that presented by ASHRAE (2001) for stack-effect pressures. Wind induced pressure difference was calculated using a modified Bernoulli equation, though there is much discussion regarding the difficulty of correctly quantifying wind induced pressure. For the studied case, experimental data showed that wind effects only marginally influenced the results. The combined pressure differences are related to velocity with the power law equation using experimentally determined pressure characteristics (i.e., flow coefficient and flow exponent). The flow distribution on either side of the shading device is treated as an input. In the model, airflow is assumed one-dimensional and in the same direction on both sides of the shading device. Saelens states that "this restricts the use of the model to multiple-skin façades with roller blinds and prohibits the simulation of rotational flow".

Saelens conducts a useful comparison between measured results and models of varying complexity. Results showed that lumping radiation and convection within the cavity was unacceptable. However, modeling a vertical temperature gradient was not as important, especially in the absence of a shading device. When a shading device was present however, the temperature gradient became more important. Three different analytical models were compared to Saelens' numerical model. For an analytical solution, a temperature profile must be chosen; therefore the three models used 1) uniform cavity temperature, 2) linear temperature profile and 3) exponential temperature profile. For the case studied, the average cavity temperature predicted by all four models was approximately the same, though the outlet temperatures differed. The outlet temperature was underestimated when a uniform cavity temperature was supposed and it was overestimated when a linear temperature distribution was supposed. The outlet temperature was also overestimated when an exponential temperature distribution was supposed, though by less. Saelens' numerical model proved to be the most accurate, since it more accurately calculates radiation heat exchange and accounts for shadowing at the top of the cavity. Saelens also warns that the use of angular solar properties and a correct modeling of the inlet temperature significantly influence the final results.

3.4.2.3 Faggembauu et al. (2003)

In their paper, Faggembauu et al. (2003) present a model to simulate both ventilated and conventional façades over a one-year time period. According to the authors, the numerical code is able to model advanced elements such as phase change materials, selective surfaces and improved glazings. The interior layer can also be partially opaque.

In the optical element, monthly-averaged, daily-integrated values of global horizontal solar radiation are used as inputs. Instantaneous values of beam, diffuse and total solar radiation as well as values on sloped surfaces are then calculated using referenced correlations. An iterative net heat radiation algorithm (Siegel & Howell, 1992) is used to determine the absorbed, reflected and transmitted solar radiation by each of the semitransparent layers.

In the thermal element, the façade is divided into 1-m vertical sections. In many instances, only references to calculations are provided. At the outdoor surface, the convective heat transfer coefficient is calculated using empirical relations based on wind speed and direction as per (Rohsenow et al., 1985). Radiative heat exchange to the sky and ground is calculated using a fourth-order Stefan-Boltzmann radiation equation including angle factors (Appendix B). The same approach is used for radiative heat exchange to the indoor environment, assuming all room walls are at a single temperature. The indoor surface convective coefficient is calculated assuming natural convection as per (Mills, 1992). Inside the cavity, convective coefficients are determined from empirical Nusselt number correlations. For a closed cavity, an expression for convection in an enclosure with isothermal walls is used (Mills, 1992). For an open cavity, developing flow is calculated as for natural convection between plates with uniform temperatures while turbulent flow is calculated as for forced convection in pipes using a friction factor. Calculations and references are provided. The authors consider the stated correlations to be the best available in published literature. Radiation heat exchange between cavity layers is determined using a fourth-order equation for net heat transfer between two infinite, parallel plates. Conduction is calculated through both glazed and opaque layers. From the continuous governing equations, a non-linear system of discrete equations is obtained, which is solved at each time step using an iterative algorithm.

In the airflow element, both open (forced and natural convection) and closed conditions are considered. Natural airflow is calculated due to buoyancy only. The method used does not

account for pressure drops due to the geometry of the inlet and outlet grids. The authors state that this is not generally important for forced convection, "but might produce significant effects in the natural convection flow rates". To calculate the buoyancy-induced pressure difference between inlet and outlet, the outlet pressure is expressed as a function of the inlet velocity and is solved using a Newton–Raphson method. Consequently, natural airflow requires a substantially higher computational time than mechanical airflow, where the flow rate is a known input. Airflow is assumed to be one-dimensional. Note that shading devices were not originally included, though a shading layer is introduced in Part II of their study. It is unclear how airflow around this layer is handled.

The model was validated using results from analytical models, reference situations and experimental results. The main identified problems were the evaluation of convective heat transfer coefficients, non-constant channel sections, and the inability to account for two-dimensional effects.

3.4.2.4 Zanghirella et al. (2010)

In this study, Zanghirella et al. (2010) attempt to provide a model to analyze DFs during the design phase, which could be easily integrated with building energy simulation tools. The authors fault other models, specifically those by Jiru & Haghighat (2008) and Faggembauu et al. (2003), because they are purpose-built and difficult for others to use, not easily adapted and difficult to couple with overall building simulation tools. Consequently, the developed model is intended to be easy to use, computationally light and adaptable to any façade design.

In the optical element, the global incident solar radiation is split into direct and diffuse fractions. Edwards' (1977) embedded method is used to account for multiple reflections, transmission and absorption in the different layers. Angle dependent, spectrally averaged values are used and polarization is not considered. Diffuse radiation is estimated using optical properties for an incidence angle of 60° (Brandemuehl & Beckman, 1980), which was also used by Saelens (2002). To incorporate the venetian blind, a similar approach to Park et al. (2004) is used, where an energy balance is applied to the fictitious cavity formed by two consecutive slats. Shaded and unshaded portions of each slat are treated separately with consideration for direct-diffuse reflection and transmission. Window frame effects are neglected.

In the thermal element, radiation calculations are not specifically described, though they are separated from convection calculations. At the outdoor surface, radiative heat exchange with the sky and outdoor ambient is considered. The convective heat exchange coefficient is calculated as the maximum caused by either buoyancy or wind. The buoyancy equation is for turbulent convection from a large surface while the wind equation is the McAdams (1954) formula. At the indoor surface, radiation heat exchange is calculated to the indoor environment, which is assessed at the indoor air temperature. The indoor surface convective coefficient is calculated using the same empirical correlations as Saelens (2002), with distinction between no heating device and a radiator or fan. Within the cavity, radiative heat exchange is calculated for indefinite parallel plates. For an open cavity, the convective coefficient is assumed the same for all surfaces and is calculated based on the air velocity using the McAdams (1954) formula ($V<5$ m/s). For an enclosed cavity, the convective coefficient is calculated from empirical Nusselt number correlations used for sealed glazing cavities. Correlations proposed by Hollands et al. (1976) are used when the cavity is inclined between 0° and 60°, while the Wright (1996) formulas are used when the cavity is inclined between 60° and 90°. Conduction through the glass layers is included, though not for the shading device. Also, thermal capacity of the glass and shading device is accounted for. The model is a transient model solved using Simulink/Matlab software, “taking approximately twenty minutes to simulate the behavior of a real façade over a week”.

In the airflow element, only mechanical ventilation is considered so the airflow rate is known. In the presence of a shading device, the cavity is separated into two independent shafts and the airflow rate in each is assumed to be proportional to the width. Airflow is assumed one-directional in the vertical plane only, without recirculation. However, the authors use the model to evaluate both roller blinds and venetian blinds.

The model was validated using a one-storey test facility and a two-storey building in Italy. The maximum error between measured and simulated layer temperatures [°C] was 11.0% for the roller blind and 12.2% for the venetian blind. Highest errors occurred at the peak temperatures of the day when incident solar radiation was high. Further difficulties that the authors describe are the time and knowledge required to set up the model and the necessity to be familiar with the inner structure of Simulink. Further research will try to incorporate natural airflow.

3.4.3 Zonal Model

The zonal model is an intermediate model between control volume and CFD models. It separates the façade into a number of control volumes, using cells larger than CFD models. Mass and energy conservation equations are then formulated for each cell. The mass flow rates through the shading device and in the façade cavities are modeled using a two-dimensional model defined by the pressure difference between neighbouring cells. The non-linear system of pressure equations is then solved and the calculated airflow rates for each cell are inserted into the energy balance equations to determine the temperature in each cell. The airflow and energy equations are solved simultaneously to get the distribution of airflow rate and temperature. Because this method accounts for pressure and airflow differences within the façade cavity, it may be used for venetian blinds. Consequently, The zonal approach can provide information on airflow and temperature distribution in a ventilated space faster than CFD, but with more accuracy and detail than lumped and control-volume models (Jiru & Haghighat, 2008).

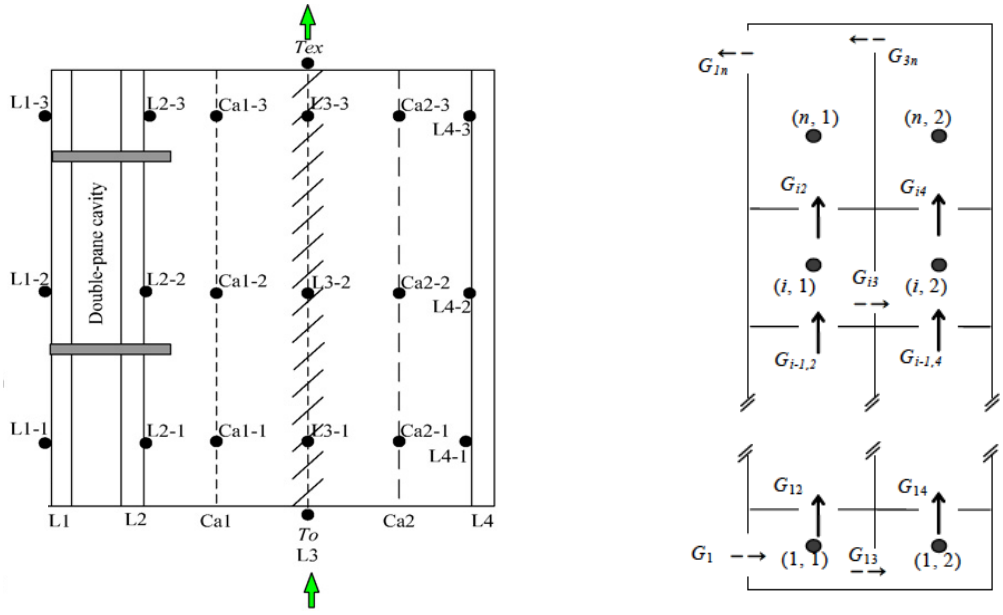

Figure 3.7 Zonal Model
Left: Cavity Divisions (Jiru & Haghighat, 2008), Right: Airflows (Yuan et al., 2007)

3.4.3.1 Yuan et al. (2007)

In this paper, Yuan et al. (2007) attempt to create a generally applicable model for architects and researchers alike. While the authors describe it as a modified lumped model, the façade is divided into multiple vertical sections and the airflow element was specifically created to include venetian blinds. While each heat transfer mechanism is discussed, the overall solution method is not provided; therefore, it is listed here as a zonal model for lack of a better category.

In the optical element, a general recursion formula is used, which is based on energy balances. In the method, multiple reflected, absorbed and transmitted components are included to determine the whole system transmittance, though it appears that solar irradiation is not separated into direct, diffuse and reflected components.

In the thermal element, it appears that radiative heat transfer to the outdoor environment is neglected. Convective heat transfer to the outdoor environment is calculated based on wind speed as per (Park et al., 2004). At the indoor surface, a combined radiation and convection heat transfer coefficient is calculated as per (ASHRAE, 2001). Within the cavity, radiative heat transfer between surfaces is calculated using a fourth-order Stefan-Boltzmann equation. The equation is not discussed, though a summation is used to account for non-isothermal walls, similar to Saelens (2002). However, neither emissivities nor angle factors are apparent in the equation. For convective heat transfer coefficients inside the cavity, a formula is presented to modify the Nusselt number found using published empirical correlations in (ASHRAE, 2001). The formula builds upon the findings of Park et al. (2004), increasing the Nusselt number due to disturbances caused by window frames and shading devices.

In the airflow element, a multi-zone, two-dimensional airflow network is introduced to calculate the mass transfer through the shading device. The cavity is separated into 2n nodes (two shafts vertically divided into n regions). Each node is connected to the nodes directly above and below it as well as to the node beside it in the adjacent shaft. The relationship between airflow rate and pressure difference between connected nodes includes a resistance coefficient that is based on pipe flow. The concept is essentially the same as that used by von Grabe (2002). Cavity channels are regarded as two rectangular pipes while the blinds are simplified into numerous tee branches. It is unclear how air velocity is calculated or how the overall system is solved; however, it appears that only natural buoyancy is considered.

The model is compared to experimental results from a previous study, showing errors in temperatures and ventilation rates around 25%. This confirms von Grabe's (2002) findings that mechanical pipe-flow loss factors do not necessarily translate to natural airflow. Other conclusions state that heat gain can be reduced if the shading device is placed closer to the inside skin, which is contrary to other findings (Saelens, 2002; Gratia & DeHerde, 2007).

3.4.3.2 Jiru and Haghighat (2008)

Jiru and Haghighat (2008) formulate a zonal model in an attempt to enhance the prediction capability of the control-volume method and expand it to include venetian blinds, without adding significant computational requirements. The model is used for a completely glazed, mechanically ventilated DF with venetian blinds at 45°.

In the optical element, incoming solar radiation is separated into direct, diffuse and reflected components. Normal incidence absorptance values are used for all layers as the authors state that optical properties "change little between 0° and 60° and most solar radiation is irradiated in this range". There is no mention of a treatment for multiple reflections within the façade or direct-diffuse reflection and transmission for the blind.

In the thermal element, combined convective and radiative heat transfer coefficients are used at the outdoor and indoor surfaces. At the outdoor surface, a standard value of 29 W/m^2K is used, which corresponds to wind speed of 6.7 m/s as per (ASHRAE, 2001). At the indoor surface, the value is calculated using an equation as per (ASHRAE, 2001). Within the cavity, radiation and convection are separated. A linearized radiative heat transfer coefficient is calculated using a view factor to account for venetian blind slat angles. The view factor is calculated using the fictitious cavity method of Rheault and Bilgen (1987). Convective heat transfer coefficients are based on empirical relations for the Nusselt number. Different relations are used for mechanical and natural airflow, similar to Saelens (2002). For mechanical convection, uniform heat flux relations for flow between parallel plates and over vertical plates are used based on the flow type (entrance region, fully developed laminar or fully developed turbulent). For natural convection, a correlation for uniform heat flux from a single vertical plate is used as per (Churchill and Chu, 1975). For the venetian blinds, the Nusselt number is estimated as for cylinders in cross flow. Calculations for both natural and forced convection are presented as per (Churchill and Chu, 1975). Conduction is included for the glazed layers but neglected for

the shading device since it is considered negligible. The energy balances are time dependent, including a term for heat storage within the layer similar to Zanghirella et al. (2010).

In the airflow element, only mechanical ventilation is considered so the inlet airflow rate is known. However, the airflow distribution is assessed using a two-dimensional zonal model in which the airflow rate through the blinds and in the air cavities is modeled using the power law. The equation is similar to that used by Yuan et al. (2007), though a flow coefficient multiplied by the cell area is used instead of a resistance coefficient. The flow coefficient values are not discussed. The non-linear system of pressure equations is solved by an iterative mass balance approach using the Newton–Raphson method. Calculated airflow rates for each cell are then inserted into the energy balance equations to calculate the temperature in each cell using the "Tri-Diagonal Matrix Algorithm".

When compared to experimental data, the prediction error increased with higher solar radiation and the highest error occurred at the top of the façade, where temperatures were highest. These findings are similar to those by Zanghirella et al. (2010). For the validation, only the total solar radiation was measured and therefore was not separated into direct, diffuse and reflected components for the numerical calculations. The authors state this simplification as one potential cause of error. Additional potential causes are "the complicated long wave exchange with the venetian blinds and the other surfaces; three-dimensional effects such as reverse flow and local short circuit caused by the outer façade frames; the complicated airflow through the venetian blinds; the heat transfer through the frames; air leakage; experimental errors; and the uncertainty of the estimated surface heat transfer coefficients". While the percent error is not given, the authors suggest that errors of the magnitude experienced would be difficult to avoid, even if CFD were employed.

3.4.4 Computational Fluid Dynamics Model

Computational fluid dynamics (CFD) is the most detailed form of modeling fluid flows. It can perform many tasks that simpler models cannot, such as determining local flow characteristics (e.g., loss and friction factors, convection coefficients, etc.) and modeling complex flow patterns (e.g., recirculation, vortexes, counterflows, etc). While CFD codes are powerful tools, the accuracy of the results strongly depends on the accuracy of the inputs.

For CFD analysis, the flow field is divided into cells using a two- or three-dimensional grid. A system of partial differential equations for the conservation of mass, momentum and energy is solved for each cell in a numerical solution. According to Manz and Frank (2005), "the equation usually solved is a Reynolds-averaged Navier–Stokes equation that predicts average velocities, temperatures, etc. for turbulent flows". Generally, k-ε style, two-equation turbulence models are used (standard, RNG or realizable). Finally, the results of the simulation may be visualized using powerful graphics workstations and visualization software. For example, temperature and velocity contours may be illustrated as in Figure 3.8. While the images are impressive to clients, they are mostly produced to visualize conceptual ideas, not for quantitative analysis.

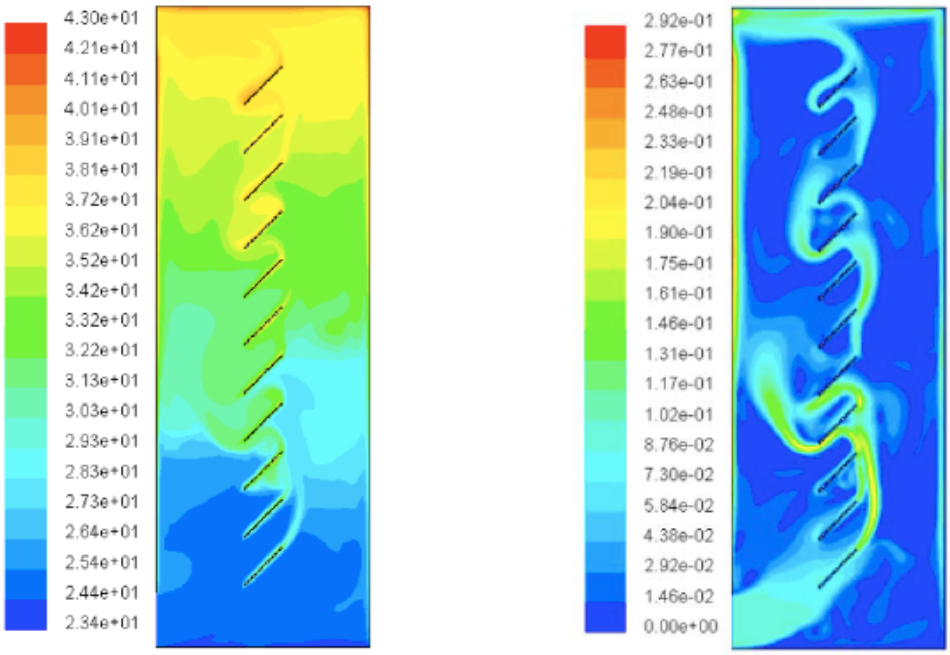

Figure 3.8 CFD Graphics for a DF with Venetian Blind (Tascon, 2008) (Left: Temperature, Right: Velocity)

Various researchers have used CFD, mostly for DF systems with venetian blinds. For example, Perez-Grande et al. (2005) use CFD to investigate the influence of different glass combinations on the heat flow into a building. Jiru et al. (2011) study the effect of blind position and slat tilt angle on the temperature and velocity distribution within the DF. Safer et al. (2005) conduct a similar study with the intent of creating a "global model of the channel" in which simplifications may be made based on the CFD results.

The successful application of CFD requires proper inputs. Coussirat et al. (2008) state that "selecting suitable sub-models for the convection, radiation and turbulence effects remains a big challenge". They investigate various sub-models, finding that the P-1 radiation model and RNG turbulence model performed best for the specific case studied. While Jiru et al. (2011) used the RNG turbulence model, other researchers used the standard k-ε model (Perez-Grande et al., 2004) or the realizable k-ε model (Safer et al., 2005; Manz & Frank, 2005). This shows that even researchers can have difficulties determining proper models. Moreover, a great number of additional input data are required for CFD analysis, often unknown during preliminary design.

Further disadvantages stated in the literature are that CFD models require large amounts of time to build, optimize and run; extensive user knowledge and experience; and proper verification, validation and reporting. Moreover, of the available CFD codes (CFX, Flovent, Fluent, Star-CD, Phoenics, etc.), few include features especially suitable for building applications (e.g., for occupant-dependent boundary conditions or specific HVAC components).

While CFD is valuable in research, it is too complex for preliminary design and is therefore not investigated in more detail for this research. However, CFD results can provide valuable information to help improve correlations used in more simplistic airflow calculations. For example, eddies and turbulence at vent openings can reduce the effective area of the opening. CFD could be used to model these complex airflows to determine more accurate discharge coefficients and effective vent areas for Griffith's (2006) calculations. Alternatively, CFD could be used to determine more accurate local loss factors for von Grabe's (2002) calculations. It is interesting to note that a CFD analysis conducted by Chiu and Shao (2000) found that cavity friction was relatively insignificant for cavity depths between 50 and 70 cm.

3.5 Conclusions

Current methods of modeling DFs were investigated, including whole building energy models, complex fenestration models and purpose-created DF models. The approaches and specific calculations used in each of the studied models are summarized in Appendix B.

In the context of DF preliminary design, several of the options can be considered unsuitable. Firstly, whole building energy models can be useful design tools; however, programs capable of modeling innovative new technologies such as DFs are often too complex for architects.

Moreover, the programs were not created to model DFs and therefore require advanced user knowledge and experience to manipulate them to do so. Secondly, complex fenestration models are powerful tools but do not incorporate the airflow element necessary to models DFs. Finally, CFD models are important research tools; however, they are too complex for preliminary design. Extensive time and knowledge are required to use them correctly and the accuracy of the results is very dependent on the inputs. However, each of these tools can play an important role in creating a more suitable DF model. Firstly, an easy-to-use whole building energy model, such as EnergyPlus or BELA, may be paired with a simple DF model to determine annual energy performance. Secondly, complex fenestration models can be used as good references for optical and thermal calculations. Finally, CFD results may be used to improve the accuracy of airflow correlations used in simpler models.

Models that are more suitable to DF preliminary design are lumped, control volume and zonal models. These models have varying levels of complexity. A lumped model may be solved analytically, though outputs are less detailed, giving only average surface temperatures. Control volume models are solved numerically and give details about the vertical temperature gradient. Zonal models are similar to control volume models but are able to model two-dimensional airflows (i.e., venetian blinds). However, both the lumped model (Park et al., 2004) and the control volume model (Zanghirella et al., 2010) have successfully been used to model DFs with venetian blinds as well.

Important findings from the studied examples show that using local loss factors and friction factors from mechanical engineering tables does not always predict resistance for natural airflow accurately (von Grabe, 2002). Furthermore, published empirical correlations may understimate the convection coefficient in a naturally ventilated DF cavity (Park et al., 2004; Yuan et al., 2007). Also, Balocco (2002) found that cavity friction reduces with increasing width between 7 and 35 cm, while Chiu and Shao (2000) found that cavity friction was relatively insifnificant for cavities between 50 and 70 cm. Saelens (2002) found that both lumped analytical models and control volume numerical models could accurately predict the average temperature in a single-storey DF cavity with natural airflow. However, the prediciton of the outlet temperature is best predicted by the numerical model. He also warns that angular solar properties and a correct modelling of the inlet temperature significantly influence final results.

Chapter 4
Development of a Double Façade Modeling Tool

4.1 Goals and Outputs

The goal of the model developed in this thesis is to aid in decision-making at the preliminary design stage of a retrofit project. At this stage, it is important to assess potential solutions based on quantitative data. While a DF may be attractive to design teams for perceived benefits, a modeling tool is needed to determine the actual benefits based on specific design intentions and climate.

To aid at the preliminary design phase, the model should require limited inputs. Furthermore, the model should be simple enough for anyone to use, not only modelers with extensive training. While the results should be sufficiently accurate to correctly assess the DF option compared to alternate solutions, high precision and detail are not required. Specific information important to a design team includes:

1) inflowing/outflowing heat flux to predict cooling and heating loads;
2) U-value (overall conductance of the assembly);
3) Solar Heat Gain Coefficient (SHGC) (ratio of transmitted solar heat gain to that incident on the outside surface);
4) airflow rate and outlet temperature of the façade cavity if natural ventilation is desired;
5) temperature of the façade perimeter to predict possible deformations and material durability; and
6) temperature of the inner surface to predict thermal comfort and condensation risk.

The inflowing/outflowing heat flux through the façade is useful to determine design loads to size mechanical equipment. This is calculated from the U-value and SHGC (Section 0), which are typical performance indices often used to compare glazing products in winter and summer respectively. Typically, U-value and SHGC can be implemented into whole building energy analyses to determine annual energy performance. However, it is important to note that the DF performance changes based on operation mode and outdoor conditions. It is a dynamic façade and therefore cannot be evaluated in an annual simulation based on static performance indices.

Any U-value and SHGC obtained for a DF represent only a snapshot in time, useful to determine design loads or performance under specified conditions.

In the case of natural ventilation, the cavity airflow rate and outlet temperature are important outputs. If the cavity air is entering the conditioned space, it affects the inflowing heat flux. Furthermore, the outlet temperature is necessary to determine which conditions would be favourable for natural ventilation or how much energy could be saved by using the cavity to preheat air to the mechanical ventilation system. Finally, surface temperatures throughout the façade yield important information for material choices and façade design. Using the above outputs, the designer would be able to assess the impact of design choices and alter their design to provide optimum performance for the specified building and climate.

To be useful for multiple projects, a DF model should be general enough to model any type of double façade configuration (i.e., any component in any sequence). Components are illustrated in Figure 4.1.

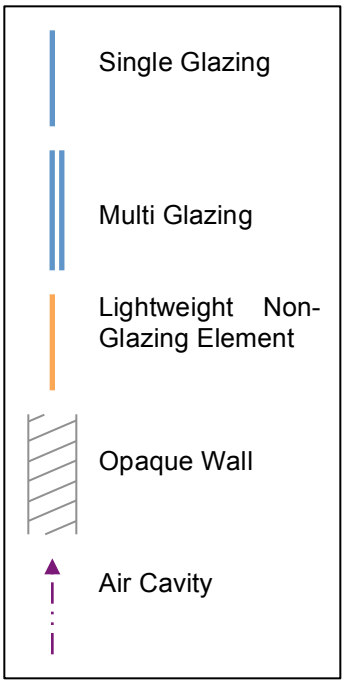

Figure 4.1 Possible Double Façade Components

The lightweight non-glazing element includes components such as shading devices. While the air cavity is illustrated with upward airflow, it may have any of the airflow modes described in Section 2.2.3. Possible component configurations are illustrated in Figure 4.2.

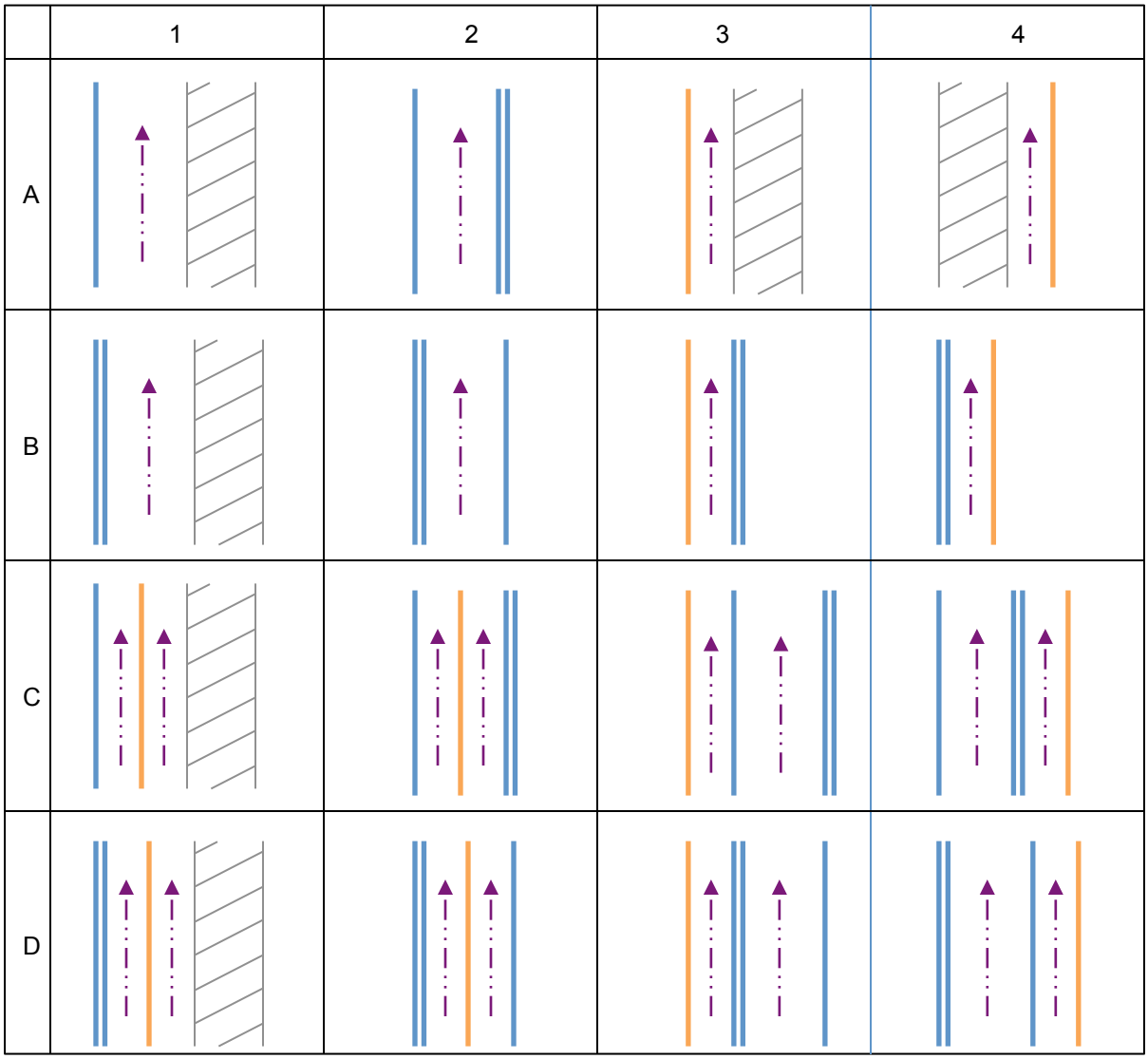

Figure 4.2 Possible Double Façade Configurations

Figure 4.2 shows some possible configurations, though many more could be designed and modeled. While the main intent is to model double façades, any assembly with ventilated cavities could be included. For example, 3A and 4A might represent PV panels on the exterior of an assembly and a ventilated cavity on the interior of an assembly. Furthermore, the tool could be used for new construction projects employing such assemblies.

4.2 Proposed Approach

A lumped model is proposed to meet the goals described above. As described in Section 3.4.1, the lumped model is a simple, one-dimensional model constructed from first principles conservation laws. Temperatures and heat transfer coefficients are averaged over the entire height of the façade so vertical stratification is neglected. This type of model was chosen because it is flexible and quick and it requires basic inputs and minimal user skill level. It can be solved analytically, does not require complex software and gives results accurate enough for design-phase decision-making. The model developed in this thesis, titled “DoFa” for double façade, is Microsoft Excel spreadsheet based. Excel is a ubiquitous program that is known and understood by architects and engineers alike.

The DoFa model begins by making initial estimates of layer temperatures based on boundary conditions and material properties. Then, heat transfer coefficients and airflow rates are calculated from the layer temperature estimates. An energy balance is then performed on each surface and cavity of the DF system. Once the set of equations has been formulated, the temperature of each layer and cavity may be solved in an iterative process. The convergence criterion is set to 100 iterations or 0.01% difference in the layer temperatures [K]. Note that heat transfer coefficients and airflow rates are recalculated for each iteration, as they are temperature dependent. Once the cavity airflow rate and temperature profile through the assembly are known, inward flowing heat flux, U-value, SHGC and cavity outlet temperature are determined. The DoFa model workflow is shown in Figure 4.3.

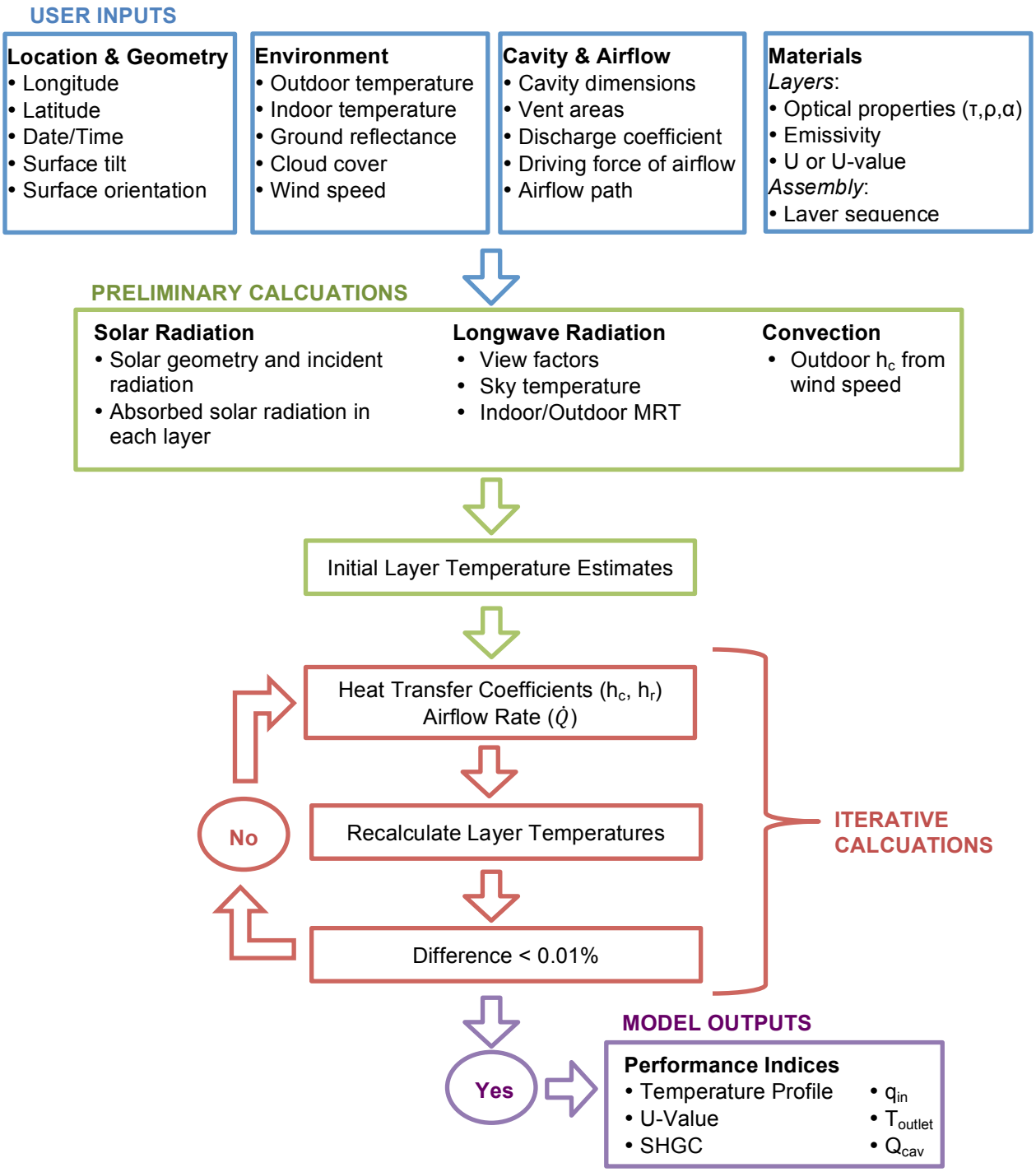

Figure 4.3 DoFa Model Flow Diagram

Such a model must incorporate all heat transfer mechanisms including radiation (shortwave and longwave), convection, conduction and airflow. The background physics behind these mechanisms are described in the following sections.

4.3 Heat Transfer Mechanisms

4.3.1 Overview

To determine the temperature of each layer within a DF, an energy balance is performed on each individual layer. It is assumed that each surface and cavity has a uniform temperature in the y-direction and that no airflow occurs through the shading device. Heat flux mechanisms for solid and fluid layers are different.

For any solid layer within an assembly, there may be heat flux from four sources: 1) solar radiation (i.e., shortwave) (q_{SWR}), 2) longwave radiation (q_{LWR}), 3) conduction (q_{cond}) and 4) convection (q_{conv}). By the law of conservation of energy, if an energy balance is performed on any solid layer, the sum of all fluxes must equal zero:

$$0 = q_{SWR} + q_{\mathrm{LWR}} + q_{cond} + q_{conv} \qquad [\mathrm{W/m^2}] \qquad \textbf{(4.1)}$$

For a fluid layer (e.g., air), solar and longwave radiation travel straight through without directly affecting the fluid temperature. In an enclosed cavity, only convection and conduction affect the layer temperature. When the layer is sufficiently wide (>13 mm), convection is the main mode of heat transfer, though conduction is included in convection calculations. In a ventilated cavity, heat flow due to airflow ($Q_{airflow}$) must be included in the energy balance. By the laws of conservation of energy and momentum, if an energy balance is performed on a fluid layer, the sum of all heat flows must equal zero:

$$0 = Q_{conv} + Q_{airflow} \qquad [\mathrm{W}] \qquad \textbf{(4.2)}$$

Note that heat loss/gain due to airflow is measured in heat flow [W], not heat flux [$\mathrm{W/m^2}$]. Therefore, when performing an energy balance on fluid layers, one must convert convective heat flux to heat flow:

$$Q_{conv} = q_{conv}A \qquad [\mathrm{W}] \qquad \textbf{(4.3)}$$

Where,

A = surface area [$\mathrm{m^2}$]

4.3.2 Optical Element: Solar Radiation

Solar energy, also known as shortwave radiation, enters the atmosphere with wavelengths in the near-ultraviolet, visible and near-infrared spectra (0.3 to 3.5 μm) (ASHRAE, 2009). When sunlight travels through the atmosphere unimpeded, it is known as direct or beam radiation. When sunlight is scattered by molecules in the atmosphere or reflected off other objects, it is known as diffuse radiation. Whether direct or diffuse, solar radiation incident on any surface may be separated into transmitted (τ), reflected (ρ) and absorbed (α) fractions. τ, ρ and α of a specific material are known as material optical properties and together they must equal unity (Figure 4.4).

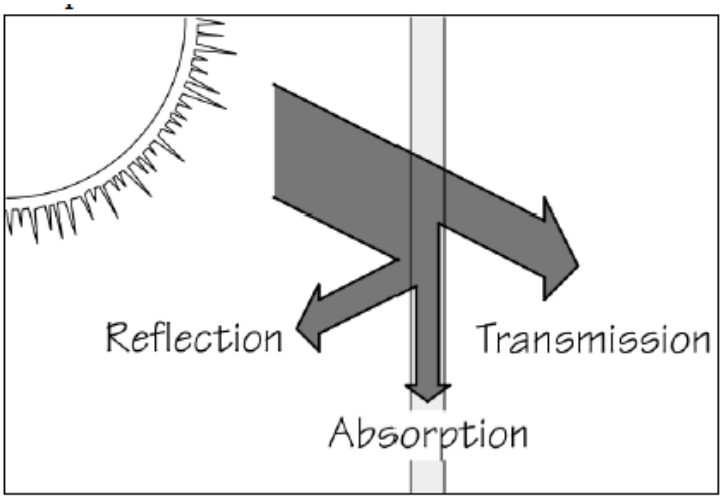

Figure 4.4 Surface Optical Properties (LBNL, 2011)

4.3.2.1 Heat Flux

Solar radiation heat flux for any given layer in a DF is the effective absorbed fraction (α_e) of the incident solar radiation (G_θ), calculated as follows:

$$q_{SWR} = \alpha_{e,D\theta} G_{D\theta} + \alpha_{e,d} G_{d\theta} \qquad [W/m^2] \qquad \textbf{(4.4)}$$

Where subscripts *D* and *d* represent direct and diffuse solar radiation respectively. Optical properties depend on the incidence angle of the sun's rays (θ); however, optical properties at normal incidence (i.e., the sun's rays are perpendicular to the surface) can be used as a simplification. In this case, direct and diffuse fractions may be combined. The implications of this simplification are discussed in Chapter 5.

$$q_{SWR} = \alpha_e G_{t\theta} \quad [W/m^2] \qquad (4.5)$$

Where,

α_e = effective absorptance at normal incidence

$G_{t\theta}$ = total incident solar radiation [W/m^2]

For brevity, Equation (4.5) is used to represent solar radiation heat flux in energy balance equations throughout this thesis, though Equation (4.4) is actually used by the DoFa model. q_{SWR} to any nth solid layer (Sn) is illustrated in Figure 4.5.

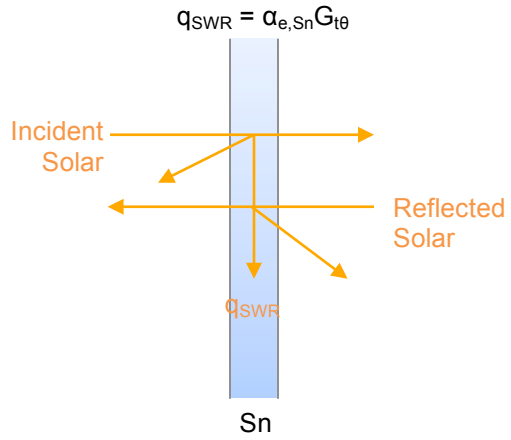

Inputs

Incident Solar Radiation (G_θ)
- Longitude
- Latitude
- Date/Time
- Surface tilt
- Surface orientation
- Clearness number
- Ground reflectance

Effective Absorptance (α_e)
- Transmitance
- Reflectance
- Absorptance

Figure 4.5 Solar Radiation Heat Flux

Note that α_e is different from α because it accounts for multiple reflections within a multi-layer enclosure. Detailed calculations for G_θ and α_e are presented in the following sections. In certain cases, the user may want to input fixed $G_{D\theta}$ and $G_{d\theta}$ values; for example, to emulate NFRC-100 design conditions. Therefore, the user has the option to use the calculated values or user-defined values. NFRC-100 $G_{t\theta}$ values used in WINDOW6.3 are 783 W/m^{2}K in summer and 0 W/m^2 in winter (LBNL, 2011).

4.3.2.2 Solar Radiation

The exact position of the sun for a given location and time may be calculated by trigonometric functions as described in various texts (Kreider et al., 2010; McQuiston et al., 2005; ASHRAE, 2009). The various angles used to calculate the solar geometry are shown in Figure 4.6. The legend on the right-hand side denotes the symbols used in this thesis for the depicted angles.

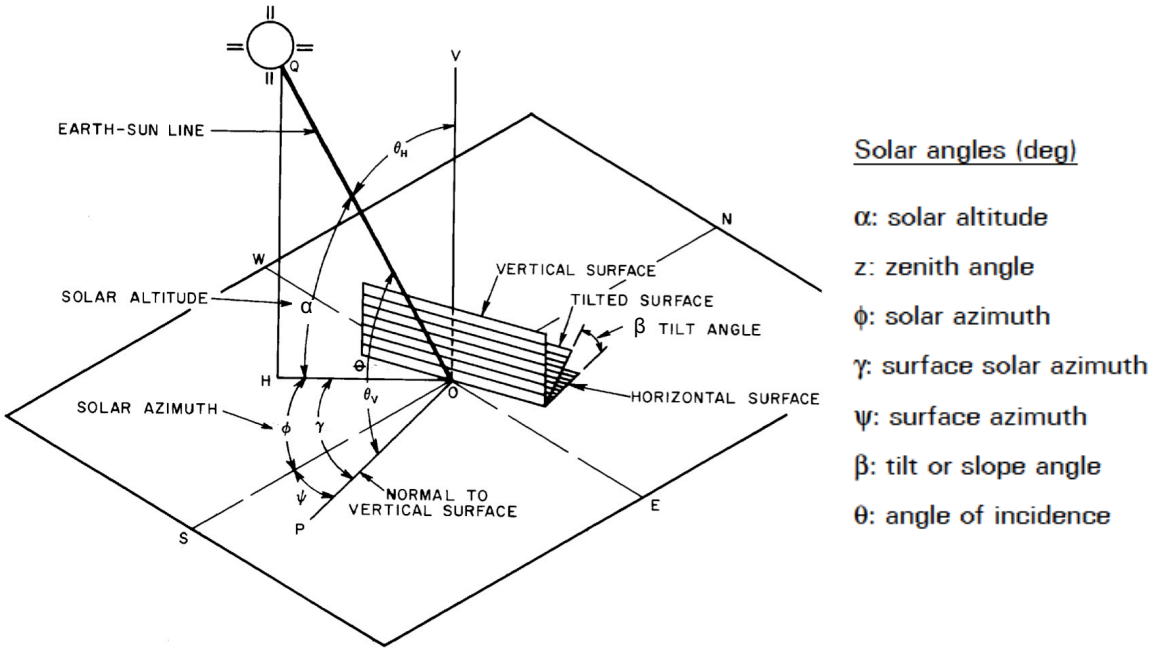

Figure 4.6 Solar Angles (ASHRAE, 2009)

The angle of incidence (θ) is defined as the angle between the incoming solar rays and a line normal to that surface (ASHRAE, 2009). This angle is important to glazing calculations and can be calculated using the following relation:

$$\cos\theta = \cos\alpha\cos\gamma\sin\beta + \sin\alpha\cos\beta \qquad \textbf{(4.6)}$$

The total irradiation incident on a vertical surface ($G_{t\theta}$) for a given incidence angle may be found by summing the direct ($G_{D\theta}$), sky diffuse ($G_{d\theta}$) and ground reflected ($G_{R\theta}$) components (ASHRAE, 1993):

$$G_{t\theta} = G_{D\theta} + G_{d\theta} + G_{R\theta} = \left[\max(\cos\theta, 0) + \frac{G_{dV}}{G_{dH}}C + \rho_g F_{wg}(\sin\alpha + C)\right] G_{DN} \qquad [W/m^2] \qquad \textbf{(4.7)}$$

Where,

G_{dV} = diffuse sky radiation on a vertical surface [W/m^2]

G_{dH} = diffuse sky radiation on a horizontal surface [W/m^2]

C = ratio of diffuse irradiation on a horizontal surface to direct normal irradiation

ρ_g = reflectance of the ground

F_{wg} = angle factor from wall to ground

G_{ND} = direct normal irradiation at the earth's surface on a clear day [W/m^2]

Calculations for G_{dV}, G_{dH}, and F_{wg} are presented by ASHRAE (1993) and McQuiston et al. (2005). Where the surface is not vertical, the term G_{dv}/G_{dh} is replaced with an angle factor from the surface to the sky (F_{ws}). Various ρ_g values for different surfaces are available (Hunn and Calafell, 1977; Threlkeld, 1970), though Kreider et al. (2010) suggest that one usually assumes 0.2 without snow cover and 0.7 with snow cover. These are the values used in the DoFa model unless overridden manually. Although calculations for ground reflected irradiance are only correct when the ground in front of the surface is not shaded, a correct calculation becomes so complicated that the gain in accuracy has usually not been deemed worth the effort (Kreider et al., 2010). Note that ground reflected radiation is assumed to be diffuse reflected and is therefore included in the diffuse component of Equation (4.4).

In order to determine the direct normal irradiation at the earth's surface on a clear day, the ASHRAE clear sky model was used:

$$G_{ND} = \frac{A}{exp\left(\frac{B}{sin\alpha}\right)} C_N \qquad [W/m^2] \qquad \textbf{(4.8)}$$

Where,

A = apparent solar irradiation at air mass equal to zero [W/m^2]

B = atmospheric extinction coefficient

C_N = clearness number

A, B, and C values are provided by ASHRAE (1993) for the 21st day of each month. These are consistent with values used in a solar calculator created by the Pacific Energy Centre (1993). C_N values are location dependent and are provided by Threlkeld and Jordan (1958) and reproduced by ASHRAE (1993). C_N values for Southern Ontario are between 1.00 and 1.05.

Note that in the current DoFa model, shading due to overhangs and frames is not included. This simplification will overestimate the direct portion of incident solar radiation and thereby overestimate solar heat gain. The degree of overestimation depends on the degree of shading. Shading effects could be added in future versions with relative ease.

4.3.2.3 Layer Optical Properties

Layer optical properties (τ, ρ and α) are user inputs. If known, the user may area-weight layer optical properties to include frames or other opaque elements in a glazing layer. Although the optical properties of glazing and shading layers are dependent on the wavelength and incidence

angle, spectrally averaged values at normal incidence can be used as a simplification. As Jiru & Haghighat (2008) argue, optical properties change little between 0° and 60° and most solar radiation is irradiated in this range. This statement is supported by graphs produced by ASHRAE (2009).

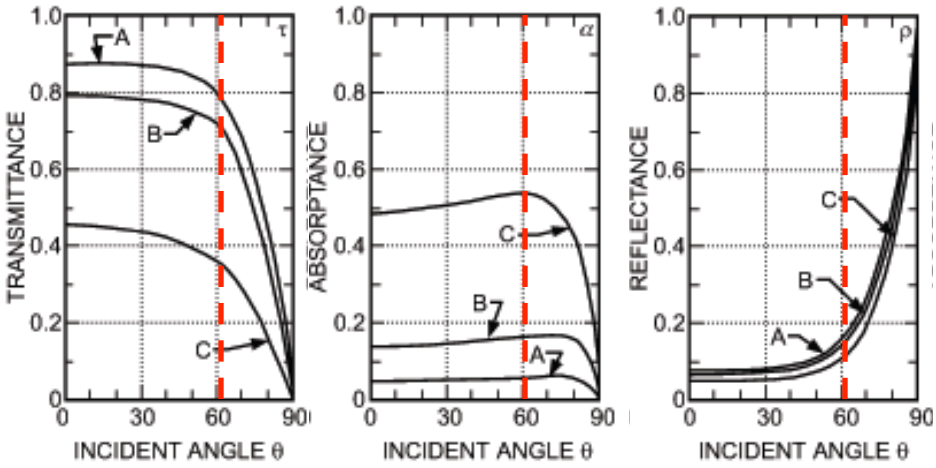

Figure 4.7 Angle-Dependent Solar-Optical Properties for (A) Double-Strength Sheet Glass, (B) Clear Plate Glass, and (C) Heat Absorbing Plate Glass (ASHRAE, 2009)

Between incidence angles of 0° and 60°, optical properties of the glazings tested changed less than 10%. However, Saelens (2002) suggests that using angle-dependent optical properties can have significant impacts on the results of a DF model. The impact of optical properties is examined in Chapter 5. It is the user's choice to use angle-dependent optical properties or not.

Furthermore, diffuse optical properties are entered separately and used in a separate calculation. Therefore, separate diffuse values can be used. Results by Brandemuehl and Beckman (1980) suggest that for vertical surfaces, the solar properties for diffuse radiation (sky diffuse and ground reflected) may be estimated by the solar properties at an effective incidence angle of 60°. However, the solar radiation calculations described previously do not account for cloud cover. If the user wishes to investigate the effects of cloudy days using separate optical properties for diffuse radiation, they should input specific $G_{D\theta}$ and $G_{d\theta}$ values with a high $G_{d\theta}$. It should be noted that the DoFa model conducts direct and diffuse calculations completely separately; therefore, only beam-beam and diffuse-diffuse transmission and reflection are considered. Rogalsky (2011) includes a treatment for beam-diffuse reflection and transmission,

which would be useful for fritted glass or diffusing shading layers. The impact of this simplification is discussed in Chapter 5.

Glazing optical properties are available from manufacturers or from the WINOW6.3 glazing library. Some shading device optical properties at normal incidence are given below.

Table 4.1 Solar-Optical Properties of Shading Devices at Normal Incidence (ASHRAE, 2001)

Indoor Shade	τ	α	ρ
Venetian Blinds*			
Light	0.05	0.4	0.55
Medium	0.05	0.6	0.35
Vertical Blinds			
White	0	0.23	0.77
Roller Shades			
Light (Translucent)	0.25	0.15	0.6
White (Opaque)	0	0.35	0.65
Dark (Opaque)	0	0.8	0.2

**ratio of slat width to slat spacing 1.2, slat angle 45°*

Once the optical properties are entered, the DoFa model determines effective absorptance (α_e) of each layer. For any single layer system, the layer absorptance equals the effective absorptance ($\alpha=\alpha_e$). However, determining specific layer α_e values becomes complicated for multi-layered systems due to multiple reflections, as shown in Figure 4.8.

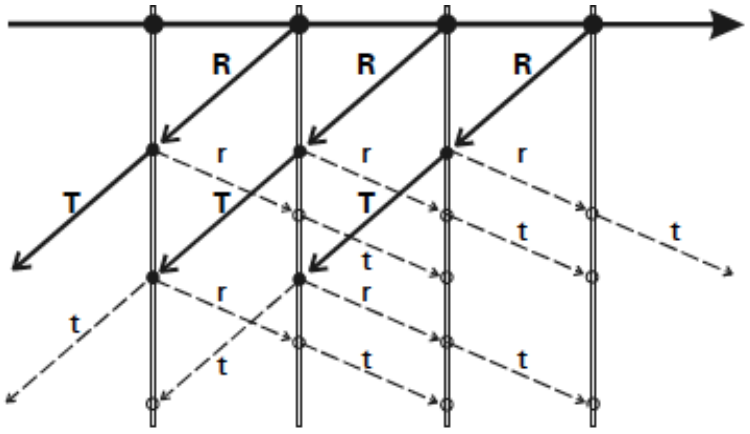

Figure 4.8 Effect of Multiple Reflections in a Multi-Layer Glazing System (Saelens, 2002)

Three different methods can be used to account for multiple reflections within the façade to obtain overall system solar properties: 1) the ray-tracing method, 2) the net radiation method and 3) the embedded or energy balance method. The embedded method proposed by Edwards (1977) is used here because of its simplicity and convenience for multiple layers with different material properties. Furthermore, Edwards (1997) states that the results obtained will be the same as those found by the other two methods. The embedded method was also the basis for optical calculations employed by Saelens (2002), Zanghirella et al. (2010) and Rogalsky (2011).

Edwards' (1977) method was originally developed for flat plate solar collectors with an absorber plate and multiple covers. In the technique, a stack of elements consisting of an absorber plate and *n* coverglasses is considered. The effect of adding one more element to the array is then formulated, making a total of *n+1* coverglasses. For an architectural application, the room becomes the absorber plate and the layers within the complex glazing system become the coverglasses.

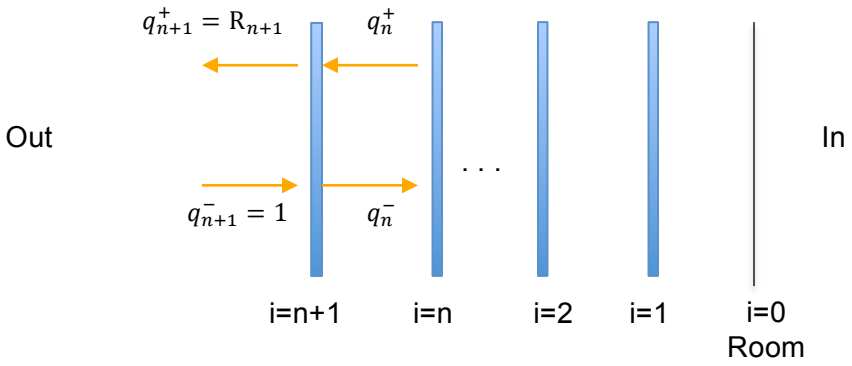

Figure 4.9 Embedding a stack of n elements

The incoming flux (q^{-}_{n+1}) outside the added *n+1* element is normalized to unity and the outgoing flux (q^{+}_{n+1}) is the overall reflectance of the array (R_{n+1}). Each flux is the combination of reflected and transmitted fluxes from the other layers.

The calculation commences with the room, where $R_0=\rho_0$ is the effective reflectance of the room. t_{n+1} and a_{n+1} are the top-of-the-stack transmittance and absorptance of the array respectively, taking into account the reflected portion of the previous layers. For the room, $t_0=0$ and $a_0=\alpha_1$ (the DoFa model assumes $\rho_0=0$ and $\alpha_0=1$ unless overridden). Then the next layer is added (innermost layer of the glazing system), making it the n+1 layer. R_{n+1}, t_{n+1} and a_{n+1} are found as follows:

$$R_{n+1} = \rho_{n+1} + \frac{\tau_{n+1}^2 R_n}{1 - \rho'_{n+1} R_n} \quad \textbf{(4.9)}$$

$$t_{n+1} = \frac{\tau_{n+1}}{1 - \rho'_{n+1} R_n} \quad \textbf{(4.10)}$$

$$a_{n+1} = a'_{n+1} R_n t_{n+1} + \alpha_{n+1} \quad \textbf{(4.11)}$$

Where,

ρ = reflectance of inside surface

ρ' = reflectance of outside surface

τ = transmittance (τ=τ' by the reciprocity principle)

α = absorptance of inside surface (α=1-ρ-τ)

α' = absorptance of outside surface (α'=1-ρ'-τ)

Allowing for different surface properties on the inside and outside surfaces of an element allows for optical coatings. However, for most layers the inside and outside values would be the same. The effective absorptance of each layer can then be determined:

$$\alpha_{e,n} = a_n t_{n+1} \quad \textbf{(4.12)}$$

For a more complete description of the method, see Edwards (1977). The DoFa model assumes that there is no source of solar radiation from the indoor environment (i.e., the room) and does not include reflections from the floor or ceiling of the cavity. These simplifications are expected to have little impact on results.

4.3.3 Thermal Element: Longwave Radiation

Longwave radiation is the radiation emitted from objects in the form of heat, or infrared radiation (3.5 - 50+ μm) (ASHRAE, 2009). It is transferred by electromagnetic waves through a gas or vacuum; therefore, a direct line of sight is required between the surfaces involved (Straube & Burnett, 2005). Longwave radiation is an important mode of heat transfer between solids. It should be noted that while solid transparent surfaces transmit a portion of solar radiation, window glass does not transmit longwave radiation.

4.3.3.1 Heat Flux

Longwave radiation heat flux can be calculated using a linearized formulation as presented in various texts (Straube & Burnett, 2005; McQuiston et al., 2005).

$$q_{LWR} = h_r(T_{S1} - T_{S2}) \qquad [W/m^2] \qquad \textbf{(4.13)}$$

Where,

h_r = radiative heat transfer coefficient [W/m^2K]

T_S = surface temperature [K]

q_{LWR} between any n^{th} and n+1 solid layers is illustrated in Figure 4.5.

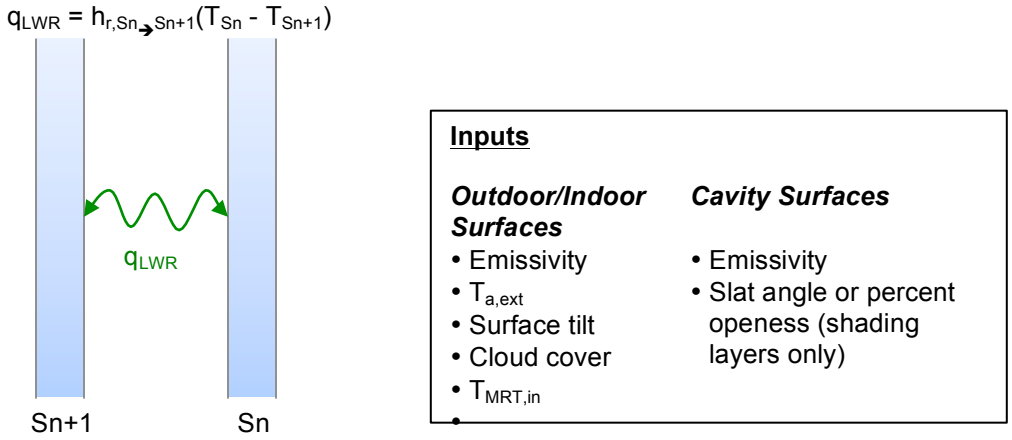

Figure 4.10 Longwave Radiation Heat Flux

h_r calculations are different for outdoor/indoor surfaces and cavity surfaces. Detailed calculations are presented in the following sections.

4.3.3.2 Radiative Heat Transfer Coefficients for Indoor/Outdoor Surfaces

For surfaces exposed to the indoor or outdoor environment, h_r between the n^{th} opaque surface and the ambient environment can be derived from the Stefan-Boltzmann equation as:

$$h_{r,Sn\rightarrow Ambient} = \frac{\varepsilon_{Sn}\sigma(T_{Sn}^4 - T_{MRT}^4)}{(T_{Sn} - T_{MRT})} = \varepsilon_{Sn}\sigma(T_{Sn}^2 + T_{MRT}^2)(T_{Sn} + T_{MRT}) \qquad [W/m^2] \qquad \textbf{(4.14)}$$

Where,

ε = surface long-wavelength emissivity

σ = Stefan-Boltzmann constant [5.67×10^{-8} W/m^2K^4]

T_{MRT} = mean radiant temperature of the ambient environment [K]

To avoid the situation where $T_{Sn}=T_{MRT}$ and the denominator becomes zero, the denominator is cancelled out by taking the difference of two squares.

For the indoor environment, $T_{MRT,int}$ is generally assumed to be equal to the indoor air temperature, which is a safe assumption where a small fenestration is exposed to a large room with surface temperatures equal to the air temperature (ASHRAE 2009). If the designer is aware that the room will contain cooled or heated surfaces, an area and emissivity-weighted mean radiant temperature should be used instead. This is user input.

For the outdoor environment, $T_{MRT,ext}$ is based on sky and ground temperatures and is therefore dependent on climatic conditions. However, $T_{MRT,ext}$ is sometimes assumed to be equal to the outdoor air temperature, as in WINDOW6.3. Therefore, the DoFa model gives the user a choice to either use the ambient temperature or the calculated temperature. When using the calculated temperature, the following relation is used:

$$T_{MRT,ext} = \left(F_g T_g^4 + F_{sky} T_{sky,e}^4\right)^{1/4} \quad \text{[K]} \qquad \textbf{(4.15)}$$

Where,

F_g = angle factor between outdoor surface and the ground (i.e., area below the horizon)

F_{sky} = angle factor between outdoor surface and the sky

T_g = ground temperature [K]

$T_{sky,e}$ = effective sky temperature for a tilted surface [K]

To calculate angle factors, it is assumed that the building sits on a featureless plain; therefore, F_g and F_{sky} are calculated as:

$$F_g = \frac{1 - \cos\beta}{2} \qquad \textbf{(4.16)}$$

$$F_{sky} = \frac{1 + \cos\beta}{2} \qquad \textbf{(4.17)}$$

However, if information is known regarding the surrounding buildings and features, the user may choose to input their own angle factors.

According to McQuiston et al. (2005), ground temperature is usually assumed to be the same as the air temperature. Note that this assumption would not be true in various cases; for example, for a wall with a significant view of an asphalt parking lot, the ground temperature would be higher on a sunny day and lower on a clear night. In the DoFa model, ground temperature is set equal to the air temperature, though this may be overridden if a detailed model of the surrounding ground is available.

There are various models and equations to estimate the sky temperature on a clear or cloudy day. The effective sky temperature for a tilted surface ($T_{sky,e}$) is estimated using an expression based on Walton's empirical model (1983):

$$T_{sky,e} = \left[\cos\left(\frac{\beta}{2}\right)\right] T_{sky} + \left[1 - \cos\left(\frac{\beta}{2}\right)\right] T_{a,ext} \qquad [K] \qquad \textbf{(4.18)}$$

Where,

T_{sky} = sky temperature for a horizontal surface [K]

$T_{a,ext}$ = outdoor air dry bulb temperature [K]

To determine T_{sky}, cloud cover (c) is introduced as a user input. The calculation is done by first estimating downward longwave radiation flux from a clear sky (I_{lwc}), then adjusting for cloud cover. Straube and Burnett (2005) state that the most widely accepted relationship for I_{lwc} was developed by Idso and Jackson (1969):

$$I_{lwc} = \left[1 - 0.261 e^{-0.000777(273 - T_{a,ext})^2}\right] \sigma T_{a,ext}^4 \qquad [W/m^2] \qquad \textbf{(4.19)}$$

To find downward longwave radiation flux from a cloudy sky (I_{lw}), Jacobs' (1978) model is used:

$$I_{lw} = I_{lwc}(1 + kc) \qquad [W/m^2] \qquad \textbf{(4.20)}$$

Where,

k = function of the type of cloud (assumed 0.26)

c = fractional cloud cover (user input)

The general relation between I_{lw} and sky temperature, assuming the sky as a black emitter, is:

$$I_{lw} = \sigma T_{sky}^4 \qquad [W/m^2] \qquad \textbf{(4.21)}$$

Therefore, rearranging for T_{sky} and substituting Equation (4.20) for I_{lw} gives:

$$T_{sky} = \left(\frac{I_{lwc}(1 + kc)}{\sigma}\right)^{1/4} \qquad [K] \qquad \textbf{(4.22)}$$

4.3.3.3 Radiative Heat Transfer Coefficients for Cavity Surfaces

Within the façade cavity, each surface is considered separately. The floor and ceiling of the cavity are excluded from radiation calculations as they are expected to have relatively little impact. For any n^{th} surface, h_r between that surface and the adjacent surface may be calculated as for two, infinite parallel plates:

$$h_{r,Sn\to Sn+1} = \frac{4\sigma T_m^3}{\frac{1}{\varepsilon_{Sn}} + \frac{1}{\varepsilon_{Sn+1}} - 1} \qquad [W/m^2] \qquad \textbf{(4.23)}$$

Where,

T_m = mean temperature of the two opposing surfaces [K]

For ease of calculations, the DoFa model was set up to calculate heat transfer between surfaces directly adjacent to each other only. However, where the adjacent surface transmits radiation (i.e., diathermanous layers), there is radiative heat transfer between the surface in question and the next two adjacent surfaces.

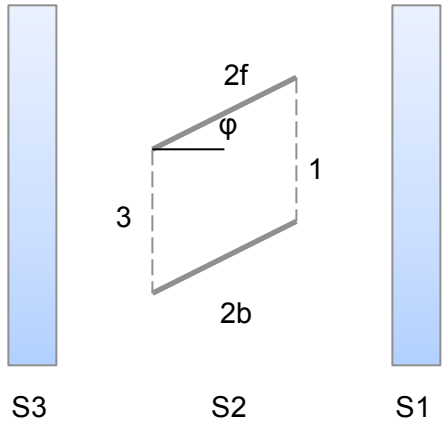

Figure 4.11 Fictitious Cavity for Calculating View Factors with Venetian Blinds

For a surface facing a diathermanous layer, the next two adjacent surfaces are combined into a single equivalent facing surface with a representative temperature and emissivity, based on Walton's mean radiant temperature/balance method (1980). For example, when evaluating S1 in Figure 4.11, the temperature and the emissivity of the equivalent facing surface ($S2_{eq}$) is:

$$T_{S2,eq} = \frac{F_{S1\to S2}\varepsilon_{S2}T_{S2} + F_{S1\to S3}\varepsilon_{S3}T_{S3}}{F_{S1\to S2}\varepsilon_{S2} + F_{S1\to S3}\varepsilon_{S3}} \qquad [K] \qquad \textbf{(4.24)}$$

$$\varepsilon_{S2,eq} = \frac{F_{S1\to S2}\varepsilon_{S2} + F_{S1\to S3}\varepsilon_{S3}}{F_{S1\to S2} + F_{S1\to S3}} \qquad \textbf{(4.25)}$$

Where,

F = angle factor between the two opposing surfaces

For any two solid, parallel layers, the angle factor is unity. For a venetian blind layer, the angle factor between the surfaces can be calculated using the fictitious cavity method developed by Rheault and Bilgen (1987) and used by Park et al. (2004) and Jiru and Haghighat (2008):

$$F_{1\to2} = F_{2\to3} = 2 - \sin\left(\frac{90+\varphi}{2}\right) - \sin\left(\frac{90-\varphi}{2}\right) \quad \textbf{(4.26)}$$

$$F_{1\to3} = \sqrt{2}\cos\left(\frac{\varphi}{2}\right) - 1 \quad \textbf{(4.27)}$$

A roller blind may also transmit longwave radiation, depending on the type of material. Therefore, the user may input a percent openness (O_p), whereby $F_{1\to2} = F_{2\to3}$ = 1 - O_p and $F_{1\to3}$ = O_p.

4.3.4 Thermal Element: Conduction

Conduction is the flow of heat through a material by direct molecular contact, either within a material or between two adjacent materials (Straube & Burnett, 2005). This is the most important mode of heat transfer within solids.

4.3.4.1 Heat flux

Conductive heat flux through a single material may be calculated using Fourier's law:

$$q_{cond} = C\left(T_{S,o} - T_{S,i}\right) \qquad [W/m^2] \quad \textbf{(4.28)}$$

$$C = \frac{k}{l} \qquad [W/m^2] \quad \textbf{(4.29)}$$

Where,

C = thermal conductance [W/m^{2}K]

k = thermal conductivity [W/m·K]

l = length/material thickness [m]

S,o = outer surface

S,i = inner surface

q_{cond} through any nth solid layer is illustrated in Figure 4.12.

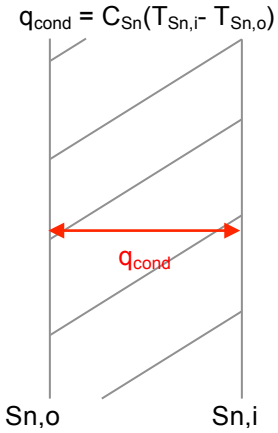

Inputs

Opaque Wall	***Multi Glazing***
• Conductance (C or U)	• Conductance (U) or U–value

Figure 4.12 Conduction Heat Flux

For multi-glazing and opaque walls with more than one material, the overall conductance (U) must be used in place of a single material conductance:

$$q_{cond} = U\left(T_{S,o} - T_{S,i}\right) \qquad [W/m^2] \qquad \textbf{(4.30)}$$

For a system of n+1 layers, U is calculated as:

$$U = \frac{1}{\sum_{i=1}^{n+1} R_i} \qquad [W/m^2K] \qquad \textbf{(4.31)}$$

Where,

R_i = resistance of the i^{th} layer [m^2K/W] = l/k

C and U are user inputs. Note that U should not include surface films (i.e., radiation and convection to the indoor and outdoor environments). For multi-glazing layers, U-values sited by manufacturers or obtained in complex fenestration models do include surface films; therefore, the distinction between U and U-value is made here. For multi-glazing layers, the user has the option to input either U or U-value, and the DoFa model performs the required conversions. (Section 4.3.4.2). Note that the entered U-value should be specified for winter conditions. To improve accuracy, the fenestration product U-value should be used, which accounts for frame effects.

4.3.4.2 Converting U-Value to U

For insulated glazing units (IGUs), the DoFa model requires the conductance of the unit without radiation or convection to the ambient. Therefore, where only U-value is known, Equation (4.32) is used to convert U-value to U.

$$U = \frac{1}{R} = \frac{1}{\left(\frac{1}{U-value} - \frac{1}{h_{int}} - \frac{1}{h_{ext}}\right)} \qquad [W/m^2K] \qquad \textbf{(4.32)}$$

Where,

R = resistance without radiation or convection to the ambient [m^2K/W]

h_{int} = indoor combined convection and radiation heat transfer coefficient [W/m^2K]

h_{ext} = outdoor combined convection and radiation heat transfer [W/m^2K]

Values for h_{int} and h_{ext} are shown in Table 4.2.

Table 4.2 Combined Convection and Radiation Heat Transfer Coefficients for Vertical Surfaces (ASHRAE, 2009)

Surface Location	Properties	h [W/m^2K]
Indoor	ε = 0.9	8.29
	ε = 0.05	3.35
Outdoor	V = 6.7 m/s (winter)	34.0

Where the indoor surface emissivity is between 0.9 and 0.05, the DoFa model interpolates to obtain h_{int}. Where the indoor surface emissivity is below 0.05, the model uses h_{int} = 3.35 W/m^2K, though an emissivity that low is unlikely for an indoor surface.

4.3.5 Thermal Element: Convection

Convection is the transfer of heat by the movement or flow of molecules (fluid) with a change in their heat content, which is important between fluids and solids (Straube & Burnett, 2005).

4.3.5.1 Heat Flux

Convective heat flux between a surface and an adjacent fluid can be expressed using Newton's Law of Cooling, written similarly to radiative and conductive heat flux equations.

$$q_{conv} = h_c(T_S - T_F) \qquad [W/m^2] \qquad \textbf{(4.33)}$$

Where,

h_c = convective heat transfer coefficient [W/m^2K]

T_F = fluid temperature [K]

q_{cond} between any n^{th} solid layer and any j^{th} fluid layer is illustrated in Figure 4.13.

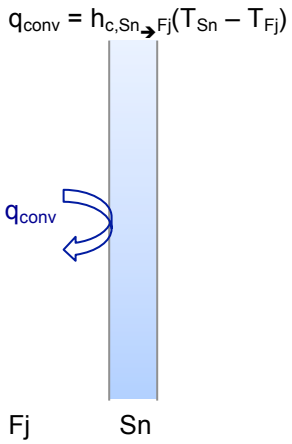

Inputs

Outdoor/Indoor Surfaces	***Cavity Surfaces***
• Wind speed	• Cavity height and depth
• $T_{a,ext}$	• Slat length (venetian blinds)
• $T_{a,in}$	• Type of airflow
• Indoor height	• Mechanical airflow rate (if applicable)
• Slat angle (venetian blinds)	

Figure 4.13 Convection Heat Flux

h_c calculations are different for outdoor/indoor surfaces and cavity surfaces. Detailed calculations are presented in the following sections.

4.3.5.2 Convective Heat Transfer Coefficients for Outdoor/Indoor Surfaces

For surfaces exposed to the outdoor environment, McAdams (1954) recommends that both forced (wind) and natural (buoyancy) convective heat transfer coefficients be calculated, and the larger of the two be used:

$$h_{c,ext} = \max\left(h_{c,for}, h_{c,nat}\right) \qquad [W/m^2K] \qquad \textbf{(4.34)}$$

In general, forced convection is larger. Straube and Burnett (2005) recommend a general coefficient relationship based on wind velocity (V), as per (McAdams, 1954):

$$V = 1 \; to \; 5 \; m/s \qquad h_{c,for} = 5.6 + 3.9V \qquad [W/m^2K] \qquad \textbf{(4.35)}$$

$$V = 5 \; to \; 30 \; m/s \qquad h_{c,for} = 7.2V^{0.78} \qquad [W/m^2K] \qquad \textbf{(4.36)}$$

However, the calculation of wind-induced heat transfer coefficients is not well established and the nature of the flow paths can change the convective coefficient drastically. Wind speed varies significantly (0.2 m/s in calm weather to >29 m/s in storm conditions), so designers often assume seasonal wind speeds of 3.4 m/s in summer and 6.7 m/s in winter (ASHRAE, 2009). In the DoFa model, users can specify a wind speed of 3.4 m/s, 5.0 m/s, 6.7 m/s or user defined. Where a user-defined wind speed is below 1 m/s, a minimum $h_{c,for}$ value of 7.5 W/m^{2}K is used, as suggested by McQuiston et al. (2005) for high-rise buildings.

Although rare, natural convection may exceed forced convection at the outdoor surface on still, sunny days. When solar heating creates a large temperature difference at the surface (~10°C+), natural convection flow can become turbulent (Straube & Burnett, 2005). For turbulent conditions, ASHRAE (2009) recommends the following relation, simplified for air at a mean temperature of 21°C:

$Turbulent \qquad h_{c,nat} = 1.26(\Delta T)^{1/3} \qquad [W/m^2]$ **(4.37)**

Where,

ΔT = temperature difference between the surface and the fluid [K]

A similar equation is used for surfaces exposed to the indoor environment. In this case, a small temperature difference is assumed, resulting in laminar airflow. For laminar conditions, ASHRAE (2009) recommends the following relation, simplified for a mean air temperature of 21°C:

$Laminar \qquad h_{c,int} = 1.46\left(\frac{\Delta T}{L}\right)^{1/4} \qquad [W/m^2]$ **(4.38)**

Where,

L = characteristic length (wall height) [m]

ΔT = temperature difference between the surface and the fluid [K]

Where heating devices are present, the correlations by Khalifa (1989) are used:

$Vertical\ walls, room\ heated\ with\ a\ radiator \qquad h_{c,int} = 2.07\Delta T^{0.23} \qquad [W/m^2]$ **(4.39)**

$Vertical\ walls, room\ heated\ with\ a\ fan \qquad h_{c,int} = 2.92\Delta T^{0.25} \qquad [W/m^2]$ **(4.40)**

However, for both outdoor and indoor convective coefficients, the user can choose to use the calculated value or input their own value. Inputting a known value may be useful in comparing the DoFa model results to other models. NFRC-100 $h_{c,ext}$ values used in WINDOW 6.3 are 15 W/m^{2}K in summer and 26 W/m^{2}K in winter (LBNL, 2011). Designers generally use an $h_{c,int}$ value between 3.2 and 3.6 W/m^{2}K (McQuiston et al., 2005; Carli, Inc., 2006).

Although the DoFa model was not specifically created to model indoor or outdoor shading devices, simple correlations may be used. It is not the intent of this thesis to investigate the convective behaviour of indoor/outdoor shading; therefore, the method presented in Appendix C of ASHRAE RP-1311 and reproduced by Rogalsky (2011) are repeated here. The method uses

a three-resistor network when shading devices are located on the interior or exterior of a glass surface (Figure 4.14).

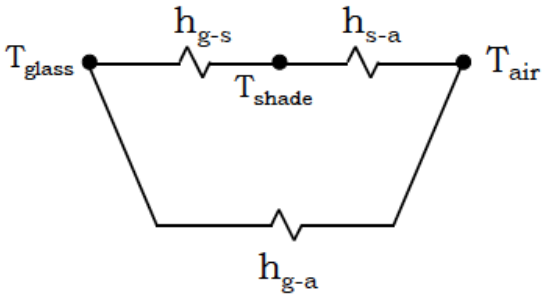

Figure 4.14 Three-Resistor Network for Convective Heat Transfer (Rogalsky, 2011)

The convective coefficient between the glass and shading device (h_{g-s}) is estimated assuming laminar flow parallel to the glass surface:

$$h_{g-s} = \frac{k}{s} \qquad [W/m^2K] \qquad \textbf{(4.41)}$$

Where,

k = air thermal conductivity [W/m·K]

s = spacing between glass and shading layers [m]

Note that the temperature difference in Equation (4.33) now becomes that between the solid surfaces. For convective heat transfer from the surfaces to the air, the following equations are used:

$$h_{g-a} = h_{c,int}\left[1 - exp\left(-4.6\frac{s}{0.1}\right)\right] \qquad [W/m^2K] \qquad \textbf{(4.42)}$$

$$h_{s-a} = h_{c,int}\left[2 - exp\left(-4.6\frac{s}{0.1}\right)\right] \qquad [W/m^2K] \qquad \textbf{(4.43)}$$

Where,

$h_{c,int}$ = reference convective coefficient calculated as per Equation (4.38) [W/m^{2}K]

The transition was scaled assuming that the two boundary layers will not interfere with each other once *s* exceeds 0.1 m (4 inches). Therefore, when s ≥ 0.1 m, $h_{g-a} = h_{c,int}$ and $h_{s-a} = 2h_{c,int}$ (i.e., both surfaces of the shading layer experience $h_{c,int}$). Where venetian blinds are used, additional airflow through the slats may increase h_{s-a} by up to 20%, depending on the slat angle:

$$h_{s-a,venetian} = h_{s-a}(1 + 0.2|sin\,(2\varphi)|) \qquad [W/m^2K] \qquad \textbf{(4.44)}$$

Note that for venetian blinds, the gap spacing (s) is determined as a function of slat angle, assuming the slats are shortened by 30%. For more details of the method, see Rogalsky (2011) and Wright et al. (2008).

For the outdoor surface, $h_{g\text{-}s} = 0$, $h_{g\text{-}a} = h_{c,ext}$ and $h_{s\text{-}a} = 2h_{c,ext}$. These are essentially the same as indoor shading with a large gap spacing. Although it seems likely that the shading device would protect the glass surface from wind and high convection rates, little is known about the influence of spacing between outdoor shading attachments and the window. Therefore, in the absence of additional information, the relationships used in ASHRAE RP-1311 are used here as well. Note that the three-resistor network describes heat transfer between layers not directly adjacent to each other, which is not supported by the calculation method used in this thesis. However, this is overcome by assuming that the cavity temperature between the shading device and glass is at ambient temperature.

4.3.5.3 Convective Heat Transfer Coefficients for Cavity Surfaces

For the DF cavity, the calculation of convection coefficients becomes more complicated. Various researchers have proposed various methods, the simplest being the use of a common value for every surface in the cavity. For example, Zanghirella et al. (2010) did so using Equation (4.35). However, many other researchers have used a more detailed approach, where h_c is calculated for each surface based on empirical information. This is the approach taken here.

The Nusselt number (Nu) is a non-dimensional quantity that relates the temperature difference between the surfaces bounding the gap to the width, height and thermophysical properties of the gap gas (LBNL, 2011). Nu is related to h_c using the following relation (ASHRAE, 2009):

$$Nu_L = \frac{convective\ heat\ transfer}{conductive\ heat\ transfer} = \frac{h_c L}{k} \qquad \textbf{(4.45)}$$

Where,

k = fluid thermal conductivity [W/m·K]

L = characteristic length, dependent on geometry [m]

By definition, the local Nusselt number in cavities is a function of the position along the height of the cavity and may vary locally due to complex inlet geometry or the presence of frames, obstacles and shading devices (Saelens, 2002). Therefore, Saelens (2002) suggests defining

an average or overall Nu, based on the surface averaged heat transfer rate. Formulas for Nu exist assuming either uniform wall temperature (UWT) or uniform heat flux (UHF). Based on experimental data from a single story cavity, Saelens (2002) recommends using UWT formulas during nighttime and periods with low solar radiation, when the vertical temperature gradient is small. However, if the solar radiation is high, the UHF formulas are recommended. Different calculations are used for the various airflow types (natural, enclosed or mechanical). The airflow type is user input.

Natural Airflow

For natural convection, the difference in Nusselt number between UWT and UHF equations is very small (typically below 1.8% for Ra < 10^{12}) (Saelens, 2002). Consequently, only UWT equations were used. Churchill and Chu (1975) developed empirical correlations for wall-averaged heat transfer rates from a vertical wall, which were reproduced by ASHRAE (2009):

$$Nu_{nat,H} = 0.68 + \frac{0.67Ra_H^{1/4}}{[1 + (0.492/Pr)^{9/16}]^{4/9}} \qquad \text{Laminar } regime\ (10^{-1} < Ra < 10^{9}) \qquad \textbf{(4.46)}$$

$$Nu_{nat,H} = \left\{0.825 + \frac{0.387Ra_H^{1/6}}{[1 + (0.492/Pr)^{9/16}]^{8/27}}\right\}^2 \qquad \text{Turbulent } regime\ (10^{9} < Ra < 10^{12}) \qquad \textbf{(4.47)}$$

Where Ra is the Rayleigh number, which is the product of the Prandtl (Pr) and Grashof (Gr) numbers, defined as (ASHRAE, 2009):

$$Ra = (Pr)(Gr) = \left(\frac{c_p \rho v}{k}\right)\left(\frac{\beta g L^3 \Delta T}{v^2}\right) \qquad \textbf{(4.48)}$$

Where,

c_p = specific heat of cavity air [approx. 1005 J/kg·K]

β = coefficient of volumetric thermal expansion [1/K]

g = acceleration of gravity [m/s^2]

v = kinematic viscosity [m^2/s]

ΔT = temperature difference between the surface and the fluid [K]

Pr for air is approximately 0.72 between -50°C and 30°C (Bejan 1993). All air properties are evaluated at the mean of the surface and fluid temperatures except for β, which is estimated at the fluid temperature. Formulas for flat plates are used under the assumption that a DF cavity will have a wide cavity. For the scenarios tested later in this thesis, the wide cavity assumption

held. However, the DoFa model should not be used for very narrow cavities without appropriate modifications.

Enclosed Cavities

For an enclosed cavity, the fluid motion becomes a recirculating flow, where it ascends along the warmer wall and descends along the colder wall. The flow characteristics depend on the aspect ratio (A_r), calculated by:

$$A_r = \frac{H}{s} \qquad \textbf{(4.49)}$$

Where,

H = cavity height [m]

s = cavity depth [m]

Most DF cavities have an aspect ratio between 5 and 40 (Saelens, 2002). For aspect ratios between 2 and 10, Catton (1978) proposed the relation:

$$Nu_s = 0.22\left(\frac{Pr}{0.2 + Pr}Ra_s\right)^{-1/4} \qquad \textbf{(4.50)}$$

For cavities with high aspect ratios, Saelens (2002) recommends using the empirically derived correlations of ElSherbiny et al. (1982):

$$Nu_s = \max\left(Nu^{ct}, Nu^{l}, Nu^{t}\right)$$

Where,

$$Nu^{ct} = \left(1 + \left(\frac{0.104 \cdot Ra_s^{0.293}}{1 + (6310/Ra_s)^{1.36}}\right)^3\right)^{1/3} \quad Conduction \text{ and } turbulent\ transition\ regime \qquad \textbf{(4.51)}$$

$$Nu^{l} = 0.242\left(\frac{Ra_s \cdot s}{H}\right)^{0.273} \quad Laminar\ boundary\ layer\ regime \qquad \textbf{(4.52)}$$

$$Nu^{t} = 0.0605 \cdot Ra_s^{1/3} \quad Turbulent\ boundary\ layer\ regime \qquad \textbf{(4.53)}$$

For enclosed cavity calculations, the characteristic length is the cavity depth and the temperature difference is that between the hot and cold pane. Although unlikely, if the aspect ratio is less than 2, Equation (4.46) or (4.47) is used as for a naturally ventilated cavity.

Forced Airflow

For forced convection, relations for external flows over flat plates (entrance region) or internal flows in ducts (fully developed region) may be used. For laminar flows, the entrance length (y) can be calculated as (Bejan, 1993):

$Flow\ Length$: $$\frac{y_f}{D_h} \cong 0.05 Re_{D_h} \quad \textbf{(4.54)}$$

$Thermal\ Length$: $$\frac{y_{th}}{D_h} \cong 0.05 Re_{D_h} Pr \quad \textbf{(4.55)}$$

Where,

D_h = hydraulic diameter = 2s [m]

Re = Reynolds number

For turbulent flow, the entrance length is much shorter and can be calculated as:

$$\frac{y_f}{D_h} \cong \frac{y_{th}}{D_h} \cong 0.05 Re_{D_h} Pr \quad \textbf{(4.56)}$$

The Reynolds number is defined as the ratio of inertial forces to viscous forces, calculated as (ASHRAE, 2009):

$$Re_L = \frac{VL}{v} \quad \textbf{(4.57)}$$

Where,

V = average fluid velocity [m/s]

Both Saelens (2002) and Jiru et al. (2008) found that the entrance length was higher than a single storey DF. For the entrance length, flat plate correlations are used for isothermal walls (ASHRAE, 2009):

$Nu_{for,H} = 0.664 Re_H^{1/2} Pr^{1/3}$ $\quad Laminar$ boundary $layer$ $(Re_H < 5\times10^5)$ **(4.58)**

$Nu_{for,H} = 0.0296 Re_H^{4/5} Pr^{1/3}$ $\quad Turbulent$ boundary $layer$ $(Re_H > 5\times10^5)$ **(4.59)**

Where the entrance length is exceeded, duct correlations are used. For fully developed laminar flows between parallel plates, Bejan (1993) gives the following UHF correlation:

$Nu_{for,D_h} = 8.235$ $\quad Laminar\ Flow$ $(Re_{D_h} < 2300)$ **(4.60)**

For fully developed turbulent flows, ASHRAE (2009) gives the following UHF correlation:

$Nu_{for,D_h} = 0.023 Re_{D_h}^{4/5} Pr^x$ $\quad Turbulent\ Flow$ $(Re_{D_h} \geq 10000)$ **(4.61)**

Where,

x = 0.3 when the fluid is cooled and n = 0.4 when the fluid is heated

Where flow is laminar for the entrance region ($Re_H < 5x10^5$) but turbulent for the developed region ($Re_{Dh} > 2300$), Saelens suggests combining Equations (4.58) and (4.59) for the average Nu valid for lengths that exceed the transition length:

$$Nu_{for,H} = 0.664 Re_y^{1/2} Pr^{1/3} + 0.0296 \left(Re_y^{4/5} - Re_y^{4/5} \right) Pr^{1/3} \quad \textbf{(4.62)}$$

Where,

Re_y = Reynolds number at the position of transition, as per Equation (4.56)

However, natural convection is also present, which may either assist or oppose the forced convection. Under the presumption that either natural or forced convection is strongly dominant, the maximum of the two Nu values is used.

Shading Devices

Where shading devices are used in the cavity space, Gratia and De Herd (2007) treat roller blinds and venetian blinds in the same manner, automatically increasing the convection coefficient by 4/3 for the gas layer adjacent to the blind to “allow for the effects of convection currents in the larger gas space enclosing the blind”. For roller blinds, Sealens (2002) treats them as any other solid layer in the façade cavity. For venetian blinds, Jiru & Haghighat (2008) suggest that the convective heat transfer between the cavity air and the slats may be estimated by assuming the slats as cylinders in cross flow, since both sides of the slats are heated or cooled.

In the DoFa model, roller blinds and closed venetian blinds (φ=90) are treated as any other solid layer. For open venetian blinds, equations for cylinders in cross flow are used. For natural convection, ASHRAE (2009) recommends the equation of Churchill and Chu (1975):

$$Nu_{Nat,D} = \left\{ 0.6 + \frac{0.387 Ra_D^{1/6}}{[1 + (0.559/Pr)^{9/16}]^{8/27}} \right\}^2 \quad 10^9 < Ra_D < 10^{13} \quad \textbf{(4.63)}$$

Where the Rayleigh number lies outside the specified range, Nu found by Equation (4.46) or (4.47) is multiplied by 4/3 as suggested by Gratia and De Herde (2007). For forced convection, ASHRAE (2009) recommends the equation of Churchill and Bernstein (1977):

$$Nu_{For,D} = 0.3 + \frac{0.62 Re_D^{1/2} Pr^{1/3}}{[1 + (0.4/Pr)^{2/3}]^{1/4}} \left[1 + \left(\frac{Re_D}{282\,000}\right)^{5/8}\right]^{4/5} \quad \textbf{(4.64)}$$

Where the characteristic length used to calculate the Rayleigh and Reynolds numbers is the diameter (D) (i.e. slat length). For forced airflow, the maximum of Equations (4.63) and (4.64) is used. For enclosed cavities, blind layers are treated as any other solid layer. Note that modeling venetian blinds is not the main focus of this thesis and should be investigated further to ensure accurate results.

4.3.6 Airflow Element

Any airflow through the cavity will either add or remove heat from the system depending on the origin and destination of the airflow. Note that heat loss/gain due to airflow is measured in heat flow (W) instead of heat flux (W/m^2). When calculating natural airflow, only buoyancy forces are considered.

4.3.6.1 Heat Flow

Heat flow due to airflow within a cavity may be estimated as (McQuiston et al., 2005):

$$Q_{airflow} = c_p \dot{m}_a (T_{inlet} - T_{cav}) \quad \text{[W]} \quad \textbf{(4.65)}$$

Where,

c_p = specific heat of cavity air [approx. 1005 J/kg·K]

m_a = mass flow rate of the air [kg/s], calculated by:

$$\dot{m}_a = \rho \dot{Q} \quad \text{[kg/s]} \quad \textbf{(4.66)}$$

Where,

ρ = average density of the cavity air [kg/m^3]

$\dot{Q}$ = volumetric flow rate [m^3/s]

$Q_{airflow}$ for any jth fluid layer is illustrated in Figure 4.15.

$$Q_{airflow} = c_p \dot{m}_{a,Fj}(T_{inlet,Fj} - T_{Fj})$$

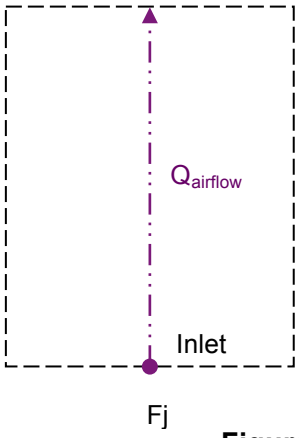

Inputs

Mechanical Airflow	***Natural Airflow***
• Airflow path	• Airflow path
• Airflow rate	• Height of cavity
	• Height to midpoint of vents
	• Vent Areas
	• Dischange coefficients
	• Cavity connections (shading devices)

Figure 4.15 Airflow Heat Flow

Detailed calculations for $\dot{Q}$ are presented in the following section.

4.3.6.2 Volumetric Airflow Rate

Airflow within a DF cavity can be natural or mechanical. For mechanical airflow, $\dot{Q}$ is a known input and the calculation is straightforward. For natural airflow, $\dot{Q}$ is induced by a pressure difference between the inlet and outlet. This may be due to natural buoyancy or wind effects. For the purposes of this study, only natural buoyancy is considered. Various authors have made the same simplification (Von Grabe, 2002; Balocco, 2002; Faggembauu et al., 2003).

Wind effects are difficult to predict accurately because the distribution of local wind pressure coefficients over the building surface depends on the building shape, wind direction, nearby buildings and terrain features (Saelens, 2002). Also, available wind speeds are typically from a local weather station that is at a different height with different shelter effects than the building in question. Furthermore, a main goal of the DoFa model is to evaluate performance under design conditions. The summer design case would generally be in still conditions, when the risk of overheating is highest. The winter design case would be in windy conditions, though the cavity would be closed and wind pressure would have no effect. For annual simulations, Saelens (2002) found that the influence of wind is relatively small. Hensen at al. (2002) found that on a summer day, the effect of wind on the cooling demand was less than 1%. Therefore, wind effects were omitted on the basis of added complexity for little to no added accuracy.

Natural buoyancy in buildings, also known as the stack effect, is caused by a decrease in density as air is heated. The heated air rises towards the outlet, hence reducing the pressure at the inlet where cooler air is sucked in. The pressure difference caused by natural buoyancy (ΔP_s) can be calculated as (ASHRAE, 2009):

$$\Delta P_s = (\rho_{inlet} - \rho_{cav})gh = \rho_{inlet} gh \left(\frac{T_{cav} - T_{inlet}}{T_{cav}}\right) \quad \text{[Pa]} \qquad \textbf{(4.67)}$$

Where,

ρ = air density [kg/m^3]

g = gravitational constant [9.81 m/s^2]

h = height to neutral pressure plane [m]

Note that the above equation, as well as all other equations in this section, neglects vertical density gradients in the cavity. In reality, there is an exponential density and temperature gradient. Therefore, the average cavity temperature and density are used here, as recommended by ASHRAE (2009) when there is vertical stratification. Where a cavity is separated into two shafts by a shading device, the average temperature of the two shafts is used. For each cavity, the user must specify whether it is connected to another cavity or not.

The height to the neutral pressure plane (*h*) is measured from the midpoint of the lower opening, calculated as (Andersen, 1995):

$$h = \frac{H}{1 + (T_{cav}/T_{inlet})(C_{d1}/C_{d2})^2 (A_1/A_2)^2} \quad \text{[m]} \qquad \textbf{(4.68)}$$

Where,

H = height between the inlet and outlet [m]

C_d = discharge coefficient of opening

A = area of opening [m^2]

The subscripts 1 and 2 refer to the lower and upper openings respectively. Note that greatest flow per unit area of openings is obtained when inlet and outlet areas are equal, corresponding to a neutral pressure plane at approximately half the cavity height. The C_d value is user input, discussed later in this section.

The flow rate through a large intentional opening can be calculated using a relationship based on the Bernoulli equation with steady, incompressible flow. ASHRAE (2009) recommends the following general equation that may include stack, wind, and mechanical ventilation pressures:

$$\dot{Q} = C_{d1} A_1 \sqrt{\frac{2\Delta P}{\rho_{inlet}}} \qquad [m^3/s] \qquad \textbf{(4.69)}$$

Where,

ΔP = pressure difference across the opening [Pa]

Therefore, combining Equations (4.67) and (4.69) gives a relation for flow caused by thermal buoyancy only:

$$\dot{Q} = C_{d1} A_1 \sqrt{\frac{2gh(|T_{cav} - T_{inlet}|)}{T_{cav}}} \qquad [m^3/s] \qquad \textbf{(4.70)}$$

Equation (4.70) is valid when $T_{cav}>T_{inlet}$. If $T_{cav}<T_{inlet}$, T_{cav} is replaced with T_{inlet} in the denominator. The discharge coefficient (C_d) is a dimensionless number that accounts for all viscous effects such as surface drag and interfacial mixing (ASHRAE, 2009). The C_d value depends on the type of opening and nature of flow. Gratia and DeHerde (2007) use a value of 0.61, which is for turbulent flow through a circular sharp-edged orifice. ASHRAE (2009) recommends a value of 0.65 for unidirectional stack-driven airflow through an orifice.

Instead of a C_d value, various authors have used loss factors from mechanical engineering tables (Balocco, 2002; von Grabe, 2002; Yuan et al, 2007). Loss factors are used to account for friction as well as losses at the inlet, outlet, bends and reductions in the hydraulic diameter of the cavity (i.e., frames, shading devices, etc.). However, von Grabe (2002) discusses the difficulties of modeling natural ventilation using loss factors, stating that doing so can produce wrong results. Since loss factors were developed for symmetric velocity profiles occurring in pipes, they do not necessarily translate to non-symmetric velocity profiles occurring in naturally ventilated cavities. Therefore, no additional loss factor was added here. While friction effects are expected to be limited due to the cavity width, obstructions and geometry (e.g., shading devices, protruding window frames, etc.) may be more important. However, more experimental and field research efforts are needed to investigate loss factors for naturally ventilated façades. At present, any additional cavity resistance should be included in the C_d value.

Similarly, when a shading device divides a cavity in two, the flow distribution depends on the flow resistance of each shaft (i.e., friction, obstructions and geometry). In experimental results, Saelens (2002) found that most of the air flows through the exterior shaft, though the distribution

was hard to measure. Results depend highly on the specific design of the DF; consequently, it is assumed here that the flow distribution is proportional to the depth distribution (i.e., the velocity will be the same in both shafts). However, the distribution may be altered by the user if one shaft is known to have a higher resistance. Furthermore, the DoFa model assumes no airflow between shafts, which Saelens (2002) proved accurate for roller blinds. However, venetian blinds, in any position other that closed, would allow airflow between shafts. Consequently, venetian blinds should be modeled with caution with special attention to the flow distribution. Finally, airflow in both shafts is assumed to be in the same direction.

4.4 Temperature Profile

In order to obtain the temperature profile through the façade, energy balances are performed on each individual component. Once the equations are formulated, the temperature of each surface is calculated with the iterative solution method. The possible components of a DF system are: 1) single glazing, 2) shading (or other lightweight non-glazing elements, 3) multi-glazing, 4) opaque wall, and 5) air cavity. Any number of layers may be included in any configuration.

4.4.1 Single Glazing and Shading

Single glazing and shading layers are treated in the same manner. Because these layers have minimal thickness and thermal resistance, the entire layer is assumed to be at a single temperature (i.e., no temperature gradient in the x-direction). Required inputs for the energy balance are the optical properties and emissivities of the outer and inner surfaces. Generally, unless there is a special coating, the inner and outer surface properties are the same. Figure 4.16 shows the different modes of heat transfer important to an energy balance for any n^{th} uniform temperature layer in a DF, where the j^{th} fluid is on the inner side and the j+1 fluid is on the outer side.

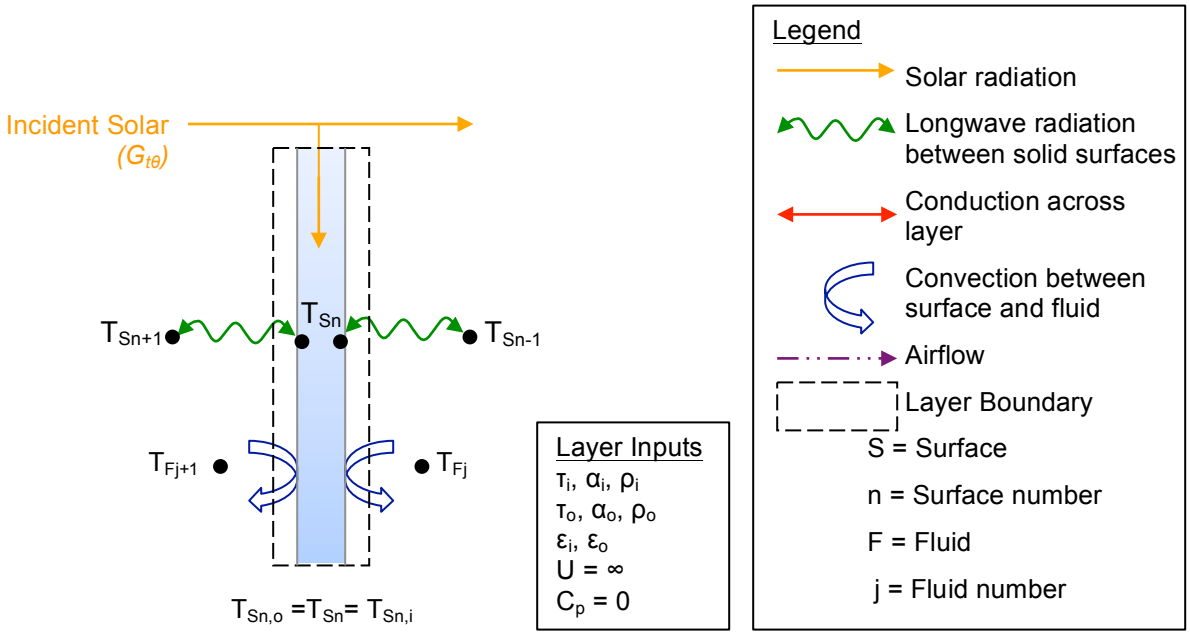

Figure 4.16 Uniform Temperature Layer Energy Balance

The energy balance on this layer is:

$$0 = G_{t\theta}\alpha_{e,Sn} + h_{r,Sn\to Sn-1}(T_{Sn-1} - T_{Sn}) + h_{r,Sn\to Sn+1}(T_{Sn+1} - T_{Sn}) + h_{c,Sn\to Fj}(T_{Fj} - T_{Sn}) + h_{c,Sn\to Fj+1}(T_{Fj+1} - T_{Sn}) \quad \textbf{(4.71)}$$

The temperature of the layer can be solved by rearranging Equation (4.71):

$$T_{Sn} = \frac{G_{t\theta}\alpha_{e,Sn} + h_{r,Sn\to Sn-1}T_{Sn-1} + h_{r,Sn\to Sn+1}T_{Sn+1} + h_{c,Sn\to Fj}T_{Fj} + h_{c,Sn\to Fj+1}T_{}}{h_{r,Sn\to Sn-1} + h_{r,Sn\to Sn+1} + h_{c,Sn\to Fj} + h_{c,Sn\to Fj+1}} \quad [K] \quad \textbf{(4.72)}$$

Note that effective absorptance (α_e) includes reflected solar radiation and considers direct and diffuse portions separately, as per Section 4.3.2.

4.4.2 Multi-Glazing

For multi-glazing layers, there is sufficient thickness and resistance to cause a temperature gradient in the x-direction. Therefore, conduction is incorporated and the inner and outer surfaces of the layer are considered at different temperatures. An energy balance must then be performed on the inner and outer surfaces separately. Required inputs for the energy balance are the optical properties of the inner and outer surfaces of each pane, the emissivities of the

innermost and outermost surfaces and the effective conductance (U) or U-value of the glazing unit.

For more accurate results, the glazing product U-value, including the frame, should be used. Figure 4.17 shows the different modes of heat transfer important to an energy balance for any n^{th} multi-glazing layer in a DF. Note that a multi-glazing layer could have any number of panes, as long as the optical properties of each pane and the overall U-value of the unit are known.

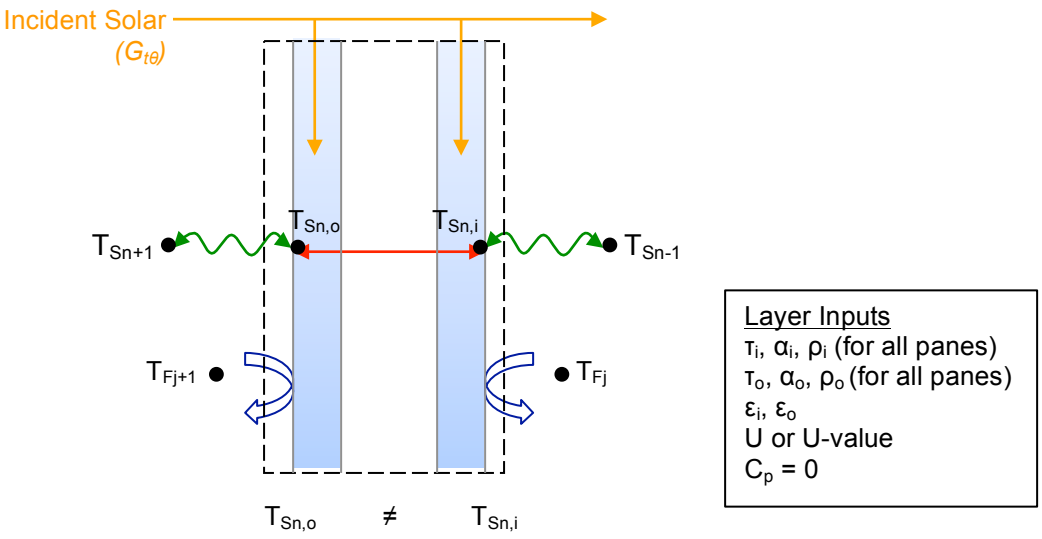

Figure 4.17 Non-Uniform Temperature Layer Energy Balance (Transparent)

The energy balances for the inner and outer surfaces are:

$$0 = G_{t\theta}\alpha_{e,Sn,i} + h_{r,Sn,i\to Sn-1}\left(T_{Sn-1} - T_{Sn,i}\right) + U_n\left(T_{Sn,o} - T_{Sn,i}\right) + h_{c,Sn,i\to Fj}\left(T_{Fj} - T_{Sn,i}\right) \quad \textbf{(4.73)}$$

$$0 = G_{t\theta}\alpha_{e,Sn,o} + h_{r,Sn,o\to Sn+1}\left(T_{Sn+1} - T_{Sn,o}\right) + U_n\left(T_{Sn,i} - T_{Sn,o}\right) + h_{c,Sn,o\to Fj}\left(T_{Fj+1} - T_{Sn,o}\right) \quad \textbf{(4.74)}$$

The inner and outer surface temperatures can be solved by rearranging Equations (4.29) and (4.33) respectively:

$$T_{Sn,i} = \frac{G_{t\theta}\alpha_{e,Sn,i} + h_{r,Sn,i\to Sn-1}T_{Sn-1} + U_nT_{Sn,o} + h_{c,Sn,i\to Fj}T_{Fj}}{h_{r,Sn,i\to Sn-1} + U_n + h_{c,\mathrm{Sn},i\to Fj}} \quad [\mathrm{K}] \quad \textbf{(4.75)}$$

$$T_{Sn,o} = \frac{G_{t\theta}\alpha_{e,Sn,o} + h_{r,Sn,o\to Sn+1}T_{Sn+1} + U_nT_{Sn,i} + h_{c,Sn,o\to Fj}T_{Fj+1}}{h_{r,Sn,o\to Sn+1} + U_n + h_{c,Sn,o\to Fj}} \quad [\mathrm{K}] \quad \textbf{(4.76)}$$

4.4.3 Opaque Wall

An opaque wall can be treated in the same manner as a multi-glazing layer, with the exception that no solar radiation is transmitted. Required inputs for the energy balance are simply the outer surface optical properties, the inner and outer surface emissivities and the wall conductance (U). Note that when calculating U, surface films should be omitted. Figure 4.18 shows the different modes of heat transfer important to an energy balance for any n^{th} opaque wall layer in a DF.

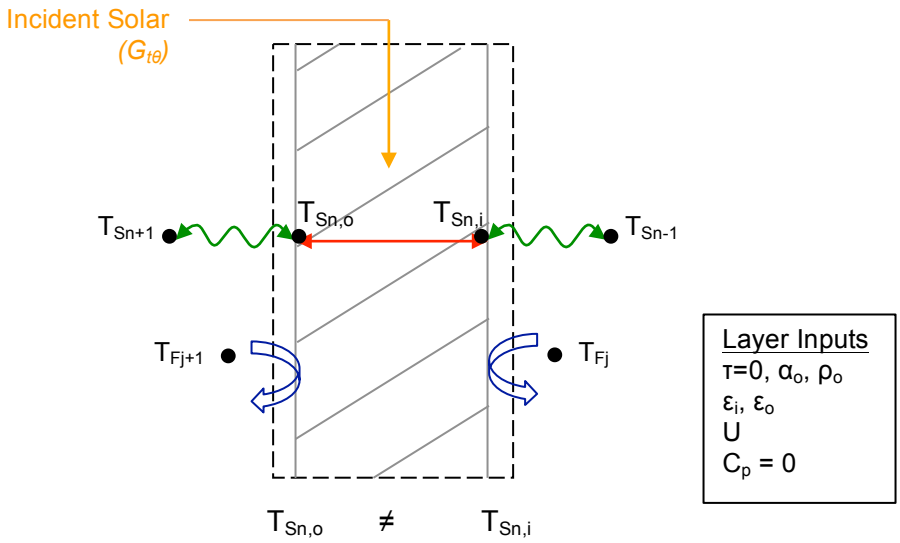

Figure 4.18 Non-Uniform Temperature Layer Energy Balance (Opaque)

The energy balance for the outer surface is the same as for a multi-glazing layer. For the inner surface, the energy balance becomes:

$$0 = G_{t\theta}\alpha_{e,Sn,o} + h_{r,Sn,o\to Sn+1}\left(T_{Sn+1} - T_{Sn,o}\right) + U_n\left(T_{Sn,i} - T_{Sn,o}\right) + h_{c,Sn,o\to Fj}\left(T_{fl,j+1} - T_{Sn,o}\right) \quad \textbf{(4.77)}$$

The inner surface temperature can be solved by rearranging Equation (4.77):

$$T_{Sn,i} = \frac{h_{r,Sn,i\to Sn-1}T_{Sn-1} + U_n T_{Sn,o} + h_{c,Sn,i\to Fj}T_{Fj}}{h_{r,Sn,i\to Sn-1} + U_n + h_{c,Sn,i\to Fj}} \quad [K] \quad \textbf{(4.78)}$$

Note that this assumes that no solar radiation is reflected from the room onto the inner wall surface. This is not in fact true, though the simplification is expected to have a minor impact. Also, thermal mass is neglected. This simplification will have a relatively larger impact, though thermal mass adds complexity beyond the scope of this thesis. Therefore, caution should be used when modeling opaque elements with considerable thermal mass.

4.4.4 Air Cavity

For a cavity layer with open vents, both solar and longwave radiation travel straight through. The cavity average temperature is affected by convection with its bounding surfaces and airflow. Figure 4.19 shows the different modes of heat transfer for any j^{th} fluid layer enclosed by surfaces n and n+1. The only required input for the energy balance is the inlet temperature (i.e., inlet source). The mass flow rate is calculated as per Section 4.3.6.1.

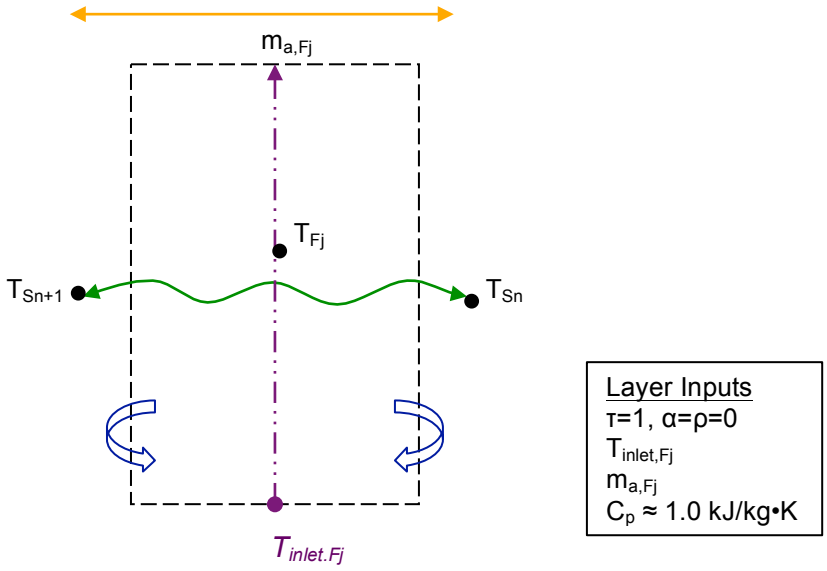

Figure 4.19 Cavity Energy Balance (Open Vents)

The energy balance for an open fluid layer is:

$$0 = A_{Sn}h_{c,Sn\rightarrow Fj}\left(T_{Sn} - T_{Fj}\right) + A_{Sn+1}h_{c,Sn+1\rightarrow Fj}\left(T_{Sn+1} - T_{Fj}\right) + \dot{m}_{a,Fj}c_p(T_{inlet,Fj} - T_{Fj}) \qquad \textbf{(4.79)}$$

The average air temperature can be solved by rearranging Equation (4.79):

$$T_{Fj} = \frac{A_{Sn}h_{c,Sn\rightarrow Fj}T_{Sn} + A_{Sn+1}h_{c,Sn+1\rightarrow Fj}T_{Sn+1} + \dot{m}_{a,Fj}c_pT_{inlet,Fj}}{A_{Sn}h_{c,Sn\rightarrow Fj} + A_{Sn+1}h_{c,Sn+1\rightarrow Fj} + \dot{m}_{a,Fj}c_p} \quad [K] \qquad \textbf{(4.80)}$$

Where the vents are closed and no airflow occurs in or out of the cavity, only convection is considered (Figure 4.20).

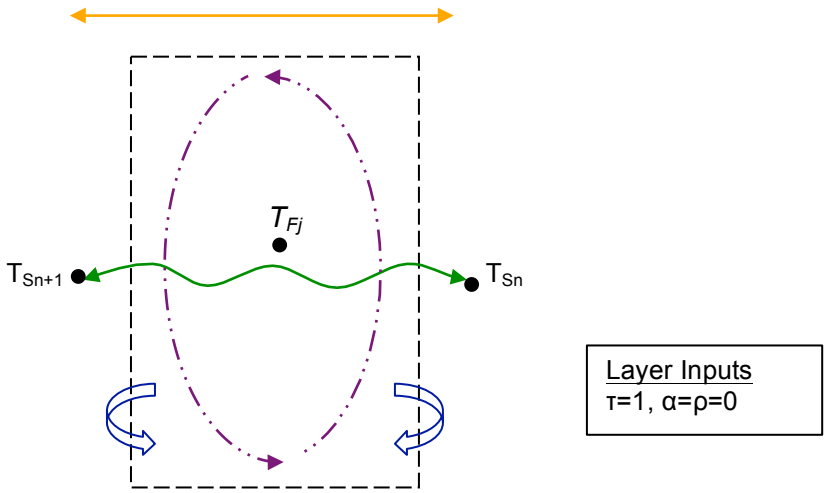

Figure 4.20 Cavity Energy Balance (Closed Vents)

The energy balance for a sealed fluid layer is:

$$0 = A_{Sn}h_{c,Sn\rightarrow Fj}\left(T_{Sn} - T_{Fj}\right) + A_{Sn+1}h_{c,Sn+1\rightarrow Fj}\left(T_{Sn+1} - T_{Fj}\right) \qquad \textbf{(4.81)}$$

The average air temperature can be solved by rearranging Equation (4.81):

$$T_{Fj} = \frac{A_{Sn}h_{c,Sn\rightarrow Fj}T_{Sn} + A_{Sn+1}h_{c,Sn+1\rightarrow Fj}T_{Sn+1}}{A_{Sn}h_{c,Sn\rightarrow Fj} + A_{Sn+1}h_{c,Sn+1\rightarrow Fj}} \quad [\text{K}] \qquad \textbf{(4.82)}$$

4.4.5 Assembled Example

To demonstrate the procedure of building a DF using the DoFa model, take for example, a DF comprised of a brick masonry interior, a roller blind and a double-glazed exterior. The heat flux across the façade may be depicted as shown in Figure 4.21.

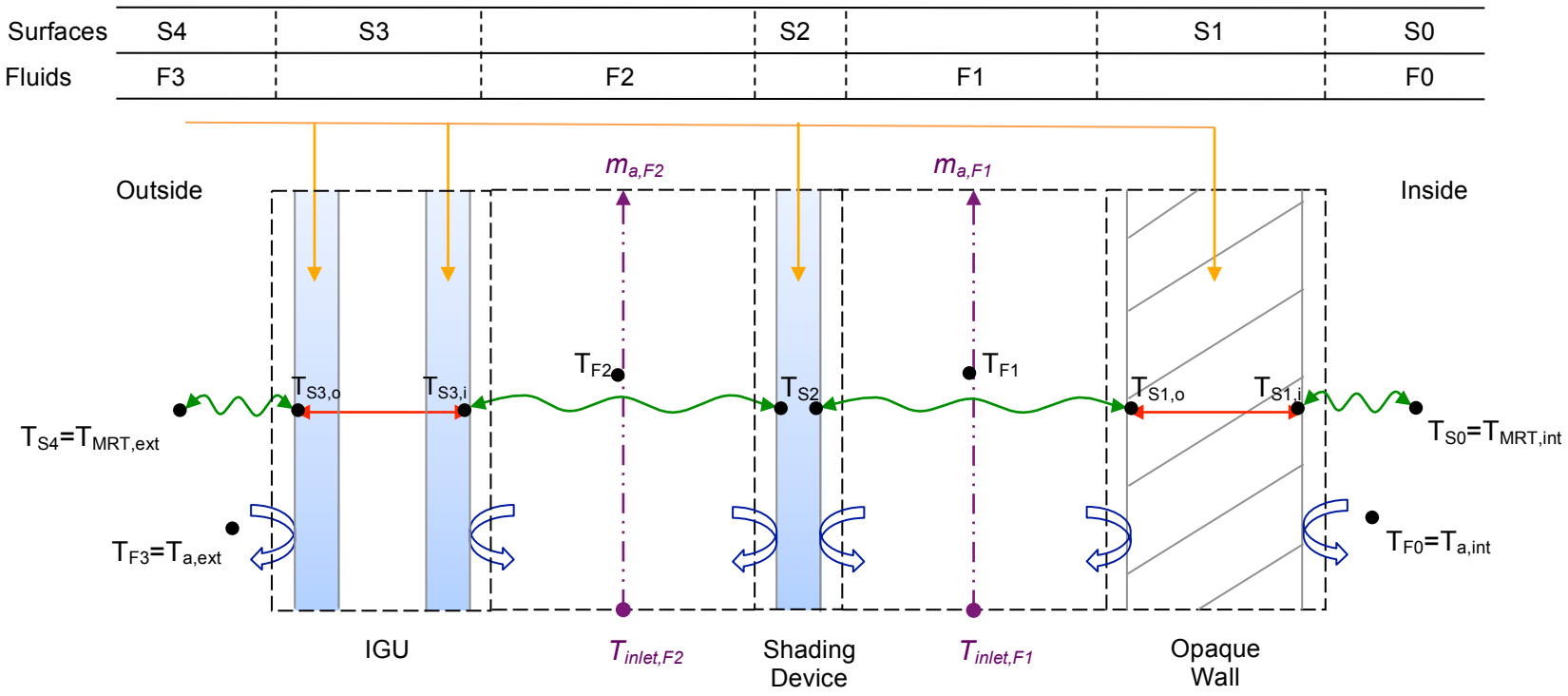

Figure 4.21 Example Layer Addition

The temperature equations are, from the innermost surface to the outermost surface:

$$T_{S1,i} = \frac{h_{r,S1\to S0}T_{MRT,int} + C_1 T_{S1,o} + h_{c,S1\to F0}T_{a,int}}{h_{r,S1\to S0} + C_1 + h_{c,S1\to F0}} \quad [K] \quad \textbf{(4.83)}$$

$$T_{S1,o} = \frac{G_{t\theta}\alpha_{e,S1,o} + h_{r,S1\to S2}T_{S2} + C_1 T_{S1,i} + h_{c,S1\to F1}T_{F1}}{h_{r,S1\to S2} + C_1 + h_{c,S1\to F1}} \quad [K] \quad \textbf{(4.84)}$$

$$T_{F1} = \frac{A_{S1}h_{c,S1\to F1}T_{S1,o} + A_{S2}h_{c,S2\to F1}T_{S2} + \dot{m}_{a,F1}c_p T_{inlet,F1}}{A_{S1}h_{c,S1\to F1} + A_{S2}h_{c,S2\to F1} + \dot{m}_{a,F1}c_p} \quad [K] \quad \textbf{(4.85)}$$

$$T_{S2} = \frac{G_{t\theta}\alpha_{e,S2} + h_{r,S1\to S2}T_{S1,o} + h_{r,S2\to S3}T_{S3,i} + h_{c,S2\to F1}T_{F1} + h_{c,S2\to F2}T_{F2}}{h_{r,S1\to S2} + h_{r,S2\to S3} + h_{c,S2\to F1} + h_{c,S2\to F3}} \quad [K] \quad \textbf{(4.86)}$$

$$T_{F2} = \frac{A_{S2}h_{c,S2\to F2}T_{S2} + A_{S3}h_{c,S3\to F2}T_{S3,i} + \dot{m}_{a,F2}c_p T_{inlet,F2}}{A_{S2}h_{c,S2\to F2} + A_{S3}h_{c,S3\to F2} + \dot{m}_{a,F2}c_p} \quad [K] \quad \textbf{(4.87)}$$

$$T_{S3,i} = \frac{G_{t\theta}\alpha_{e,S3,i} + h_{r,S2\to S3}T_{S2} + U_3 T_{S3,o} + h_{c,S3\to F2}T_{F2}}{h_{r,S2\to S3} + U_3 + h_{c,S3\to F2}} \quad [K] \quad \textbf{(4.88)}$$

$$T_{S3,o} = \frac{G_{t\theta}\alpha_{e,S3,o} + h_{r,S3\to S4}T_{MRT,ext} + U_3 T_{S3,i} + h_{c,S3\to F3}T_{a,ext}}{h_{r,S3\to S4} + U_3 + h_{c,S3\to F3}} \quad [K] \quad \textbf{(4.89)}$$

This leaves 7 equations and 19 unknowns (temperatures, heat transfer coefficients and airflow rates). All calculations are interdependent, hence requiring the iterative calculation method. Once solved, the temperature profile through the assembly is known. The temperature profile output for the described assembly on a sunny summer day would resemble Figure 4.22.

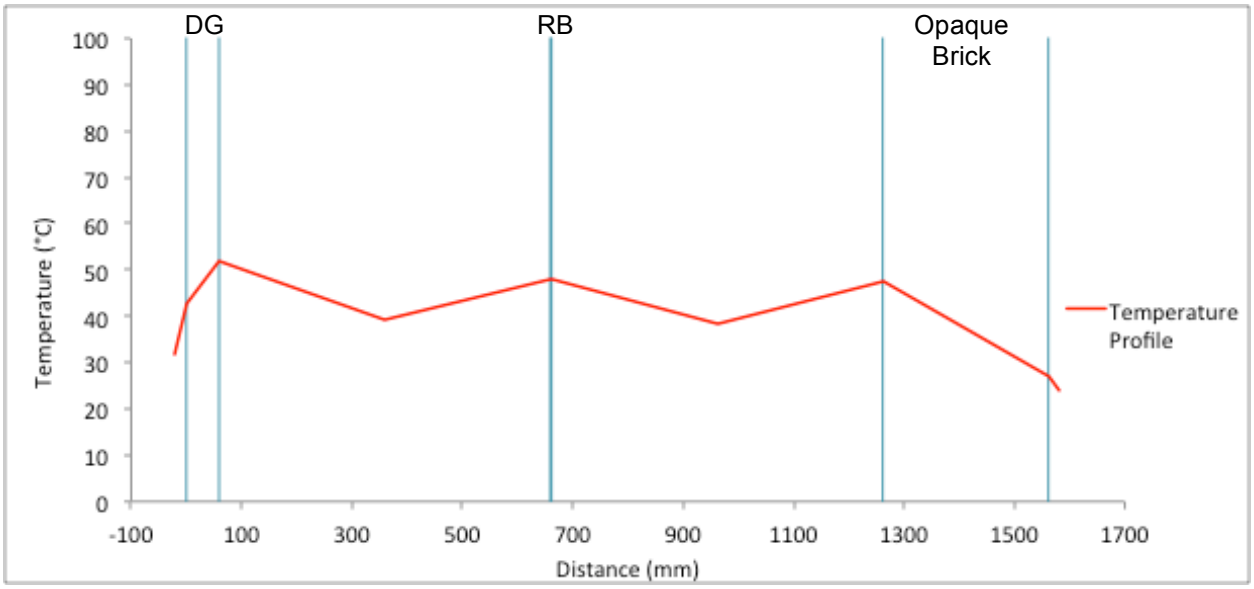

Figure 4.22 Temperature Profile Example

4.5 Additional Outputs

From the temperature profile through the assembly, important performance indices may be determined. In the energy balance calculations, each layer temperature is determined along with the cavity airflow rate. The remaining desired outputs are inflowing heat flux, U-value, SHGC, cavity outlet temperature and condensation risk. These are discussed in the following sections.

4.5.1 Inflowing Heat Flux

Inflowing heat flux is an important measure for design teams. It allows them to determine the heating or cooling load of a building under certain environmental conditions, such as design conditions for sizing HVAC equipment. The basic equation for steady state heat flux through a fenestration product, as presented by ASHRAE (2009), is:

$$q_{in} = U\text{-}value\left(T_{a,ext} - T_{a,int}\right) + (SHGC)G_t \qquad [W/m^2] \qquad \textbf{(4.90)}$$

Where,

U-value = total assembly U-value including surface films [W/m^2K]

SHGC = total assembly Solar Heat Gain Coefficient

The first term of Equation (4.90) deals with heat transfer caused by an indoor/outdoor temperature difference, assuming no sunlight, air infiltration or moisture condensation. The second term deals with solar heat gain, separated into directly and indirectly transmitted solar radiation (i.e., the inward flowing fraction of absorbed solar radiation). U-value and SHGC are steady-state performance indices commonly used to evaluate fenestration products.

4.5.2 U-value and Solar Heat Gain Coefficient

Design teams often use U-value and SHGC as a measure of performance to compare alternative design solutions. These performance indices can be used as stand-alone indicators or as inputs in whole building annual energy simulations. However, U-value and SHGC for typical enclosures depend largely on material properties and thickness of the assembly layers. For a DF assembly, system properties become important as well, such as the airflow path and rate, the position of the shading device, etc (Saelens, 2002). Therefore, the U-value and SHGC calculated for a DF signify performance under specific environmental conditions only, not to be

used in annual simulations. Potential use of U-value and SHGC outputs in whole building energy models is discussed in Chapter 7.

Within the DoFa model, the U-value [W/m^{2}K] of a DF system is calculated using the heat flux from the indoor surface as a reference. The calculation assumes zero solar radiation ($G_{t\theta}$=0); therefore, heat flux to/from all layers is equal.

$$\textit{U-value} = \frac{q_{th,Gt=0}}{\left(T_{a,out} - T_{a,in}\right)} = \frac{h_{r,S1\rightarrow S0}\left(T_{S1,i} - T_{MRT,in}\right) + h_{c,S1\rightarrow F0}\left(T_{S1,i} - T_{a,in}\right) + q_{airflow}}{\left(T_{a,out} - T_{a,in}\right)} \quad \textbf{(4.91)}$$

Where,

$q_{th,Gt=0}$ = heat flux due to indoor/outdoor temperature difference [W/m^2]

Where air flows from the cavity to the indoor environment, heat flux due to airflow ($q_{airflow}$) must be considered. This is calculated using Equation (4.65), though the temperature difference becomes that between the cavity outlet and the indoor environment:

$$q_{airflow} = \frac{c_p \dot{m}_a (T_{outlet} - T_{a,int})}{A} \quad [\text{W/m}^2] \quad \textbf{(4.92)}$$

Where,

A = heat transfer area (i.e., indoor wall area) [m^2]

Air properties are taken at T_{outlet}. For indoor shading, the cavity between the shading device and the glass would technically be vented to the indoor environment. However, it is assumed that this cavity air is at indoor conditions and extra heat flux due to airflow is included in the additional convection coefficients to the indoor environment (Section 4.3.5.2).

The SHGC is the ratio of solar heat flux that enters the building to that incident on the outdoor surface:

$$SHGC = \frac{q_{dir} + q_{ind}}{G_t} \quad \textbf{(4.93)}$$

Where,

q_{dir} = direct solar heat flux [W/m^2]

q_{ind} = indirect solar heat flux [W/m^2]

The direct portion is easily calculated and depends only on the optical properties of the assembly.

$$q_{dir} = \alpha_{e,0,d} G_d + \alpha_{e,0,D\theta} G_{D\theta} \quad [\text{W/m}^2] \quad \textbf{(4.94)}$$

Where,

$\alpha_{e,0}$ = effective absorptance of the room (i.e., the overall transmittance of the assembly)

Where properties are assumed equal for direct and diffuse radiation, the two terms in Equation (4.94) may be combined. The indirect portion consists of the absorbed portion of the incoming radiation that is subsequently conducted, convected or radiated to the interior of the building. This is the difference between the thermal inflowing heat flux for the boundary conditions and that when the solar radiation is set to zero.

$$q_{ind} \cong q_{th,Gt} - q_{th,Gt=0} \qquad \textbf{(4.95)}$$

Both heat fluxes in Equation (4.95) are calculated from the indoor surface to the room.

4.5.3 Outlet Cavity Temperature

The temperature profile in the cavity is assumed to be exponential, which is the expected temperature profile for a ventilated cavity (Saelens, 2002). The cavity temperature at any given distance from the inlet is calculated as per (Carli, Inc., 2004), which is referenced by WINDOW 6.3 (LBNL, 2011):

$$T_{Fj}(y) = T_{m,j} - (T_{m,j} - T_{Fj,inlet})e^{-y/H_{0,j}} \qquad \text{[K]} \qquad \textbf{(4.96)}$$

Where,

y = height above inlet [m]

$T_{m,j}$ = average temperature of the surfaces bounding the glazing cavity [K], given as:

$$T_{avg,j} = \frac{T_{Sn} + T_{Sn+1}}{2} \qquad \text{[K]} \qquad \textbf{(4.97)}$$

Where,

$H_{0,j}$ = characteristic height (temperature penetration length) [m], defined by:

$$H_{0,j} = \frac{\rho_j c_p s_j V_j}{h_{c,Sn\rightarrow Fj} + h_{c,Sn+1\rightarrow Fj}} \qquad \text{[K]} \qquad \textbf{(4.98)}$$

Where,

ρ_j = density of air at average cavity temperature T_{fj} [K]

c_p = specific heat capacity of the air [1005 J/kg·K]

s_j = width of the j^{th} cavity [m]

V_j = mean velocity in the j^{th} cavity [m/s]

To find the outlet temperature, the height (y) in Equation (4.96) is set as the outlet height (H_j):

$$T_{Fj,outlet} = T_{avg,j} - (T_{avg,j} - T_{Fj,\text{inlet}})e^{-H_j/H_{0,j}} \quad [\text{K}] \qquad \textbf{(4.99)}$$

4.5.4 Condensation Risk

Surface temperatures are important to determine expected material durability, potential deformations, occupant comfort and condensation risk. If any surface of the façade drops below the adjacent air dewpoint temperature, condensation will form. This can create mold or rot if condensation occurs regularly on moisture sensitive materials. For glazed surfaces, it is unsightly and restricts the view. Therefore, DoFa calculates the dewpoint temperature of indoor and outdoor air to evaluate condensation risk.

The dewpoint temperature (T_{dp}) can be calculated as (Straube & Burnett, 2005):

$$T_{dp} = \frac{4030}{18.689 - ln\left(\frac{P_w}{133}\right)} - 235 \quad [°\text{C}] \qquad \textbf{(4.100)}$$

Where,

P_w = partial water vapour pressure [Pa], calculated by:

$$P_w = P_{ws} \cdot RH \quad [\text{Pa}] \qquad \textbf{(4.101)}$$

Where,

RH = relative humidity [%], user input

P_{ws} = saturation vapour pressure [Pa], calculated by:

$$P_{ws} = 1000 \cdot e^{\left[52.58 - \frac{6790.5}{T} - 5.028 \cdot \ln(T)\right]} \quad [\text{Pa}] \qquad \textbf{(4.102)}$$

Where,

T = air temperature [K]

The dew point temperature for the indoor and outdoor air is compared to the indoor and outdoor façade surfaces to determine condensation risk. Furthermore, the dewpoint temperature of the cavity air is the same as the inlet source (i.e., indoor or outdoor conditions), so the condensation risk within the cavity space is also easily evaluated.

Chapter 5
Validation and Evaluation

5.1 Validation with Existing Models

Given the lack of solid experimental data of different DF systems, the proposed DF modeling tool (DoFa) was validated and its accuracy assessed by comparison to other computer models. WINDOW6.3 (LBNL, 2011) and VISION5 (Rogalsky, 2011) were used for comparison. Although these programs are not meant to model DFs, they can be used to model glazing system configurations similar to a DF system.

5.1.1 Model Differences

The main difference between DoFa, VISION and WINDOW is the treatment of solar and longwave radiation. In the DoFa model, optical properties are user input and are regarded as fixed values, while both VISION and WINDOW convert normal incidence optical properties to off-normal properties for glazing and shading layers. For venetian blinds, VISION and WINDOW employ shading models that use the profile angle of the sun, slat solar properties and the slat dimensions to provide beam and diffuse reflecting and transmitting characteristics. Furthermore, WINDOW uses spectral libraries to perform radiation calculations wavelength by wavelength and uses weighting factors to determine total solar, visible, and thermal infrared properties. Both DoFa and VISION assume spectral broadband solar properties and diffuse longwave properties (i.e., material properties are independent of wavelength).

To determine equivalent absorptance of each layer, the DoFa model uses Edwards' (1977) embedded method with beam-beam and diffuse-diffuse reflection and transmission. VISION uses the same method, though a treatment for beam-diffuse reflection and transmission is included. WINDOW uses similar recursive equations written with a spectral dependency.

For longwave radiation exchange within cavities, the DoFa model uses the Stefan-Boltzmann equation to determine linearized radiative heat transfer coefficients valid for net radiation exchange between two non-blackbody plane surfaces of equal area. When a layer is not opaque to longwave radiation, it is combined with the next layer to form a single equivalent surface with a representative temperature and emissivity weighted by angle factors. In contrast,

both VISION and WINDOW calculate surface radiosity, which is the net radiation leaving a surface including emitted, reflected and transmitted portions. In VISION, a thermal resistance network allows radiant heat transfer between any two layers via jump resistors. Radiosity energy balances are solved through matrix inversion and the resulting relative radiosities are used to calculate radiative heat transfer coefficients between any two layers. In WINDOW, the radiosities are solved in one matrix solution along with all other unknowns in the overall energy balances. A summary of the differences is presented in Table 5.1.

Table 5.1 Summary of Differences Between Compared Models

	DoFa	VISION	WINDOW
Solar Radiation			
Material Properties	- Spectral broadband - Fixed, user input	- Spectral broadband - Converted from normal to off-normal incidence	- Spectrally dependent - Converted from normal to off-normal incidence
Calculations	- Edwards (1977) embedded method	- Edwards (1977) embedded method with treatment for beam-diffuse reflection and transmission	- Recursive equations similar to Edwards (1977) written with spectral dependence
Longwave Radiation			
Material Properties	- Independent of wavelength and direction	- Independent of wavelength and direction	- Spectrally dependent - Independent of direction
Calculations	- Emissivity and angle factors used to determine equivalent h_r between two parallel surfaces	- Relative surface radiosities used to find h_r between any two layers	- Surface radiosities used to solve overall energy balances
Performance Indices			
SHGC	- Specified conditions ($T_{int,a} - T_{ext,a} \neq 0$)	- Specified conditions ($T_{int,a} - T_{ext,a} \neq 0$)	- Assumes no Indoor/outdoor ΔT ($T_{int,a} - T_{ext,a} = 0$)
U-Value	- Assumes no solar radiation ($G_{t\theta} = 0$)	- Specified conditions ($G_{t\theta} \neq 0$)	- Assumes no solar radiation ($G_{t\theta} = 0$)

5.1.2 Comparison Outline

The limitations of WINDOW and VISION dictated the types of systems that could be compared. Therefore, the following limitations were applied for the comparison:

- 1.0-m height;
- maximum 0.1-m cavity depths;
- center of glazing results; and
- airflow in innermost/outermost cavities only (VISION).

Furthermore, it was necessary to match the inputs as closely as possible to facilitate a direct comparison. Therefore, NFRC-100 environmental conditions were chosen as a basis of comparison (LBNL, 2011):

Summer	Winter
$G_{D\theta}$ = 783 W/m^2	$G_{t\theta}$ = 0 W/m^2
$G_{d\theta}$ = 0 W/m^2	$G_{d\theta}$ = 0 W/m^2
$h_{c,ext}$ = 15 W/m^{2}K	$h_{c,ext}$ = 26 W/m^{2}K
$T_{MRT,ext} = T_{a,ext}$ = 32 °C	$T_{MRT,ext} = T_{a,ext}$ = -18 °C
$T_{MRT,int} = T_{a,int}$ = 24 °C	$T_{MRT,int} = T_{a,int}$ = 21 °C

The $h_{c,int}$ value is not explicitly stated, therefore fixed values of 3.6 and 3.4 W/m^{2}K were used for summer and winter respectively. Several different cases were tested under summer and winter conditions with normal incident solar radiation (θ = 0). In each case, cavity depths were set to the maximum, as this is more applicable to DF systems. Exceptions are indoor and outdoor shading cavities.

Table 5.2 System Dimensions

Dimension	Measurement [m]
Height	1.0
Width	1.0
Cavity Depth (DF)	0.1
Cavity Depth (Shading)	0.0254

The specific glazing and shading layer optical properties entered into DoFa are presented in Appendix C. Note that the front reflectance of the low-E layer was slightly different in WINDOW (0.509 instead of 0.562). However, various comparisons using the DoFa model showed that this slight difference in reflectance had very little impact on the results. In some cases, an insulated glazing unit was used (Table 5.3).

Table 5.3 Multi Glazing Properties

Name	Description	U [W/m^{2}K]	Pane 2	Fill	Pane 1
DG	Low-E double glazing	1.66	Low-E 0.02	10% Air, 90% Argon (12.7 mm)	Clear

The cases used for comparison are presented in Table 5.4.

Table 5.4 Case Descriptions

		Layer				
Type	**Case**	**S3**	**F2**	**S2**	**F1**	**S1**
Triple Glazed	1	Clear	100 mm, enclosed	Clear	100 mm, enclosed	Clear
	2	Clear	100 mm, enclosed	Low-E 0.02	100 mm, enclosed	Clear
	3	Low-E 0.02	100 mm, enclosed	Low-E 0.02	100 mm, enclosed	Clear
Intermediate Shading	4a	Clear	100 mm, enclosed	VB/RB1	100 mm, enclosed	Clear
	4b	Low-E 0.02	100 mm, enclosed	VB/RB1	100 mm, enclosed	Clear
	5a	Clear	100 mm, enclosed	VB/RB1	100 mm, enclosed	DG
	5b	Low-E 0.02	100 mm, enclosed	VB/RB1	100 mm, enclosed	DG
Indoor/ Outdoor Shading	6a	Clear	100 mm, enclosed	DG	25.4 mm, open	VB/RB1
	6b	Low-E 0.02	100 mm, enclosed	DG	25.4 mm, open	VB/RB1
	7a	VB/RB1	25.4 mm, open	Clear	100 mm, enclosed	DG
	7b	VB/RB1	25.4 mm, open	Clear	100 mm, enclosed	DG

The low-E coating chosen (0.02) is very low to simulate a high performing, solar control glazing. The following sections describe the results of the comparisons.

5.1.3 Triple Glazed Systems

To begin, a simple assembly of three glass layers was examined to determine if the DoFa model could produce similar results to the compared models. The effect of adding a low-E coating was investigated.

Cases 1 through 3 are triple glazed systems with enclosed cavities. Figure 5.1 and Figure 5.2 show the temperature profiles for Case 1 in summer and winter conditions respectively.

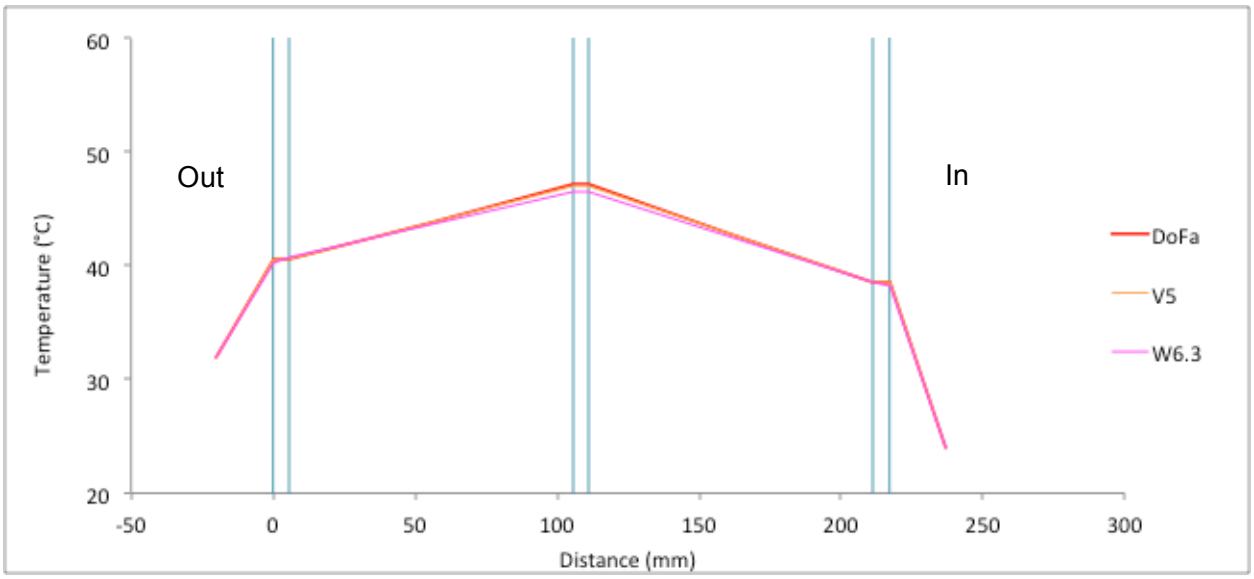

Figure 5.1 Case 1 Summer Temperature Profile

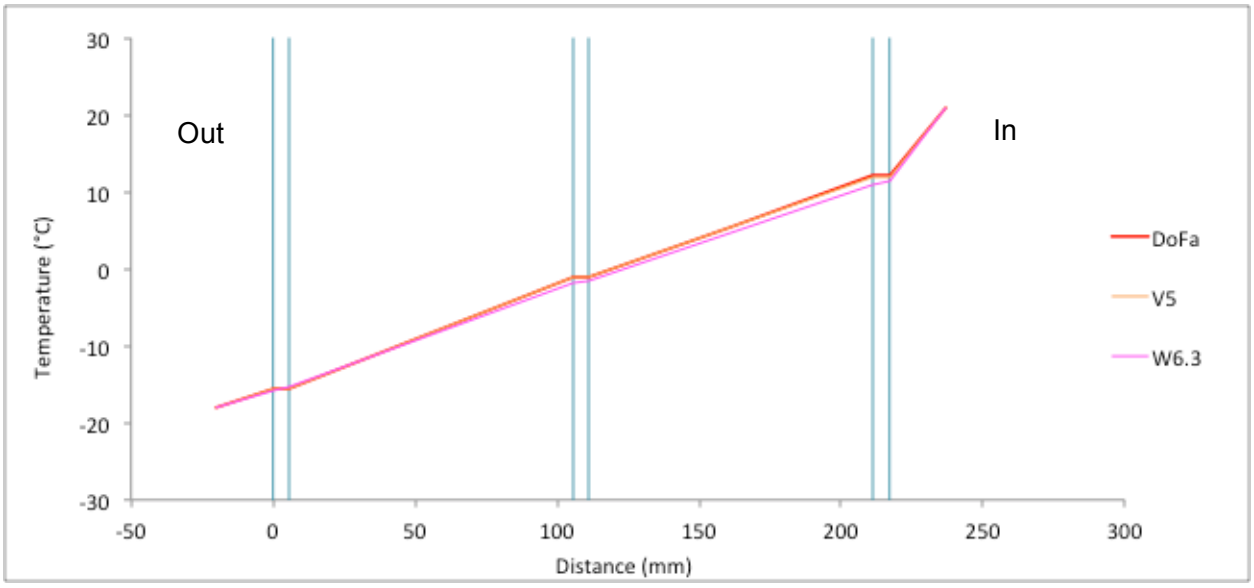

Figure 5.2 Case 1 Winter Temperature Profile

In Case 1, the temperature profiles showed good agreement. Note that in winter conditions, the temperature profiles showed good agreement for all cases; therefore, no further winter profiles are included. Table 5.5 shows the design indices.

Table 5.5 Case 1 Design Indices

Conditions	Measure	Unit	DoFa	V5	W6.3
Summer	SHGC	N/A	0.61	0.61	0.62
	Difference	%		0.3%	0.8%
Winter	U-Value	W/m^2K	1.83	1.85	1.76
	Difference	%	-	1.3%	3.7%

For Case 1, the DoFa model showed good agreement with the other models in winter and summer conditions.

When a low-E coating was added to various layers throughout the assembly, there was a slightly larger difference between models. In winter, the temperature profiles remained well matched. In summer, there were some variations (Figure 5.3 and Figure 5.4).

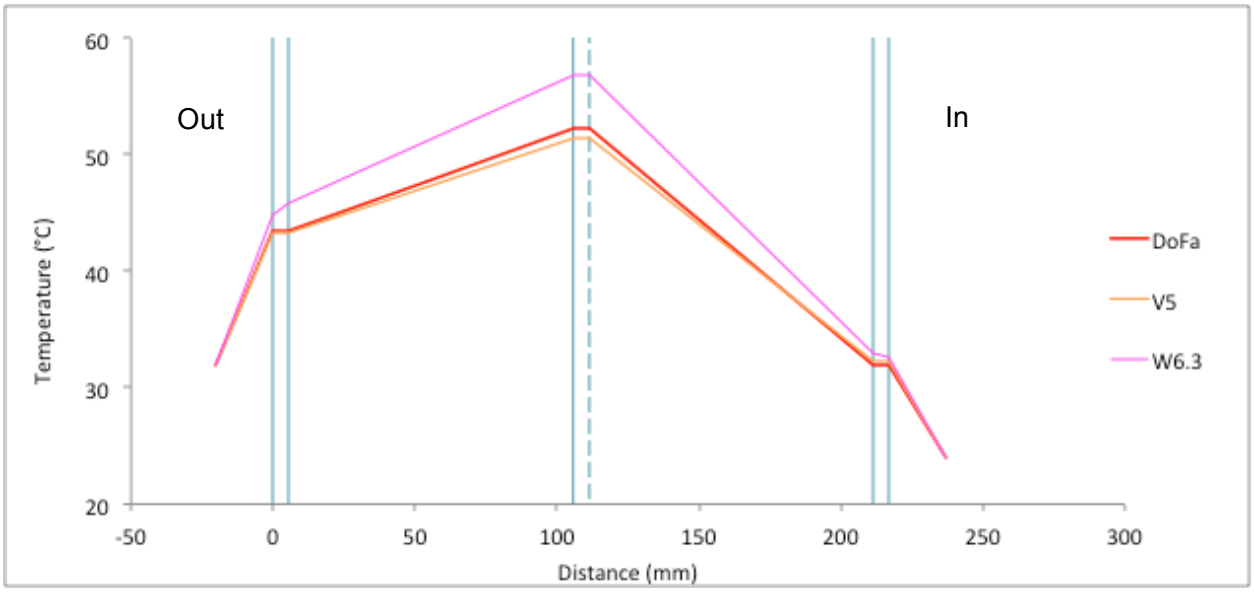

Figure 5.3 Case 2 Summer Temperature Profile

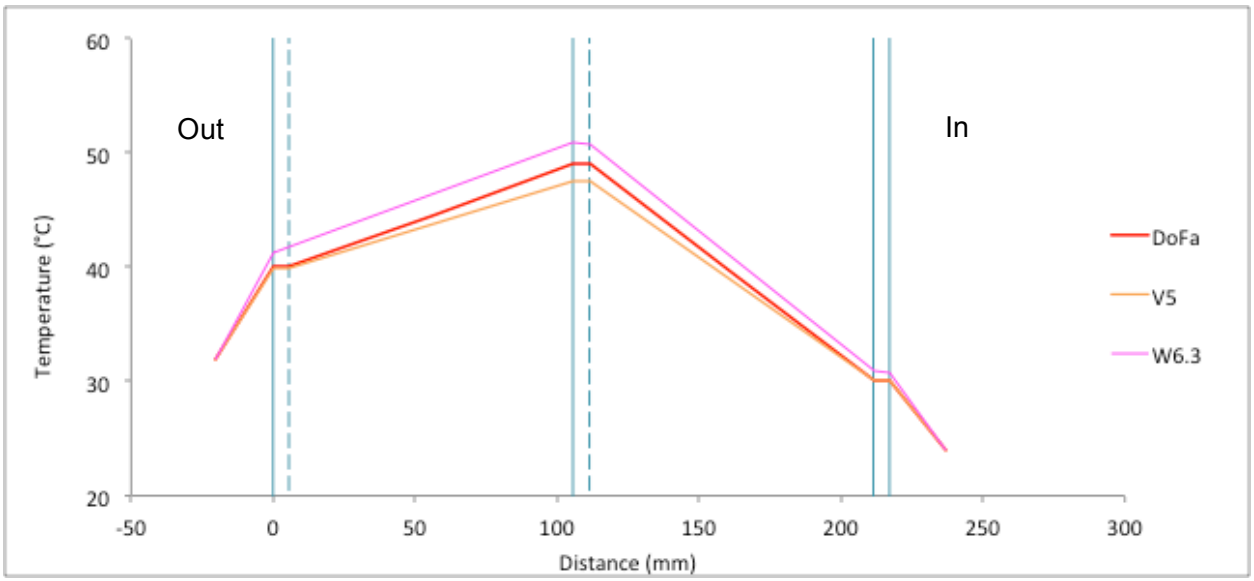

Figure 5.4 Case 3 Summer Temperature Profile

In general, the summer temperature profiles showed good agreement; however, the WINDOW profile was slightly higher in both cases. The cause could be that WINDOW calculates spectrally dependent surface properties. When examining the effective absorptance of each layer, DoFa and VISION calculated the same values while WINDOW values differed (Table 5.6).

Table 5.6 Cases 2 and 3 System Optical Properties

			Effective Absorptance (α_e)		
Case	**Model**	**τ_{total}**	**S3**	**S2**	**S1**
2	DoFa/V5	0.182	0.227	0.129	0.037
	W6.3	0.216	0.240	0.174	0.012
3	DoFa/V5	0.093	0.194	0.066	0.019
	W6.3	0.159	0.224	0.077	0.007

The effective absorptance for S2 was higher in WINDOW for both cases, which explains the higher S2 temperatures seen in Figure 5.3 and Figure 5.4. Also, the differing layer absorptances resulted in a higher total transmittance in WINDOW for both cases. This difference is reflected in the performance indices (Table 5.7).

Table 5.7 Cases 2 and 3 Performance Indices

			Case 2			Case 3		
Conditions	**Measure**	**Unit**	**DoFa**	**V5**	**W6.3**	**DoFa**	**V5**	**W6.3**
Summer	SHGC	N/A	0.26	0.26	0.29	0.16	0.15	0.22
	Difference	%	-	0.5%	10.8%	-	3.3%	32.9%
Winter	U-Value	W/m^2K	1.21	1.25	1.22	0.88	0.92	0.92
	Difference	%	-	3.4%	0.8%		4.2%	3.9%

While winter performance was generally the same between models, summer heat gain predicted by WINDOW was higher than the other two models. This reflects the difference in total transmittance. The number of low-E layers seems to directly increase the percent difference between models. Reasons for the difference could be that the low-E layer in WINDOW reflects 10% less than DoFa and VISION, WINDOW uses spectrally-dependent surface properties and WINDOW's SHGC calculations assume no temperature difference between indoors and outdoors. Nevertheless, a difference of 33% seems large for a relatively simple glazing system (Case 3) .

5.1.4 Intermediate Shading

Shading devices were introduced in Cases 4 and 5 to add an extra layer of complexity. A venetian blind (light, $\varphi = 60°$) and roller blind (light, $O_p = 0.14$) from the VISION shading library were used. To replicate the shading layers in WINDOW, new shading layers were built. For the venetian blind, a light aluminum slat material was created to match the material properties in VISION. The slat angle (60°), spacing (10.6 mm) and length (12.7 mm) were then matched to VISION. For the roller blind, it proved difficult to match shading material properties to VISION. Therefore, an equivalent glass layer was used instead with the desired optical and thermal properties. Note that these shading layers did not have spectral files; therefore, WINDOW assumed a flat spectral behaviour based on the stated properties.

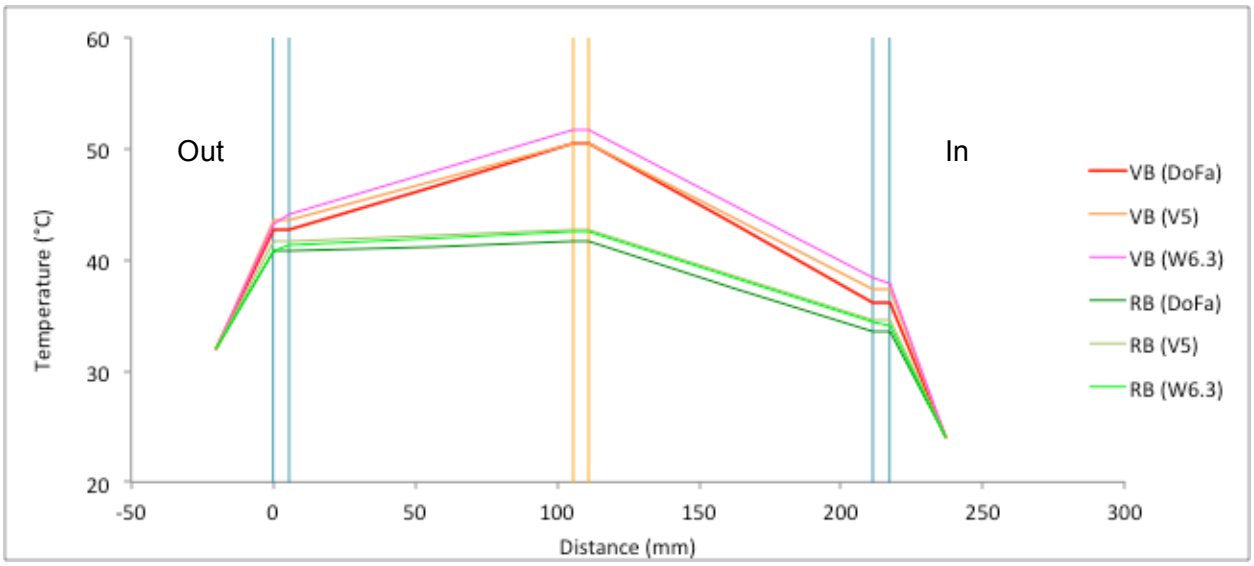

Figure 5.5 Case 4a Summer Temperature Profile

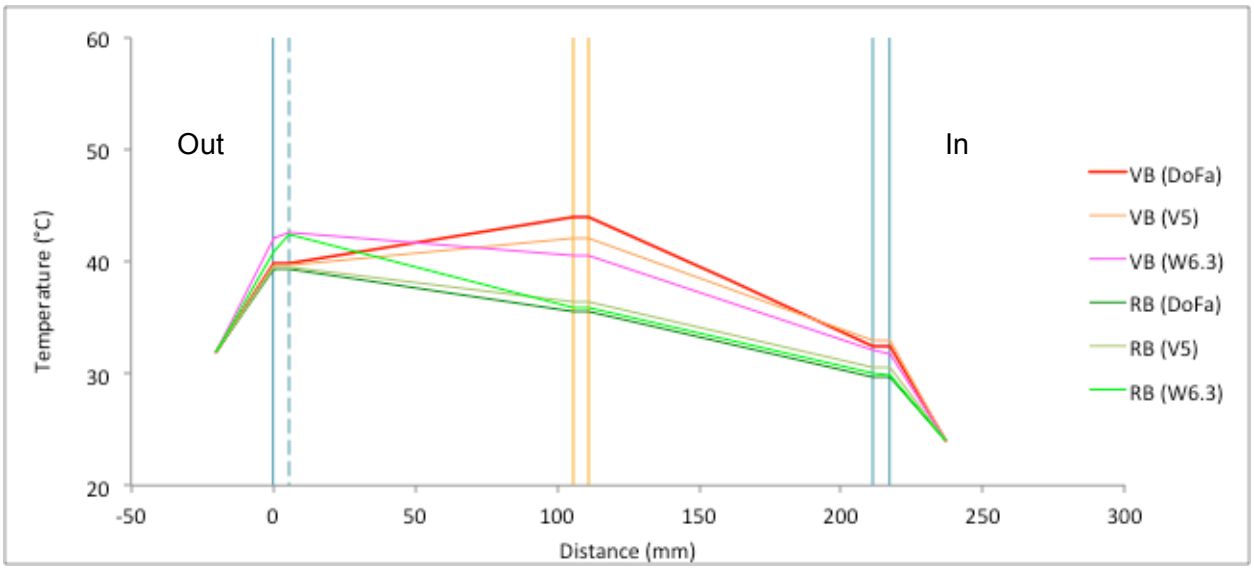

Figure 5.6 Case 4b Summer Temperature Profile

The summer temperature profiles showed good agreement between models; however, WINDOW showed a higher outdoor surface temperature for Case 4b. Also, the system transmittance and effective absorptances were not the same between DoFa and VISION with the inclusion of shading devices. VISION accounts for beam-diffuse reflection and transmission, which occurs in shading layers, and DoFa does not. Performance indices are shown in Table 5.8.

Table 5.8 Case 4 Performance Indices

				Venetian Blind (60°)			Roller Blind		
Conditions	**Case**	**Measure**	**Unit**	**DoFa**	**V5**	**W6.3**	**DoFa**	**V5**	**W6.3**
Summer	4a	SHGC	N/A	0.23	0.24	0.23	0.28	0.29	0.29
		Difference	%	-	4.3%	1.3%	-	3.0%	4.0%
	4b	SHGC	N/A	0.15	0.16	0.11	0.16	0.16	0.15
		Difference	%	-	8.1%	28.3%	-	0.4%	4.1%
Winter	4a	U-Value	W/m^2K	2.02	2.04	1.92	1.99	2.07	1.92
		Difference	%	-	0.8%	5.3%	-	4.1%	3.3%
	4b	U-Value	W/m^2K	1.23	1.32	1.29	1.25	1.33	1.30
		Difference	%	-	7.3%	5.3%	-	6.0%	3.4%

The difference between models ranged significantly, though it was generally less than 10%. Note that the difference between VISION and WINDOW results is not reported in Table 5.8; however, it was comparable to the difference between DoFa and either of the other two models.

In general, the roller blind results were well matched between all models; however, venetian blind results were not. In summer, WINDOW predicted lower heat gain due to lower system transmittance, which was magnified in the presence of a low-E exterior pane (similar to Case 3). In all appearances, the venetian blind layers (geometry and material properties) were identical in VISION and WINDOW; however, the resulting layer optical properties differed (Table 5.9).

Table 5.9 Venetian Blind Layer Optical Properties at Normal Incidence

Model	**τ**	**ρ**	**α**	**ε**	**ε'**
V5	0.174	0.626	0.200	0.840	0.840
W6.3	0.145	0.645	0.210	0.840	0.840

A second test, whereby the WINDOW venetian blind optical properties were entered into DoFa, resulted in a 23.4% difference between DoFa and WINDOW for the 4b summer case. Therefore, the majority of the difference is likely due to the difference in calculation methods. Consequently, the following discussion regarding venetian blinds pertains to the difference between DoFa and VISION, which is more easily analyzed.

For the venetian blind summer cases, DoFa underestimated the heat gain. One reason is that the DoFa model uses fixed front and back optical properties with no beam-diffuse reflection or transmission. Therefore, in the absence of diffuse solar radiation, all properties used by DoFa are for 100% direct radiation. This is not a problem for layers with relatively similar properties for direct and diffuse radiation, such as glazing layers and roller blinds. However, venetian blinds have a higher transmittance for diffuse radiation (0.334 vs. 0.174 in this case). Therefore,

any direct radiation diffusely reflected from the slats to the exterior glass and back to the slats would have a higher transmitted fraction than assumed in DoFa. In contrast, VISION assumes that all direct radiation incident on venetian blind slats is reflected diffusely, which is then addressed in a separate diffuse calculation with corresponding diffuse properties. Therefore, the overall system transmittance is increased. Table 5.10 shows the difference in total transmittance between models.

Table 5.10 Difference in Total Transmittance for Case 4 with Venetian Blind

	Case	
Model	**4a**	**4b**
DoFa	0.114	0.061
V5	0.114	0.072
Difference	0.0%	16.5%

In Case 4a, the exterior glass was clear with a reflectance of 0.072. Therefore, the diffuse radiation reflected from the venetian blind was mostly transmitted back to the outdoors. In Case 4b however, the exterior glass had a reflectance of 0.562. Therefore, over half of the diffuse radiation reflected from the venetian blind was re-reflected back. This accounts for the larger difference in Case 4b for venetian blinds in summer conditions.

In winter conditions, both blind types showed larger differences in the presence of a low-E coating (4b). This difference is likely due to the treatment of longwave radiation transfer in the presence of diathermanous layers. The roller blind is mostly opaque to longwave radiation (86%), which reduces the impact. The venetian blind, which is more open, had a larger difference between models, though the difference in results between DoFa and either of the other two models was still less than 8%.

In Case 5, a multi-glazing element was added. Figure 5.7 and Figure 5.8 show the summer temperature profiles for Cases 5a and 5b respectively.

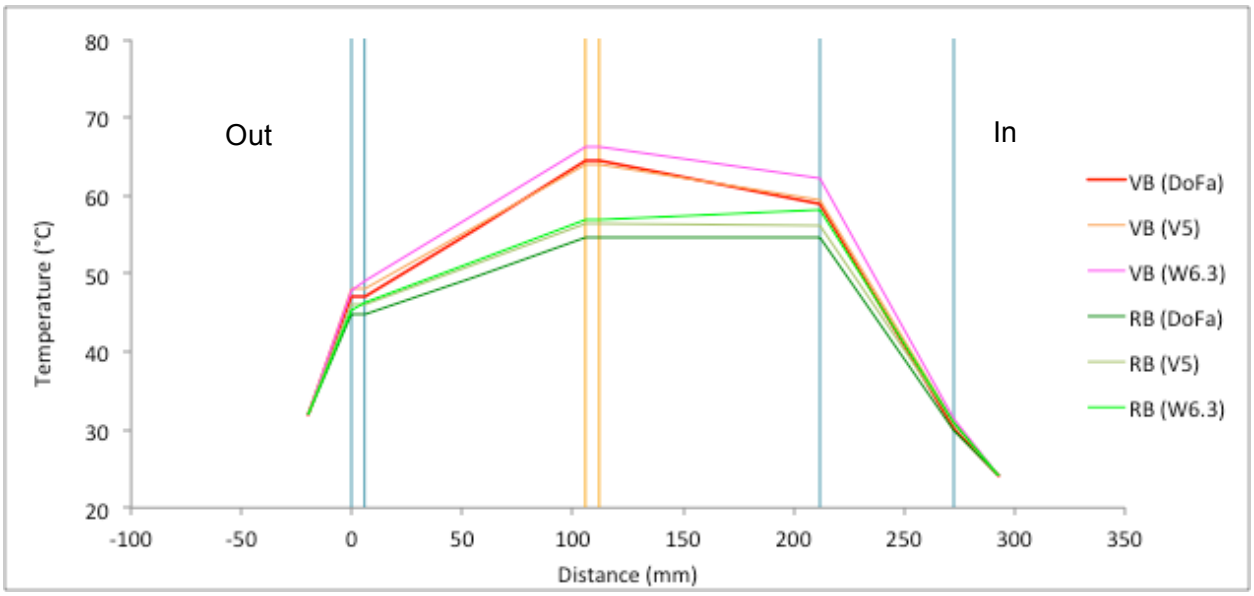

Figure 5.7 Case 5a Summer Temperature Profile

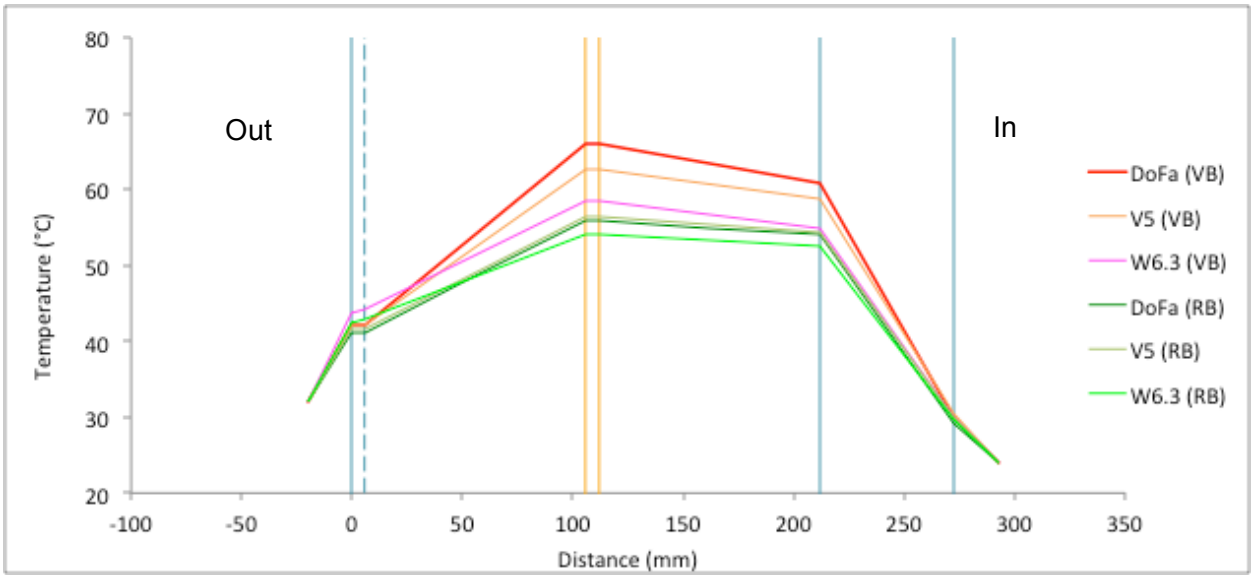

Figure 5.8 Case 5b Summer Temperature Profile

The summer temperature profiles showed relatively good agreement between models; however, there was a wider spread in Case 5a with venetian blind. Performance indices are shown in Table 5.11.

Table 5.11 Case 5 Performance Indices

Conditions	Case	Measure	Unit	Venetian Blind (60°)			Roller Blind		
				DoFa	V5	W6.3	DoFa	V5	W6.3
Summer	5a	SHGC	N/A	0.11	0.11	0.10	0.14	0.14	0.15
		Difference	%	-	2.1%	10.5%	-	1.8%	7.7%
	5b	SHGC	N/A	0.09	0.09	0.08	0.10	0.10	0.12
		Difference	%	-	1.6%	16.6%	-	2.0%	12.8%
Winter	5a	U-Value	W/m^2K	0.85	0.85	0.84	0.84	0.86	0.83
		Difference	%	-	0.0%	0.8%	-	1.9%	2.0%
	5b	U-Value	W/m^2K	0.65	0.66	0.66	0.65	0.66	0.66
		Difference	%	-	2.3%	1.7%	-	1.1%	0.5%

Results reflect those from Case 4. Once again, WINDOW SHGC results for summer conditions with venetian blinds were lower than the other two models. However, the DoFa and VISON results for the same case were actually better matched. The addition of an insulating layer on the interior lessened the difference caused by intermediate shading.

5.1.5 Indoor/Outdoor Shading

Assemblies with indoor and outdoor shading were modeled to test this element of the DoFa model. WINDOW was not used in the comparison because it does not provide an airflow option. Both Cases 6a and 6b showed similar temperature profiles; therefore, only 6a is shown.

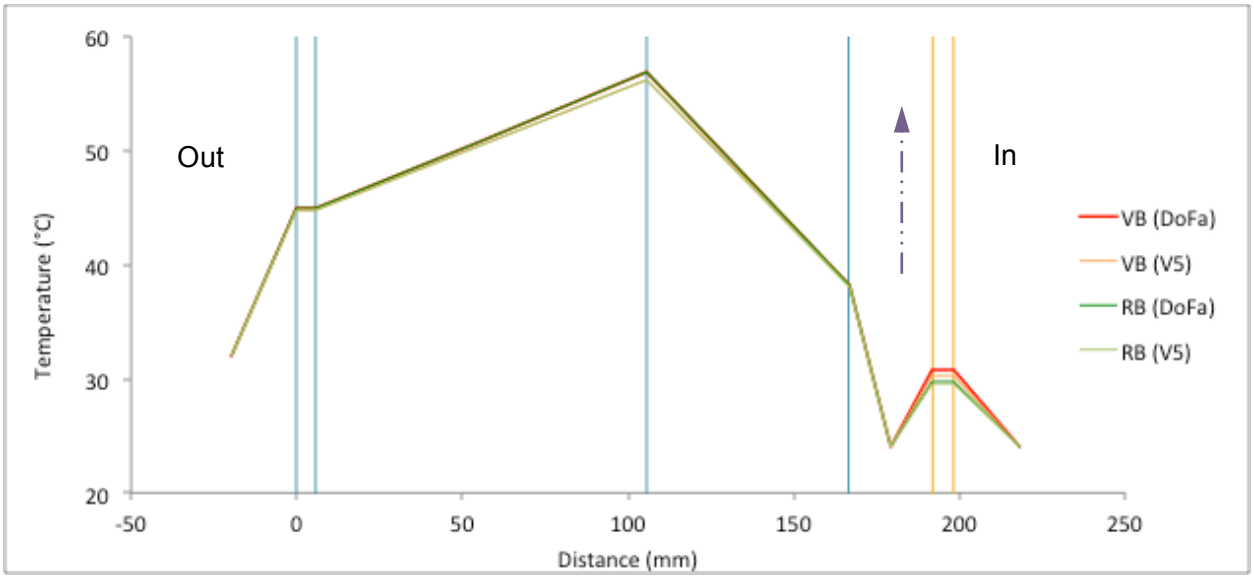

Figure 5.9 Case 6a Summer Temperature Profile

The temperature profiles showed good agreement between models. Performance indices are shown in Table 5.12. In this case, the total inflowing heat fluxes predicted by the two models were compared as well. While VISION does not expressly give the q_{in} value, the values shown in Table 5.12 were calculated from the given SHGC and U-value using Equation (4.90).

Table 5.12 Case 6 Performance Indices (Summer)

			Venetian Blind (60°)		Roller Blind	
Case	**Measure**	**Unit**	**DoFa**	**V5**	**DoFa**	**V5**
6a	SHGC	N/A	0.19	0.20	0.19	0.20
	q_{in}	W/m^2	156.6	165.5	158.6	165.4
	Difference (q_{in})	%	5.5%		4.2%	
6b	SHGC	N/A	0.13	0.13	0.13	0.13
	q_{in}	W/m^2	102.9	108.1	103.7	108.1
	Difference (q_{in})	%	5.0%		4.1%	

The agreement between models was good. The SHGCs were generally the same, though the q_{in} values varied slightly due to differences in calculated U-values. For U-value calculations, DoFa assumes no solar radiation while VISION includes solar radiation. However, the difference between models was less than 6%.

In Case 7, the shading device was moved to the outside of the façade. Again, Cases 7a and 7b showed similar temperature profiles; therefore, only 7b is shown here.

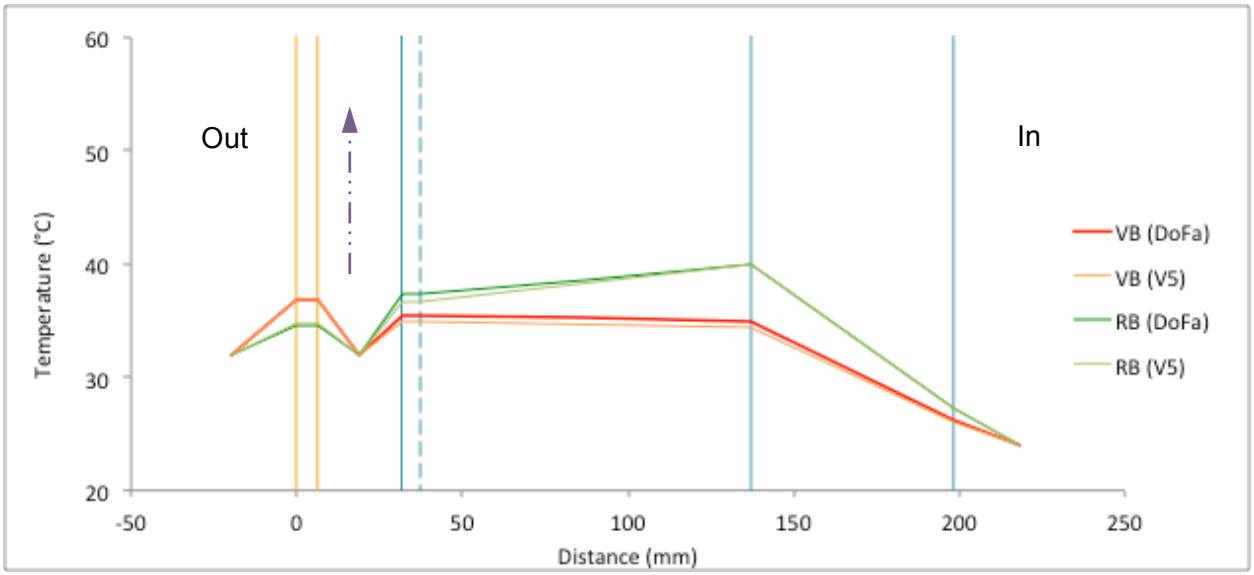

Figure 5.10 Case 7b Summer Temperature Profile

The summer temperature profiles showed good agreement between models. Performance indices are shown in Table 5.13, again including inflowing heat flux. Note that the SHGCs for exterior shading are very low.

Table 5.13 Case 7 Performance Indices (Summer)

			Venetian Blind (60°)			Roller Blind		
Case	**Measure**	**Unit**	**V5**	**DoFa**	**DoFa***	**V5**	**DoFa**	**DoFa***
7a	SHGC	N/A	0.05	0.06	0.05	0.09	0.10	0.09
	q_{in}	W/m^2	47.5	56.5	48.6	79.0	89.9	76.1
	Difference (q_{in})	%	-	17.4%	2.4%	-	12.9%	3.7%
7b	SHGC	N/A	0.03	0.04	0.04	0.07	0.07	0.06
	q_{in}	W/m^2	27.4	39.8	35.1	60.1	63.7	55.9
	Difference (q_{in})	%	-	36.8%	24.6%	-	5.9%	7.2%

** Diffuse optical properties used for inner layers*

When the shading device is located on the outside, it changes the fraction of beam and diffuse solar radiation incident on all other layers. Because DoFa does not account for beam-diffuse reflection and transmission, a second test was conducted where diffuse properties were used for all layers to the interior of the shading device. The results using diffuse properties were better matched to VISION results, with the exception of Case 7b with roller blind. Also, the difference in q_{in} for Case 7b with venetian blind remained high. The reason is similar to Case 4, though with the opposite effect.

DoFa does not account for beam-diffuse transmission; therefore, it overestimates the amount of transmitted radiation for outdoor venetian blinds. In reality, any radiation transmitted diffusely through the blind and reflected from the exterior glazing would be transmitted back to the outside according to the diffuse transmittance of the shading device (0.334 in this case). However, the DoFa model uses the beam transmittance (0.174), resulting in more reflection towards the interior and a higher overall transmittance. This was especially true in Case 7b, when the reflectance of the exterior glazing was high. However, it should be noted that for outdoor shading, the SHGC is so small that a very slight change leads to a large percent difference. For example, the difference of 24.5% in Case 7b amounted to only 7.7 W/m^2. Nevertheless, caution should be exercised when modeling venetian blinds using DoFa. Special attention should be paid to the location of the blind within the assembly and the optical properties of adjacent layers.

5.1.6 Variable Optical Properties

In all previous cases, incoming solar radiation was set to 100% direct at normal incidence. Several of the previous cases were retested under two different solar radiation conditions: 1) 50% diffuse solar radiation and 2) 45° incidence angle. Results were compared to VISION because incidence angle and diffuse fraction can be changed easily in this model. The optical properties for the tested solar radiation conditions were obtained from VISION (Appendix C).

The results for the 50% diffuse test case are presented in Table 5.14. Testing was conducted under summer conditions only, since solar optical properties make no difference under the specified winter conditions.

Table 5.14 Performance Indices with 50% Diffuse Solar Radiation (Summer)

				Venetian Blind (60°)		Roller Blind	
Measure	**Model**	**1**	**2**	**4a**	**4b**	**4a**	**4b**
SHGC	V5	0.54	0.24	0.27	0.17	0.27	0.15
	DoFa	0.55	0.24	0.26	0.16	0.26	0.15
Difference		1.4%	0.6%	1.9%	8.8%	2.9%	0.3%
q_{in} [W/m^2]	V5	443.8	197.0	230.8	135.7	230.8	125.4
	DoFa	443.8	194.2	224.4	128.9	221.1	124.5
Difference		0.0%	1.4%	2.8%	5.2%	4.3%	0.7%

In general, the agreement was good. In the presence of shading devices, the difference was actually improved from the 100% direct solar radiation case. This supports the theory that the previous difference was due to the consideration of beam-diffuse reflection and transmission, especially for venetian blinds.

The second test case investigated performance with a 45° incidence angle (Table 5.15).

Table 5.15 Performance indices for 45° Incidence Angle (Summer)

				Venetian Blind (60°)		Roller Blind	
Measure	**Model**	**1**	**2**	**4a**	**4b**	**4a**	**4b**
SHGC	V5	0.55	0.24	0.18	0.14	0.26	0.15
	DoFa	0.55	0.24	0.16	0.11	0.26	0.15
Difference		0.9%	0.3%	11.7%	23.8%	0.3%	1.2%
q_{in} [W/m^2]	V5	449.7	198.1	160.9	116.9	226.0	125.9
	DoFa	449.6	194.9	142.4	93.3	218.6	123.5
Difference (q_{in})		0.0%	1.6%	12.2%	22.4%	3.3%	1.9%

In general, differences for all cases were similar to the normal incidence cases. The exception was the venetian blind, where the difference doubled at 45° incidence. This is because at off-

normal incidence, the venetian blind had an even lower transmittance for direct radiation. Therefore, users should be cautious when using DoFa to model venetian blinds at off-normal incidence angles, unless the blind transmittance is altered accordingly.

In contrast, roller blind results were quite well matched. Therefore, further incidence angles were investigated to determine if this was generally true. Case 5 was taken as the test case.

Table 5.16 Effects of Incidence Angle (Roller Blind)

		5a				5b			
Measure	**Model**	**0**	**20**	**45**	**60**	**0**	**20**	**45**	**60**
SHGC	V5	0.14	0.14	0.13	0.11	0.10	0.10	0.09	0.08
	DoFa	0.14	0.14	0.13	0.11	0.10	0.10	0.09	0.08
Difference		2.8%	2.1%	0.0%	2.4%	4.2%	0.8%	3.9%	4.0%
q_{in} [W/m^2]	V5	119.9	117.7	108.5	95.9	82.4	81.6	77.6	70.0
	DoFa	119.8	119.1	108.9	95.4	86.3	83.5	77.8	69.8
Difference (q_{in})		0.1%	1.2%	0.3%	0.6%	4.6%	2.3%	0.3%	0.3%

Results show that DoFa can accurately reproduce VISION results at off-normal incidence angles for roller blinds. However, the optical properties for each incidence angle were manually entered into the DoFa model, since the model does not calculate them itself. Therefore, changing incidence angles is a somewhat tedious task. If DoFa is used to model various options for direct comparison, using normal optical properties would be sufficient. However, if performance information is desired for different incidence angles, angle specific optical properties should be used. Note that the change in total inflowing heat flux between 0° and 60° is relatively large. The effect of incidence angle is discussed in more detail in Section 5.3.5.

5.1.7 Conclusions

Comparisons with WINDOW and VISION showed that the DoFa model can provide equally accurate results for enclosed glazing systems with roller blinds at normal and off-normal incidence. However, differences were apparent in specific cases, including multiple low-E layers, venetian blinds and outdoor shading.

The presence of multiple low-E layers side by side (Case 3) caused differing results between models. However, it was WINDOW that gave differing results while DoFa and VISION results were similar. Furthermore, the difference was only apparent in situations with incoming solar radiation. Potential causes of the difference is slightly different solar optical properties, the use of spectral broadband optical properties (DoFa and VISION) versus spectrally dependent

properties (WINDOW) and the manner of calculating SHCG. The large difference between models was repeated in other summer cases, especially those with a low-E exterior layer and venetian blinds (Cases 4b and 5b). However, in these cases the DoFa results were intermediary between VISION and WINDOW results. Therefore, the accuracy of DoFa was no worse than the other two models for the cases tested.

The presence of venetian blinds caused DoFa and VISION results to differ. This is because the DoFa optical model does not account for beam-diffuse reflection or transmission, which is a problem for layers that have widely differing properties for diffuse and direct radiation (e.g., venetian blinds). Therefore, caution should be exercised when using DoFa to model venetian blinds. To improve accuracy, the transmittance of the blind may be altered to account for beam-diffuse reflection and transmission. However, this is not advised unless the user has detailed knowledge of the expected behaviour of the assembly. The transmittance of a venetian blind should be increased or decreased depending on the location of the blind within the façade and the optical properties of the other layers.

Finally, the presence of outdoor shading caused differing results. Once again, the cause is that the DoFa optical model does not account for beam-diffuse transmission. The comparison with VISION showed that using diffuse properties for the interior layers generally reduced the difference between models. Therefore, this strategy may be employed to increase accuracy when diffusing layers are located on the outside of the assembly. When shading layers were located in the intermediate space or on the inside, the difference was under 10%.

A variety of glazing combinations were compared to existing models to validate the DoFa model. However, due to limitations of existing models, the airflow element could not be tested. While VISION can be used to model indoor and outdoor shading cavities with airflow, airflow through intermediate cavities is not possible. Furthermore, a cavity with deliberate ventilation openings does not behave in the same way as a shading cavity. Therefore, measurements were necessary to compare DoFa to actual DF systems.

5.2 Validation with Measurements

In order to validate the DoFa model in the presence of natural airflow, experimental data was necessary. However, there is currently little to choose from. Many researchers have developed

models and presented results without experimental validation (e.g., Hensen et al., 2002; Yilmaz & Cetintas, 2004; Griffith, 2006). Other researchers have presented experimental data without providing adequate detail to reproduce it, such as optical properties or opening areas (e.g., Von Grabe, 2002; Yuan et al., 2007). Furthermore, some researchers provided adequate input details though presented limited results, making it difficult to conduct a meaningful comparison (e.g., Manz, 2004). While Tascon (2008) presented extensive experimental data in his PhD thesis, many outcomes were reported separately and it is difficult to link situations to make a direct comparison (e.g., surface temperatures provided without airflow rate). Furthermore, from the literature review it became apparent that important performance indices such as inflowing heat flux, U-value and SHGC were rarely discussed. While further studies addressed mechanically ventilated façades (e.g., Manz et al, 2004; Corgnati et al., 2007; Haase et al, 2009), validating mechanical ventilation is beyond the scope of this thesis.

Ultimately, experimental results from two publications were used for comparison: (Saelens, 2002) and (Park et al., 2004). While neither provided adequate input and output data for a comprehensive comparison, a basic comparison was possible. More experimental data is required to confirm the validation of the DoFa model.

While experimental data is extremely important, the accuracy is variable. It is difficult to measure glass temperatures because solar radiation may heat the measurement equipment relative to the glass. Furthermore, instrument and installation error can cause variations in results. Therefore, one must acknowledge that the measured data has a degree of uncertainty.

5.2.1 Saelens (2002)

5.2.1.1 Experimental Setup

In his PhD thesis, Saelens (2002) conducted experiments using the Vliet test cell in Belgium to validate his numerical model. His results are some of the most exhaustive, where actual optical properties and airflow rates were reported. The setup consisted of a one-storey, southwest-facing, exterior air curtain DF with natural airflow (Figure 5.11).

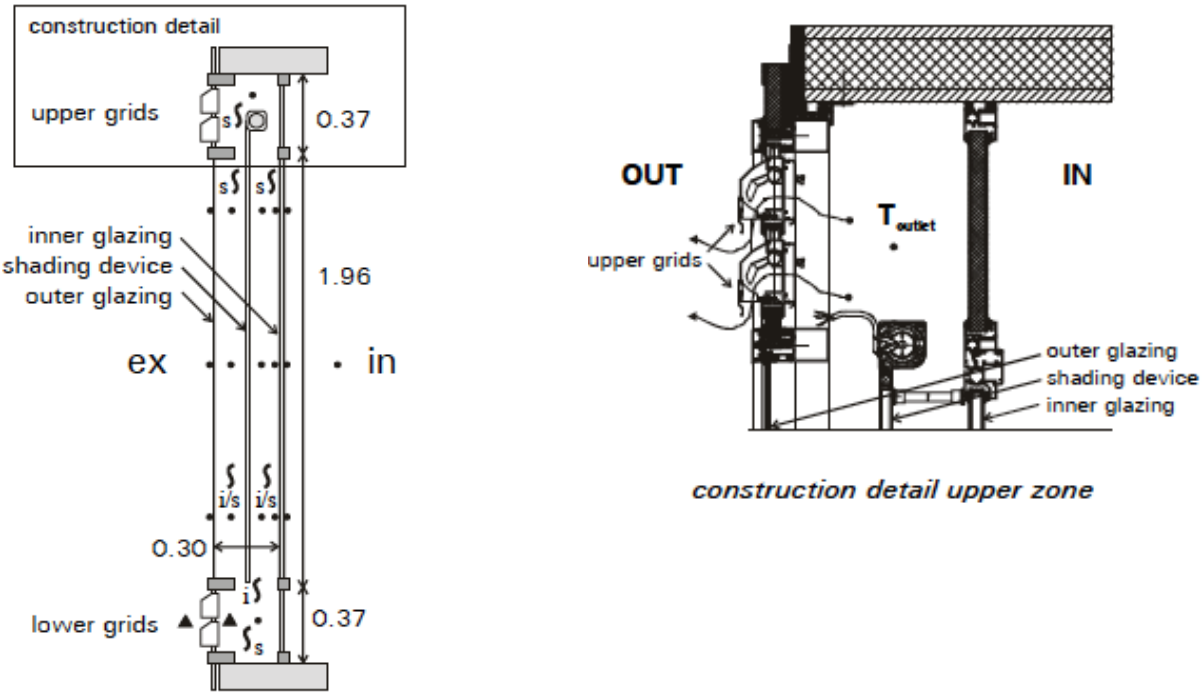

Figure 5.11 Vliet Test Cell Experimental Setup (Saelens, 2002)

Pappas and Zhai (2008) also used Saelens' (2002) experimental results to validate their CFD model. Therefore, results from both researchers were considered. To begin, it was necessary to characterize the façade geometry, presented in

Table 5.17. Layer optical properties are presented in Appendix C.

Table 5.17 System Properties

Item	Description
Height	2.7 m
Width	1.2 m
Depth	0.3 m
Outdoor Surface	Single Glazing (Clear)
Shading Device	Roller Blind (RB)
Indoor Surface	Double glazing (Clear+Argon+Low-E 0.09) U-value = 1.23 W/m^{2}K

One problem in modeling the Vliet DF was characterizing the inlet/outlet grids. Pappas and Zhai (2008) found the same problem, stating that the complex geometry was difficult to replicate precisely. They suggested that an effective opening area of 0.026 m^2 and a C_d value of 1.0 gave results nearest to the measured data. This was used as a starting point.

The second problem came with characterizing the flow distribution. Although Saelens (2002) claimed that the majority of air flowed through the exterior cavity, his results suggested otherwise. His results consistently showed a higher temperature in the exterior cavity, which Saelens (2002) attributed to higher solar radiation and surface temperatures. However, all results using DoFa suggested that the interior cavity was warmer when double glazing was located on the interior (see Case 5 of Section 5.1.4). Therefore, the fraction of air flowing through the exterior cavity was varied in an attempt to replicate Saelens' (2002) results.

5.2.1.2 Temperature Profiles and Airflow Rates

Sealens (2002) provided a horizontal temperature profile for the three cases presented in Table 5.18. Therefore, these temperature profiles were reproduced and compared to the results obtained using DoFa.

Table 5.18 Test Cases

Case	$G_{t\theta}$ [W/m^2]	$T_{a,ext}$ [°C]	$T_{a,int}$ [°C]	Time	Open Grids
1S	487	5.0	19.5	14:30	2
2S	614	26.0	21.5	16:30	1
3S	295	3.6	18.8	15:00	1

Note that all test cases were conducted in the afternoon, when the incidence angle would be closer to normal.

In the first test case, exterior cavity flowing fractions of 0.5 and 0.23 were compared. Note that Saelens (2002) did not measure the temperature of the shading device, so the temperature shown in Figure 5.12 is only estimated.

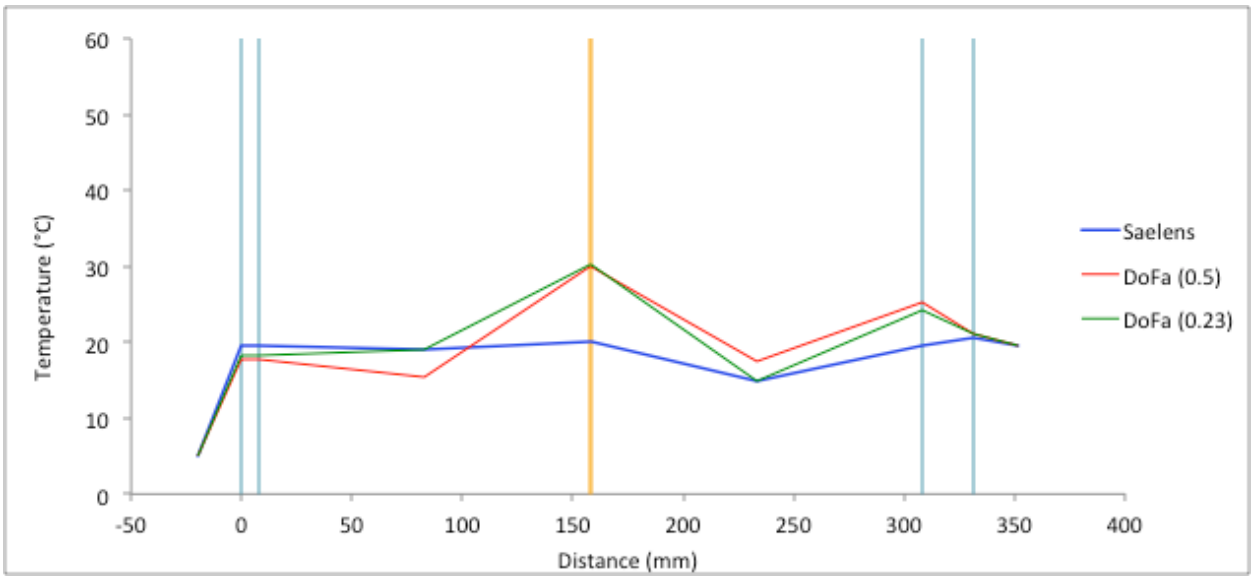

Figure 5.12 Case 1S Temperature Profile

When assuming an equal flow distribution, DoFa under-predicted the exterior cavity temperature and over-predicted the interior cavity temperature. The 0.23 exterior cavity flow fraction matched the measured results more closely. DoFa calculated a total cavity airflow rate of 93.5 m^3/h. Although Saelens (2002) did not report the airflow rate for this case, a case with similar outdoor conditions and two open grids resulted in an airflow rate of 92 m^3/h. Therefore, it appears that the relation suggested by Pappas and Zhai (2008) corresponds well with two open grids.

Saelens (2002) provided more data for cases with one open grid. Therefore, the correlation empirically derived by Saelens (2002) was used to characterize pressure difference as a function of temperature difference and wind speed.

$$\Delta P = 0.033\Delta T_{avg} - 0.011V^2 \qquad \text{[Pa]} \qquad \textbf{(5.1)}$$

Where,

ΔT_{avg} = difference between average cavity and inlet temperatures [°C]

V = wind speed [m/s]

This correlation relates to low wind speeds; therefore, a value of V = 1 m/s was chosen. The pressure difference is then related to the airflow rate through the ventilation grid:

$$Q = 57 \cdot \Delta P^{0.51} \qquad [m^3/s] \qquad \textbf{(5.2)}$$

Using the airflow distribution established in Case 1S and the new flow relationship, Cases 2S and 3S were modeled (Figure 5.13).

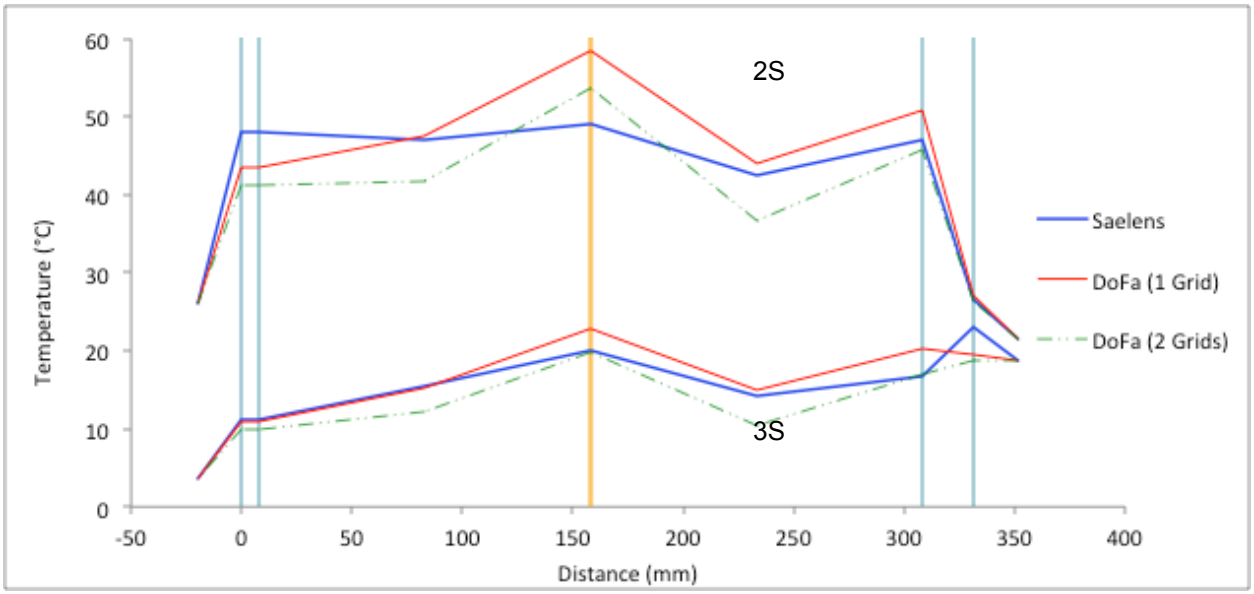

Figure 5.13 Cases 2S and 3S Temperature Profiles

Note again that the shade temperature was not measured by Saelens (2002). The temperature profiles for one open grid were similar to the measured data in both cases. However, DoFa overestimated the interior cavity surface temperature, which was also true for Case 1S. This is likely due to the calculated convection coefficient at this surface (see

Table 5.22). Furthermore, while the incidence angles were close to normal, the diffuse fraction was unknown. The DoFa model assumed 100% direct incident solar radiation, which may have caused some difference in results.

In Case 3S. Saelens (2002) reported measured and calculated airflow rates.

Table 5.19 Case 3S Airflow Rate Comparison

	Saelens		DoFa
	Measured	Calculated	Calculated
Airflow Rate [m^3/h]	30.4	35.6	34.4

The airflow rate calculated by DoFa was closely matched to Saelens' (2002) results; however, the correlation used is only valid for the Vliet test cell. This shows the importance of characterizing the inlet/outlet grids to predict accurate airflow rates and temperature profiles. If

Cases 2S and 3S were repeated for two open grids, the results would be different. The dotted green lines in Figure 5.13 show the profiles for two open grids, which underestimated the cavity temperatures.

Unfortunately, Saelens (2002) did not report SHGC or U-value to compare. Instead he uses the results from his numerical model in a building simulation program to calculate overall energy loads. However, he did report inflowing heat flux from the indoor surface for Case 3S in day and night conditions. In Table 5.20, Saelens' (2002) calculated results are compared to DoFa. Airflow rates were fixed to reduce variables.

Table 5.20 Case 3S Thermal Heat Flux

	Airflow Rate	Thermal Heat Flux [W/m^2]		
Time	[m^3/h]	Saelens	DoFa	Difference
Day	30.4	7.0	6.2	12.6%
Night	16.2	-9.4	-9.6	2.4%

For the daytime case, the measured indoor surface temperature was higher than that predicted by DoFa (Figure 5.13). Whether this was due to instrument error or higher absorptance in that pane, the result is a higher inflowing heat flux. However, the thermal heat flux is only a portion of the total heat flux in the daytime (approximately 30% for this case). At nighttime, thermal heat flux and total heat flux are equivalent. The DoFa results matched Saelens' (2002) results relatively well in this case.

5.2.1.3 Inlet Temperatures and Convection Coefficients

Other than airflow, both inlet temperature and cavity convection coefficients affect the average cavity temperature. Sealens (2002) provided a vertical temperature profile for the two cases presented in Table 5.22. These temperature profiles were used to compare the effects of inlet temperature and cavity convection coefficients on average cavity temperature.

Table 5.21 Test Cases

Case	$G_{t\theta}$ [W/m^2]	$T_{a,ext}$ [°C]	$T_{a,int}$ [°C]	T_{inlet} [°C]	Open Grids	Q [m^3/h]
4S	575	9.8	20.0	18.0	1	50
5S	542	4.9	21.5	9.8	2	92

Note that the measured inlet and average cavity temperatures reported in this section are approximate values estimated from the vertical temperature profiles.

Saelens (2002) stresses the importance of modeling the correct inlet temperature. In times of high solar radiation, air flowing through the inlet is warmed as it comes in contact with the grids. The rise in temperature depends on the flow rate, with lower flows corresponding to higher temperature rises. In winter, Saelens (2002) found a temperature increase over the inlet grid of approximately 8°C for one open grid (Case 4S) and 5°C for two open grids (Case 5S).

With respect to cavity convection coefficients, Saelens (2002) reported calculated values for Case 3S of the previous section. The same naming convention used in Section 4.4.5 is used here, with surface numbers increasing from inside out (Figure 5.14).

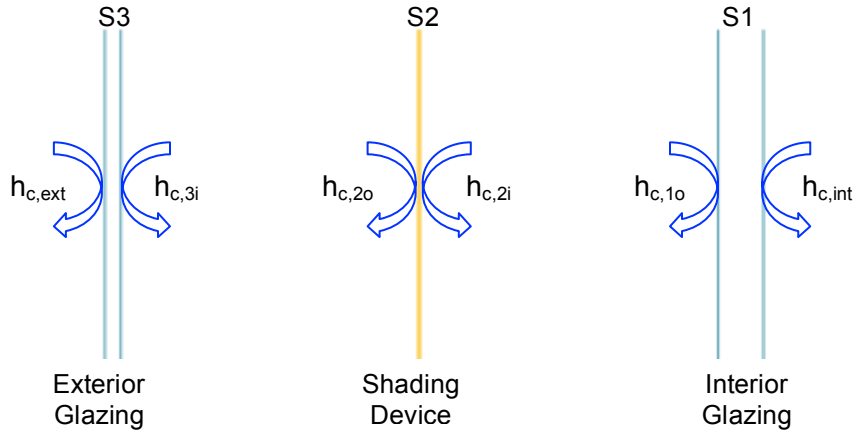

Figure 5.14 Convection Coefficient Naming Convention

Saelens' (2002) convection coefficients were calculated using similar empirical correlations to those used in DoFa; however, the average surface and fluid temperatures were determined by integrating over the height of the façade. Furthermore, a correction term was used to account for using the fluid temperature instead of the free stream fluid temperature. While it is unclear how the free stream fluid temperature was calculated, the correction caused Saelens' (2002) h_c values to differ from those calculated in DoFa.

Table 5.22 Open Cavity Convection Coefficients [W/m^{2}K]

Model	$h_{c,3i}$	$h_{c,2o}$	$h_{c,2i}$	$h_{c,1o}$
Saelens	0.6	6.8	7.1	9.1
DoFa	2.49	2.81	2.78	2.34

Table 5.22 suggests that empirical relations for flat plates may underestimate actual convection coefficients in a naturally ventilated DF with solar radiation. At nighttime when the shading device was raised, the convective coefficients were slightly better matched.

Table 5.23 Enclosed Cavity Convection Coefficients [W/m^{2}K]

Model	$h_{c,3i}$	$h_{c,1o}$
Saelens	1.50	3.1
DoFa	1.25	1.77

Recognizing the potential error caused by inlet temperature and convection coefficients, DoFa results were compared to the measured data for Cases 4S and 5S. To begin, a base case was modeled using the outdoor temperature as the inlet temperature and calculated convection coefficients. Three modified cases were then tested to determine if the accuracy of the DoFa model could be improved. The three cases used 1) modified inlet temperatures measured by Saelens (2002), 2) fixed convection coefficients from Table 5.22 and 3) both modified inlet temperatures and fixed convection coefficients. Table 5.24 shows the results. Airflow rates were fixed to reduce variables.

Table 5.24 Average Cavity Temperatures Depending on Inlet Temperature

			Saelens	DoFa			
Case	Measure	Unit	Measured	Base	T_{inlet}	h_c	$T_{inlet} + h_c$
4S	T_{avg}	°C	30.0	27.1	31.0	30.9	35.3
	Difference	%	-	10.3%	3.4%	2.8%	16.1%
5S	T_{avg}	°C	20.0	16.9	20.0	19.0	22.4
	Difference	%	-	16.8%	0.2%	5.2%	11.5%

Altering the inlet temperature or the h_c value improved the accuracy of the DoFa model. This was more important for Case 5S, where high airflow extracted more heat from the cavity. However, when both modifications were made simultaneously, the cavity temperature was overestimated. However, the fixed h_c values were only approximate. Values calculated for Case 3S would not be the same for Cases 4S and 5S. The influence of inlet temperature and convection coefficients on overall system performance will be discussed in Section 5.3.

5.2.2 Park et al. (2004)

5.2.2.1 Experimental Setup

Park et al. (2004) conducted experiments at the Smart Façade Demo Unit (SFDU) in Atlanta, Georgia. The setup consisted of a one-storey, south-facing DF with natural airflow. The airflow

path was switched between 10 different modes during the experiments. Therefore, a time when the façade was set to the interior air curtain mode was chosen because this would exclude wind effects. The time chosen was approximately 12:30 pm on March 25, 2003.

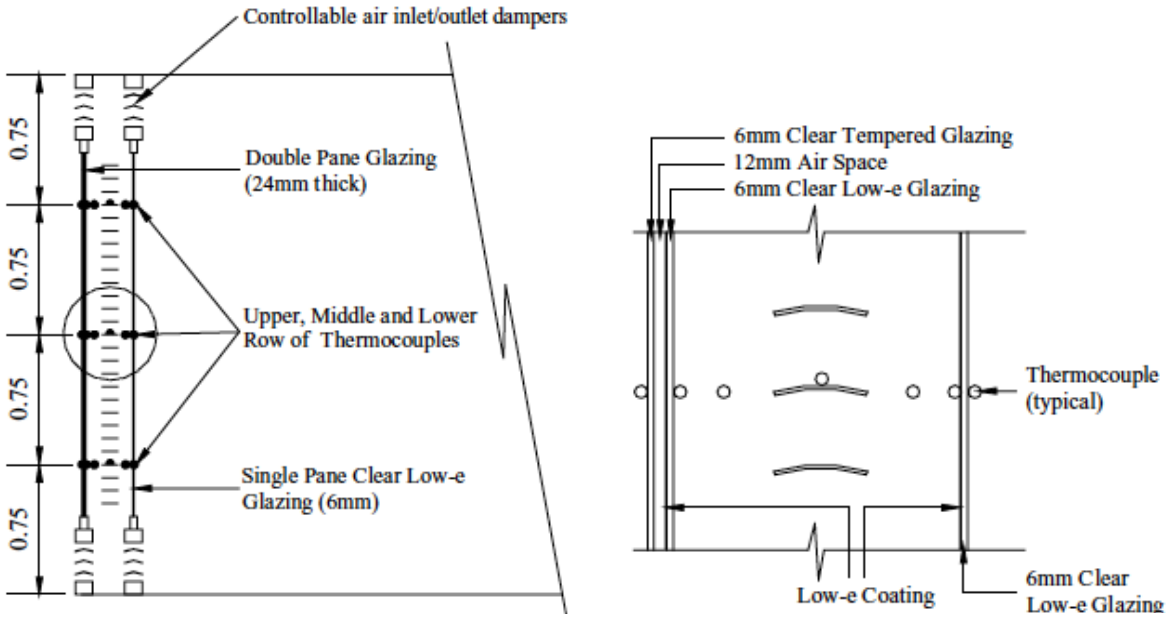

Figure 5.15 SFDU Experimental Setup (Park et al., 2002)

The façade geometry and composition are described in Table 5.25. Note that in this case, the double glazing U-value was not provided. Because the fill was air, it could be modeled using DoFa as two single glazing layers and an enclosed cavity. However, if the fill was a gas mixture other than air, it would need to be modeled as multi glazing with a U-value obtained from WINDOW or VISION.

Table 5.25 System Properties

Item	Description
Height	3.0 m
Width	1.2 m
Depth	0.3 m
Outdoor Surface	Double glazing (Clear+12mm Air+Low-E 0.05)
Shading Device	Venetian Blind, 10-cm wide, yellow PVC, centered in cavity
Indoor Surface	Single glazing (Clear)

There were various difficulties in replicating the experiment, largely because optical properties were not provided. However, a detailed discussion of h_c values was presented. Therefore, an

attempt was made to model the façade to make a general comparison of h_c values. The chosen optical properties are presented in Appendix C.

The next step was characterizing the inlet/outlet dampers. To account for the obstruction caused by the dampers, half of the opening area (0.27 m^2) was chosen with a C_d value of 0.65. This seemed to accurately predict airflows within the cavity (26 cm/s or 337 m^3/h).

5.2.2.2 Comparison Results

Results reported by Park et al. (2004) were compared with results obtained using DoFa. However, note that all values from Park et al. (2004) are approximate values estimated from graphs, including indoor and outdoor boundary conditions. The resulting temperature profiles are presented in Figure 5.16.

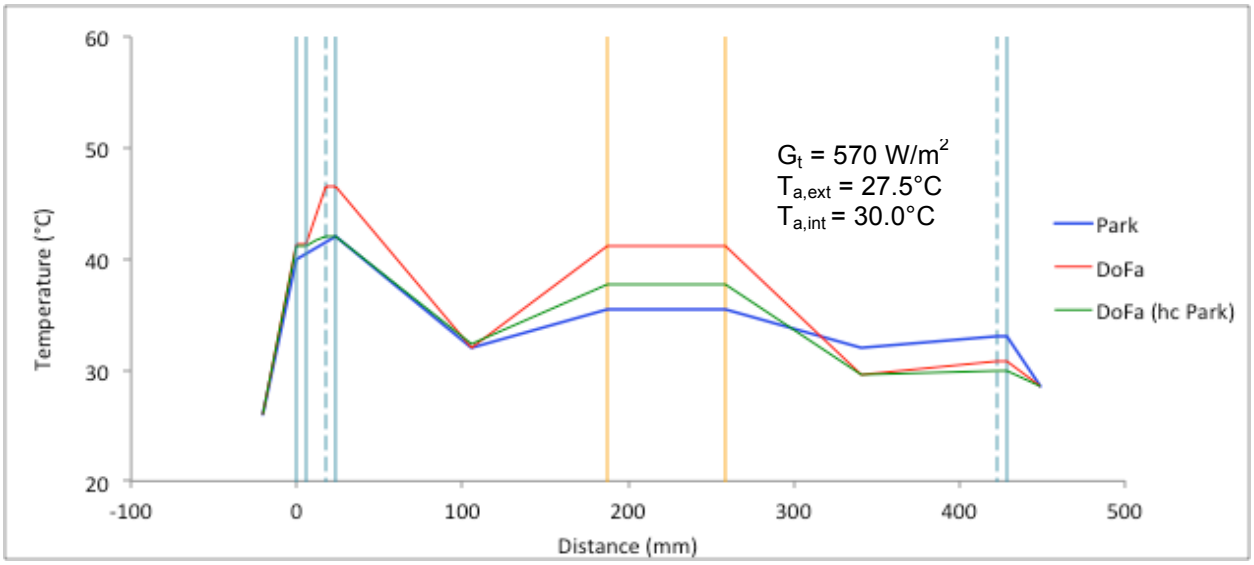

Figure 5.16 Temperature Proflie for SFDU

A first scenario uses h_c values calculated by DoFa while the second uses empirically calibrated average h_c values by Park et al (2004). As was expected, using Park's h_c values resulted in a more accurate temperature profile. Note that Park et al. (2004) only reported one cavity temperature, so both cavities were assumed to have the same temperature in Figure 5.16. Table 5.26 lists the two sets of h_c values.

Table 5.26 Convective Coefficient Comparison [W/m^{2}K]

Model	$h_{c,ext}$	$h_{c,3i}$	$h_{c,2o}$	$h_{c,2i}$	$h_{c,1o}$	$h_{c,int}$
Park	9.16	7.03	7.23	7.23	9.5	3.83
DoFa	9.50	3.29	3.82	4.07	1.7	1.75

While Park et al. (2004) did not explicitly state average indoor and outdoor h_c values, their empirically-calibrated equations were used to calculate the values provided in Table 5.26. Once again, experimental results indicate that empirical relations published in the literature underestimate convective coefficients. Park et al. (2004) suggest that this is also true for an enclosed cavity. In their paper, they state that literature h_c values "are empirically derived for an enclosed cavity with both vertical sides insulated. Thus, those empirical values from the literature, which do not account for lateral heat losses, might cause a significant error in predicting the system's behaviour, if not calibrated or cautiously used."

5.2.3 Conclusions

Comparisons with empirical results showed that DoFa can accurately predict temperature profiles for double façades with natural airflow. However, the comparisons showed that the accuracy depends on certain parameters such as inlet/outlet grid characterization, flow distribution, inlet temperature and cavity convection coefficients. The effect of these parameters on façade performance will be examined in the following section.

5.3 Parametric Evaluation

The comparisons conducted in the previous sections suggest that results can be sensitive to some of the assumed input values. Therefore, a parametric study was conducted. The configuration from Case 5B in Section 5.1.4 was used because it represents a likely DF; however, the low-E coating on the exterior glazing was changed to 0.10 to model a more durable coating that would be required in a DF cavity. Note that 0.10 is still very low for a durable coating. The setup is described in Table 5.27.

Table 5.27 Double Façade Setup for Parametric Study

Item	Description
Height	3.0 m
Width	1.0 m
Depth	0.6 m
Vent Areas	0.2 m^2
C_d	0.65
Outdoor Surface	Single Glazing (Low-E 0.10)
Shading Device	Roller Blind (RB1), centered in cavity
Indoor Surface	Double glazing U = 1.66 W/m^2K

The optical properties used for the new low-E glazing are presented in Appendix C. The following sections discuss the impacts of convection coefficients, airflow distribution, airflow rate, inlet temperature and optical properties. All comparisons were conducted under summer NFRC-100 conditions unless otherwise specified.

5.3.1 Convection Coefficients

Experimental results from Saelens (2002) and Park et al. (2004) indicated that cavity convection coefficients for DFs with natural airflow are greater than equations in the literature suggest. Therefore, the effect of increasing convection coefficients was examined (Table 5.28).

Table 5.28 Effect of Cavity Convection Coefficients: Open Vents Day

Measure	Units	Base	1A	1B	1C	1D
$h_{c1,o}$	W/m^2K	2.7	5.5	8.0	8.0	9.0
$h_{c3,I}$, $h_{c2,o}$, $h_{c2,i}$	W/m^2K	2.8	5.5	5.5	8.0	7.0
Thermal Heat Flux	W/m^2	33.5	29.2	28.2	27.8	27.6
Change	%	0.0%	-12.8%	-15.7%	-17.0%	-17.4%
Total Heat Flux	W/m^2	86.0	81.7	80.7	80.3	80.1
Change	%		-5.0%	-6.1%	-6.6%	-6.8%

In the base case, h_c values calculated by DoFa were used. However, the values suggested by Saelens (2002) and Park et al. (2004) were much higher, similar to Case 1D. Temperature profiles for the base case and Case 1D are compared in Figure 5.17.

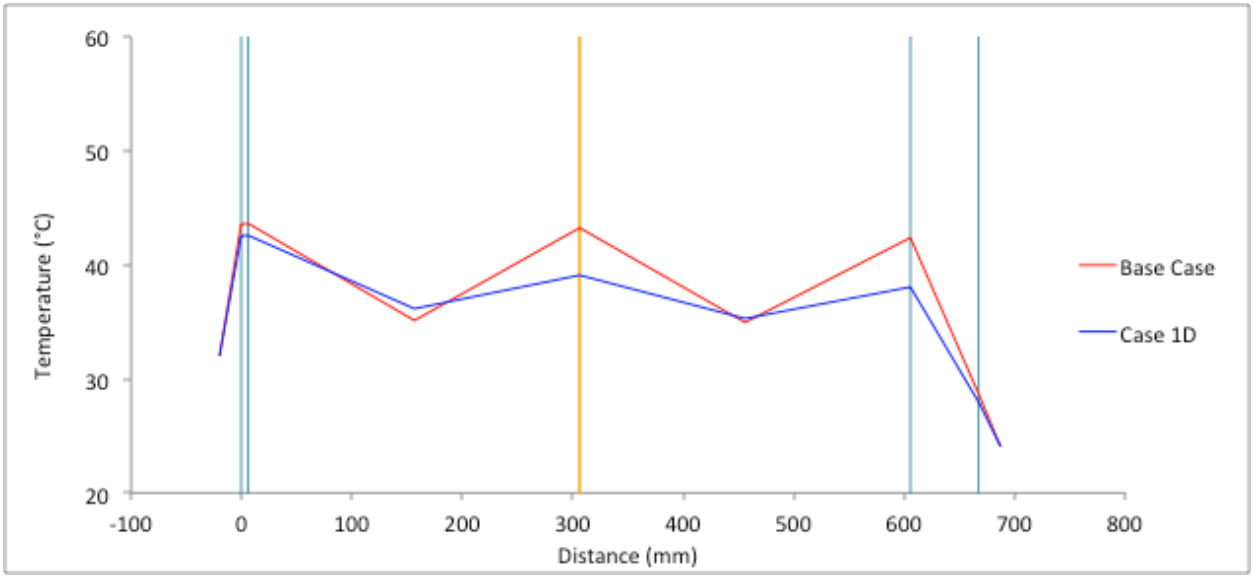

Figure 5.17 Effect of Cavity Convection Coefficients: Summer Conditions

Note that the base case estimated higher shading device and interior cavity surface temperatures, similar to comparisons with Saelen's (2002) results in Section 5.2.1.2. Between the base case and Case 1D, the decrease in thermal heat flux was over 17%. However, the decrease in total heat flux was under 7%. This is because in periods of high solar radiation, the majority of incoming heat flux is due to direct solar gains.

At nighttime, the airflow through the cavity and resulting convection coefficients are lower. For comparison, two situations representative of nighttime cooling were modeled with an indoor temperature of 24°C. Results using h_c values calculated by DoFa were compared to results using h_c values suggested by Saelens (2002).

Table 5.29 Effect of Cavity Convection Coefficients: Open Vents Night

		$T_{a,ext}$ = 19°C		$T_{a,ext}$ = 15°C	
Measure	**Units**	**h_c Calc**	**h_c Fixed**	**h_c Calc**	**hc Fixed**
$h_{c1,o}$	W/m^2	1.6	3.0	1.85	3.00
$h_{c2,i}$, $h_{c2,o}$, $h_{c3,i}$	W/m^2	1.0*	1.5	1.31*	1.50
U-Value	W/m^2	0.87	0.94	0.92	0.96
Total Heat Flux	W/m^2	-4.4	-4.7	-8.3	-8.7
Change	%	-	-7.9%	-	-4.9%

** Average of* $h_{c2,i}$, $h_{c2,o}$ and $h_{c3,i}$

For nighttime cases, the change in total heat flux was under 8%.

Park et al. (2004) suggested that equations in the literature also underestimate convection coefficients for enclosed cavities. Therefore, the effect of increasing convection coefficients for an enclosed cavity was examined using NFRC-100 winter conditions (Table 5.30).

Table 5.30 Effect of Cavity Convection Coefficients: Closed Vents Night

Measure	**Units**	**Base**	**2A**	**2B**	**2C**	**2D**
$h_{c1,o,}$, $h_{c2,i}$	W/m^2K	1.4	3.0	3.0	5.5	8.0
$h_{c3,l}$, $h_{c2,o}$	W/m^2K	1.8	1.5	3.0	5.5	5.5
U-Value	W/m^2K	0.70	0.74	0.82	0.95	0.98
Heat Flux	W/m^2	-27.4	-28.7	-32.1	-37.2	-38.1
Change	%	0.0	-4.5%	-16.8%	-35.5%	-38.9%

The values suggested by Park et al. (2004) resemble Case 2D. Temperature profiles for the base case and Case 2D are compared in Figure 5.18.

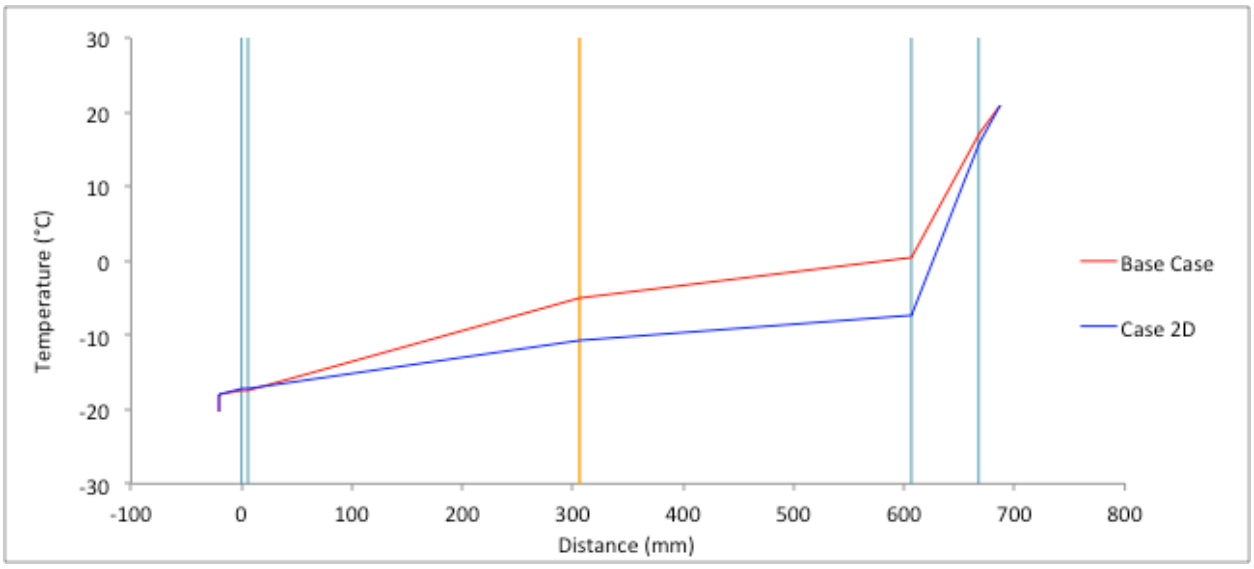

Figure 5.18 Effect of Cavity Convection Coefficients: Winter Conditions

Using h_c values suggested by Park et al. (2004) resulted in an increase in outflowing heat flux of 39%. However, Park et al. (2004) conducted their experiments over a 72-hr period during which solar heating would have increased the average h_c values. Furthermore, the experiments were conducted in Georgia, where winter temperatures are not as extreme. A more likely case might be 2B, which resulted in a 17% increase in outflowing heat flux. Further experimental results are needed to confirm enclosed-cavity convection coefficients.

Indoor and outdoor convection coefficients were also examined to determine the effect on overall performance. Summer and winter results are presented in Table 5.31.

Table 5.31 Effect of Indoor/Outdoor Convection Coefficients

	Summer			Winter		
Measure	**Base**	**3A**	**3B**	**Base**	**4A**	**4B**
$h_{c,ext}$ [W/m^{2}K]	18.9	18.9	7.5	31.7	31.7	15.0
$h_{c,int}$ [W/m^{2}K]	2.3	3.6	2.3	2.2	3.4	2.2
Thermal Heat Flux [W/m^2]	33.5	34.2	34.2	-27.4	-27.9	-27.0
Percent Change	-	2.3%	2.3%	-	-1.5%	1.5%
Total Heat Flux [W/m^2]	86.0	86.7	86.7	-	-	-
Percent Change	-	0.9%	0.9%	-	-	-

The indoor and outdoor convection coefficients were altered In Cases A and B respectively. In both summer and winter cases, a small change in the $h_{c,int}$ was equivalent to a larger change in

$h_{c,ext}$. However compared to cavity h_c values, indoor and outdoor values had relatively little effect on the final heat flux through the façade.

5.3.2 Airflow Distribution

As discovered in the comparison with Saelens (2002), the flow distribution can be important to correctly estimate cavity temperatures. Therefore, the effect of the exterior flowing fraction (Fe) was investigated.

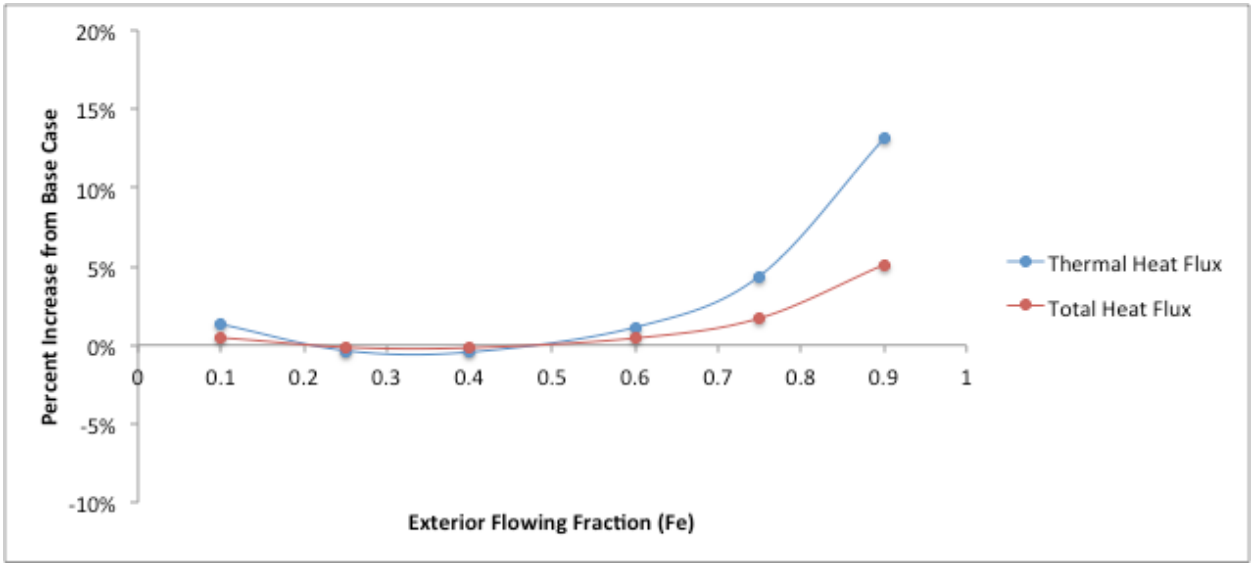

Figure 5.19 Effect of Exterior Flowing Fraction

Figure 5.19 suggests that an Fe above 50% increases the inflowing heat flux. However, reducing the Fe below 50% had very little effect. Therefore, locating the shading device directly in front of the interior façade would be unwise because airflow would not be able to extract the absorbed heat. On the other hand, locating the shading device directly behind the exterior façade also caries a small energy penalty. For the configuration studied, an exterior flowing fraction between 0.2 and 0.5 would provide the most heat extraction from the cavity.

5.3.3 Airflow Rate

Comparisons with empirical results showed that correctly characterizing the inlet/outlet openings is very important to the cavity airflow rate. Therefore, the importance of inlet/outlet characterization to overall façade performance was investigated. A base case of A = 0.1 m^2

and C_d = 0.65 (C_dA = 0.065 m^2) was chosen. The C_dA product was then altered to determine the effect on inflowing heat flux. Figure 5.20 illustrates the results.

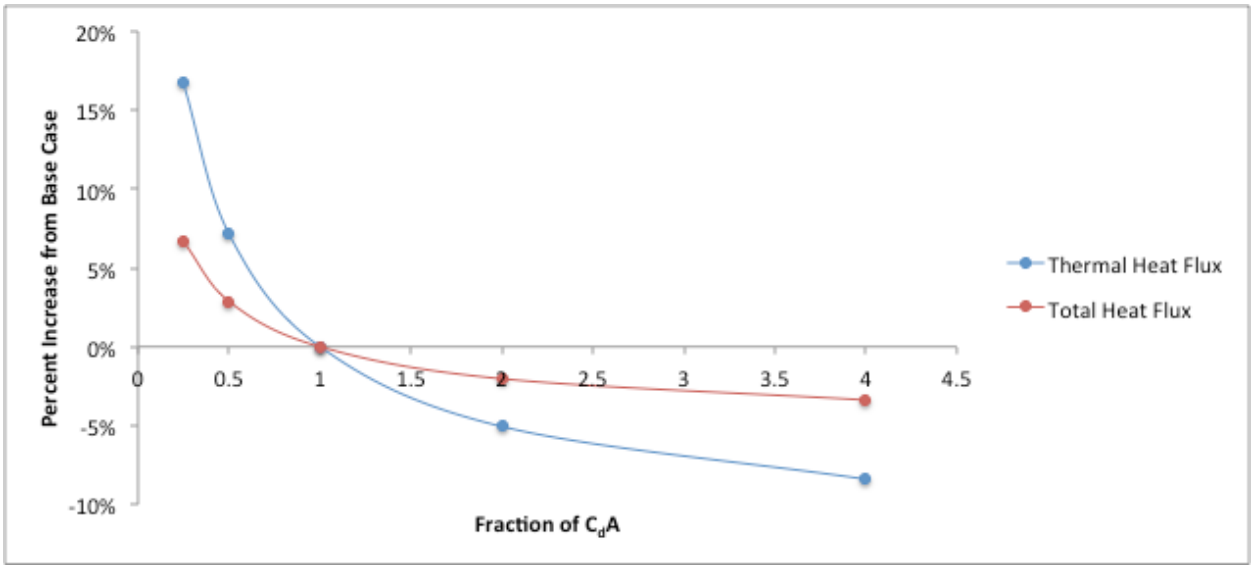

Figure 5.20 Effect of Airflow Rate

The relationship between C_dA product and inflowing heat flux is an exponential curve. Decreasing the C_dA product had a relatively significant effect, while increasing the C_dA product past double had very little additional effect. Note that C_dA product and airflow rate are directly related. For the cases examined, airflow rates ranged from 49 m^3/h (2.3 cm/s) to 361 m^3/h (16.7 cm/s), which are realistic rates for a one-storey DF (Saelens, 2002; Park et al., 2004). The average rate for the base case was 137 m^3/h (6.7 cm/s).

5.3.4 Inlet Temperature

Saelens (2002) discusses the importance of properly modeling the inlet temperature. However, when the interior layer is double glazing, the effect of the cavity temperature on inflowing heat flux is moderated. Therefore, a second common DF configuration was investigated, where the double glazing was located on the exterior and a clear, single glazing was located on the interior. It was expected that cavity temperature would be more important in this case. In Figure 5.21, DG and SG denote the double-glazing interior and single-glazing interior cases respectively.

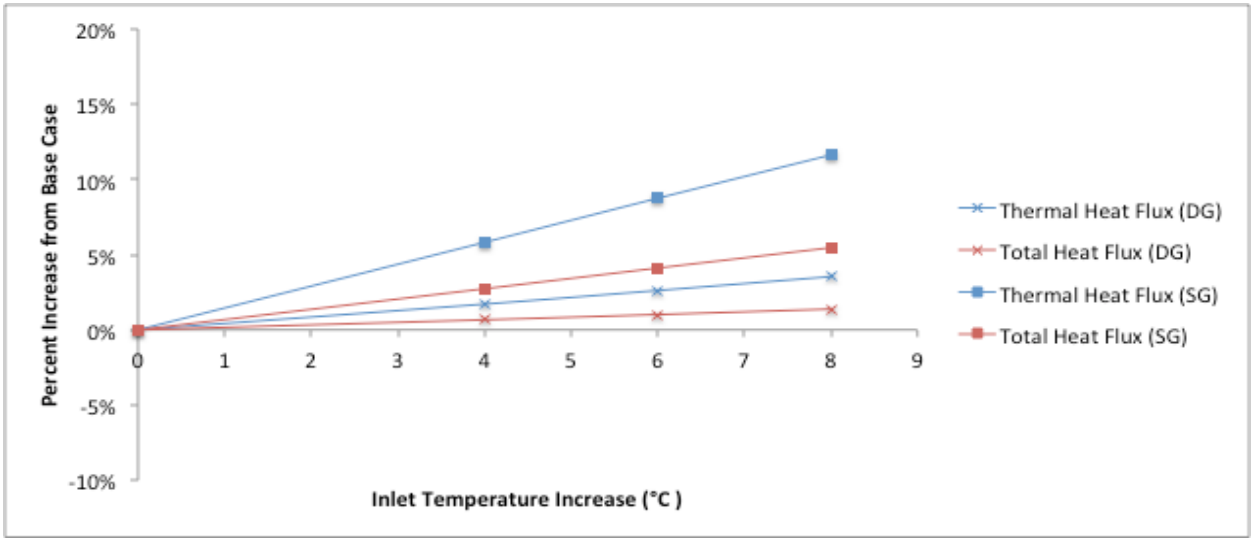

Figure 5.21 Effect of Inlet Temperature

As expected, inflowing heat flux was more affected in the SG case. This would also be true for other parameters affecting the cavity temperature, such as airflow distribution and rate.

5.3.5 Optical properties

Correct optical properties of each layer are important to accurately predict the behaviour of the façade. Therefore, the impacts of diffuse solar radiation and off-normal incidence angles were investigated. Figure 5.22 illustrates the results.

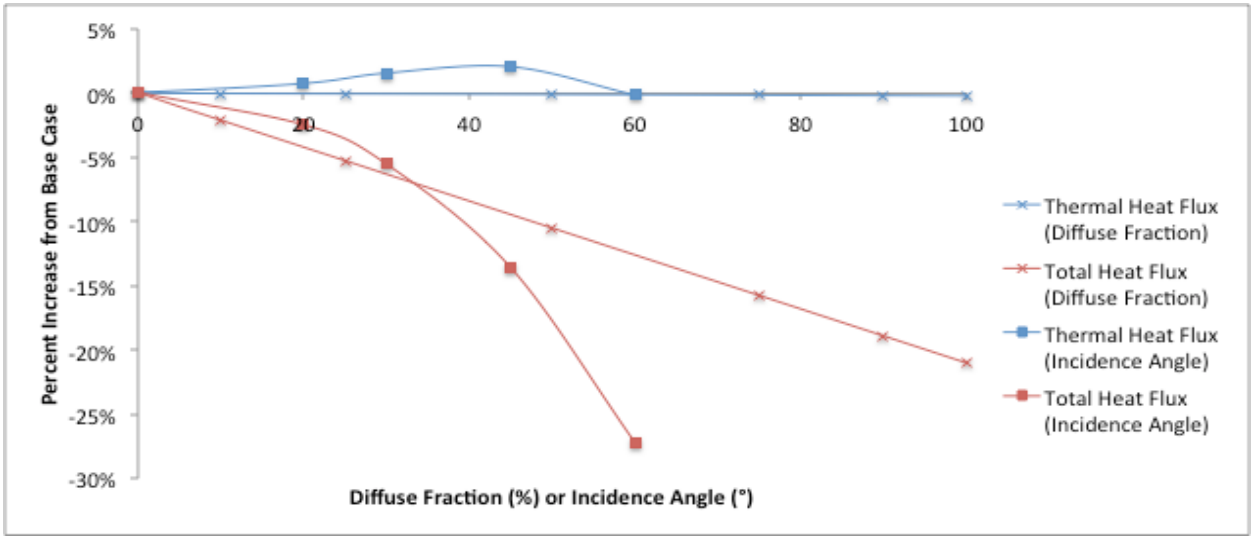

Figure 5.22 Effect of Incidence Angle and Diffuse Fraction

While optical properties had little effect on thermal heat flux, they had a significant effect on the total heat flux. This is because the overall transmittance of the façade is decreased with incidence angle. For the tested case, fully diffuse incident radiation was equivalent to an incidence angle between 50° and 60°. This agrees with the results by Brandemuehl and Beckman (1980), which suggest that solar properties for diffuse radiation on a vertical surface are equivalent to solar properties at an incidence angle of 60°. Note that the results would be different for a venetian blind.

5.3.6 Outlet Temperature

The previous sections examined the effect of various input parameters on heat flux through the façade. However, outlet temperature is also an important output of a DF model. For example, correct outlet temperature is needed to estimate when cavity air could be used for natural ventilation or to quantify potential energy savings associated with using cavity air as preheated ventilation air. Therefore, the effect of the previously described parameters was examined with respect to peak temperature difference between outlet and outdoor conditions. Figure 5.23 shows the effects of airflow rate, airflow distribution and inlet temperature. The effects of convection coefficients and optical properties were excluded because they were minimal.

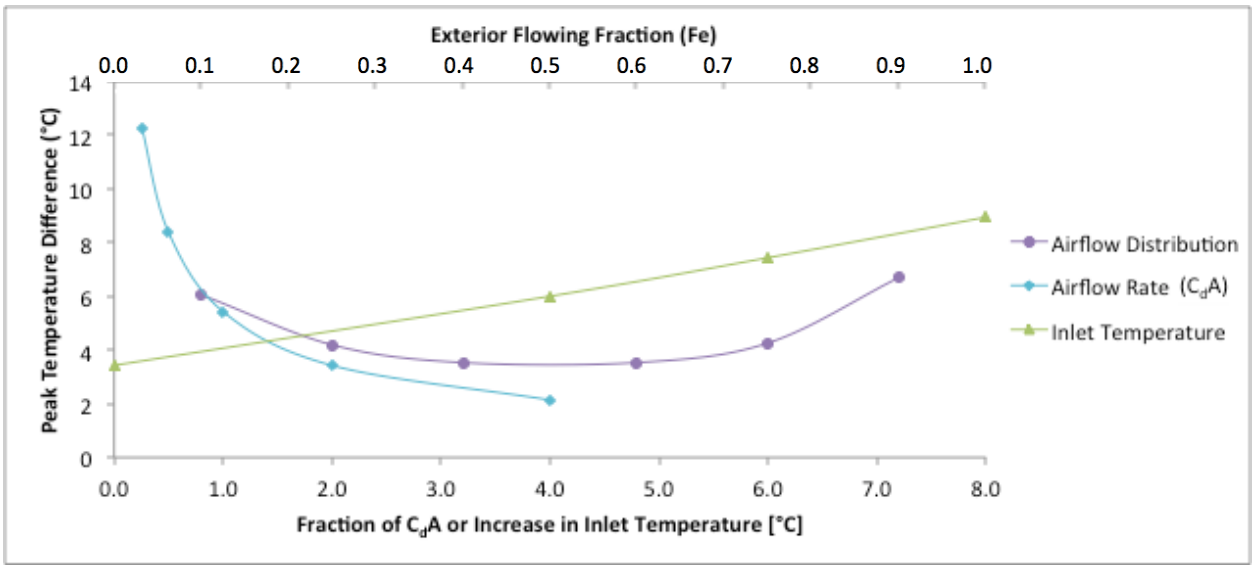

Figure 5.23 Impact of Input Parameters on Peak Temperature Difference (airflow distribution uses top x-axis)

The airflow rate (C_dA) had the largest effect, though it also had the largest testing range (¼ to 4 times the original C_dA product). In many DF systems, the inlet/outlet opening size can be varied to obtain the desired airflow rate. However, the designer must be able to correctly characterize the inlet/outlet openings to determine the maximum size required. For the cases tested, the maximum increase in peak temperature difference between inlet and outlet was approximately 8.8°C (C_dA fraction = 0.25) over the base case (C_dA fraction = 1.0).

The inlet temperature had the second largest effect. Unfortunately the increase in inlet temperature cannot be predicted in a simple way, as it depends on the incident solar radiation, inlet grid configuration and materials, airflow rate and climatic conditions. The designer may input a inlet temperature increase into the DoFa model if a specific value is expected. For the cases tested, the maximum increase in peak temperature difference between inlet and outlet was approximately 5.5°C (T_{inlet} increase = 8°C) over the base case (T_{inlet} increase = 0°C).

When the airflow distribution was not equal between the exterior and interior cavities, the outlet temperature increased. However, airflow distribution had the smallest effect of the three parameters. For the cases tested, the maximum increase in peak temperature difference between inlet and outlet was approximately 3.2°C (Fe = 0.9) over the base case (Fe = 0.5).

5.3.7 Conclusions

A summary of the parametric study findings are presented in Table 5.32.

Table 5.32 Parametric Study Summary

Parameter	Change with Maximum Effect	Increase from Base Case: Thermal Heat Flux	Increase from Base Case: Total Heat Flux	Increase from Base Case: Outlet Temp [°C]
Convection Coefficients	$h_{c,cav}$, Case 1D	-17.4%	-6.8%	0.80
	$h_{c,ext}$, Case 3B	2.3%	0.9%	0.65
Airflow Distribution	Fe=0.9	13.1%	5.1%	3.17
Airflow Rate	C_dA = ¼(0.065)	16.7%	6.7%	8.80
Inlet Temperature	$T_{a,ext}$ + 8°C	3.5%	1.4%	5.52
Optical Properties	θ = 60°	-0.1%	-27.2%	0.39

The results presented in Table 5.32 are for an open cavity and summer conditions. For the case studied, cavity convection coefficients had the largest effect on thermal heat flux while optical properties had the largest effect on total heat flux. Cavity airflow rate had the largest effect on the outlet temperature.

For a closed cavity and winter conditions, many of the parameters do not apply. However, cavity convection coefficients were found to be very important to the overall performance of the façade. Altering the cavity h_c values from those calculated by DoFa resulted in an average 17% increase in outflowing heat flux.

In the DoFa model, the user is responsible for C_dA values, flow distribution, inlet temperature and optical properties. However, the DoFa model is responsible for cavity convection coefficients. From comparisons with empirical results, it is apparent that the DoFa model underestimates convection coefficients for natural airflow in the presence of solar radiation. Further experimental results are needed to confirm convection coefficient relationships for both open and closed DF cavities.

5.4 Model Simplifications and Limits

While the DoFa model can be a useful design tool, one must understand the simplifications made and the modeling limits. Firstly, various simplifications were made because the effect was deemed insignificant for the required accuracy:

1) Incident solar radiation: calculations are for a clear sky only. If performance on a cloudy day is being investigated, the user should choose “user defined” values with a high diffuse fraction. Also, shading caused by frames or building geometry is not accounted for, though the user can account for these by modifying layer thermal/optical properties and the fraction of diffuse incident radiation.
1) Absorbed solar radiation: calculations are based on the assumption that no source of solar radiation exists on the inside (i.e., the room) and reflections from the floor or ceiling of the cavity are not included.
2) Conduction: thermal resistance of single glazing and shading devices is assumed negligible.
3) Longwave radiation: calculations within the cavity space assume infinite parallel plates; therefore, the cavity floor and ceiling are excluded.
4) Convection within the cavity: coefficient calculations for natural airflow are valid for wide cavities.

Based on the approach and calculations used, there are also several limits to DoFa's modeling capabilities:

1) Absorbed solar radiation: optical properties are user input and are treated as fixed values (i.e., normal optical properties are not converted to equivalent off-normal properties) and beam-diffuse reflection and transmission is not accounted for. Consequently, DoFa does not accurately predict the effective optical properties of venetian blinds. If no alterations are made to the blind transmittance, DoFa will overestimate or underestimate the overall system transmittance depending on the location of the blind within the assembly.
2) Cavity convection: coefficients are calculated using empirical Nusselt number correlations from the literature. Validation with experimental results suggests that these underestimate convection coefficients in the presence of natural airflow and solar radiation. This would cause the model to overestimate cooling loads in summer. Note that mechanical convection coefficients were not validated with experimental results.
3) Airflow rate: natural airflow is calculated from buoyancy forces only. Therefore, natural airflow predictions may be inaccurate in windy locations, though a windless day is usually considered for design conditions. Also, calculations are dependent on characterization of inlet areas and flow coefficients, which are user input.
4) Airflow distribution: not modeled in detail. In a cavity separated by a shading device, airflow is assumed to have the same direction in both shafts, which prohibits the simulation of rotational flow. Airflow is also assumed one-dimensional in the vertical direction, preventing the simulation of diagonal flow through a shading device (i.e., venetian blind). However, the flow distribution on either side of the shading device is user input and may be altered accordingly.
5) Thermal mass: not accounted for since DoFa uses steady-state energy balances. Therefore, surfaces with thermal mass would heat and cool more slowly than predicted by the DoFa model.
6) Results: predict instantaneous loads and performance. At present, the model results should not be used for annual simulations. Furthermore, results predict general performance (e.g., average surface temperatures and bulk airflows). For detailed design requiring local airflow distribution or surface temperatures, a more complex modeling

tool would be needed.

7) Applications: developed for assembly sections with uniform layers. Users can account for mixed opaque/glazed layers (e.g., masonry with punched windows) by area-weighting the thermal and optical properties of the layer. However, in cases where a layer is present in one section and not in another (i.e., shading device), area weighting does not work. A method is presented in Chapter 6 for vertically stacking uniform sections to create an overall assembly. The method is simplified and should not be used without further development and validation.

It is important that designers consider the limits listed above to understand the accuracy of their results. Future model development should aim to minimize the listed limits.

Chapter 6
Applications

6.1 Glazing Analysis

One application of the DoFa model is to make direct comparisons between glazing systems. Therefore, a comparison was conducted to demonstrate how the DoFa model might be used. The relative performance of a variety of DFs was assessed with respect to conventional glazing units. Comparisons were conducted in summer and winter design conditions as well as average conditions.

6.1.1 Case Descriptions

The cases examined in the comparison are presented in Table 6.1.

Table 6.1 Case Descriptions

Name	Description	S3	S2	S1
DG	Insulated double glazing unit	N/A	Low-E 0.02	Clear
	Double glazing with intermediate shading	N/A	Low-E 0.10	Clear
TG	Insulated triple glazing unit	Low-E 0.04	Low-E 0.02	Clear
	Triple glazing with intermediate shading	Low-E 0.10	Low-E 0.03	Clear
DF-A	Low-E exterior, clear interior	N/A	Low-E 0.10	Clear
DF-B	DG exterior, clear interior	Low-E 0.02	Clear	Clear
DF-C	Clear exterior, DG interior	Clear	Low-E 0.02	Clear
DF-D	Low-E exterior, DG interior	Low-E 0.10	Low-E 0.02	Clear

All layer optical properties are provided in Appendix C. For the double and triple glazing units, a shading device was placed on the outside, inside or in between panes. Cavity depths were different depending on the cavity type, as presented in Table 6.2.

Table 6.2 Cavity Descriptions

Cavity	Depth [mm]	Fill	Airflow
Insulated glazing	12.7	10% Air, 90% Argon	Sealed
Intermediate shading	22.5	Air with shading device	Sealed
Outdoor/Indoor shading	24.5	Air	Natural
Double façade	800	Air with shading device	Natural

VISION was used to test the insulated double and triple glazing units while DoFa was used to test the remainder of the cases. The test cases are illustrated in Figure 6.1.

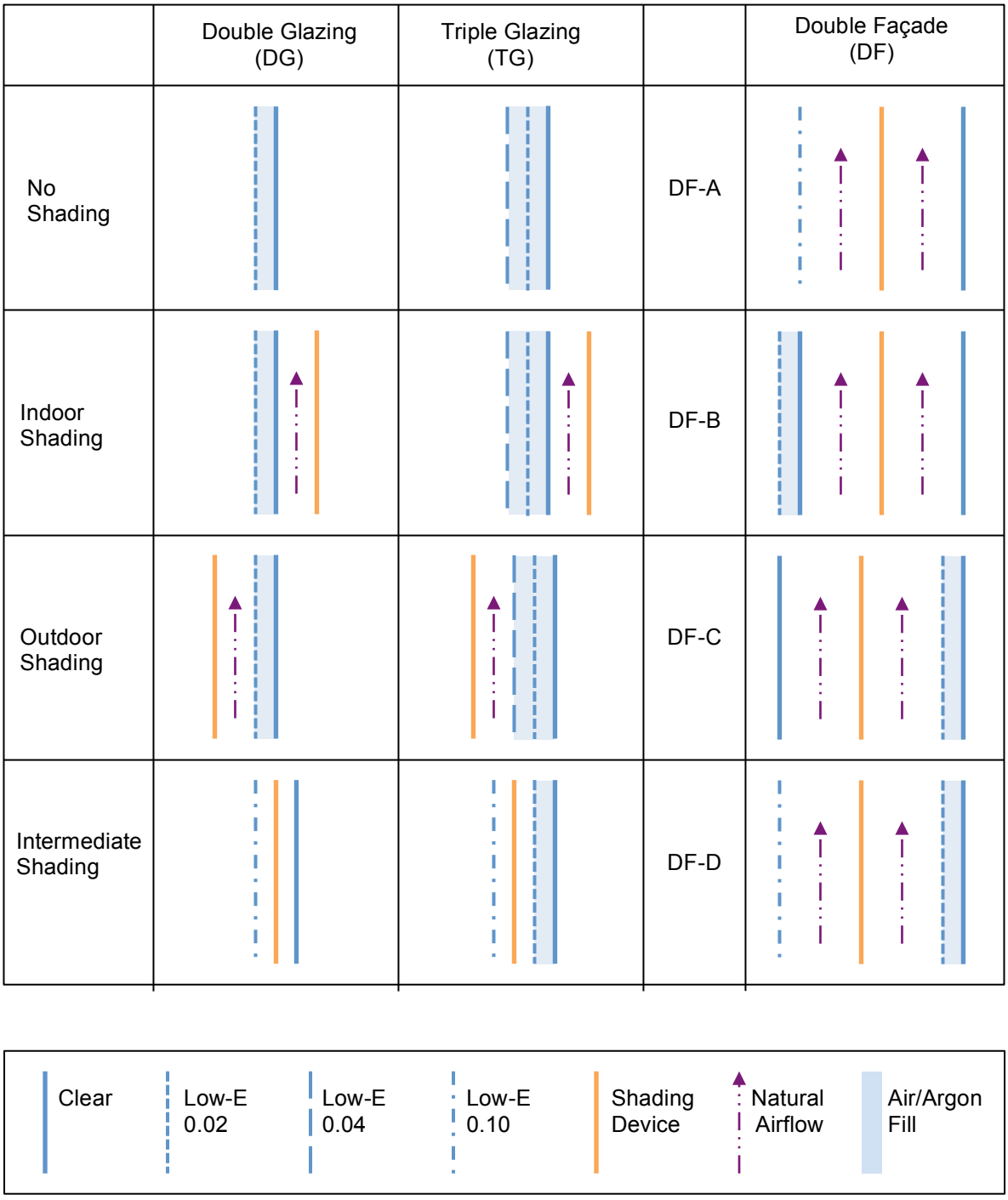

Figure 6.1 Glazing Configurations

The DF configurations were intended to represent possible retrofit scenarios. For DF options A and B, single glazing was used for the interior façade to represent a scenario where the original façade was left untouched (e.g., a historic building). For DF options C and D, double glazing was used for the interior façade to represent scenarios where the interior glazing was either upgraded or already double glazed. The DF inputs are presented in Table 6.3.

Table 6.3 Double Façade Inputs

Item	Description
Height	3.6 m
Width	1.5 m
Depth	0.8 m
Vent Areas	0.1 m^2
Discharge Coefficient	0.65
Double Glazing U	1.66 W/m^2K

The shading device was placed in the center of the cavity, assuming an even flow distribution. Two different roller blinds were tested, since the DoFa model proved to be more accurate with roller blinds. RB1 and RB2 are both light in colour with 14% and 5% openness respectively. Complete optical properties are presented in Appendix C.

6.1.2 Design Conditions

To begin, the glazing cases were tested under NFRC-100 summer and winter conditions. Figure 6.2 and Figure 6.3 illustrate the summet results with RB1 and RB2 respectively.

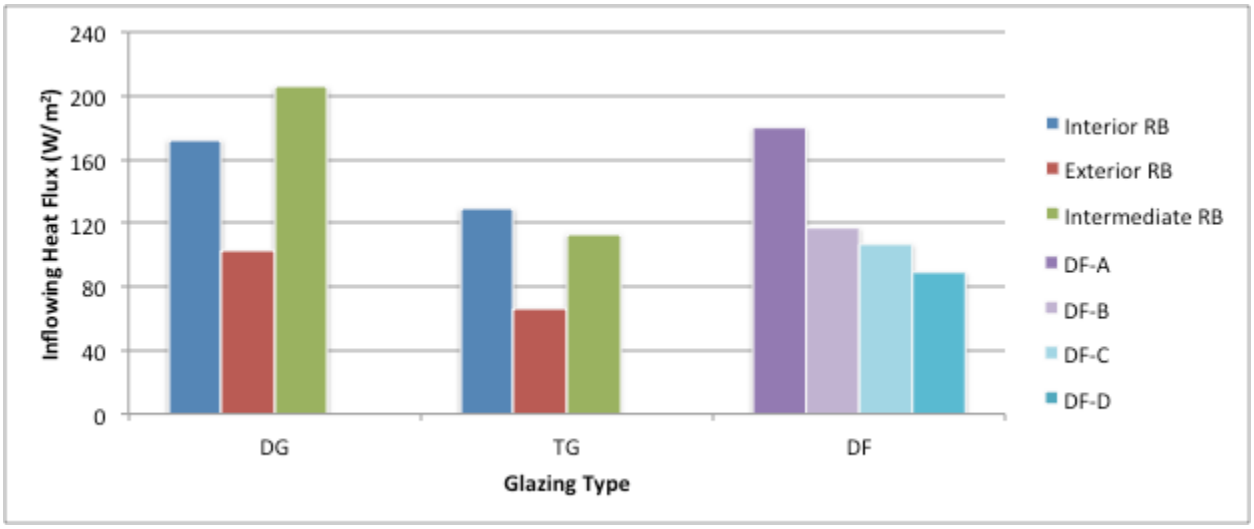

Figure 6.2 Results for Summer Conditions (RB1)

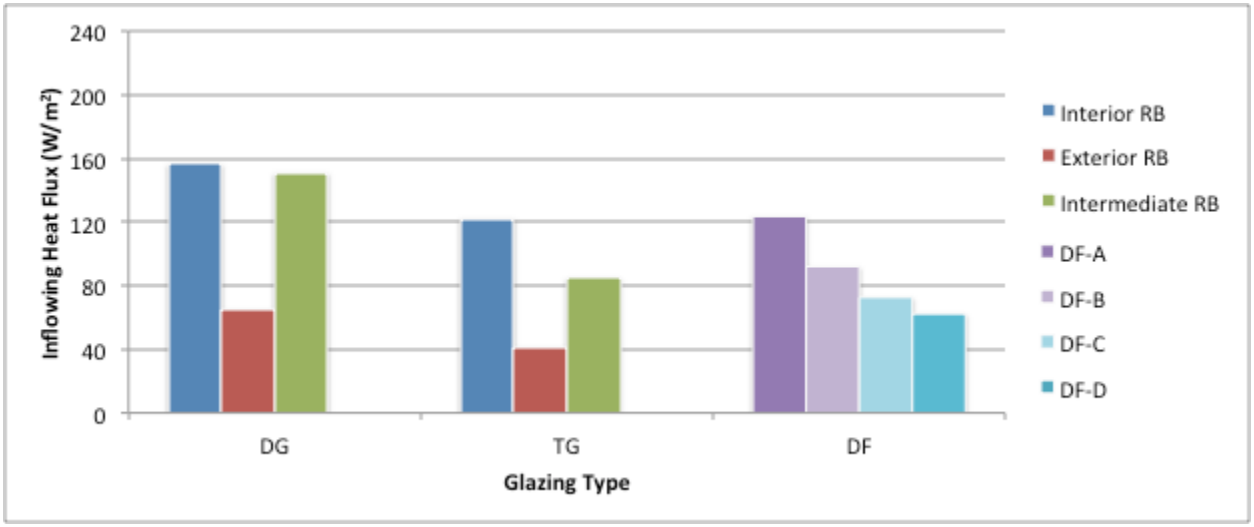

Figure 6.3 Results for Summer Conditions (RB2)

Firstly, the results from the double and triple glazing units showed that outdoor shading was by far superior to indoor shading. Moving the shade to the outside presented a 41% to 66% decrease in heat gain for the cases examined. Intermediate shading generally provided a benefit over indoor shading, with the exception of double glazing with RB1. In this case, the heat gain was actually increased with intermediate shading due to the increased transmittance of the system. In the intermediate shading cavity, a more durable low-E coating was used and the layer transmittance was approximately twice the transmittance of the non-durable low-E layer. Furthermore, the fill in the intermediate shading cavity was air instead of an argon mix, thereby reducing the thermal performance of the window because air has a higher conductivity.

For double façades, all options performed better than conventional glazing with indoor shading except DF-A with RB1. DF-A is the most basic DF option and is essentially the same as double glazing with intermediate shading; however, the cavity space is deeper and open to airflow. DF–B performed comparably to triple glazing with intermediate shading while DF-C performed slightly better. DF-D, which was the best performing DF, performed comparably to double glazing with outdoor shading. However, triple glazing with outdoor shading performed better than all DFs.

For a more definitive comparison, all options were put in order of performance compared to double glazing with indoor shading, which can be considered standard (Figure 6.4).

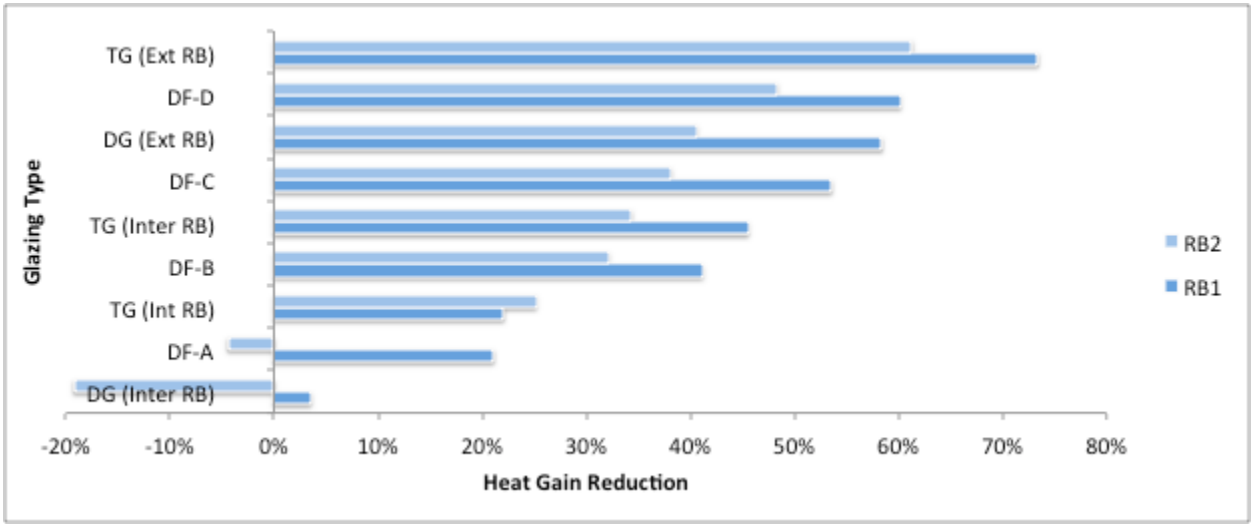

Figure 6.4 Heat Gain Reduction from Double Glazing with Indoor Shading

Triple glazing showed the highest reduction in heat gain, while DF-D was the second best.

The summer performance of the DFs was directly linked to the overall transmittance; therefore, attention should be paid to the transmittance of the chosen glazing layers. Each DF option used different layers and layer sequences, which resulted in different overall transmittances. Figure 6.5 illustrates the relationship between SHGC and transmittance for the cases examined.

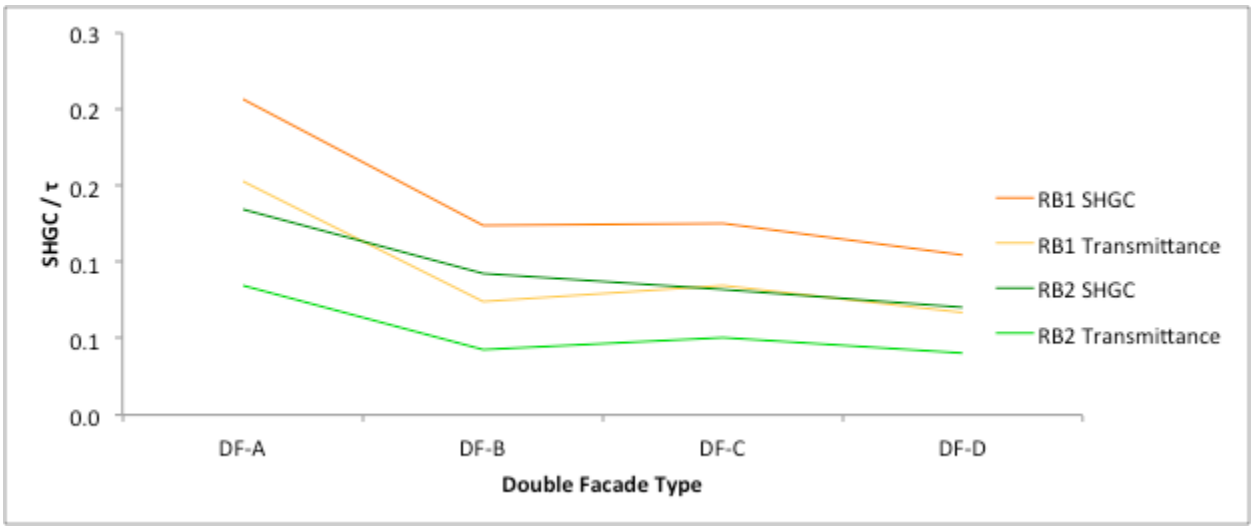

Figure 6.5 Double Façade Transmittance and SHGC

The airflow rates experienced in the DF cavities ranged from 118 to 161 m^3/h (4.1 to 5.6 cm/s); which are suitable rates for a single story DF.

In winter, both shading devices performed similarly, so only RB2 is shown in Figure 6.6.

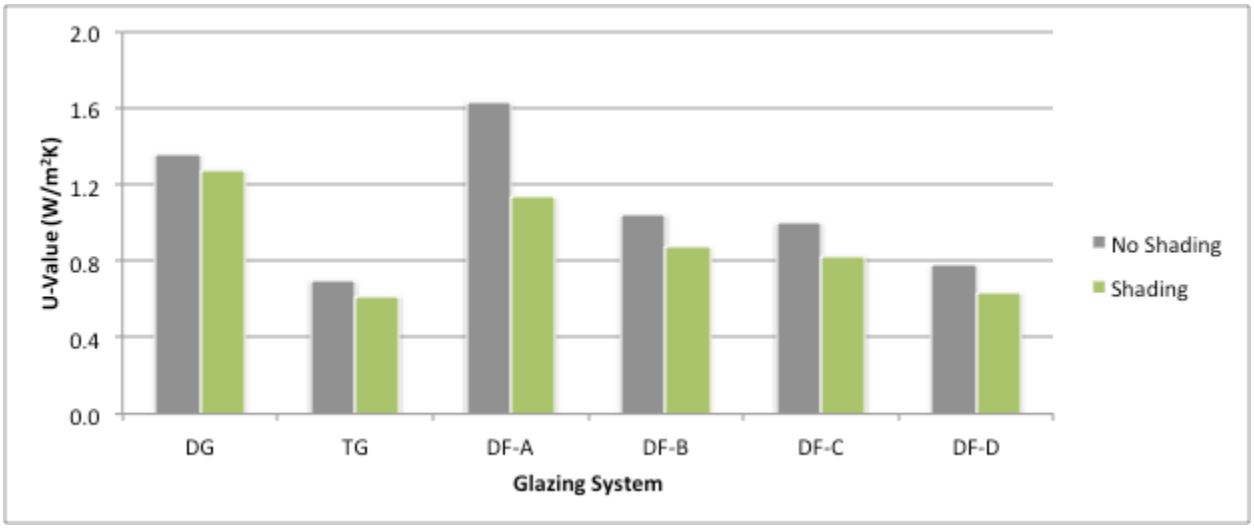

Figure 6.6 Results for Winter Nighttime Conditions, RB2

In winter conditions, the DFs performed better with lowered shading. The shading device prevents radiation between the inner and outer glazings, hence improving the U-value of the assembly. With lowered shading, all DFs performed better than the double glazing. DF-D even performed comparably to triple glazing, with U-values of 0.64 and 0.62 W/m^2 for DF-D and triple glazing respectively.

6.1.3 Average Conditions

Although design conditions are important, performance under average conditions is more representative of annual performance. Therefore, two average situations were examined.

Table 6.4 Average Environmental Conditions

Item	Unit	1	2
$G_{D\theta}$	W/m^2	300	600
$G_{d\theta}$	W/m^2	0	0
$h_{c,ext}$	W/m^{2}K	17	20
$h_{c,int}$	W/m^{2}K	3.5	3.5
$T_{MRT,ext} = T_{a,ext}$	°C	5	-10
$T_{MRT,int} = T_{a,int}$	°C	21	21

Case 1 represents a mild day with low solar radiation while Case 2 represents a cold day with high solar radiation. Different modes of operation were tested for the DFs to either maximize or minimize solar heat gain. The tested modes include no shading (NS) or roller blind (RB) with

vents open or closed. Results for Case 1 are presented in Figure 6.7 and Figure 6.8 for RB1 and RB2 respectively.

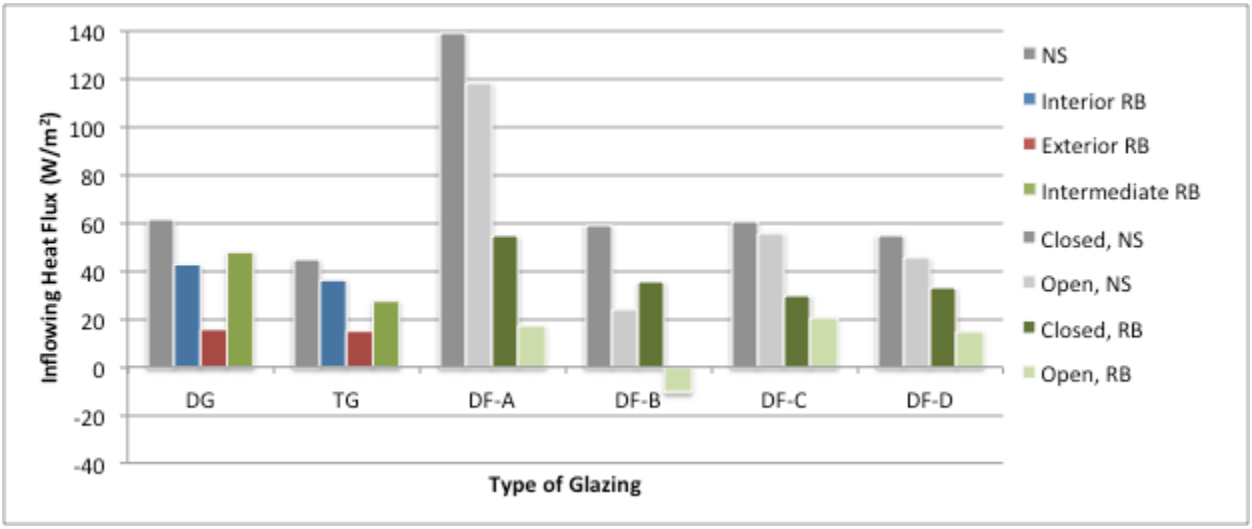

Figure 6.7 Results for Average Conditions Case 1 (RB1)

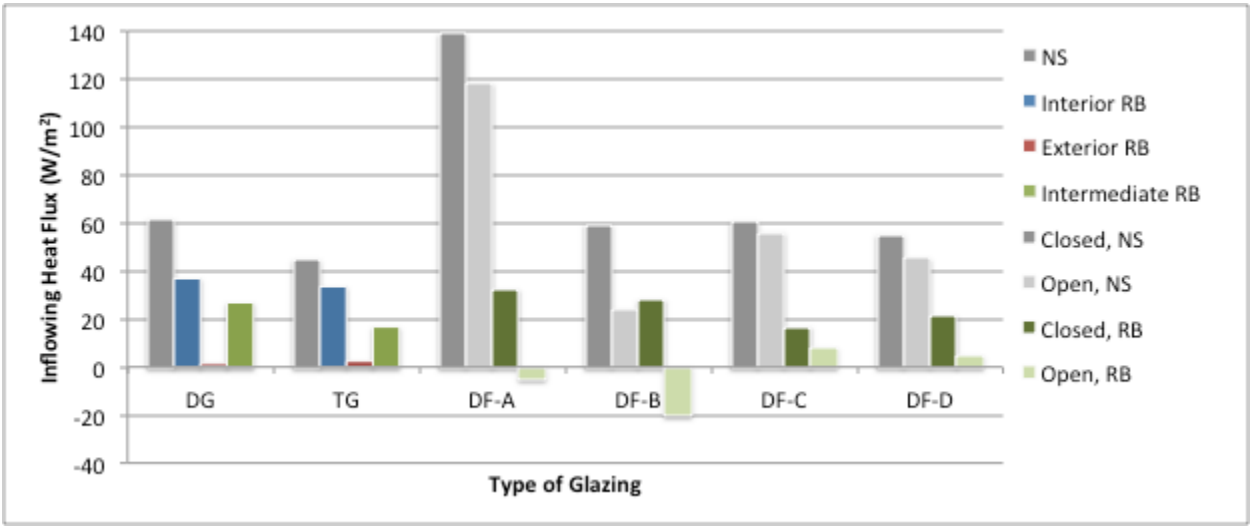

Figure 6.8 Results for Average Conditions Case 1 (RB2)

In shoulder seasons, the benefit of the DF is that it is a dynamic façade that can provide a wide range of performance. If solar gain is desired, the vents may be closed and the shading raised. In this mode, the DFs performed similarly to double glazing without shading. The exception is DF-A, which transmits a large amount of solar radiation to the inside with raised shading. If solar gain is not desired, the vents may be opened and the shading lowered. In this mode, the

DFs performed similarly to double and triple glazing with outdoor shading. For DF-B, the low transmittance combined with a single glazed interior resulted in heat loss through the façade for both shading types. Whether more or less heat gain is desired depends on the specific building design and occupancy. In many commercial buildings, solar heat gain is undesirable in average conditions because of high internal gains

In Case 2, incident solar radiation was higher, which resulted in higher inflowing heat fluxes for configurations without shading. Results for Case 2 are presented in Figure 6.9 and Figure 6.10 for RB1 and RB2 respectively.

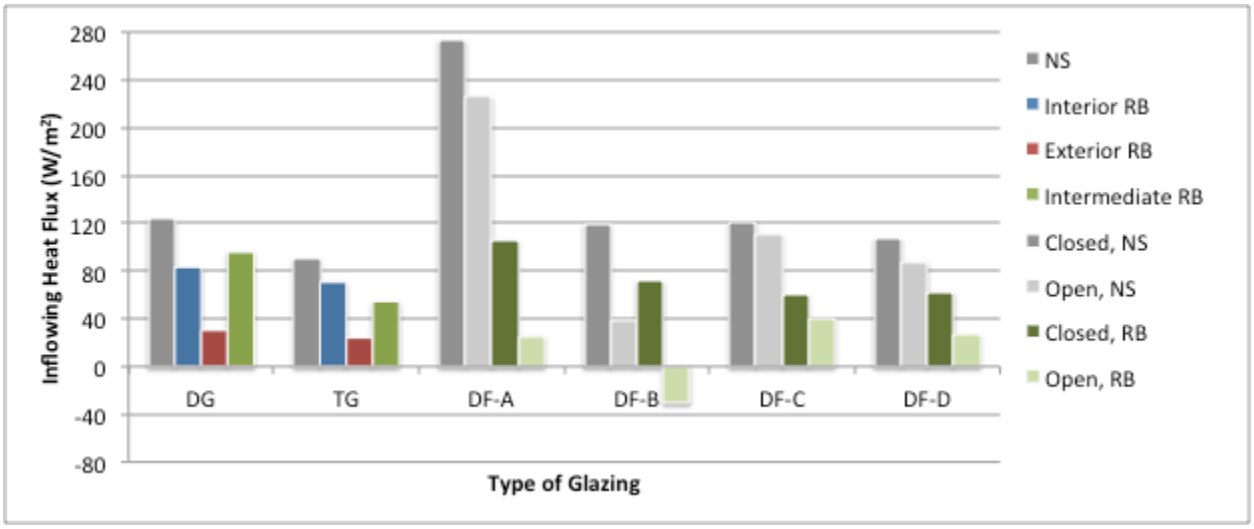

Figure 6.9 Results for Average Conditions Case 2 (RB1)

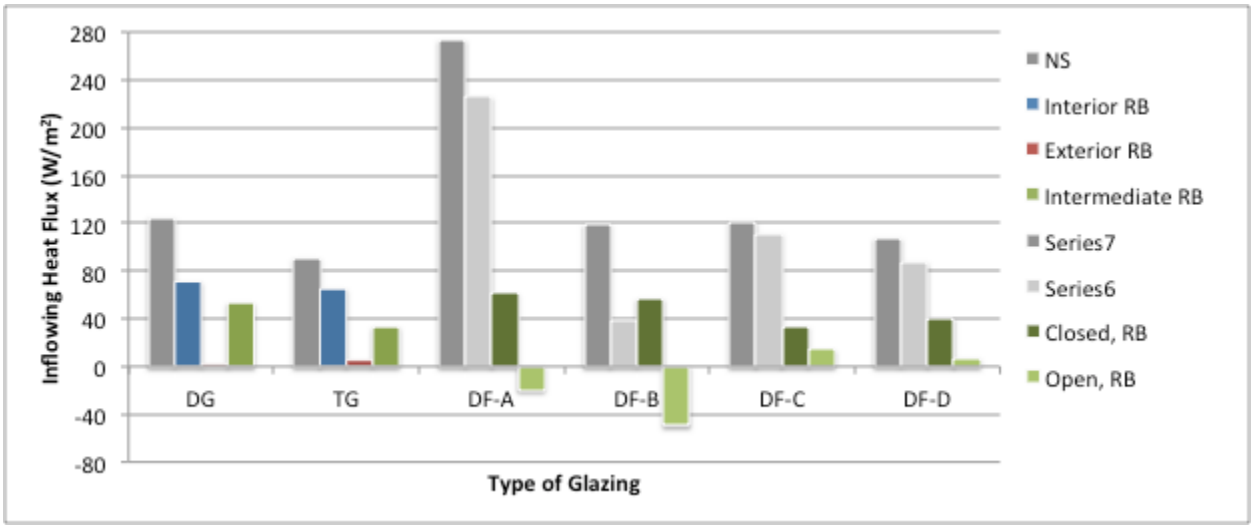

Figure 6.10 Results for Average Conditions Case 2 (RB2)

Although the outdoor temperature was lower in Case 2, the high incident solar radiation increased the inflowing heat flux. Regardless, the relative results were similar to Case 1. Note that without shading, DF-A had a high transmittance and the resulting level of solar heat gain would likely be undesirable. This illustrates how important the transmittance of the system is to overall performance.

When allowing airflow through DFs in cold outdoor conditions, the indoor surface temperature may become a problem. If it drops too low, it could affect the comfort of the occupants or drop below the dew point of the indoor air, causing condensation. With open vents and shading lowered, the indoor surface temperature for DF-B dropped to 11.7°C. If the indoor air were kept at 30%RH, the dew point would be 3.7°C. However, in a museum situation where the indoor air is kept at 50% RH, the dew point would be 10.0°C. These conditions would present a risk of condensation for DF-B.

6.1.4 Conclusions

The DoFa model was used to compare the performance of various DF options to more traditional glazing units. Of the DF options, DF-D performed the best in summer and winter conditions. This façade was comprised of a double-glazed interior and a single-glazed, low-E exterior. In summer, the performance was comparable to double glazing with outdoor shading. In winter, the performance was comparable to triple glazing.

In average conditions, a DF may be opened or closed and shading raised or lowered to maximize or minimize solar heat gains. However, when opening the façade in cold weather, the indoor surface temperature may become a concern. Special attention should be paid to the indoor surface temperature to assess the risk of condensation and occupant discomfort.

Note that the comparison made here is only valid for the tested glazing systems. There is a wide variety of possible glazing layers and configurations, for which results may be quite different.

6.2 Future Development and Application to Buildings

While DoFa may be used to compare glazing options on a unit-to-unit basis, it is more interesting to look at an entire building. If a DF is being considered in a retrofit project, a

comparison to other retrofit options on a whole-building scale is more useful. Therefore, the DoFa model was modified to facilitate a complete enclosure comparison. Note that the method used is a simplified method that needs validation and further development; however, it shows how the DoFa model might be used in the future. The modified tool was used in a case study to compare possible retrofit options.

6.2.1 Approach

Previously, the DoFa model was used to analyze enclosures with a uniform interior façade (e.g., curtain wall). However, many enclosures consist of non-uniform interior façades (e.g., masonry with punched windows). Users can account for mixed opaque/glazed layers by area-weighting the thermal and optical properties of the layer; however, this does not work in cases where a layer is present in one section and not in another (i.e., shading device).

When modeling an enclosure with non-uniform sections, it is proposed that the enclosure be divided into smaller, uniform sections that can be modeled separately. The performance indices of the individual sections can then be area weighted to determine performance indices of the entire façade. This method is analogous to determining overall performance indices for traditional enclosures, where the U-value of windows and walls are area weighted to find the overall U-value. However, in a traditional enclosure, the window and wall U-values are constant. For a DF, the window and wall U-values are height dependent because they are linked by the cavity space. Consequently, some modifications were made to the DoFa model to account for vertically linked sections.

To begin, a façade may be divided into horizontal sections based on composition. For example, suppose a DF retrofit were being considered for a one-storey masonry building with punched windows (Figure 6.11).

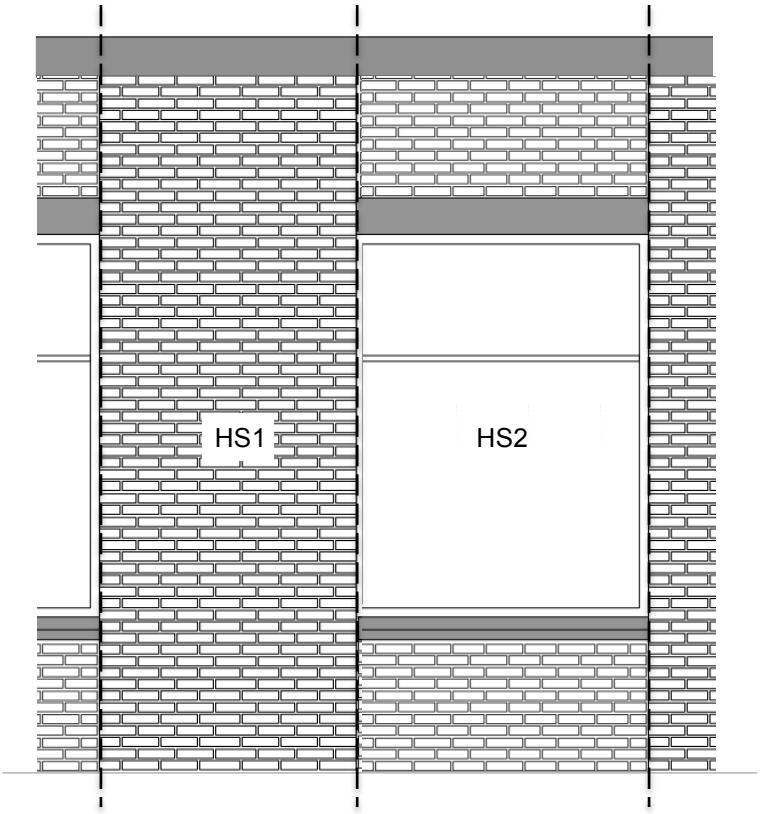

Figure 6.11 Horizontal Section Division

The façade may be divided into two horizontal sections of masonry and punched windows (HS1 and HS2 respectively). The horizontal sections are assumed to be separate and are assessed separately. If the cavity extends over multiple horizontal sections, they will in fact be linked by the cavity. However, the method used here is only an approximation. In the future, the effect of this simplification should be tested and the method modified accordingly.

The horizontal sections are then divided further into stacked vertical sections of uniform composition, which are solvable using DoFa. The stacked vertical sections are linked by the cavity airflow and temperature; therefore, the airflow rate and inlet temperature are calculated for each vertical section and treated as fixed inputs. While the airflow rate is constant for the stack, the inlet temperature varies depending on the vertical position of the section. The method for determining the airflow rate and inlet temperatures is described in Section 6.2.2.

Looking at the example building, HS1 consists of only one vertical section and can be solved without further division. HS2 consists of three vertical sections with two different compositions; therefore, it is divided into three stacked vertical sections.

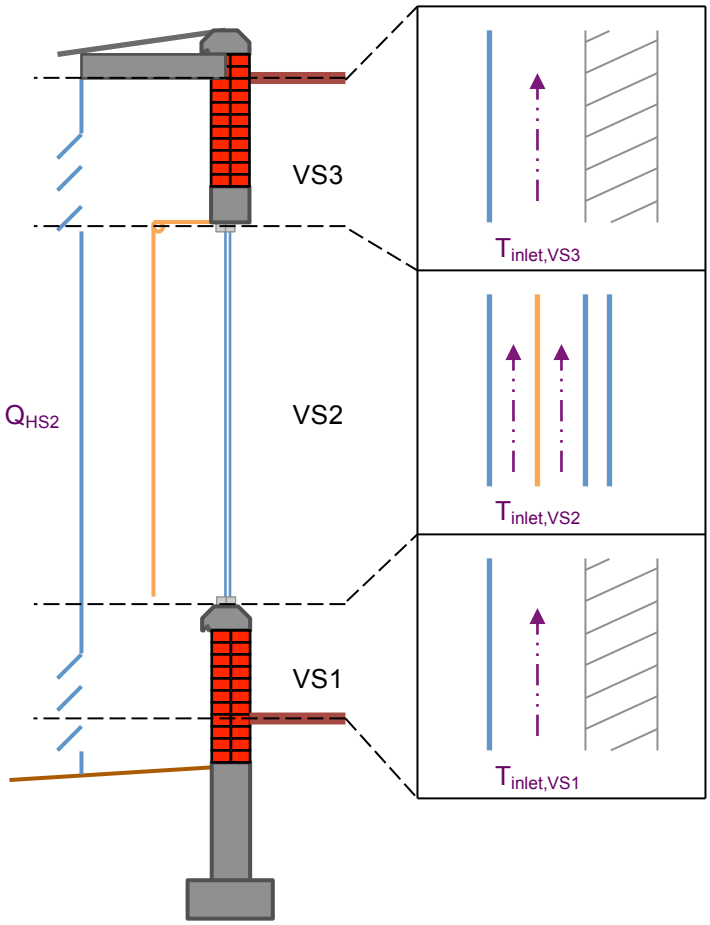

Figure 6.12 Vertical Section Division, HS2

Note that the only difference between VS1 and VS3 is the inlet temperature. Once the performance indices are determined for each vertical section, they are area weighted to determine the performance indices of the horizontal section. These, in turn, are area weighted to determine the performance indices for the entire façade. The method presented here is a quick and easy solution to modeling non-uniform façades using DoFa.

6.2.2 Vertical Section Calculations

When sections are stacked vertically, they are connected by airflow and cavity temperature. Therefore, a simplified method is proposed to determine the airflow rate and inlet temperature for each stacked vertical section.

To begin, the user must create individual vertical sections as described in Chapter 4. Then, the user must specify the sequence of vertical sections and the height of each section. As an initial trial, the DoFa model was modified to allow a maximum of three different vertical section compositions with a maximum of five sections in a stack. However, when stacking sections, they must be linked by the cavity. If the cavity is separated by storey, the storeys should be modeled separately.

For each different vertical section, the DoFa model determines the average airflow rate and outlet temperature as if the section were the entire height of the stack. The results are then area weighted to determine the overall stack averages. For example, the overall outlet temperature for a stack of *n* vertical sections may be found by:

$$T_{outlet,avg} = \frac{\sum_{i=1}^{n} T_{outlet,i} H_i}{H_{total}} \qquad [K] \qquad \textbf{(6.1)}$$

Where,

$T_{outlet,avg}$ = overall outlet temperature of the stack [°C]

$T_{outlet,i}$ = outlet temperature for the i^{th} vertical section assuming H_{total} [°C]

H_{total} = overall height of the stack [m]

H_i = height of the i^{th} vertical section [m]

Note that if a vertical section has two connected cavities separated by a shading device, the average outlet temperature of the two cavities is used. The same method is used for the airflow rate. Note that area weighting the outlet temperature and airflow rate is not standard practice, but was done for lack of a better method. The accuracy of the method has not been tested and should be investigated in the future.

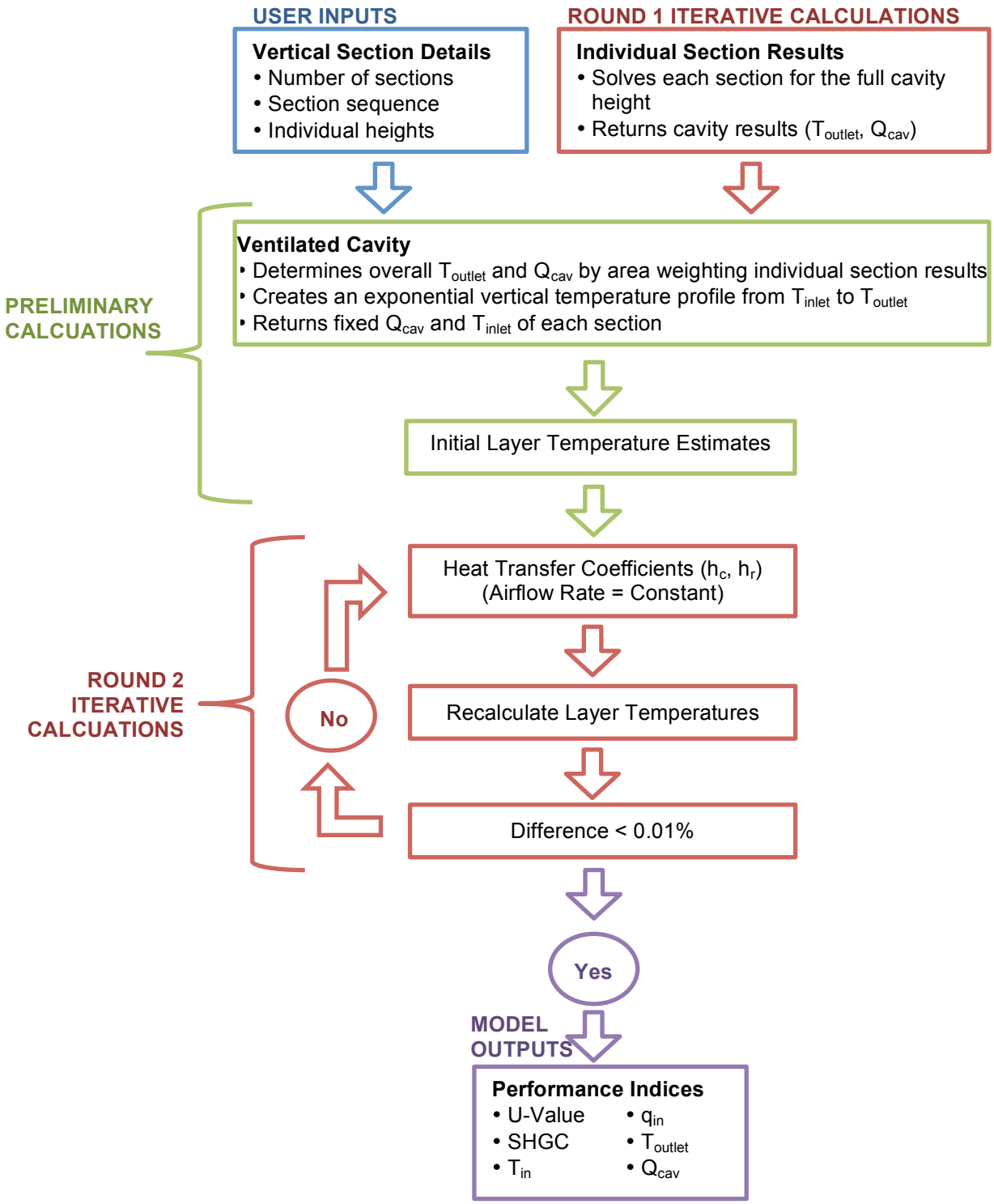

Figure 6.13 Flow Diagram for Solving Stacked Vertical Sections

The overall stack outlet temperature and airflow rate are then used in a second round of calculations using the specified vertical section heights. The airflow rate is used as a fixed input while the outlet temperature is used to find the inlet temperature of each vertical section. An exponential vertical temperature profile is assumed between the inlet and outlet, using Equation (4.96) to determine the temperature at each vertical section inlet height. The horizontal temperature profile through each vertical section is then solved and the performance indices are area weighted to determine the overall performance indices of the stack. Figure 6.13 illustrates the process of solving the vertical sections within a stack.

6.2.3 Case Study

As an example of how the DoFa model could be used to analyze a whole building, a case study was chosen. The building examined was the University of Waterloo School of Architecture in Cambridge, Ontario. The original masonry structure was built in 1919 as the Riverside Silk Mill (Cambridge Times, 2012). In 2004, the building was renovated to house the University of Waterloo School of Architecture. Much of the historic character was retained in the retrofit, with high ceilings, large windows and exposed brick masonry. Although windows were upgraded from single to double glazing, the remainder of the enclosure was largely left untouched.

Figure 6.14 University of Waterloo School of Architecture Building

Although the building has already been retrofitted, a DF could have easily been a retrofit option. Therefore, various DFs were compared to more conventional retrofit strategies to demonstrate how DoFa might be used in a whole-building application. To make the comparison straightforward, only two storeys were considered, assuming a pattern of equal-width window sections and masonry columns. The dimensions are provided in Figure 6.15.

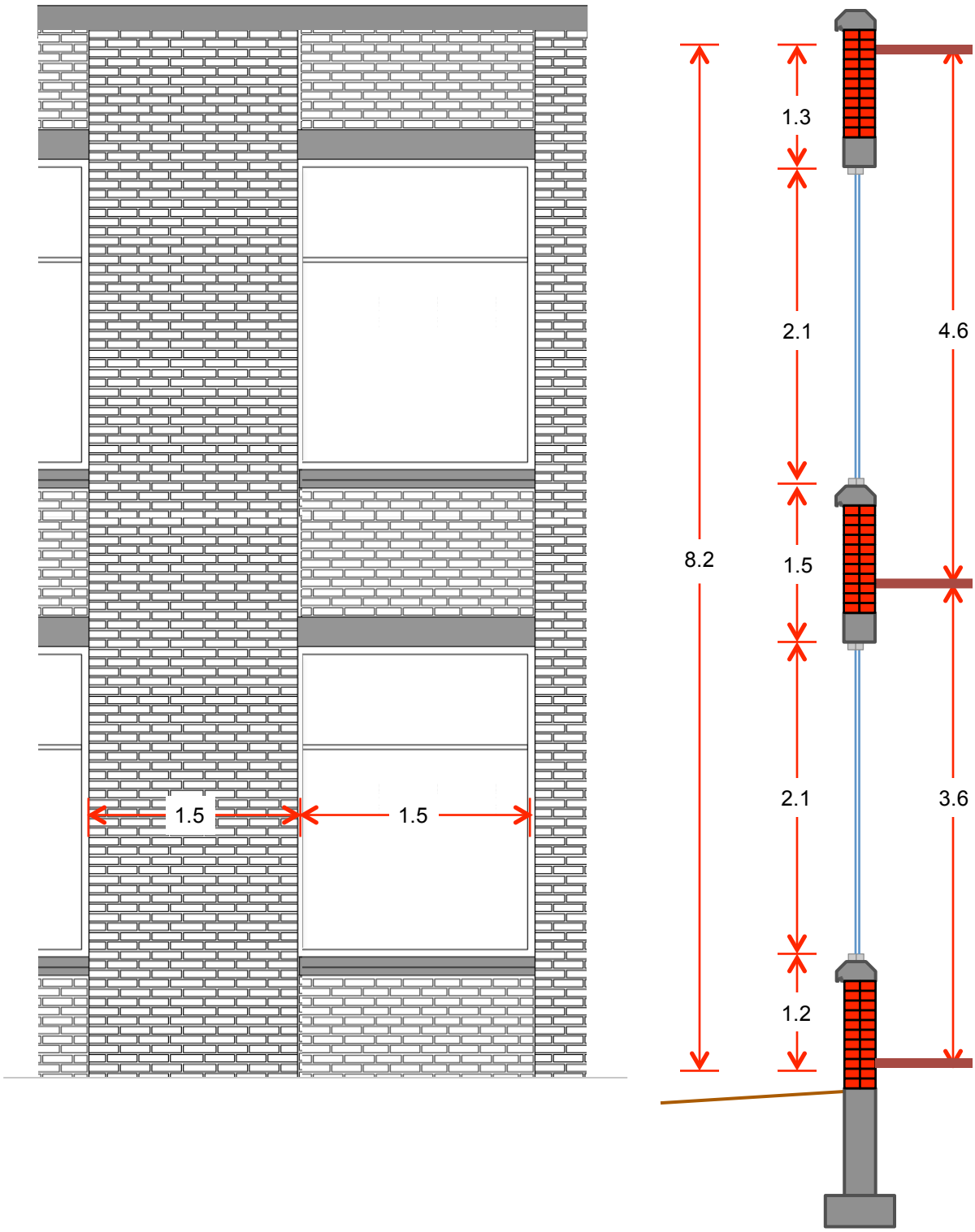

Figure 6.15 Case Study Building Dimensions [m]

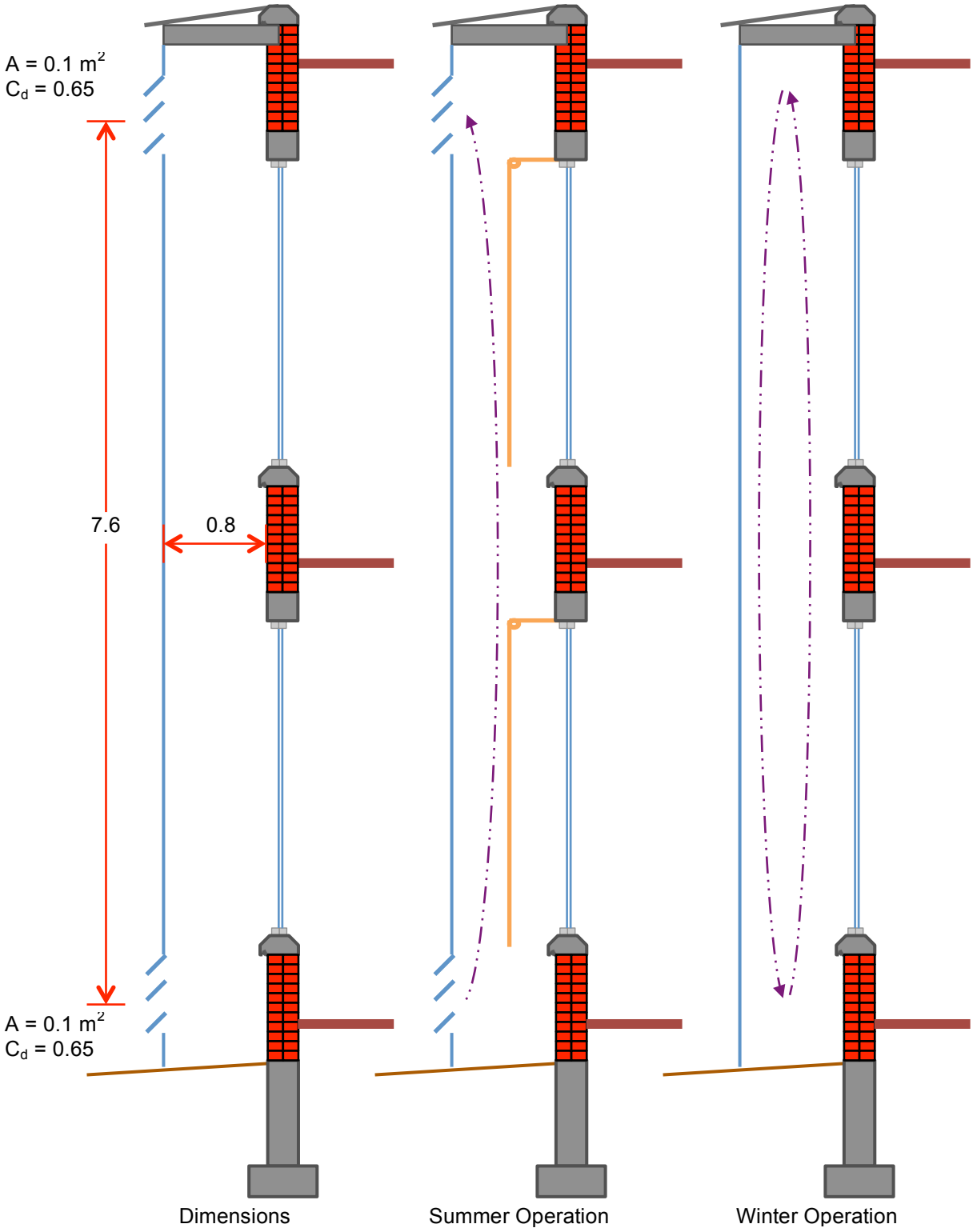

Figure 6.16 Double Façade Retrofit Configuration [Dimensions in Meters]

Note that the comparison here does not represent the actual design options considered in the 2004 retrofit. Furthermore, the U-values used are estimates and do not represent the actual building component U-values. The estimated values are presented in Table 6.5.

Table 6.5 Component U-Values

Opaque Component	U-Value [W/m^{2}K]	Glazed Component	U-Value [W/m^{2}K]
1) Original Masonry	0.97	1) Single	5.99
2) Insulated Masonry	0.36	2) Double	1.36
		3) Triple	0.70

A more common measure of performance for opaque components is the R-value [h·ft²·°F/Btu]. The original and insulated masonry components are equivalent to R-5 and R-15 respectively.

The conventional retrofit options were to improve the opaque components, glazed components or both. The DF options were DF-A, B, C and D. In these options, the opaque components would remain unchanged while the glazed components would be altered or not depending on the DF. A multi-storey DF was used, as this presents little interference with the original façade. The configuration and operation modes are illustrated in Figure 6.16. RB1 from Section 6.1 was used for the shading device. For the conventional glazing options, indoor and outdoor shading was considered. For the DF options, the shading device was placed in the center of the cavity and equal flow distribution was assumed. The façades were tested under summer and winter design conditions as well as average conditions.

6.2.4 Results

Figure 6.17 illustrates the summer results. While the DFs generally performed better than single glazing, the problem of overheating was apparent. With high incident solar radiation, the DFs create a warmer microclimate outside the interior façade, thereby increasing thermal heat gain through the glazed and opaque components. While this may be desirable in winter, it is undesirable in summer. DF options B, C and D performed slightly better than the double-glazing option with indoor shading and original masonry. However, when insulation was added to the masonry, the double glazing performed better. Furthermore, both double-glazing options with outdoor shading as well as all triple-glazing options performed better than the DFs.

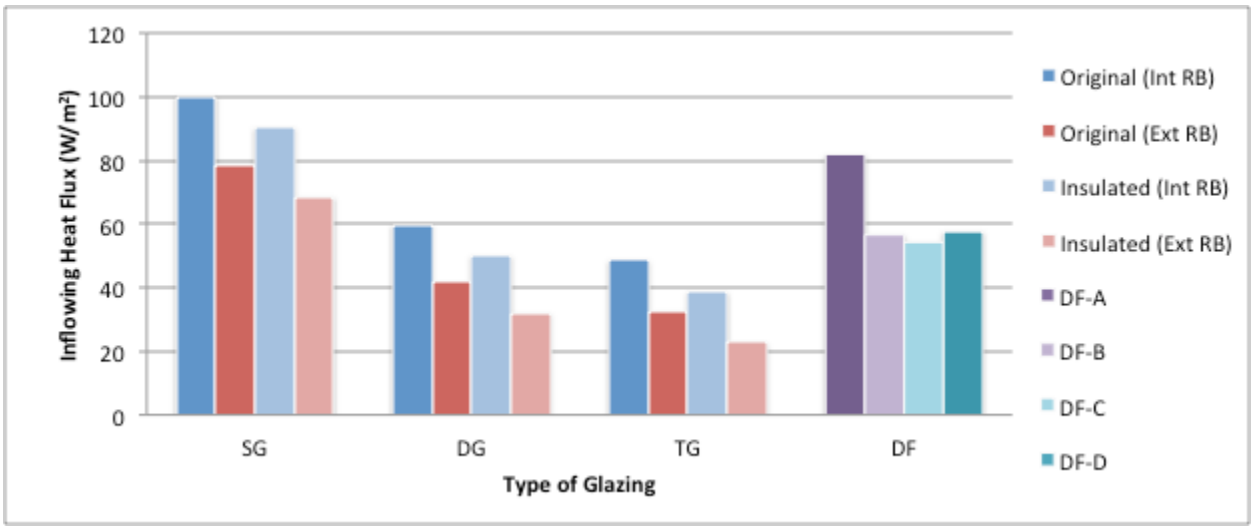

Figure 6.17 Results for Summer Conditions

In winter conditions, all options were compared without shading devices Figure 6.18).

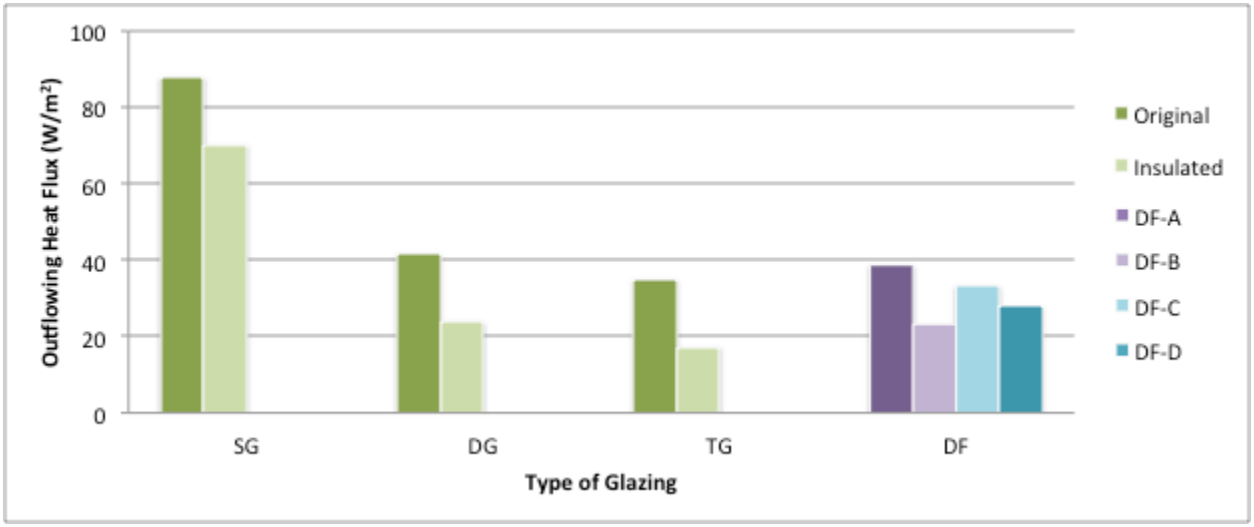

Figure 6.18 Results for Winter Conditions

The DF options generally performed better than the traditional retrofit options that addressed only one component of the façade. Simply insulating the opaque components had little effect when single glazing was retained. Replacing the single glazing with double or triple glazing had a much larger effect, even without insulating the opaque elements. DF options C and D were slightly better than the triple glazing retrofit without insulation. DF-B performed the best of the

DF options, which was comparable to the double-glazing retrofit with insulation. Triple glazing with insulation remained the best performing option.

In the shoulder seasons, the façade may be opened and shading lowered to reduce solar heat gain. However, the indoor surface temperature is also important because a very low temperature may cause discomfort to occupants and surface condensation. Results are presented in Figure 6.19 and Figure 6.20.

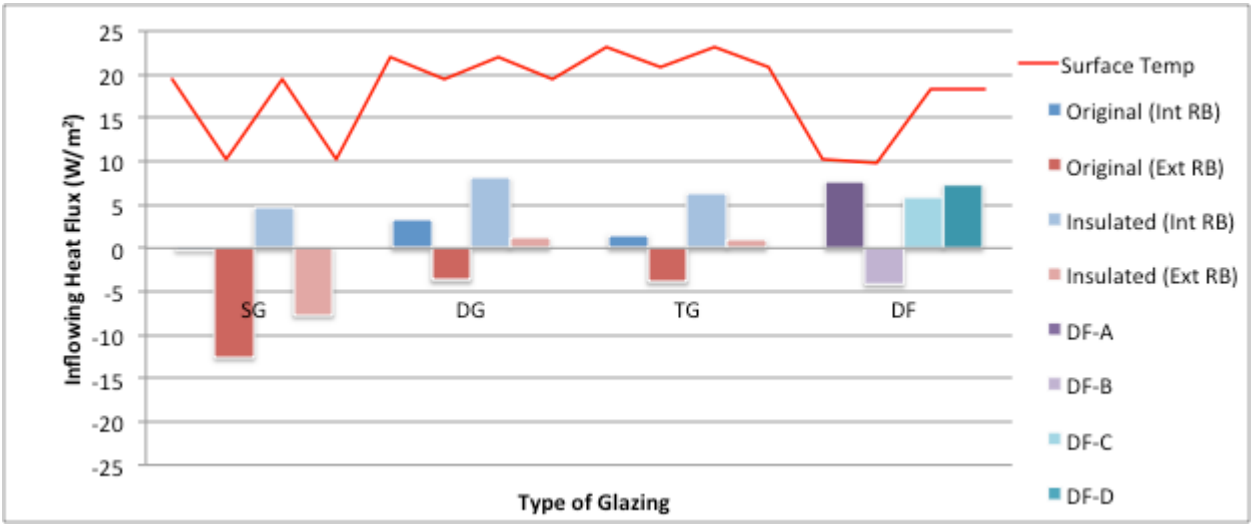

Figure 6.19 Results for Average Conditions Case 1 (G_t = 300 W/m^2, $T_{a,out}$ = 5°C)

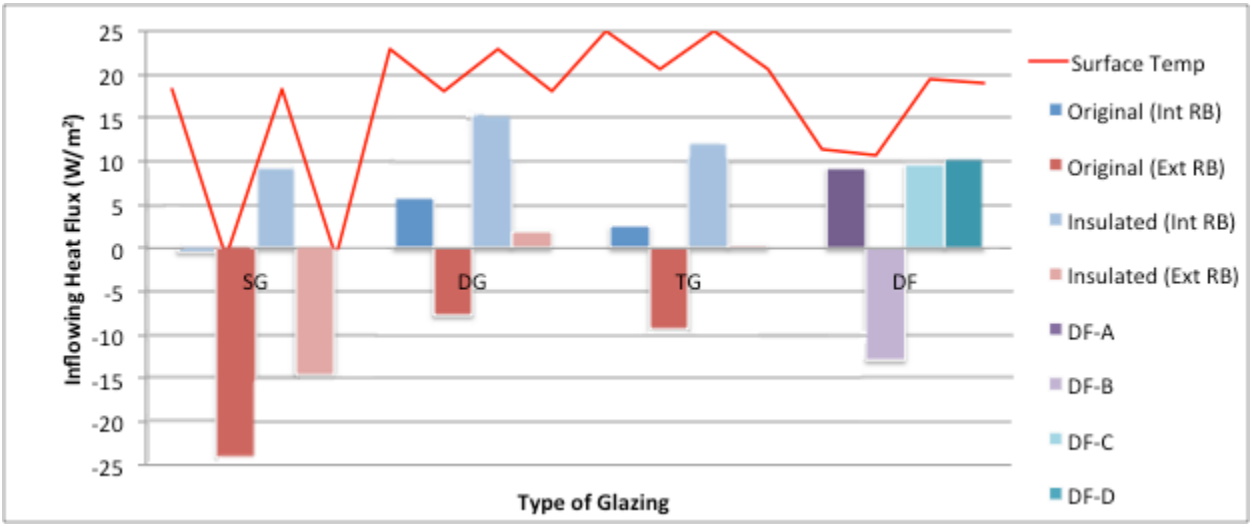

Figure 6.20 Results for Average Conditions Case 2 (G_t = 600 W/m^2, $T_{a,out}$ = -10°C)

Note that the shading may be raised to increase solar heat gain if desired. In both average condition cases, all glazing options were similar. The double and triple-glazing options with insulated masonry were essentially zero, while the other options were just below or above.

Surface temperatures for DF options A and B were quite low for the tested operation mode; therefore, occupant comfort and condensation risk would need to be assessed. On average, the DF options showed a temperature difference between inlet and outlet of 4.3°C for Case 1 and 7.1°C for Case 2. This information could be used to assess the option of using cavity air as preheated ventilation air. Furthermore, vent openings and cavity airflow could be reduced to allow further air preheating if desired. The average airflow rates were 8.9 cm/s for Case 1 and 11.5 cm/s for Case 2. All this information would be useful to a design team to create a proper design and operation strategy.

6.2.5 Conclusions

The DoFa model was used to analyze an entire façade using a simplified method of adding horizontal and vertical sections. While the method still requires validation, preliminary results were used to compare various retrofit options for a masonry building with single-glazed windows.

In summer conditions, DFs presented the risk of overheating. The DFs performed better than single glazing but worse than most double-glazing and all triple-glazing options. No DF option performed notably better than the others. In winter conditions, DF-B performed the best, which was comparable to double glazing with insulated masonry. This shows that DFs are a valid retrofit solution to increase winter performance.

In the specific case study examined, the actual retrofit solution was to retain the original masonry and replace the windows with double glazing with indoor shading. Therefore, this solution was compared directly to DF-B (Table 6.6).

Table 6.6 Inflowing Heat Flux [W/m^2]

	Actual	DF-B
Summer	59.7	52.0
Winter	-41.7	-23.0

Based on performance in design conditions, DF-B is preferable. However, further examination of performance under average conditions would be necessary to determine expected annual

performance as well as optimal DF operation strategies (e.g., vents and shading devices). In cold outdoor conditions, it would be advisable to either completely or partially close the vents in the outer façade to avoid cold indoor surface temperatures. Proper operation is essential to achieve good performance of the façade.

If preservation were the goal of the retrofit, DF-B is a good solution. The DF-B option involves adding a double-glazed façade to the exterior of the existing building, thereby leaving the original building completely unchanged. With the new exterior façade, the original building would be protected from weather and any further degradation. Furthermore, the retrofit would present little interference with the indoor space, allowing the building to stay occupied throughout construction. However, a DF retrofit would undeniably cost more and it would alter the outer appearance of the building. Whether a DF is the right solution for a specific building depends on the design intentions, project goals, etc. Regardless, DoFa can give quantitative results helpful in making design decisions. Furthermore, after choosing the DF option, various design parameters such as shading type and location, cavity depth, vent areas, etc. could be tested to determine the optimal design.

Chapter 7
Conclusions and Recommendations

7.1 Conclusions

The North American commercial building stock is aging and many buildings will need to be upgraded from both a durability and energy performance standpoint in the near future. While demolition and reconstruction is an option, retrofitting the existing buildings requires fewer materials and reduces landfill waste. Typically, enclosure retrofits involve adding insulation to either the interior or the exterior of the existing façade. While exterior insulation is superior from a performance perspective, interior insulation is often chosen for historical retrofits where the exterior appearance must be retained. However, adding interior insulation to old masonry façades presents various performance problems, including brick damage by freeze-thaw, surface condensation and deterioration of embedded timber floor beams. Consequently, an alternative retrofit strategy was investigated in this thesis, whereby a second glass skin is added to the exterior of the existing structure to create a double façade. This approach also allows for interesting opportunities regarding aesthetics.

Double façades have traditionally been used in new construction in an attempt to improve the performance of all-glazed façades. However, reducing the glazing quantity while increasing the glazing quality presents a much better technical solution. For retrofit however, double façades could be a more competitive solution. Applying a second glazed skin to an existing building preserves and protects the building without completely covering it up. Furthermore, the retrofit presents little interference with the indoor space, allowing the building to remain occupied during construction. Also, a double façade does not decrease useable floor space and could modernize the appearance of an older, outdated façade. However, double façades present various drawbacks, mainly the risk of overheating, fire-protection difficulties, noise transfer within the cavity space and additional costs for construction, operation and maintenance. Whether a double façade is a good choice for a specific building depends on the design intentions and goals of the project. A tool is needed to assess the energy performance of a double façade with respect to other retrofit options.

In this thesis, a simple, spreadsheet-based tool (DoFa) was developed to model double façades in the preliminary design phase. The DoFa model is a lumped model, which is a one-dimensional model constructed from first principles. Temperatures and heat transfer coefficients are averaged over the entire height of the façade so vertical stratification is neglected. This type of model was chosen because it is flexible and requires basic inputs and minimal user skill level. It also facilitates quick simulations and gives results sufficiently accurate for design-phase decision-making. Outputs of the model are the horizontal temperature profile, U-value, SHGC, heat flux, airflow rate and outlet temperature.

The DoFa model was validated by comparing results to two widely used and accepted glazing system modeling tools, WINDOW6.3 and VISION5. The comparisons showed that the DoFa model can provide accurate results for enclosed glazing systems with roller blinds. However, caution should be exercised when using DoFa to model venetian blinds. At present, the DoFa optical model does not account for beam-diffuse reflection or transmission, which is a problem for layers that are directionally selective (e.g., venetian blinds). Similarly, DoFa results differed when diffusing layers were located on the outside (e.g., shading). However, using diffuse optical properties for the interior layers generally reduced the discrepancy between models.

Further validation was conducted using empirical results. However, the lack of detailed published results made comprehensive comparisons difficult. Comparisons with Saelens (2002) and Park et al. (2004) showed that the DoFa model can analyze the field performance of double façades with natural airflow. However, the accuracy depends on certain parameters such as inlet/outlet grid characterization, flow distribution, inlet temperature and cavity convection coefficients. Therefore, a parametric study was conducted to determine which inputs were most important. For the case studied, cavity convection coefficients had the largest effect on thermal heat flux while optical properties had the largest effect on total heat flux. Cavity airflow rate had the largest effect on the outlet air temperature.

The DoFa model was used in two applications to demonstrate its usefulness. The first application compared a variety of double façades to more traditional glazing systems. The best performing double façade consisted of a single-glazed, low-E exterior with a double-glazed, low–E interior. In summer, the performance was comparable to double glazing with outdoor

shading. In winter, the performance was comparable to triple glazing. Of course, the results are only valid for the chosen glazing systems.

In the second application, the DoFa model was used to compare whole-building retrofit options for the University of Waterloo School of Architecture building located in Cambridge, Ontario. To make the comparison, the DoFa model was modified to allow the addition of vertically-stacked, non-uniform sections. Note that the method used is a simplified method that needs validation and further development. In summer, conventional retrofits generally performed better than double façades, especially when outdoor shading was used with double or triple glazing. In winter, double façades performed comparably to conventional retrofits. The best performing double façade consisted of a double-glazed, low-E exterior with the original interior (i.e., masonry and single glazing). When compared to the chosen retrofit solution of upgrading the windows to low-E double glazing with indoor shading, the double façade option performed better in summer and winter. Therefore, a double façade could have been a good retrofit solution for the chosen building. However, the performance of a double façade is very dependent on proper design and operation. The DoFa model can be very useful in creating the proper preliminary design and operation strategies, though more advanced modeling tools may be necessary in the detailed design stage.

7.2 Recommendations

The DoFa model is a simple model that could benefit from further development. Additional experimental results are needed to further validate the model and assess the accuracy. At present, identified areas of improvement are:

1) Beam-diffuse transmission and reflection: the DoFa model only allows beam-beam and diffuse-diffuse transmission and reflection. This is a problem for venetian blinds and for diffusing layers located near the exterior of the façade. Beam-diffuse calculations should be investigated for potential inclusion in the DoFa calculations. Similarly, calculations to determine off-normal optical properties from the normal optical properties could also be investigated.
2) Shading: the DoFa model does not account for shading caused by glazing frames or building geometry. Currently, the user may account for these in the optical and thermal properties of glazing layers and by increasing the diffuse fraction of incoming solar

radiation. However, DoFa could easily be modified to include calculations for frames and shading based on geometry and solar angles.

3) Cavity convection coefficients: empirical results indicate that the DoFa model underestimates convection coefficients for natural airflow in the presence of solar radiation. Further experimental results are needed to confirm convection coefficient relationships for both open and closed DF cavities.
4) Thermal mass: the DoFa model neglects thermal mass because the necessary calculations are complex and time dependent. Future development could investigate the impact and importance of thermal mass and how it might be incorporated.
5) Annual simulations: the DoFa model uses steady-state energy balances to determine instantaneous performance indices. However, it would be beneficial to input performance indices into whole-building simulations to determine annual performance. Therefore, the DoFa calculations could be embedded into a computer code to quickly test performance under multiple boundary conditions. The results could be used to create a performance map or relationship between boundary conditions and performance, which could be used as input into an annual energy simulation. For example, based on the incident solar radiation and outdoor temperature, the established relationship could determine the corresponding SHGC and U-value. Alternatively, the DoFa model could be altered so that it could be paired with a whole building energy model such as EnergyPlus or BELA to continuously update performance indices based on changing boundary conditions (e.g., Wright et al., 2011).
6) Non-uniform assemblies: a method was developed in Chapter 6 of vertically stacking sections to create an overall assembly (i.e., masonry interior with punched windows and cavity shading only at window locations). This is a simplified method that should receive further development and validation to accurately model whole building façades with non-uniform composition.

As noted previously, more test data and field results are needed to validate the DoFa model. Furthermore, it is important that researchers report all inputs and material properties so that their experiments can be reproduced. A catalogue or library of typical inputs would be very useful for DoFa users; for example, optical properties of glazing/shading layers, R-values of older building assemblies and flow coefficients for various opening types and sizes.

References

[BPIE] Buildings Performance Institute Europe. (2011). *Europe's Buildings Under a Microscope - A country-by-country review of the energy performance of buildings.* Buildings Performance Institute Europe.

Andersen, K. T. (1995). Theoretical considerations on natural ventilation by thermal buoyancy. *ASHRAE Transactions , 101* (2), 1103-1117.

ASHRAE. (1993). *1993 ASHRAE Handbook - Fundamentals.* Atlanta, GA, USA: American Society of Heating, Refrigerating and Air-Conditioning Engineers, Inc.

ASHRAE. (2001). *2001 ASHRAE Handbook - Fundamentals.* Atlanta, GA, USA: American Society of Heating, Refrigerating and Air-Conditioning Engineers, Inc.

ASHRAE. (2009). *2009 ASHRAE Handbook - Fundamentals.* Atlanta, GA, USA: American Society of Heating, Refrigerating and Air-Conditioning Engineers, Inc.

Baker, N. V. (2009). *The Handbook of Sustainable Refurbishment: Non-Domestic Buildings.* London, UK: Earthscan.

Ballestini, G., De Carli, M., Masiero, N., & Tombola, G. (2005). Possibilities and limitations of natural ventilation in restored industrial archaeology buildings with a double-skin façade in Mediterranean climates. *Building and Environment , 40*, 983-995.

Balocco, C. (2002). A simple model to study ventilated façades energy performance. *Energy and Buildings , 34*, 469-475.

Barnaby, C. S., Wright, J. L., & Collins, M. R. (2009). Improving Load Calculations for Fenestration with Shading Devices. *ASHRAE Transactions , 115, Pt. 2*.

Bejan, A. (1993). *Heat Transfer.* New York: Wiley.

Boake, T. (2006). *The Tectonics of the Double Skin: Green Building or Just more Hi-Tech Hi-Jinx?* Case Study, University of Waterloo, School of Architecture, Waterloo.

Braham, W. W. (2005). Active Glass Walls: A Typological and Historical Account. *AIA Convention* (pp. 1-4). Las Vegas: University of Pennsylvania.

Brandemuehl, M. J., & Beckman, W. A. (1980). Transmission of Diffuse radiation through CPC and Flat Plate Collector Glazings. *Solar Energy , 24* (5), 511-513.

Brunoro, S. (2008). An assessment of energetic efficiency improvement of existing building envelopes in Italy. *Management of Environmental Quality: An International Journal , 19* (6), 718-730.

Cambridge Times. (2012, September 10). *Doors Open features University of Waterloo School of Architecture*. Retrieved December 13, 2012, from CambridgeTimes: http://www.cambridgetimes.ca/community/article/1499879

Carli, Inc. (2006). *TARCOG: MATHEMATICAL MODELS FOR CALCULATION OF THERMAL PERFORMANCE OF GLAZING SYSTEMS WITH OR WITHOUT SHADING DEVICES.* Amherst: Carli, Inc.

Catton, I. (1978). Natural Convection in Enclosures. *Proc. 6th Int. Heat Transfer Conf.*, *6*, pp. 13-31. Toronto.

Charbonneau, M. (2011). *Simulating the Effects of Enclosure Retrofits on Post-War High-Rise Apartment Buildings in Cold Climates .* University of Waterloo, Civil and Environmental Engineering. Waterloo: University of Waterloo.

Chiu, Y.-H., & Shao, L. (2000). *An Investigation into the Effect of Solar Double Skin Façade with Buoyancy-Driven Natural Ventilation.* University of Nottingham, Institute of Building Technology, School of Built Environment. Nottingham: University of Nottingham.

Churchill, S. W., & Berstein, M. (1977). A correlating equation for forced convection from gases and liquids to a circular cylinder in cross flow. *Journal of Heat Transfer , 99*, 300.

Churchill, S. W., & Chu, H. H. (1975). Correlating equations for laminar and turbulent free convection from a horizontal cylinder. *International Journal of Heat and Mass Transfer , 18* (9), 1049-1053.

CIBSE. (1999). *CIBSE Guide A3: Thermal Properties of Building Structures.* London: Chartered Institution of Building Services Engineers.

Corgnati, S. P., Perino, M., & Serra, V. (2007). Experimental assessment of the performance of an active transparent façade during actual operating conditions. *Solar Energy , 81*, 993-1013.

Coussirat, M., Guardo, A., Jou, E., Egusquiza, E., Cuerva, E., & Alavedra, P. (2008). Performance and influence of numerical sub-models on the CFD simulation of free and forced convection in double-glazed ventilated façades. *Energy and Buildings , 40*, 1781-1789.

CRGBC. (2001). *Telus William Farrell Building.* Cascadia Region Green Building Council. Vancouver: U.S. Green Building Council.

CS™. (2012). C/S Solarmotion® Dynamic Solar Façades. Mississauga, ON, Canada: Construction Specialties.

Danish Architecture Centre. (2012, December 21). *DAC & LIFE*. Retrieved Februrary 7, 2013, from Industry's New House: http://m.dac.dk/en/dac-life/copenhagen-x-gallery/ongoing-or-future-projects/industrys-new-house/

Dickson, A. (2004). *Modelling Double-Skin Façades.* University of Strathclyde, Department of Mechanical Engineering. Glasgow: University of Strathclyde.

Ebbert, T. (2011). Integrated refurbishment planning for sustainable office buildings. *Proceedings of the ICE - Structures and Buildings* .

Ebbert, T., & Knaack, U. (2007). *Office Refurbishment by means of Façades with Integrated Building Services .* Delft niversity of Technology, Faculty of Architecture, Delft.

Ebbert, T., & Knaack, U. (2007). *Office Refurbishment by means of Façades with Integrated Building Services.* Delft University of Technology, Faculty of Architecture, Delft.

Edwards, D. K. (1977). Solar absorption by each element in an absorber-coverglass array. *Solar Energy , 19*, 401-402.

Eicker, U., Fuxa, V., Bauer, U., Mei, L., & Infield, D. (2008). Façades and summer performance of buildings. *Energy and Buildings , 40*, 600-611.

ElSherbiny, S. M., Raithby, G. D., & Hollands, K. G. (1982). Heat Transfer by Natural Convection Across Vertical and Inclined Air Layers. *Journal of Heat Transfer , 104*, 96-102.

ERGO Italia. (2009). *Ergo Italia: ultimato il progetto di riqualificazione energetica della sede italiana.* Milano: ERGO Versicherungsgruppe AG.

Faggembauu, D., Costa, M., Soria, M., & Olivia, A. (2003). Numerical analysis of the thermal behaviour of ventilated glazed façades in Mediterranean climates. Part I: development and validation of a numerical model. *Solar Energy , 75*, 217-228.

Filonenko, G. K. (1954). Hydraulic Resistance in Pipes. In E. e. Schlunder, *Heat Exchanger Design Handbook, Teploenergetika* (Vol. 1). Hemisphere Publishing Corporation.

Flamant, G., Heigmans, N., & Guiot, E. (2004). *Determination of the energy performances of ventilated double façades by the use of simulation integrating the control aspects - Modelling aspects and assessment of applicability of several simulation software.* Belgian Building Research Institute, Department of Building Physics, Indoor Climate and Building Services. Brussels: Belgian Building Research Institute.

Gratia, E., & De Herde, A. (2007). The most efficient position of shading devices in a double-skin façade. *Energy and Buildings , 39*, 364-373.

Griffith, B. (2006). A MODEL FOR NATURALLY VENTILATED CAVITIES ON THE EXTERIORS OF OPAQUE BUILDING THERMAL ENVELOPES. *Second National IBPSA-USA Conference* (pp. 153-159). Cambridge: Simbuild 2006.

Høseggen, R., Wachenfeldt, B. J., & Hanssen, S. O. (2008). Building simulation as an assisting tool in decision making Case study: With or without a double-skin façade? *Energy and Buildings , 40*, 821-827.

Haase, M., Wong, F., & Amato, A. (2007). Double-Skin Façades for Hong Kong. *Surveying and Built Environment , 18* (2), 17-32.

Hagentoft, C.-E. (2001). *Introduction to Building Physics.* Lund, Sweden: Studentlitteratur.

Hanam, B. (2010). *Development of an Open Source Hourly Building Energy Modeling Software Tool.* University of Waterloo, Department of Civil and Environmental Engineering. Waterloo: University of Waterloo.

Hens, H., Saelens, D., De Meulenaer, V., & Elsen, P. (2008). Multiple-skin façades: high tech blessing or not? *Proceedings of the 8th Symposium on Building Physics in the Nordic Countries edition:8*, (pp. 1-8). Copenhagen.

Hensen, J., Bartak, M., & Drkal, F. (2002). Modeling and Simulation of a Double-Skin Façade System. *ASHRAE Transactions , 108, Part 2*, 1251-1259.

Hilmarsson, J. G. (2008). *Double Skin Façade: Evaluating the Viability of the Component.* Copenhagen Technical Academy. Copenhagen: Copenhagen Technical Academy.

Hoffmann, C. (2006). Was wissen wir über den Gebaüdebestand an Nichtwohn- und Wohngebaüden in Deutschland und Europa? – Eine Literaturrecherche. *Gesundheitsingenieur – Haustechnik – Bauphysik – Umwelttechnik , 127*, 69-75.

Hollands, K. G., Unny, T. E., Raithby, G. D., & Konicek, L. (1976). Free convective heat transfer across inclined air layers. *AIChE--ASME National Heat Transfer Conference. 98:2*, pp. 189-193. San Francisco: Journal of Heat Transfer.

Hottel, H. C. (1954). Radiant Heat Transmission. In W. H. McAdams, *Heat Transmission.* New York, NY, USA: McGraw-Hill.

Hunn, B. D., & Calafell, D. D. (1977). Determination of average ground Reflectivity for solar collectors. *Solar Energy , 19* (1), 87-89.

Idso, B. S., & Jackson, D. R. (1969). Thermal radiation from the atmosphere. *Journal of Geophysical Research , 74* (23), 5397-5403.

Intelligent Energy Europe. (2008). *BESTFACADE: Best Practice for Double Skin Façades, EIE/04/135/S07.38652.* Brussels, Belgium: European Commission.

Jacobs, J. D. (1978). Radiation climate of Broughton Island. *Energy Budget Studies in Relation to Fast-Ice Breakup Processes in Davis Strait , 26*, 105-120.

Jiru, T. E., & Haghighat, F. (2008). Modeling ventilated double skin façade—A zonal approach. *Energy and Buildings , 40*, 1567-1576.

Jiru, T. E., Taob, Y.-X., & Haghighat, F. (2011). Airflow and heat transfer in double skin façades. *Energy and Buildings , 43*, 2760-2766.

Khalifa, A. J. (1989). *Heat Transfer Processes in Buildings.* University of Wales, College of Cardiff. Cardiff: University of Wales.

Kotey, N. A. (2009). *Measurements and Models Related to Solar Optics in Windows with Shading Devices .* University of Waterloo, Department of Mechanical Engineering. Waterloo: University of Waterloo.

Kreider, J. F., Curtiss, P. S., & Rabl, A. (2010). *Heating and Cooling of Buildings: Design for Efficiency* (Revised Second Edition ed.). Boca Raton, FL, United States of America: CRC Press - Taylor & Francis Group.

Kurstjens, T., Vrins, E., & Leenaerts, C. (2004). The Revival of the Albatross. *Plea2004 - The 21th Conference on Passive and Low Energy Architecture* (pp. 19-22). Gouda-Tilburg: W/E consultants.

Lancour, X., Deneyer, A., Blasco, M., Flamant, G., & Wouters, P. (2004). *Ventilated Double Facades: Classification & illustration of façade concepts.* Belgian Building Research Institute, Department of Building Physics, Indoor Climate & Building Services. Belgian Building Research Institute.

LBNL. (2011). *THERM 6.3 / WINDOW 6.3 NFRC Simulation Manual.* Berkeley: Lawrence Berkeley National Laboratory.

Loveday, D. L., & Taki, A. H. (1996). Convective heat transfer coefficients at a plane surface on a full-scale building façade. *International Jourcal of Heat and Mass Transfer , 39*, 1729-1742.

Manz, H., & Frank, T. (2005). Thermal simulation of buildings with double-skin façades. *Energy and Buildings , 37*, 1114-1121.

McAdams, W. H. (1954). *Heat Transmission* (3rd Edition ed.). New York: McGraw-Hill.

McQuiston, Parker, & Spitler. (2005). *Heating, Ventilating, and Air Conditioning: Analysis and Design* (Sixth Edition ed.). Hoboken, NJ, United States of America: John Wiley & Sons, Inc.

Mills, A. (1992). *Heat Transfer.* Irwing.

Moshfegh, B., & Sandberg, M. (1996). Investigation of fluid flow and heat transfer in a vertical channel heated from one side by PV elements, Part I numerical study and PartII experimental study. *WREC* , 248-253 and 254-258.

Natural Resources Canada. (2003). *Commercial and Institutional Building Energy Use Survey 2000 Summary Report.* Office of Energy Efficiency. Ottawa: Energy Publications.

NRCan. (2012). *A Grander View of the Future: A Case Study of Enermodal Engineering's New Building.* Ottawa: Natural Resources Canada.

NRCan. (2008, December). *Natural Resources Canada*. Retrieved July 11, 2012, from Recommissioning Project Synopsis: TELUS House, Vancouver, British Columbia: http://oee.rncan.gc.ca/node/9658

NRCan. (2010, June 22). *Natural Resources Canada*. Retrieved February 15, 2011, from Energy Efficient Buildings: http://canmetenergy.nrcan.gc.ca/buildings-communities/energy-efficient-buildings/2007

Oesterle, E., Lieb, R.-D., Lutz, M., & Heusler, W. (2001). *Double-Skin Façades—Integrated Planning.* Munich, Germany: Prestel Verlag GmbH + Company.

oikos. (2001). *Telus: Revitalization of an Office Building*. (Iris Communications, Inc.) Retrieved April 30, 2012, from http://oikos.com/library/showcase/telus/index.html

Pappas, A., & Zhai, Z. (2008). Numerical investigation on thermal performance and correlations of double skin façade with buoyancy-driven airflow. *Energy and Buildings , 40*, 446-475.

Park, C.-S., Augenbroe, G., Messadi, T., Thitisawat, M., & Sadegh, N. (2004). Calibration of a lumped simulation model for double-skin façade systems. *Energy and Buildings , 36*, 1117-1130.

Perez-Grande, I., Meseguer, J., & Alonso, G. (2005). Influence of glass properties on the performance of double-glazed façades. *Applied Thermal Engineering , 25*, 3163-3175.

Poirazis, H. (2006). *Double Skin Façades for Office Buildings.* Lund University, Department of Construction and Architecture, Division of Energy and Building Design. Lund: Lund University.

Prasad, D., & Snow, M. (2005). *Designing with Solar Power: A Source Book for Building Integrated Photovoltaics [BiPV].* Mulgrave, Victoria, Australia: The Images Publishing Group Pty Ltd & Earthscan.

Reindl, D. T., Beckman, W. A., & Duffie, J. A. (1990). Diffuse Fraction Correlations. *Solar Energy , 45*, 1-7.

Rheault, S., & Bilgen, E. (1987). Heat transfer optimization of an automated venetian blind window system. *Proceedings from the ASES 12th National Passive Solar Conference.* Portland.

Rogalsky, C. (2011). *Application of a Network Solution to Complex Fenestration Systems.* University of Waterloo, Mechanical Engineering. Waterloo: University of Waterloo.

Roshenow, W., Hartnett, J., & Ganic, E. (1985). *Handbook of Heat Transfer Applications.* New York: McGraw-Hill.

Rowe, J. D., Pressnail, K. D., & Richman, R. (2010). *Evaluating the Performance of a Double Façade in a Cold Climate.* Case Study, Toronto.

Saelens, D. (2002). *Energy Performance Assessment of Single Storey Multiple-Skin Façades.* Katholieke Universiteit Leuven, Department of Civil Engineering. Leuven: Katholieke Universiteit Leuven.

Schumacher, C. (2011). Assessing the Freeze-Thaw Resistance of Clay Brick for Interior Retrofit Projects. *Building America Expert Meeting - Interior Insulation Retrofit of Mass Masonry Wall Assemblies.* Boston: Building Science Corporation.

Shewen, E. C. (1986). *A Peltier effect technique for natural convection heat flux measurements applied to the rectangular open cavity.* University of Waterloo, Department of Mechanical Engineering. Waterloo: University of Waterloo.

Siegel, R., & Howell, J. R. (1992). *Thermal Radiation Heat Transfer.* New York: McGraw-Hill.

Solaripedia. (2008). *Project: Albatros (Netherlands)*. Retrieved May 14, 2012, from Solaripedia: http://www.solaripedia.com/13/10/albatros_%28netherlands%29.html

Straube, J. (2008). Can Highly Glazed Building Façades be Green? *Building Science Insight , 006*, 1-4.

Straube, J., & Burnett, E. (2005). *Building Science for Building Enclosures.* Westford, MA: Building Science Press Inc.

Straube, J., & Schumacher, C. (2007). Interior Insulation Retrofits of Load-Bearing Masonry Walls in Cold Climates. *Building Science Digest , 114*, 1-16.

Straube, J., & Van Straaten, R. (2001). *The Technical Merits of Double Façades for Office Buildings in Cool Humid Climates.* University of Waterloo, Civil and Environmental Engineering. Waterloo: University of Waterloo.

Tascon, M. H. (2008). *Experimental and Computational Evaluation of Thermal Performance and Overheating in Double Skin Façades.* University of Nottingham. Nottingham: University of Nottingham.

Taylor, H. G. (2010). *Green Commercial Real Estate: Office Assets.* University of British Columbia, Sauder School of Business. Vancouver: University of British Columbia.

Threlkeld, J. L. (1970). *Thermal environmental engineering* (2nd Edition ed.). Englewood Cliffs, NJ, United States of America: Pretince-Hall.

Threlkeld, J. L., & Jordan, R. C. (1958). Direct solar radiation available on clear days,. *ASHRAE Transactions , 64*, 44-48.

Todorovic, B., & Maric, B. (1998). *The influence of double façades on building heat losses and cooling loads.* Belgrade University, Faculty of Mechanical Engineering. Belgrade: Belgrade University.

U.S. Department of Energy. (2006). *Commercial Buildings Energy Consumption Survey (CBECS) - Table C3A.* Washington D.C.: U.S. Department of Energy.

Ueno, K. (2011). Masonry Wall Interior Insulation Retrofit - Embedded Beam Simulations. *Building America Experts Meeting: Interior Masonry Insulation Retrofits.* Boston: Building Science Corporation.

Uuttu, S. (2001). *Study of Current Structures in Double-Skin Façades.* Helsinki University of Technology, Department of Civil and Environmental Engineering. Helsinki: Helsinki University of Technology.

von Grabe, J. (2002). A prediction tool for the temperature field of double façades. *Energy and Buildings , 34*, 891-899.

Walton, G. N. (1980). A New Algorithm for Radiant Interchange in Room Loads Calculations. *ASHRAE Transactions , 86* (2), 190-208.

Wright, J. L. (1996). A Correlation to Quantify Convective Heat Transfer Between Vertical Window Glazings . *ASHRAE Transactions , 102* (Pt. 1), 940-946.

Wright, J. L. (2008). Calculating center-glass performance indices of glazing systems with shading devices. *ASHRAE Transactions , 114* (Pt 1), 471-482.

Wright, J. L., & Kotey, N. A. (2006). Solar Absorption by Each Element in a Glazing/Shading Layer Array. *ASHRAE Transactions , 112* (2), 3-12.

Wright, J. L., Barnaby, C. S., Collins, M. R., & Kotey, N. A. (2009). *Improving Cooling Load Calculations for Fenestration with Shading Devices.* ASHRAE Research Project 1311-RP.

Wright, J. L., Barnaby, C. S., Niles, P., & Rogalsky, C. J. (2011). Efficient Simulation of Complex Fenstration Systems in Heat Balance Room Models. *Proceedings of Building Simulation 2011* (pp. 2851-2858). Sydney: 12th Conference of International Building Performance Simulation Association.

Yilmaz, Z., & Cetintas, F. (2005). Double skin façade's effects on heat losses of office buildings in Istanbul. *Energy and Buildings , 37* (691), 697.

Yuan, Y., Zeng, J., Zhu, Y., & Lin, B. (2007). A Lumped Model of Double Skin Façade with Cavity Shading. *Proceedings: Building Simulation* (pp. 211-216). Beijing: International Building Performance Simulation Association.

Zanghirella, F. (2008). *Le prestazioni energetiche delle facciate trasparenti attive: metodi di analisi sperimentale e modellazione numerica.* Politecnico di Torino. Torino: Politecnico di Torino.

Zerofootprint. (2011). *Finalist: ERGO Tower - Milan, Italy*. Retrieved May 16, 2012, from Zerofootprint Re-Skinning Awards: http://2011.reskinningawards.com/commercialindustrial/ergo-towers/

Zerofootprint. (2010). *MOED de Armas - 100 Park Ave. (Large Commercial)*. Retrieved May 5, 2011, from Zerofootprint Reskinning Awards: http://reskinningawards.com/winners/single/moed-de-armas-100-park-ave/

Zollner, A. (2001). *Experimentelle und theoretische Untersuchung des kombinierten W€armetransports in Doppelfassaden.* Technical University of Munich. Garching: Technical University of Munich.

Appendix A

User Manual

A.1 Overview

The DoFa model is based in Microsoft Excel and is therefore, relatively simple to use. Various tabs exist for inputs and calculations. Input tabs are for overall boundary conditions ("Inputs"), solid layer properties ("Single Glazing", "Shading", "Multi-Glazing" and "Opaque Wall") and cavity layer properties and creating vertical sections ("VS"). Cells that require user inputs are coloured green. There is also a tab labeled "Data Tables" that provides references for user inputs (e.g., clearness numbers, ground reflectivity, example optical properties). The remainder of the tabs are for calculations and are hidden from the user.

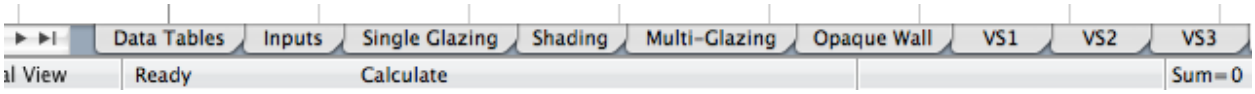

Figure A-1 Tabs

A.2 "Inputs" Tab: General Inputs

To begin, the user must go to the "Inputs" tab and specify whether to use calculated incident solar radiation values or user-defined values. Where the calculated values are used, the location data must be entered. The user can then model their design at any hour of the day. Note that the solar calculations are for clear days; therefore, user-defined values should be used to simulate a cloudy day. In this case, the location data is not necessary (Figure A).

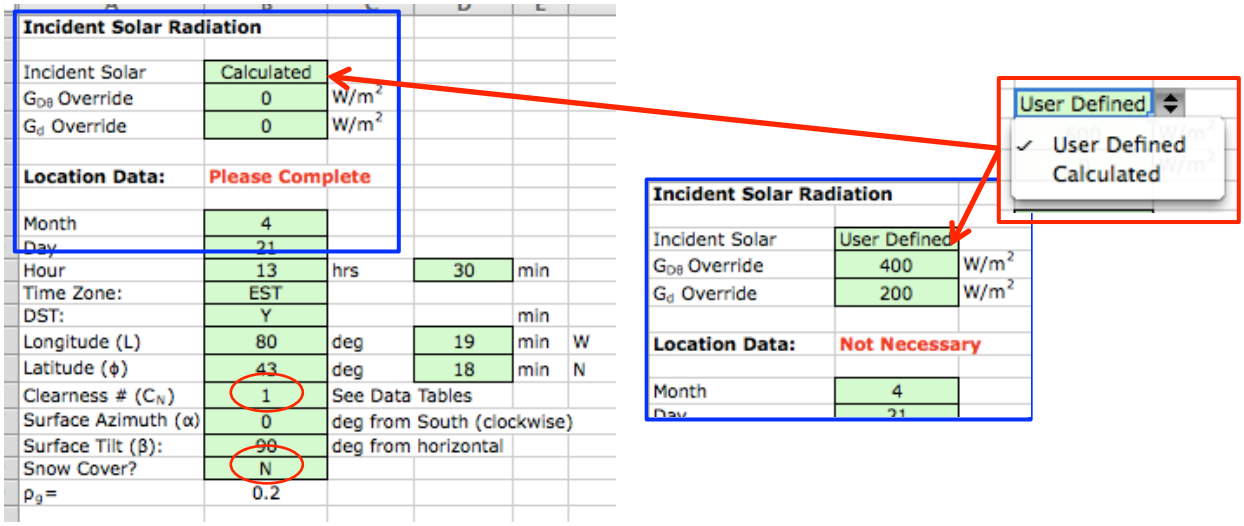

Figure A-2 "Inputs" Tab: Solar Radiation Inputs

Clearness numbers for the United Sates and the southern edge of Canada are provided in the "Data Tables" tab. Values range between 0.9 and 1.1; therefore, a value within this range may be assumed if no information is provided for a particular location. The ground reflectivity is calculated separately for snow cover (Y) or no snow cover (N), though the user may input a value manually (reference values are also provided in the "Data Tables" tab).

In addition, indoor and outdoor boundary conditions and façade dimensions must be entered in the same general "Inputs" tab.

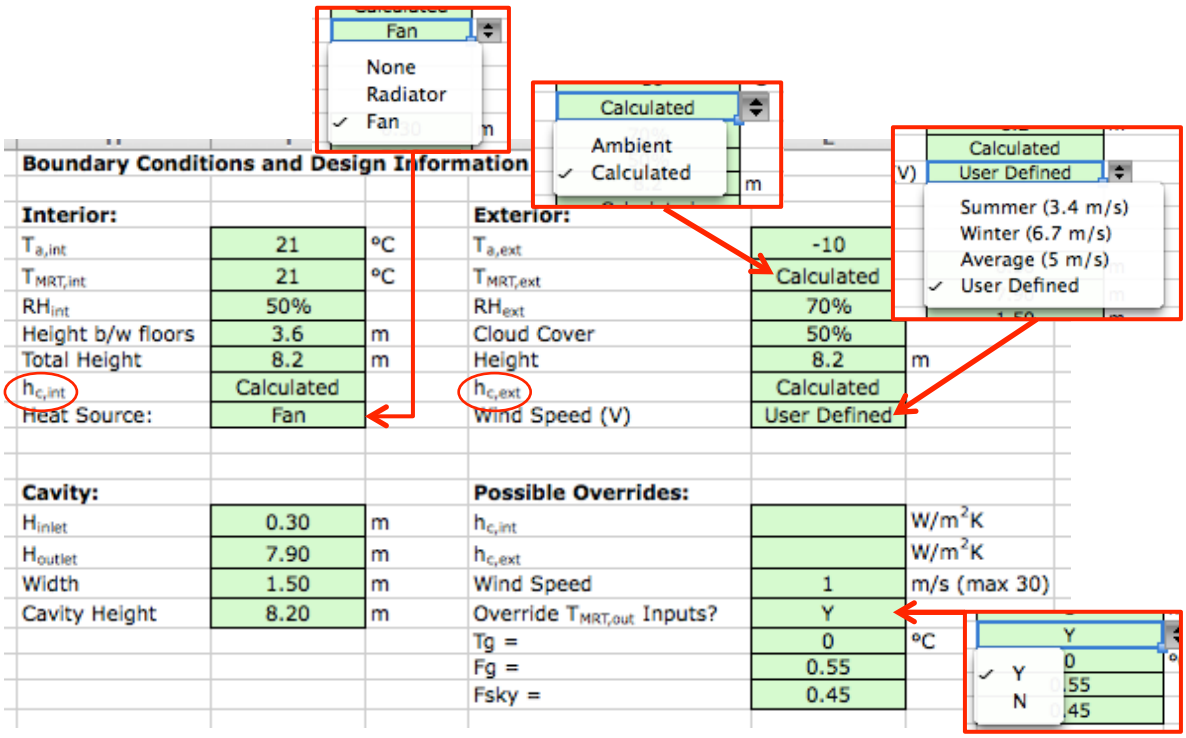

Figure A-3 "Inputs" Tab: Boundary Conditions and Dimensions

The analyst can override both the indoor and outdoor convective coefficients by selecting "User Defined" instead of "Calculated" and entering values in the "Possible Overrides" section. If so, the indoor heat source and the outdoor wind speed are not necessary. If "Calculated" convective coefficients are selected, then the analyst must choose a heat source (none, radiator or fan) and a wind speed (summer, winter, average or user defined). If a user-defined wind speed is selected, the wind speed must be entered in the "Possible Overrides" section. The possible overrides were intended to give the analyst maximum flexibility.

The other possible overrides pertain to the outdoor MRT ($T_{ext,MRT}$). If "Ambient" is selected, $T_{ext,MRT}$ is set to the outdoor air temperature and no other inputs are necessary. If "Calculated" is chosen, $T_{ext,MRT}$ is calculated from the sky and ground (surroundings) temperatures and the analyst must complete the "Override $T_{ext,MRT}$ Inputs?" cell. If "N" is selected, the default inputs for ground temperature and angle factors are used ($T_g = T_{a,ext}$ and $F_g = F_{sky} = 0.5$). If "Y" is selected, the analyst must enter their own values. This may be useful in an urban setting, where the wall has a limited view of the sky (i.e., $F_g > F_{sky}$) or where a wall has a significant view of an asphalt parking lot on a sunny day ($T_g > T_{a,ext}$). Once the "Inputs" tab is complete, the user must create the solid layers.

A.3 Component Tabs: Solid Layer Inputs

There is a tab for each type of solid component where the user can enter layer properties: "Single Glazing", "Shading", "Multi-Glazing" and "Opaque Wall". The inputs for single glazing are shown in Figure .

Layer ID:	Clear_6						
Thickness:	5.7	mm					
	Emissivity		Transmittance	Reflectance		Absorptance	
	out	in		out	in	out	in
Beam			0.771	0.073	0.072	0.156	0.157
Diffuse			0.677	0.130	0.130	0.193	0.193
Layer	0.840	0.840					

Figure A-4 "Single Glazing" Tab: Example Inputs

The inputs include thermal and optical properties. Based on the transmittance and reflectance input values, DoFa calculates the corresponding absorptance. As shown, the diffuse properties are entered separately.

For shading layers, there are some additional inputs. According to the blind type, the user must either input the slat angle and length (venetian blind) or openness (roller blind).

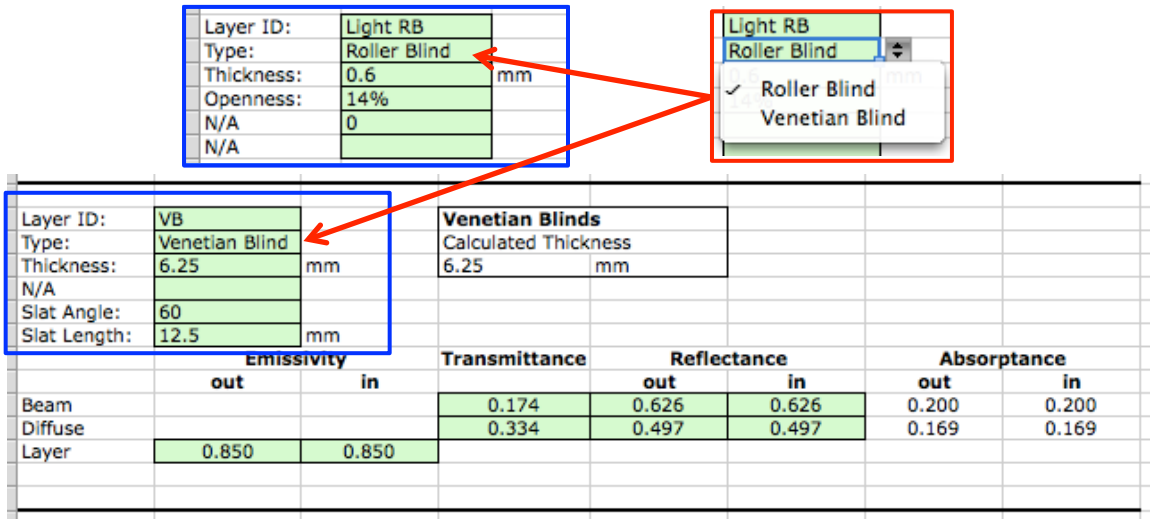

Figure A-5 "Shading" Tab: Example Inputs

For venetian blinds, DoFa calculates the thickness of the blind based on the slat angle and length. The result is displayed in the box outlined in the top centre. The analyst can then input this value into the "Thickness" cell without doing any calculations themselves. Note that the shading thickness is only important for the results graph. For roller blinds, the openness applies to longwave radiation only. For solar radiation, the openness should be included in the blind transmittance.

Multi-glazing layers can have up to four panes. The analyst must specify the number of panes and enter optical properties for each. It is very important to enter the correct number of panes because DoFa will only model the number of panes specified, even if optical properties are provided for all panes,

Layer ID:	DG Low-E Avg									
Panes:	2									
Thickness:	60.9	mm								
		U-Value	Emissivity		Transmittance	Reflectance		Absorptance	
		W/m²K	out	in		out	in	out	in
Pane 1	Beam				0.771	0.073	0.072	0.156	0.157
	Diffuse				0.677	0.130	0.130	0.193	0.193
Pane 2	Beam				0.281	0.562	0.562	0.157	0.157
	Diffuse				0.247	0.589	0.589	0.164	0.164
Pane 3	Beam								
	Diffuse								
Pane 4	Beam								
	Diffuse								
Layer	U-Value	1.32	0.841	0.840					
	U	1.66							
	U Calc =	1.66	h_{int} =	7.94					

Figure A-6 Multi-Glazing Tab: Example Inputs

Note that the bottom cell labeled “U Calc” is calculated from the entered U-value. The user can either use the calculated U, or input a value of their choosing. U signifies the component conductance without surface films.

For opaque layers, direct optical properties are entered only for the outdoor surface. It is assumed that opaque optical properties change little with incidence angle and that no source of solar radiation exists on the inside (i.e., the room).

Layer ID:	Masonry						
Thickness:	300	mm					
	R-Value	U	Emissivity		Reflectance	Absorptance	
	h·ft²·°F/Btu	W/m²K	out	in	out	out	
Layer	5.0	1.136	0.900	0.900	0.630	0.370	
	U Calc =	1.136					

Figure A-7 "Opaque Wall" Tab: Example Inputs

Here, the bottom cell labeled “U Calc” is calculated from the entered imperial R-value. The imperial R-value is more commonly used and is therefore an easier input. Note that the R-value should not include surface films. The analyst may use the calculated U, or input a value of their choosing. In each component tab, there is space to enter three different layers. The layer ID should describe the layer, as it will be used to build vertical sections.

A.4 “VS” Tab: Vertical Section Inputs

The next step is to build a vertical section in the “VS” tab, using the created components. First, the analyst must enter how many solid layers make up the section. The model automatically assumes that a cavity layer exists between any two solid layers.

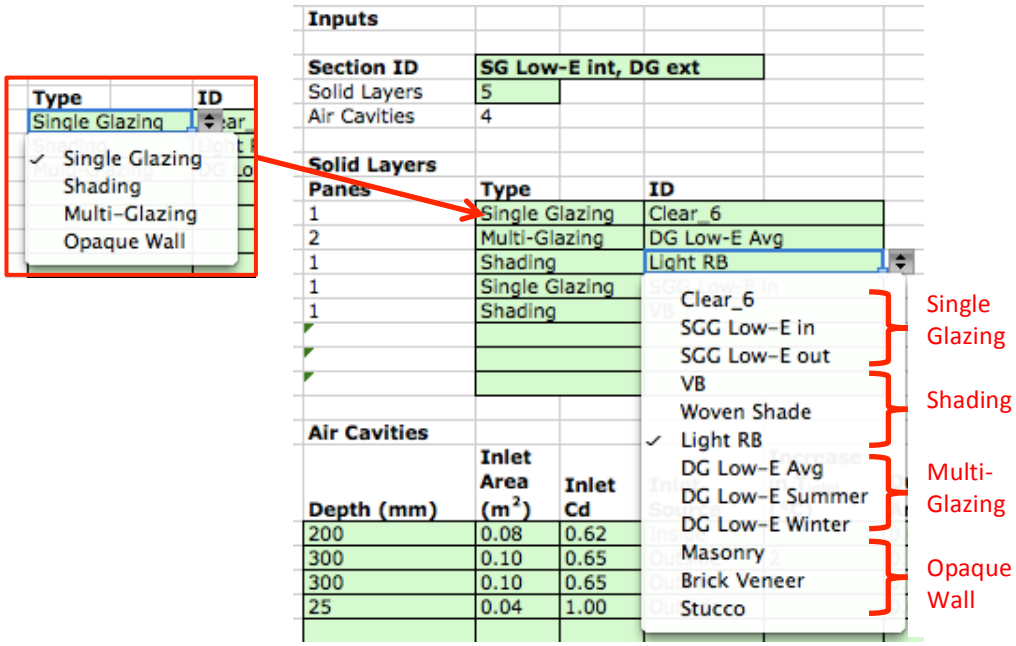

Figure A-8 “VS” Tab: Example Section Inputs

Next, the analyst must specify the layer sequence by choosing the type and ID for each layer. Note that the layer numbers increase from the inside to the outside. The layer IDs created in each of the component tabs show up in the ID dropdown menu. There are three IDs for each component type, corresponding to the three different layer inputs in each component tab.

On the same tab, the analyst must define the air cavities. Note that all cavities are assumed to be air and are not intended for IGU cavities (e.g., argon fill). IGUs should be treated as multi-glazing components, where the cavity is incorporated into the U-value.

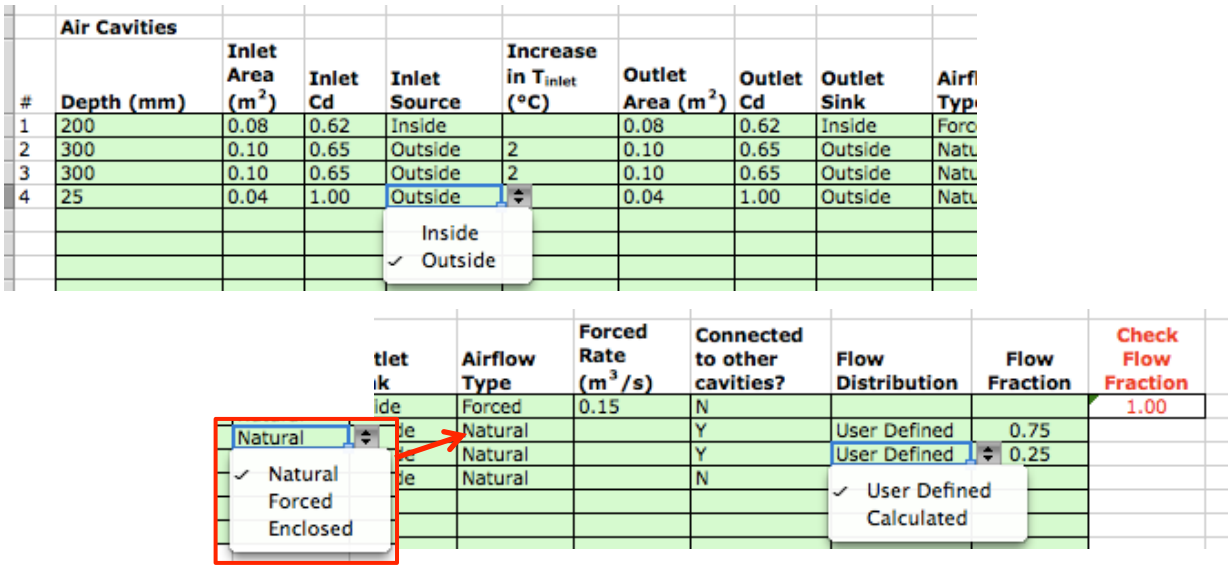

Figure A-9 "VS" Tab: Air Cavity Inputs

Beginning from the left, the analyst must enter the cavity depths as well as the flow characteristics (A and C_d) for the inlet and outlet. The inlet source is important as it determines the inlet temperature of the cavity, which is needed for natural ventilation as well as cavity temperature calculations. Beside the inlet source, there is a column to add an increase to the inlet temperature. This is to account for temperature increases over the inlet opening; however, it can be left blank if unknown. The outlet sink is only important if "Inside" is specified, as this affects the heat flux into the building. However, if the cavity air is to be fed into the HVAC system and not directly into the conditioned space, the outlet sink should be specified as "Outside". This way, HVAC calculations can be conducted separately.

The airflow type is important to the convection calculations as well as the airflow calculations. Where "Forced" is chosen, a rate must be entered in the adjacent cell in m^3/s. Also, the analyst must specify whether or not a cavity is connected to other cavities. If "Y" is chosen, this represents the case where two cavities are separated by a shading device but are ultimately connected at the top and bottom. The DoFa model assumes that any cavity with a "Y" in the "Connected to other cavities?" column is connected to all other cavities marked with a "Y". Therefore, any number of cavities can be connected, though there cannot be separate sets of connected cavities. It is important that inputs be entered only for cavity layers present, as a "Y" in a later row would alter the results.

Where connected cavities exist, the analyst may choose to either define a flow distribution or use the calculated flow distribution. In the first case, a flow fraction must be entered in the adjacent cell. The summation of flow fractions for the connected cavities should equal 1. In the second case, DoFa assumes a flow distribution proportional to the width distribution. Once all the inputs have been entered, the results show up in the same “VS” tab. Note that there are currently three “VS” tabs so that the analyst may test different systems (Figure).

A.5 “VS” Tab: Results

The results include the temperature profile, performance indices and airflow. Results are shown here for the inputs from the previous sections. Note that this system is simply for demonstration and would not likely be used in practice. The solid layers, from inside to outside, are single glazing (SG), double glazing (DG), roller blind (RB), single glazing (SG) and a venetian blind (VB). The layers are labeled for clarification, with solid layer labels on the bottom and cavity layer labels on the top (Figure).

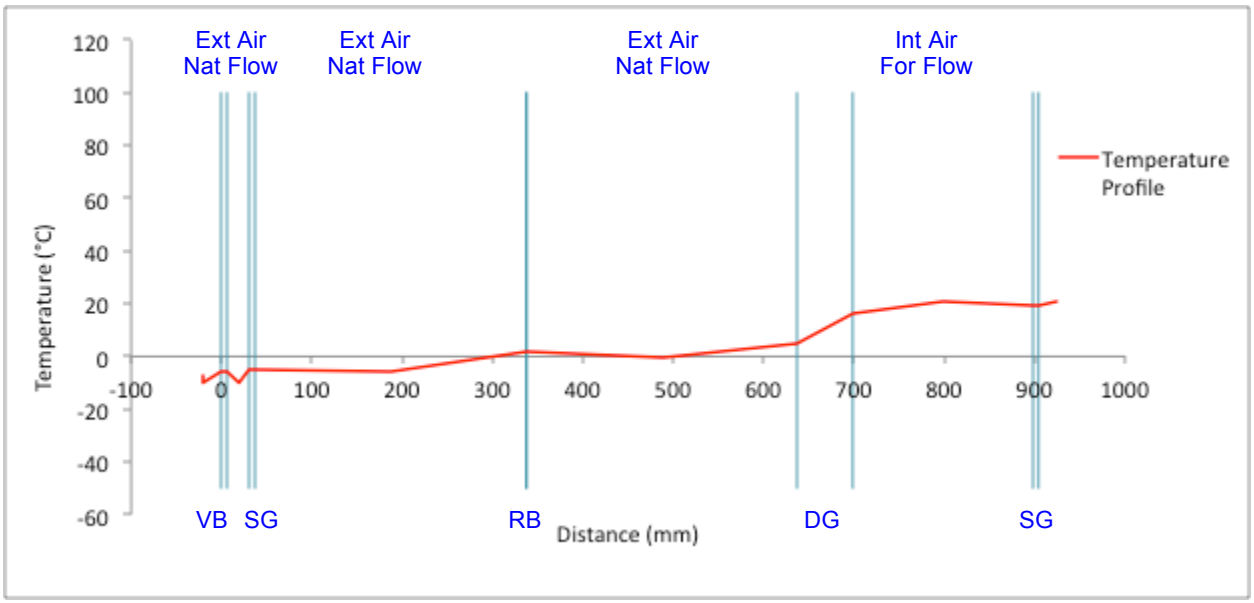

Figure A-10 "VS" Tab: Temperature Profile

A vertical line represents the outdoor and indoor surface of each layer. Note that for multi-glazing components, the intermediate panes are not illustrated. The temperature profile is also presented in table format, along with all other outputs.

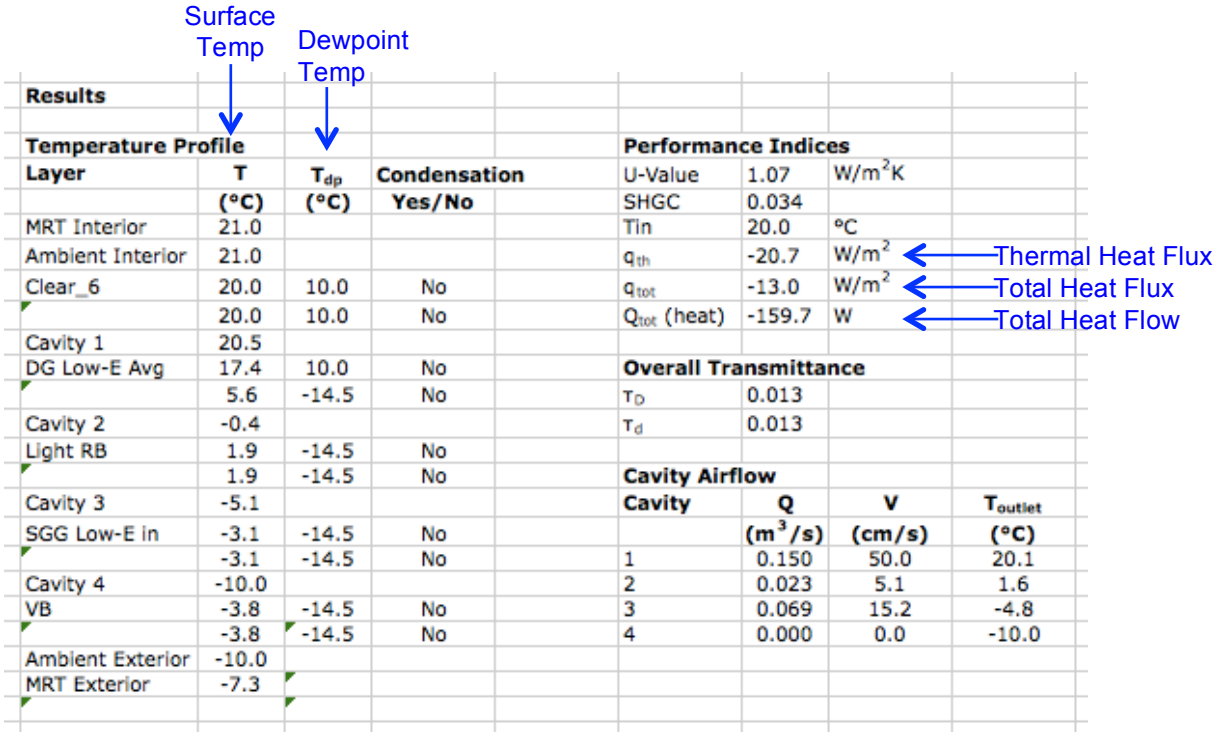

Results

Temperature Profile

Layer	T (°C)	T_{dp} (°C)	Condensation Yes/No
MRT Interior	21.0		
Ambient Interior	21.0		
Clear_6	20.0	10.0	No
	20.0	10.0	No
Cavity 1	20.5		
DG Low-E Avg	17.4	10.0	No
	5.6	-14.5	No
Cavity 2	-0.4		
Light RB	1.9	-14.5	No
	1.9	-14.5	No
Cavity 3	-5.1		
SGG Low-E in	-3.1	-14.5	No
	-3.1	-14.5	No
Cavity 4	-10.0		
VB	-3.8	-14.5	No
	-3.8	-14.5	No
Ambient Exterior	-10.0		
MRT Exterior	-7.3		

Performance Indices

U-Value	1.07	W/m^2K
SHGC	0.034	
Tin	20.0	°C
q_{th}	-20.7	W/m^2
q_{tot}	-13.0	W/m^2
Q_{tot} (heat)	-159.7	W

Overall Transmittance

τ_D	0.013
τ_d	0.013

Cavity Airflow

Cavity	Q (m^3/s)	V (cm/s)	T_{outlet} (°C)
1	0.150	50.0	20.1
2	0.023	5.1	1.6
3	0.069	15.2	-4.8
4	0.000	0.0	-10.0

Figure A-11 "VS" Tab: Results

For each surface, the dewpoint of the adjacent air is provided to determine if condensation occurs. The overall performance indices are presented on the top right, while the overall transmittance of both direct and diffuse light are presented just below. The airflow rate, velocity and outlet temperature in each cavity are presented on the bottom right.

It is important to realize which inputs have the largest impact on the results. For total heat flux/flow, layer optical properties are most important. For airflow rate and outlet temperature, inlet/outlet characteristics (A and C_d) are most important. Also, venetian blinds should be modeled with caution as the accuracy of results is variable.

Appendix B

Summary of Model Approaches and Calculations

Table B-1 Complex Fenestration Models (Lumped)

Authors	Configuration Modeled	Optical Element	Thermal Element		Airflow Element	Validation
			Radiation	Convection		
VISION5 (Rogalsky, 2011)	**Height**: Unit height **Layers**: Uniform (glazed) **Shading**: Any **Cavity depth**: 10 cm max b/w any 2 layers	**Incident Radiation:** User input, including diffuse fraction. **Absorbed Fraction:** Edwards' (1977) method to account for multiple reflections. Treatment of diffuse radiation, and beam-to-diffuse reflection and transmission.	**Outdoor/Indoor:** MRT user input. **Cavity:** Temperature dependent coefficients based on radiosities calculated as per (Wright, 2008).	**Outdoor/Indoor:** User input. **Cavity:** Calculated using empirically derived relations for Nusselt number as per (Wright, 1996) for sealed cavities with aspect ratios > 40. $N_{u1} = 0.0673838 R_a^{1/3} \;;\; 5\cdot10^4 < R_a$ $N_{u1} = 0.028154 R_a^{0.4134} \;;\; 10^4 < R_a \le 5\cdot10^4$ $N_{u1} = 1 + 1.7596678\cdot10^{-10} R_a^{2.2984755} \;;\; R_a \le 10^4$	None. Airflow allowed in outdoor/indoor shading cavities through altered convective coefficients. Indoor: $h_{g\text{-}s} = \frac{k_{air}}{b} \qquad h_{g\text{-}a} = h_c\left(1-\exp\left(-4.6\frac{b}{0.1}\right)\right)$ $h_{s\text{-}a} = h_c\left(2-\exp\left(-4.6\frac{b}{0.1}\right)\right)$ Venetian Blinds (max 20% increase): $h_{s\text{-}a} = h_c\left(2-\exp\left(-4.6\frac{b}{0.1}\right)\right)\cdot\left(1+0.2\left\|\sin(2\phi)\right\|\right)$ Outdoor: $h_{g\text{-}s} = 0 \qquad h_{g\text{-}a} = h_c \qquad h_{s\text{-}a} = 2\,h_c$ g = glass, s = shading device, b = gap depth, Φ = slat tilt angle	Tested against published data (ASHRAE handbook).
WINDOW 6.3 (LBNL, 2011)	**Height**: Center of glazing: Unit height Glazing product: User defined **Layers**: Uniform (glazed) **Shading**: Any **Cavity depth**: Any	**Incident Radiation:** NFRC 100 - 783 W/m^2, direct, normal incidence **Absorbed Fraction:** Iterative equations written with spectral dependence (uses a multi-band model requiring a spectral data file). Accounts for multiple reflections.	**Outdoor/Indoor:** MRT equal to ambient for NFRC conditions. $h_{r,out} = 4\sigma\varepsilon_{f,1}\left(\frac{T_{rm,out}+T_{f,1}}{2}\right)^3$ **Cavity:** Radiosity of each surface calculated from the Stefan-Boltzmann law using the surface infrared hemispherical emissivity and temperature.	**Outdoor:** $h_{c,out} = 4 + 4w_s$ w = wind speed **Indoor/Cavity**: Empirically derived relations for Nusselt number based on tilt angle.	None.	Yes.

Table B-2 Double Façade Models (Lumped)

Authors	Configuration Modeled	Optical Element	Thermal Element		Airflow Element	Validation
			Radiation	Convection		
Todovoric & Maric (1998)	**Height:** Single storey **Layers:** Mixed (glazed and opaque) **Shading:** None **Cavity depth**: Varied	**Incident Radiation:** Input. No separation between direct and diffuse. **Absorbed Fraction:** No consideration of multiple reflections.	**Opaque Wall:** Not included (considered negligible). **Glazing:** Outdoor, indoor and cavity: $Q=\varepsilon A\sigma\beta(T_s-T_m)$ β = temperature coefficient (1.1) (T_s-T_m) = temperature difference between surface and adjacent air	Calculations not presented.	Air velocity must be known.	None.
*von Grabe (2002)	**Height:** Single storey **Layers:** Uniform (glazed) **Shading:** Roller blind **Cavity depth:** 24 cm	Not described.	**Outdoor/Indoor:** Combined radiation/convection heat transfer coefficients as per CIBSE Guide A3 (1999). **Cavity:** linearized heat transfer coefficients for infinite parallel plates. $h_{r,m,i-j}=\frac{C_{i-j}}{100^4}[(T_{i,m}+T_{j,m})^3 - 2(T_{i,m}+T_{j,m})T_{i,m}T_{j,m}]$	**Indoor/Outdoor:** Combined radiation/convection heat transfer coefficients as per CIBSE Guide A3 (1999). **Cavity:** Calculated separately for each shaft using the approach of Michejew for free convection at vertical planes (Elsner, 1992/1993; Elsner et al., 1993).	Natural airflow (buoyancy only). One-dimensional in the y-plane. 2 shafts treated separately. $w_{m,S1}=\sqrt{\frac{2(\rho_{EX}-\rho_{m,S1})gH}{\rho_{m,S1}(1+\sum_i\zeta_{i,effective,S1})}}$ w = velocity ζ = loss factor (determined as per turbulence losses in pipes: orifices, flanges and diffusers)	Test facility.
Yılmaz & Cetintas (2004)	**Height:** Single storey **Layers:** Mixed (glazed and opaque) **Shading:** None **Cavity depth:** 60 cm	Same as Todorovic, except separated into direct and diffuse	Only included between opaque wall and cavity air, otherwise neglected. Calculation same as Todorovic.	**Outdoor/Indoor:** Calculations not presented. **Cavity:** *V = 5 to 30 m/s* $hc = 7.3V^{0.78}$ *V < 5 m/s* $hc = 5.6 + 4V$	N/A. Only for closed cavity.	None.

**Modified lumped model to account for vertical temperature gradient in the cavity air.*

Table B-2 Double Façade Models (Lumped Cont'd)

Authors	Configuration Modeled	Optical Element	Thermal Element		Airflow Element	Validation
			Radiation	Convection		
Park, Augenbroe, Messadi, Thitisawat, Sadegh (2004)	**Height:** Single storey **Layers**: Uniform (glazed) **Shading**: Venetian blind **Cavity depth**: 30 cm	**Incoming Radiation:** Separated into direct and diffuse. **Absorbed Fraction:** Net radiation method by Rheault and Bilgen (1989) accounts for multiple reflections.	**Outdoor/Indoor:** Not described. **Cavity:** Calculated according to Rheault and Bilgen (1989) for net radiation.	Convective coefficients found using a parameter estimation technique based on extensive data points. **Outdoor h_c:** $= 5.678\left[0.9244 + 0.5564\left(\frac{V_{out}}{0.3048}\right)^{0.4594}\right]$ **Indoor h_c:** $= 3.8249\left(\frac{\Delta T}{L}\right)^{0.0144}$ **Cavity:** Outer glazing h_c = $2.2024 + 1.1934(\Delta T)^{0.3890} + 0.2652(V_{ca})^{0.8749}$ Blind h_c = $2.1064 + 1.8809(\Delta T)^{1.0135} + 0.2652(V_{ca})^{0.8749}$ Inner glazing h_c = $2.6205 + 2.6845(\Delta T)^{1.0196} + 0.2652(V_{ca})^{0.8749}$	Natural airflow for 10 regimes calculated for 3 main flow paths. 1) Interior air curtain: Buoyancy only. $V_{ca,b} = \sqrt{2}\frac{OH}{D}\sqrt{\frac{gL}{f}\frac{\lvert T_{ca} - T_{in}\rvert}{T_{in}}}$ OH = open height of vents D = depth, L = height, f = form loss factor 2) Exterior air curtain: Buoyancy/ wind. $V_{ca,w} = \frac{c}{A_e}\left(C_p\rho\frac{V_{out}^2}{2}\right)^n$ if $C_p \geq 0$ $\begin{cases} \text{if } V_{ca,b} \geq V_{ca,w}: & V_{ca} = \sqrt{V_{ca,b}^2 - V_{ca,w}^2} \\ \text{elseif } V_{ca,b} < V_{ca,w}: & V_{ca} = -\sqrt{V_{ca,w}^2 - V_{ca,b}^2} \end{cases}$ elseif $C_p < 0$: $V_{ca} = \sqrt{V_{ca,b}^2 + V_{ca,w}^2}$ 3) Supply/Exhaust: Buoyancy, wind and mechanical pressures combined. $Q_{ca} = c(\Delta p)^n = c(p_b + p_w + p_m)^n$	Test facility.
Griffith (2006)	**Height:** Horizontal cavity (roof) **Layers:** Uniform (opaque) **Shading:** None **Cavity depth:** 5 cm	**Incoming Radiation:** Calculated. Separated into direct and diffuse, using sky, solar, and shading models as per EnergyPlus. **Absorbed Fraction:** Only for outside baffle (opaque).	Calculations not presented. **Outdoor:** Exchange between sky, air and ground using linearized coefficients (Stefan-Boltzmann law and view factors). **Indoor:** Not applicable (not modeled). **Cavity:** Linearized heat transfer coefficient.	Calculations not presented. **Outdoor:** Undefined. Same as EnergyPlus. **Indoor:** Not applicable (not modeled). **Cavity:** Based on those used for window gaps in ISO 15099.	Natural airflow. Buoyancy: $\dot{V}_{thermal} = C_D A_{in}\sqrt{2g\Delta H_{NPL}\frac{(T_{a,cav} - T_{amb})}{T_{a,cav}}}$ Wind: $\dot{V}_{wind} = C_v A_{in} U_\infty$ Total: $\dot{V}_{tot} = \dot{V}_{wind} + \dot{V}_{thermal}$ C_d = discharge coefficient C_v = effectiveness of openings (0.25-0.6)	None. Requires "subsequent research to derive input data from empirical measurements".

Table B-3 Double Façade Models (Control Volume)

Authors	Configuration Modeled*	Optical Element	Thermal Element		Airflow Element	Validation
			Radiation	Convection		
Balocco (2002)	**Height:** Multi storey (6 and 14 m) **Layers:** Uniform (opaque) **Shading:** None **Cavity depth:** 7-35 cm	**Incoming Radiation:** Input. No separation between direct and diffuse. **Absorbed Fraction:** Only for outside layer (opaque).	Calculations not presented **All surfaces:** Linearized heat transfer coefficients.	**Outdoor:** v < 4 m/s Nusselt number correlation for vertical walls (ASHRAE, 1997) v > 4 m/s McAdams (1954) formula: $h_e = 5.7 + 3.8 \times v_v$ **Indoor:** Not described (could be included in U-value) **Cavity:** (Holman, 1991; Warren et al., 1998) $Nu_i = \frac{fat \times Re \times Pr}{1.07 + 12.7 \times fat^{0.5}(Pr^{2/3} - 1)}$ where $fat = \frac{1.82}{8}(\log_{10} Re - 1.64)^{-2}$	Natural airflow (buoyancy only). One-dimensional in the y-plane. $v^2 = 2gH\frac{(t_{ma}/t_e - 1)}{(\lambda H/D + 2.5)}$ $\lambda = 0.0055\left[1 + \left(2 \times 10^4 \frac{\varepsilon}{D} + \frac{10^6}{Re}\right)^{1/3}\right]$ H = height D = equivalent diameter λ = friction factor ε = roughness of granite panel (1.5) Re = Reynolds number	Compared to literature experimental data (Moshfegh & Sandberg, 1996).
Saelens (2002)	**Height:** Single storey **Layers:** Uniform (glazed) **Shading:** Roller blind **Cavity depth:** Varied	**Incident Radiation:** Calculated. Separated into direct and diffuse (Reindl model, 1990). **Absorbed Fraction:** Edwards' (1977) method to account for multiple reflections. Angle of incidence and partial shading of the panes is also taken into account.	**Indoor/Outdoor**: If inadequate information available, radiative and convective heat transfer may be combined (h_{int} = 8 W/m^{2}K and h_{ext} = 23 W/m^{2}K). Otherwise, outdoor: $q_{lw,k} = \frac{\varepsilon_{lw,k}\sigma}{2}\left[\left(T_{sky}^4 - T_k^4\right) + \left(T_{sur}^4 - T_k^4\right)\right]$ Indoor calculations not presented. **Cavity:** Net-radiation method by Hottel (1954). $q_{r,k} = q_{o,k} - q_{i,k}$ $q_{o,k} = \varepsilon_{lw,k}\,\sigma\,T_k^4 + (1 - \varepsilon_{lw,k})q_{i,k}$ $q_{i,k} = \sum_{j=1}^{N} F_{kj}\,q_{o,j}$ Subscripts: r =net, o = outgoing, i = incoming	**Outdoor:** Correlations for hc by Loveday and Taki (1996) depending on wind speed and direction. **Indoor:** 1) No heating device (Alamdari and Hammond, 1983): $h_{c,i} = \left[\left(1.50\left(\frac{\Delta\theta}{H}\right)^{0.25}\right)^6 + \left(1.23(\Delta\theta)^{0.33}\right)^6\right]^{\frac{1}{6}}$ 2) Radiator (Khalifa, 1989): $h_{c,i} = 2.07\,\Delta\theta^{0.23}$ 3) Fan (Khalifa, 1989): $h_{c,i} = 2.92\,\Delta\theta^{0.25}$ **Cavity:** Based on the Nusselt number. Distinction is made between natural, forced and mixed convection for both wide and narrow channels.	Mechanical and natural airflow. One-dimensional in the y-plane. Distribution on either side of blind is input. Buoyancy ΔP (Liddament, 1996): $\Delta p_{buoy} = \rho_o \cdot g \cdot H \cdot \left(\frac{T_{cav}}{T_e} - 1\right)$ Wind ΔP: $p_v = \rho_o U_h^2 / 2$ $p_s = C_p\,p_v$ Tot= a Δp˘ ѡ: Q a and b determined experimentally U_h = wind speed at height h	Test facility.

Table B-3 Double Façade Models (Control Volume Cont'd)

Authors	Configuration Modeled*	Optical Element	Thermal Element		Airflow Element	Validation
			Radiation	Convection		
Faggembauu, Costa, Soria, Olivia (2003)	**Height:** Single storey **Layers:** Mixed (glazed and opaque) **Shading:** Roller blind **Cavity depth:** 24 cm	**Incident Radiation:** Calculated. Separated into direct and diffuse using Collares-Pereira–Rabl correlations (1979). Values on sloped surfaces as per (Liu & Jordan, 1962). **Absorbed Fraction:** Iterative net heat radiation algorithm (Siegel and Howell, 1992) accounts for multiple reflections.	**Outdoor:** $q = \epsilon_o(\sigma(F_{f-g}(\epsilon_g T_g^4 + (1-\epsilon_g)T_{sky}^4) + (1-F_{f-g})T_{sky}^4) - \sigma T_{wo}^4)$ **Indoor:** $q = \epsilon_i\sigma(T_{wi}^4 - T_{walls}^4)$ **Cavity:** Infinite parallel plates. $q_{rn} = \frac{\epsilon_i\epsilon_{i+1}\sigma(T_i^4 - T_{i+1}^4)}{\epsilon_{i+1} + \epsilon_i(1-\epsilon_{i+1})}$	**Outdoor**: Correlation for h_c based on wind speed and direction (Rohsenow et al., 1985) **Indoor/Closed Cavity:** Calculated for natural convection (Mills, 1992) **Cavity**: Developing flow (Gnielinski, 1983): $Nu = 3.78 + \frac{0.0156\left[Pe\frac{w}{h}\right]^{1.14}}{1 + 0.058\left[Pe\frac{w}{h}\right]^{0.64}Pr^{0.17}}$ Turbulent flow (Filonenko, 1954): $Nu = \frac{(f_t/8)(Re-1000)Pr}{1+12.7\sqrt{f_t/8}(Pr^{2/3}-1)}\left[1+\left(\frac{d}{h}\right)^{2/3}\right]$ $f_t = (1.82\log Re - 1.64)^{-2}$	Mechanical and natural airflow (buoyancy only). The effect of pressure drops due to the geometry of the inlet and outlet ports are not considered. Inlet pressure: $P_{in} = -\frac{1}{2}\rho V_{in}^2$ Outlet pressure: $P_{out}(V_{in}) = -\rho_o g h$ A Newton–Raphson method is used to solve this equation	Compared to analytical solutions, reference situations and experimental set-ups (European Joule Project - Costa et al., 2000; Soria et al., 2000).
Zanghirella, Perino, Serra (2010)	**Height:** Single and double storey **Layers:** Uniform (glazed) **Shading:** Roller/venetian blind **Cavity depth:** Varied	**Incident Radiation:** Calculated. Separated into direct and diffuse though method not described. **Absorbed Fraction:** Edwards' (1977) method accounts for multiple reflections. For venetial blinds, direct-to-diffuse and diffuse-to-diffuse reflected portions treated separately.	Calculations not presented. **Outdoor:** Exchange with sky and surroudings. **Indoor:** MRT assumed to be equal to air temperature **Cavity**: Assumed indefinite parallel plates.	**Outdoor:** max of buoyancy or wind $h_c = \max(h_{c1}, h_{c2})$ $h_{c1} = 1,52 \cdot \lvert\Delta T\rvert^{1/3}$ $h_{c2} = 5.62 + 3.9 \cdot v$ **Indoor:** Same as Saelens. Plus fan with known velocity: $h_c = 5.34 + 3.27 \cdot v$ **Cavity**: Open cavity uses McAdams (1954) formula (same for both shafts) $h_c = 5.62 + 3.9 \cdot v \quad v < 5\,\mathrm{m/s}$ Closed cavity uses empirically derived relations for Nusselt number based on tilt angle.	Mechanical airflow, flow rate is known. One-dimensional in the y-plane. Distribution on either side of blind is assumed proportional to the shaft widths.	Test facility and existing building (SOMEC Headquarters in Italy).

Table B-4 Double Façade Models (Zonal)

Authors	Configuration Modeled*	Optical Element	Thermal Element		Airflow Element	Validation
			Radiation	Convection		
Yuan, Jianlong, Yingxin, Borong (2007)	**Height:** Single storey **Layers:** Uniform (glazed) **Shading:** Venetian blind **Cavity depth:** 80 cm	**Incident Radiation:** Not described. **Absorbed Fraction:** General recursion formula based on energy balances (Yi Jiang, 1980) accounts for multiple reflections.	**Outdoor:** Not included. **Indoor:** Combined convective/radiative heat transfer coefficient (ASHRAE 2001). $h_6 = 1.46\left[\frac{(T_7 - T_m)}{H}\right]^{0.25} + e\sigma(T_7 - T_m)$ **Cavity:** Stefan-Boltzmann equation used with summation for net radiation between non-isothermal walls. $q = \sum_k \sigma_{i,j\to k} A_i \left(T_k^4 - T_{i,j}^4\right)$	**Outdoor**: As per (Park et al., 2004) $h_1 = 5.68\left(0.92 + \left(\frac{V}{0.3}\right)^{0.46}\right)$ **Indoor:** Combined with radiation (see radiation). **Cavity**: Based on modified Nusselt number. $Nu_{DSF} = C_M Nu_{em} = C_A C_T C_H Nu_{em}$ C_A = extra area introduced by window frames and shadings (>1) C_T = averaged temperature of transparent and opaque surfaces (>1) C_H = transfer enhancement due to disturbances (frame and shading) (1-2)	Natural airflow (buoyancy only). Two-dimensional airflow network. Unspecified how velocity is calculated. $\Delta P = \zeta_{(i-1,1)\to(i,1)} \frac{\rho_{(i,1)} v^2_{(i-1,1)\to(i,1)}}{2}$ ΔP = pressure difference between nodes ζ = loss factor determined as per turbulence losses in pipes (Qingyao Lu., 1987)	Test facility.
Jiru & Haghighat (2008)	**Height:** Single storey **Layers:** Uniform (glazed) **Shading:** Venetian blind **Cavity depth:** 15-30 cm	**Incident Radiation:** Input. Separated into direct and diffuse. **Absorbed Fraction:** Normal incidence absorption used. No mention of multiple reflections or direct-to-diffuse reflection of the blinds.	**Outdoor/Indoor:** Combined convective/radiative heat transfer coefficients. h_{ext} = 29 W/m^{2}K $h_{int} = 1.48\left(\frac{T_{L4} - T_{indoor}}{H}\right)^{0.25} + \frac{T_{L4}^4 - T_{indoor}^4}{T_{L4} - T_{indoor}}$ **Cavity:** A view factor accounts for diathermanous layers. $h_r = \frac{4\sigma T_m^3}{(1/F_{Li,Li+1}) + (1-\varepsilon_{Li}/\varepsilon_{Li}) + (1-\varepsilon_{Li+1}/\varepsilon_{Li+1})}$ View factor as with fictitious cavity (Rheault & Bilgen, 1989). $F_{L2,L3} = 2 - \sin\left(\frac{90+\varphi}{2}\right) - \sin\left(\frac{90-\varphi}{2}\right)$ $F_{L2,L4} = \sqrt{2}\cos\left(\frac{\varphi}{2}\right) - 1 \quad F_{L3,L4} = F_{L2,L3}$ L2, L4 = glass surfaces, L3 = shading in between, ϕ = slat tilt angle	**Outdoor/Indoor:** Combined with radiation (see radiation). **Cavity:** *Natural Airflow* Glass: $Nu_H = (0.825 + 0.328 Ra_H^{1/6})^2 \quad 0.1 < Ra_H < 10^{12}$ Blinds: $Nu_D = (0.60 + 0.322 Ra_D^{1/6})^2 \quad 0.1 < Ra_D < 1012$ *Mechanical Airflow* Glass: Entrance - $Nu = 0.906 Re^{1/2} Pr^{1/3}$ Laminar - $Nu = 8.235$ Turbulent - $Nu = 0.023 Re^{4/5} Pr^{1/n}$ Blinds: $Nu_D = 0.51 Re_D^{0.5} Pr^{0.37} \quad 40 < Re_D < 103$	Mechanical airflow, Inlet and outlet flow rates are know. Two-dimensional flow. Conservation of mass: $\sum_{j=1}^{n} m_j + S_M = 0$ Mass flow rate between cells modeled using the Power Law Model: $m_j = KA\rho\left(\frac{2\Delta P}{\rho a}\right)^{1/2}$ S_M = mass source K = flow coefficient A = area of cell ΔP = pressure difference between neighbouring cells	Test facility.

Appendix C

Glazing and Shading Layer Properties

Table C-1 Normal Glass Layer Properties

Name	Description	ID	l [mm]	τ	ρ	ε	ε'
Clear	PPG Clear_6	5012	5.7	0.771	0.072	0.840	0.840
Low-E 0.02	PPG SB70XL Strph-6	5439 (W6.3) 5000 (V5)	5.7	0.281	0.562	0.018	0.838
Low-E 0.10	SGG Planitherm T	11032	6.0	0.571	0.156	0.837	0.103
Low-E 0.04	Cardinal LoE287	2014	5.7	0.409	0.417	0.840	0.042

Table C-2 Normal Shading Layer Properties

Name	Description	Slat Angle/ Openness	l [mm]	τ	ρ	ε	ε'
VB	Light Al venetian blind, slat length = 12.7 mm, slat spacing = 10.6 mm	60°	6.25	0.174	0.626	0.850	0.850
RB1	White roller blind	14%	0.60	0.300	0.620	0.900	0.900
RB2	Chalk roller blind	5%	0.80	0.160	0.740	0.900	0.900

Table C-3 Off-Normal and Diffuse Glass and Shading Layer Properties

Name	Condition	τ	ρ	ε	ε'
Clear	Diffuse	0.677	0.013	0.840	0.840
	θ = 45°	0.725	0.084	0.840	0.840
Low-E 0.02	Diffuse	0.247	0.589	0.018	0.838
	θ = 45°	0.264	0.568	0.018	0.838
VB	Diffuse	0.334	0.497	0.850	0.850
	θ = 45°	0.089	0.732	0.850	0.850
RB1	Diffuse	0.262	0.620	0.900	0.900
	θ = 45°	0.271	0.620	0.900	0.900

Table C-4 Glazing and Shading Layer Optical Properties for Saelens (2002)

Layer	τ	ρ	α	ε	ε'
RB	0.100	0.510	0.390	0.900	0.900
Low-E 0.09	0.583	0.302	0.115	0.090	0.840
Clear	0.826	0.075	0.099	0.840	0.840

Table C-5 Glazing and Shading Layer Optical Properties for Park et al. (2004)

Layer	τ	ρ	α	ε	ε'
VB	0.307	0.485	0.208	0.900	0.900
Low-E 0.05	0.500	0.350	0.150	0.050	0.840
Clear	0.650	0.072	0.278	0.840	0.840

‘ Interior-facing surface (i.e., back side)